M.Sc. ABSTRACT Geography Department

WEATHER SYSTEMS AND PRECIPITATION CHARACTERISTICS OVER THE ARCTIC ARCHIPELAGO IN THE SUMMER OF 1968

Stephen Fogarasi

Weather systems over the Canadian Archipelago are specified twice daily in terms of surface pressure patterns and these patterns are grouped into 22 types with Lund's method. These pressure types, with the assumption of geostrophic flow, are interpreted using tendency equations expressed in terms of thickness, vorticity advection, and velocity divergence. Within this system of classification, large and some small-scale features are distinguished and their synoptic characteristics are detected. Pressure types and their station precipitations do not show persistent relationships because the connection between the assumed geostrophic circulation and the actual flow pattern is not persistent. Precipitation is, however, in close relationship with the 3 dimensional variation of vertical velocity as is demonstrated in two cases. Discrepancies between the calculated and measured precipitations are considered to be due to the sparse observation network, organized boundary layer vertical velocities, and the shortcomings of the model used for the calculation of total vertical velocities.

WEATHER SYSTEMS ~~AND PRECIPITATION CHARACTERISTICS~~
OVER THE ARCTIC ARCHIPELAGO ~~IN THE SUMMER~~ OF 1968

WEATHER SYSTEMS AND PRECIPITATION CHARACTERISTICS OVER THE ARCTIC ARCHIPELAGO IN THE SUMMER OF 1968

by

Stephen Fogarasi
McGill University
Montreal

WEATHER SYSTEMS AND PRECIPITATION CHARACTERISTICS OVER THE ARCTIC ARCHIPELAGO IN THE SUMMER OF 1968

by

STEPHEN FOGARASI

A Thesis submitted to
the Faculty of Graduate Studies and Research
in partial fulfilment of the requirements
for the degree of Master of Science

Department of Geography
McGill University
Montreal

March 1971

ACKNOWLEDGMENTS

The writer is greatly indebted to the Glaciology Subdivision of the Inland Waters Branch for making this study possible, for its acquisition of weather data from the Meteorological Branch of the Department of Transport, Toronto, the U.S. Department of Commerce, National Weather Records Center, Ashville, North Carolina, and the Danske Meteorologiske Institut, Copenhagen, and for providing programming, computer, and drafting facilities.

The author extends his gratitude to the Central Analysis Office, Dorval, to the Uplands Airport Forecast Office, Ottawa, to Professor B.J. Garnier for providing weather maps, and to the Satellite Data Laboratories, Malton, for kindly providing access to their archives and for supplying selected satellite pictures.

The author tenders his sincere thanks to Mr. Kunio Shimizu and his assistant, Mrs. M. Patterson, Geological Survey Branch of the Department of Energy, Mines and Resources in Ottawa, for the provision of the correlation, mean, and standard deviation programs used for weather classification, also for the sorting program of the precipitation data, and for the vertical velocity program used in precipitation analysis.

The writer's special thanks are hereby extended to: Mr. H.L. Ferguson, Hydro-Meteorology Section of the Meteorological Branch, Toronto,

for providing precipitable water overlay, advection scale, and valuable advice on upper level advection; Mr. E.C. Jarvis and N.H. Kagawa, Research and Training Section of the Meteorological Branch, Toronto, for their comment on the applicability of streamline analysis on the arctic; Professor S. Orvig, Department of Meteorology, McGill University, for his assistance in the derivation of vertical velocity equation; Professor R.A. Bryson, Department of Meteorology, Wisconsin University, and Dr. R.G. Barry, Associate Professor, Arctic and Alpine Research, Boulder, Colorado, for their encouragement and valuable comments; and Miss J.M. Pazdzior for assisting in air pressure data extraction and in the compilation of the simplified orography of the arctic.

CONTENTS

LIST OF TABLES

LIST OF FIGURES

List of Symbols Used

g	acceleration of gravity, 9.81 m sec^{-2}
R	gas constant of dry air, 6.857×10^{-2} cal/gram ^{o}C
ρ	density of the air, g m^{-3}
Z	height above the sea surface in geopotential metres
ϕ	geographical latitude
f	Coriolis parameter, $(2\hat{\omega}\sin\phi)$, in 10^{-5} sec^{-1}, where $\hat{\omega}$ is for the angular velocity of the earth
$\vec{V}$	wind vector in m sec^{-1}
p_o	surface air pressure in mb
p	upper level air pressure in mb
$\frac{\partial p_o}{\partial t}$	local surface pressure change at a point in a fixed coordinate system
$\frac{\partial p}{\partial t}$	local upper level pressure change at a point in fixed coordinate system
$\frac{dp}{dt}$	individual change of pressure at a point in a moving coordinate system
Tm	mean virtual temperature of the 1000 - 500 mb layer
$\frac{\partial Tm}{\partial t}$	local change of the mean virtual temperature of the 1000 - 500 mb layer in a fixed coordinate system
Δp_o	local surface pressure change in 12 hours
Δp	local upper level pressure change in 12 hours
$div\rho\vec{V}$	mass divergence
$Div\vec{V}_1$ or $\vec{V}_2$	velocity divergence at level 1 or 2, in 10^{-5} sec^{-1}
$\frac{d\alpha}{dn}$	confluence of the streamlines, where $d\alpha$ indicates the deviation of the streamline from the straight line, and n is normal to the streamline

$\frac{\partial V}{\partial s}$	velocity divergence, where ∂V is the velocity change, and ∂s is an infinitely small path run by the air along the streamline
u	zonal wind component along the axis x in Carthesian coordinate system; westerly wind positive, easterly negative, in m sec^{-1}
v	meridional wind component along axis y in Carthesian, coordinate system, southerly wind positive, northerly negative; in m sec^{-1}
∇p	pressure gradient
$\nabla \rho$	density gradient
C	velocity of the moving coordinate system
$A\zeta_a$	geostrophic advection of absolute vorticity in m/3 hours
A_h	geostrophic thickness advection in m/3 hours
W	vertical velocity in cm sec^{-1}
ω	vertical velocity through pressure surfaces in 10^{-3} mb sec^{-1}

INTRODUCTION

The weather and precipitation of a region are its important "natural resources". Knowledge of the spatial distribution of the amount of precipitation and an understanding of the weather systems yielding precipitation are essential prerequisites to the formulation of a model for the study of the arctic atmospheric water balance. This goal is still far away since, at present, arctic precipitation is being measured only at a few scattered rain gauges and snow plots. Therefore, the object of this study is to see if it is possible to identify precipitation characteristics based on the analysis of weather systems and, on the bases of the characteristics deduced, to make suggestions for the establishment of an atmospheric water balance model. For this analysis the summer of 1968 has been chosen. The fact that there were in existence well organized collections of data and reliable precipitation measurements for summer day conditions in 1968 was a deciding factor in the selection of this particular summer.

Since the analysis of weather is an important aspect of this study, an attempt will be made to classify weather types and to seek a connection between weather systems and their related precipitation conditions. This connection, whether it is a direct or an inverse connection will be explained by assessment of the current, large-scale kinetic and hydro-dynamic characteristics associated with at least some of the weather systems. Such an appraisal of the kinetic or thermo-dynamic characteristics of arctic weather systems and the local influences on the circulation within given states of weather may lead to a better understanding of the particular large-scale

vertical motion fields as precipitation producing systems. The kinetic characteristics of the weather systems will be determined by wind field analysis, and the thermo-dynamic conditions will be determined by the advection of heat and of cyclonic rotation as measured on the 500 mb weather maps.

The sparse records, both in terms of space and time, of arctic precipitation form a major difficulty for the study of arctic climatology. In this study, therefore, synoptic-analytical methods are invoked to assess the physical characteristics related to the horizontal distribution of precipitation. Interpolation between the precipitation values of instantaneous weather systems is not justifiable. However interpolation between temperature and pressure values is quite acceptable. The analysis of weather elements other than precipitation measured at distant points frequently involves the use of interpolation and extrapolation at intermediate or edge locations. Although the main area of interest of this study is the Canadian Archipelago, difficulty of extrapolating atmospheric wind conditions over this area of interest suggested the analysis of a region larger than the Canadian Archipelago itself in order to reduce errors in analysis around the edge of this region. The surface and upper air stations used in this study are shown in Figure 1 with the extent of the area of interest outlined with dash-lines. The observation network is discontinued outside the northern and northwestern edge of the Canadian Archipelago; therefore, the surface and upper level maps will be analysed to estimate the possible weather elements along the edge zone.

The sequence of the steps for the execution of the analysis will

be the identification or specification of the weather systems, their classification, and their interpretation in terms of kinetic and thermo-dynamic processes producing given precipitation fields. Finally, suggestions for the establishment of an atmospheric water balance model will be made.

CHAPTER 1

PRINCIPLES FOR THE SPECIFICATION OF THE WEATHER SYSTEMS

a) Approximating the wind fields of the weather systems with pressure patterns

Large-scale vertical velocity, the main factor causing organized precipitation, depends largely on the speed and direction of the wind in relation to pressure systems, topography, land-ocean distribution and moisture sources. A survey of the horizontal wind field within synoptic-scale motion systems is a major prerequisite for the estimation of the instantaneous precipitation patterns. If the wind field of the instantaneous weather systems were devoid of local and temporal disturbances and remained stationary, continuous in space at least for a short time, (Jarvis 27), the synoptic pressure maps would be considered as the mean flow charts of at least a few minutes showing the average state of the general circulation in a spatial context. For the consideration of the geostrophic flow the pressure maps represent smoothed motion patterns containing only the large-scale circulation features. Therefore the assumption of geostrophic condition can be regarded as a very general approximation of the representative wind field.

According to Saltzman (47), and Petterssen (44), (45) the actual circulation patterns of the arctic undergo periodic fluctuations due to the fact that they maintain their statistical quasi-balanced normal state. In

the second approximation of the description of the wind field, therefore, the fluctuating nature of the circulation types must be taken into consideration. A stratified sampling of arctic circulation will establish motion types and thus can be expected to demonstrate the spatial and short term characteristics of each fluctuation. Some variability within each motion type is however likely to occur. The operational twice-daily (00 and 12 GMT) surface pressure maps seem to be sufficient sources for the separation of the fluctuations in the arctic tropospheric motion since, according to Petterssen (44), only small pressure pattern changes can be expected during a 12 hourly period. The limitations of these pressure maps when used for wind analysis, however, cannot be disregarded. In the proximity of the ground, the motion field is essentially modified by frictional forces, whereas in the free atmosphere semibalanced geostrophic conditions prevail. Pressure patterns of the free atmosphere, therefore, may diverge from the surface patterns, and the upper geostrophic circulation may, according to Petterssen (44) and Hromov (24), even be opposite to the lower geostrophic motion. Surface pressure maps reflect the large scale geostrophic wind conditions above the boundary layer, and pressure charts of the standard isobaric surfaces represent the generalizations of the upper air motions. Since the periodic fluctuations of the characteristic wind field in weather systems are largely represented by instantaneous surface pressure patterns, one may assume that the characteristic large-scale vertical velocities are similarly associated with particular surface pressure patterns. Court (9), for example, recommended the application of the principles of map pattern climatology to the study of instantaneous weather and large-scale precipitation systems, since large-scale weather patterns are frequently associated with particular precipitation fields.

Therefore, it would seem justifiable to substitute surface pressure patterns for the physical characteristics of the lower troposphere. Consequently, attention will now be drawn to the description of the physical characteristics pertaining to the surface pressure patterns. Large-scale organized precipitation and its vertical velocity field, according to Jarvis (26), always possess recognizable physical characteristics of propagation components. These components, such as, the advected sensible heat, the cyclonic rotation patterns, the precipitable water content of the advected warm air, and the confluence or difluence of the isobars and upper level baroclinic waves are always associated with particular pressure features of the upper and lower layers (Jarvis, 26). The main regulators of the lower pressure features, the upper tropospheric baroclinic waves, are recognizable on the pressure maps of the free atmosphere. The surface pressure features, overlapped by the baroclinic waves, are more or less the modified expressions of the map patterns at the upper standard pressure surfaces. The overwhelming dominance of the surface circulation in the formation of the arctic weather beneath the region of the upper baroclinic wave pattern cannot be emphasized enough. For this reason, then, in this thesis the study of surface circulation will take precedence and the analysis and consideration of these baroclinic waves will be omitted.

The successive assessment of the physical characteristics and the propagation components of the large-scale precipitation of the weather systems are very complicated to analyse. Consequently, several scientists have recommended the consideration of a more accessible parameter. For example, Saltzman (47), Bryson and Kuhn (7), Hastenrath (23), and Lydolph (37) have called attention to the fact that the differences in the physical

processes in the free atmosphere and in the boundary layer of the air-sea-land interface bring about localized friction-induced velocity divergence and the deflections of the large-scale currents. Jarvis (27), Soucier (48), Petterssen (44), and Kagawa (29) agree that pressure features are associated with particular streamline systems. These systems, with the exception of the boundary layer, agree well with the geostrophic conditions. Significant discrepancies exist near the ground between the surface pressure patterns and the actual wind conditions, and these discrepancies are necessarily reflected in the related streamline patterns. For the purpose of generalization it is assumed that, although a shallow boundary layer can alter the local appearances of the macro-synoptic conditions near the ground, an instantaneous modification of the synoptic conditions by surface friction and localized diabatic processes can hardly affect the general character of the atmospheric circulation when the oscillating circulation is investigated over a large region during a short period of time.[1] The frequency distributions of divergences and convergences for both cyclonic and anticyclonic flow patterns given in Figures 33 and 34 (a detailed discussion of these figures will be given later) clearly indicate that the highest frequencies are associated with zero divergence, that is, with a flow that behaves like a geostrophic wind devoid of acceleration, confluence, and difluence. Therefore the delineation of the current circulation patterns in time and space can conveniently be based on the related surface pressure charts representing the geostrophic flow patterns rather than on the surface streamline patterns.

---

[1] This statement is based on the personal communication between the writer and E.C. Jarvis, O'Neil, H.L. Ferguson, Department of Transport of Canada, Meteorological Branch, and Professor R.A. Bryson, Wisconsin University, Department of Meteorology, Madison, Wisconsin.

In the present study the weather types are classified in terms of surface pressure patterns and their characteristic streamlines are used for selected analyses and illustrations. The actual streamline-pictures present the true flow patterns of the pressure maps, but they still show static and instantaneous images of the wind fields with the exclusion of the time-dependent variation of the circulation.

b) Interpreting the time-variation of the pressure patterns with tendency equations

According to Hromov (24), Jarvis (25), Lee (35), and McPherson et al. (38) a measured surface pressure is a report of a given thermo-dynamic condition in the vertical column of air and local pressure changes are equivalent to changes in the thermo-dynamic conditions above. The time-dependent fluctuating weather systems, when classified in terms of pressure patterns, are delineated on the basis of the variable thermo-dynamic conditions of the lower troposphere. This type of interpretation of pressure fields is undertaken in order to bridge the gap between the problem of air pressure and the complex vertical velocity problem. The principle can be expanded and clearly illustrated by means of arguments borrowed from synoptic meteorologists.

Thus, following Hromov's (24) example, one can write the logarithmic form of the static equation of pressure differentiated with respect to time, as

$$\frac{\partial p_o}{\partial t} = \frac{p_o}{p}\frac{\partial p}{\partial t} - p_o \frac{g z}{R \bar{T}_m}\frac{\partial T_m}{\partial t} . \qquad (1)$$

By replacing the differentials with finite differences, as measured during the period Δt = 12 hours, the following tendency equation is obtained:

$$\Delta p_o = \frac{p_o}{p} \Delta p - p_o \frac{g z}{R T_m} \Delta T_m \cdot \qquad (2)$$

Equations (1) and (2) are valid if the requirements for a static equilibrium are satisfied; that is if the vertical pressure gradient is able to counterbalance the weight of the unit mass of air, and if there is no vertical acceleration. According to Hromov (24) the latter can exist for a short distance for a brief time in the case of strong convection, which is however very rare over the arctic.

If the upper level pressure change Δp is equal to zero in equation (2) then the change of surface pressure Δp_o is made up entirely by the second part of the same equation. The change of the mean virtual temperature, ΔT_m, in the upper layer is associated with heat advection, vertical motion, release of latent heat, mixing and radiation.

If isothermal conditions are maintained, that is T_m = constant, then ΔT_m is equal to zero. The upper level pressure change in this case is made up entirely of upper tropospheric divergence which is not detected in the surface flow pattern. Isothermal conditions of the arctic circulation are frequently encountered in the so-called "cold lows" in which the isotherms are parallel with the isobars. This condition has also been pointed out by Hare (19) who showed that arctic weather systems are frequently associated with cold lows and concentric isotherms, that is, with a lack of temperature discontinuities along the flow lines.

Hromov (24), and Petterssen (44) indicated that the upper divergence is reflected in the value of Δp, since

$$\frac{\partial p}{\partial t} = - \int_{z}^{\infty} g \, \mathrm{Div}_{\rho} \vec{V} \, dz \, . \qquad (3)$$

Namias (39) has shown that the effects of topography, surface friction, and kinematic disturbances in the lower boundary layer can all be expressed in terms of divergence at upper levels despite the upper geostrophic conditions assumed. Namias' reasoning is fully explained by the Bjerknes equation quoted in Hromov (24),

$$\frac{\partial p}{\partial t} = - \int_{z}^{\infty} g\rho \vec{V} \frac{d\alpha}{dn} \, dz - \int_{z}^{\infty} g\rho \frac{\partial v}{\partial s} dz - \int_{z}^{\infty} (g\vec{V} \cdot \nabla\rho) \, dz + (g\rho w)z \, , \qquad (4)$$

where the first term on the right represents the horizontal confluence of the streamlines, and the second term indicates the horizontal velocity divergence along the streamlines. The third integral is for the density advection represented by the scalar product of the density gradient, $\nabla\rho$, and the horizontal wind vector, $\vec{V}$. The fourth expression for the consideration of the sea level pressure changes can be disregarded since $w = 0$ on the surface.

Since equation (4) as it stands is very difficult to interpret and calculate, it is customary to introduce simplifications. This can be achieved by following the arguments of McPherson et al. (38) where it is shown that the first two terms on the right can be replaced by the integrated value of velocity divergence in the vertical column and the third term can be replaced by the temperature or thickness advection of the 1000 - 500 mb layer. Furthermore Jarvis (25) has pointed out that the divergence

term comprising the first two terms on the right of equation (4) can be approximated with the absolute vorticity advection at 500 mb level. Therefore it follows that equation (4) can be calculated in terms of two relatively simple elements: thickness advection, and the vorticity advection on the 500 mb level.

The approximate relationship between the pressure tendency and the advection of the absolute vorticity at the 500 mb level can be rapidly and easily expressed by Ferguson's (15) equation for the lower troposphere. Accordingly,

$$\frac{\partial p_o}{\partial t} \propto - c \frac{1}{2.65} \left[A_{\zeta a} \right]_{500} , \qquad (5)$$

where c is a coefficient expressing the effect of the diabatic processes and vertical motions and $A\zeta_a$ is measured from the 500 mb vorticity chart by using Ferguson's (15) "Geostrophic Advection Scale" and Harley's (20) correction factor.

Ferguson's (15) other approximative tendency formula

$$\frac{\partial p}{\partial t} \propto - c \left[A_h \right]_{p}^{p_{500}} \qquad (6)$$

utilizes the geostrophic advection of the mean virtual temperature, A_h, or simply the thickness advection between the surface and 500 mb level as measured with Ferguson's (13) advection scale. The interpretation of equations (5) and (6) seems to be more convenient than that of equation (4) and these two components are easily accessible from the 500 mb charts.

Penner (43), on the bases of the two components, vorticity advection and thickness advection, introduced his equation of the large-scale vertical velocity for the 600 mb level as adjusted for the polar stereographic charts, 1:20,000,000 scale in the form

$$-\omega_6 = \frac{0.16}{f} A_{\zeta a} + \frac{0.12}{f} A_h \cdot \qquad (7)$$

Hence it follows that pressure tendencies in the form of either equation (4), (5), or (6) serve not only to explain the thermo-dynamic changes of the time dependent pressure patterns but also to describe the large-scale vertical velocity potentials of the pressure changes. These thermo-dynamic conditions are localized in certain parts of the pressure field and according to Petterssen (44): ..."a rapid pressure decrease and cloud formation are most likely over the regions of strong positive (cyclonic) vorticity advection, and cyclonic vorticity advections are associated with warm advection beneath the 500 mb level in the warm sector of the lows and highs, that is, in the southerly confluence zone between the foreparts of the lows and the rear of the highs". Lee (35) expressed the same philosophy based on equation (3) by saying that surface pressure falls are associated with net divergence and warm advection, while pressure rises are associated with net convergence and cold advection in the vertical column of air. It follows from equations (3) and (4) that constant atmospheric surface pressure can still be associated with vertical velocity aloft under certain conditions, as for example, when a low-level velocity divergence is overlapped by a convergence field above it. Equations (5) and (6) can similarly indicate constant surface pressure values when the sign of the thickness and vorticity advection changes with elevation and the upper level values are

able to counterbalance the magnitude of the lower ones. These conditions occur in the majority of the cases.

Ferguson (13), Harley (20), McPherson (38), Penner (42), (43), Petterssen (44), and Sutcliffe et al. (49) suggested that equation (7) is applicable to a model atmosphere which is composed of baroclinic waves of the upper levels overlapping the pressure features of the lower levels. This model applies to weather systems with closed contours near the surface and an upper trough. This is the type of weather which produces the most vertical motion.

It will be apparent from the foregoing discussion that the complicated link between the surface pressure changes and the lower tropospheric motion can be looked upon as the product of a number of thermodynamic processes inherent in the motion field associated with the fluctuating and travelling pressure features provided that geostrophic conditions are present in the free atmosphere. By using equation (7) the complicated and multi-layered atmosphere can be reduced to a single layer model of the 1000 - 500 mb levels. Hence the baroclinic weather systems classified in terms of the surface pressure patterns can be expected to represent a particular distribution of vertical velocity provided that baroclinic conditions prevail. In cold lows associated with a baratropic atmosphere, when equation (7) is not applicable due to the lack of advection at the 500 mb level, the effect of the lower levels is dominant in the creation of a vertical velocity field. Under these conditions the confluence and difluence zones of the pressure types can be expected to be associated with vertical velocity fields. A multi-layered divergence calculation for a

barotropic atmosphere, according to Bellamy (5), Kuhn (33), Landers (34), and Thompson (52), can provide an accurate estimate of the large-scale vertical velocity field. The vertical velocity in pressure coordinates on the top of a layer can be expressed by means of the average velocity divergence of the top and bottom of the layer as

$$\omega_2 = \omega_1 + \frac{1}{2}\left(\mathrm{Div}\,\vec{V}_1 + \mathrm{Div}\vec{V}_2\right)(p_1 - p_2) \times 10^{-3} \text{ mb sec}^{-1} \cdot \qquad (8)$$

One might conclude from the previous discussion of equations (7), and (8) that if geostrophic conditions are maintained characteristic pressure features will produce typical vertical velocity fields and precipitation characteristics. This is, however, not the case since low- and upper-level divergences do frequently modify the distribution of vertical velocities. Before commencing the analysis of vertical velocities, therefore, it will be necessary to classify the weather systems in terms of pressure patterns.

CHAPTER 2

CLASSIFICATION

a) Description of the method and technique of classification

In the present thesis the quantitative classification of the surface pressure maps has been carried out on 246 sets of numerical data. Each pressure map has been numerically specified. For this specification the pressure samples were extracted for the months of May, June, July, and August, 1968, from the 00 and 12 GMT surface maps at the scale of 1:20,000,000 published by the Central Analysis Office of the Canadian Department of Transport in Montreal. Sea-level pressure values read at 25 points were used to describe the map patterns for each of the 246 surface maps. The location of the sampling points used for classification is presented in Figure 2. Each row of the sampling network is separated by a distance of 5 degrees latitude. The position of the points along each row is subjectively determined in order to avoid using pressure readings from mountainous terrain since surface reduced pressure fields over high mountains bear little relation to the winds at the gradient wind level. The sampling network is believed to provide an adequate general summary of the pressure maps. The method of classification used has taken into account the objective that the existence of the general synoptic patterns should be recognizable and that the localized small-scale pressure features of the weather systems, possibly of great importance for the local climate, should not be sacrificed and filtered out with the method used. The classification of the sea-level pressure maps was done according to Lund's (36) method.

The essence of Lund's method is to seek out individual maps which show great resemblance to other pressure maps. The resemblance or similarity between pressure patterns is determined quantitatively with linear correlation. The correlation is performed in such a way that each of the digitized 25 pressure values of the first map is correlated with the corresponding value on the successive second, third, and finally n-th map. The mean correlation coefficients of the first map with the second, and the first with the third, and so on successively to the n-th map are calculated. Then in turn the second map is correlated with the third, fourth, to the n-th map, the third with the fourth and successive maps, and continuing in this way to the correlation of the (n-1) map with the n-th map. The resulting vast number of correlation coefficients are organized and recorded in a correlation matrix and the classification of the pressure patterns is performed on the matrix.

The classification is carried out by counting row-wise and column-wise the correlation coefficients above 0.7. The reason why 0.7 has been selected will be discussed later. The individual map which resembles most closely the most weather charts is indicated by the highest number of counts and considered by Lund to be representative of that group within which a high correlation of the pressure values can be expected. This group is called a type. By disregarding all the maps of the first type, a second count will result in the establishment of another type. The process is repeated until there are no maps left to count.

In the present work the computerized calculation of the correlation coefficients for the 246 maps required 42 minutes on the CDS 3100 computer. The results of the correlation values equal to or higher than +0.70 along

with the lower and upper confidence limits on 5% confidence level were listed on the output sheets and the correlation values were manually plotted on a 246 x 246 symetric correlation matrix. Table 1 shows a part of the correlation matrix with the sum of the row and column totals on the right side of the table as obtained at the first count. The first values on the left in the count column are the enumerations of the cases when the row-dated maps correlated with other maps at a correlation coefficient equal to or higher than +0.7. The second number on the left represents the column counts. The subdivision of the totals into row and column subtotals made count-checking easier. The maps associated with the most correlation coefficients of $\geq$0.7 were selected and designated as type A. For the first count, both column- and row-wise, there were 44 maps whose correlation with the map of July 3, 1968, 12 GMT, equalled or exceeded 0.70. Therefore the surface map, July 3, 12 GMT, was selected as the representative map of the type A group. The relationships between the map of July 3, 12 GMT and the similar charts are expressed through their correlation coefficients circled on Table 1. This table shows only a small portion of the matrix. All the type A cases were removed from further consideration by crossing out with a thin line all the correlation values associated with these maps along the appropriate rows and columns of the correlation matrix. The maps to be disregarded for the next recounting are checked off on the right side of Table 1. All the totals and subtotals were erased on the original matrix before recounting. The recounting of the high correlation values was made on the rest of the maps and type B was selected as Map July 28, 00 GMT, which was highly correlated with 24 other maps. The above process was repeated until no cases remained with correlations of 0.70 or higher.

After the process of recounting and the separation of the 22 types there remained only a few maps having no correlation with each other and any other maps already classified. This group of pressure patterns is declared unclassifiable and indicated with the letter W. For each pressure type a list has been set up by enumerating all the individual-member maps and their correlation coefficients with the type-representative map within that group in a succeeding time sequence. This list has been checked against the computer printout of the correlation coefficients and a search was made to find out whether individual maps already classified had higher correlation with other type-representative maps or not. In a number of cases a rearrangement or reclassification of the individual maps was found to be necessary. Information about the types, the representative surface maps of the types, the result of the reclassification, and the mean correlation coefficient within each type is shown in Table 2. The discussion of column number 5 in this Table will be presented in the next chapter. The summary of the whole classification is presented in the Map Type Calendar, Table 3. In this table correlation values of three digit numbers are indicated on the right side of the class-name of each individual map. Since type-representative maps correlate with themselves at a value of 1.0, these units are not shown. Similarly unclassifiable cases are not designated with any correlation value in Table 3. The final demonstration of the weather types is presented in a series of maps beginning with Figure 3 and ending with Figure 24. In each of these figures there are four maps. Each map designated A in this series of figures is a type-representative map which is sufficiently representative of the established weather types. The B figures represent the mean pressure patterns of the individual maps for the type. The deviation of the instantaneous pressure

patterns from the mean is represented by a series of C maps. The detailed discussion and the interpretations of these and the series D maps are reserved for the forthcoming chapters.

At this stage the preliminary work on the classification has been completed. However before one can begin to interpret the results, one major subjective point of the classification, the effect of the acceptable lowest limit of the correlation coefficients on the validity of the classification, requires further explanation.

b) Acceptable correlation coefficient

By following Lund's (36) reasoning the assumption is made that by lowering the lowest limit of the correlation coefficients, the number of cases within each group can be increased. According to Lund exactly the same map would have been chosen as a member of a certain type if either +0.90 or +0.60 had been used instead of +0.70 as the "lowest acceptable correlation coefficient". The use of a lower "value", results in the inclusion of more cases in each type but it definitely does not cancel out existing high correlations with other established types already taken into consideration, since maps being correlated with two or more types were assigned to the type with which they were most highly correlated within the narrowest confidence limits. This rearrangement has previously been shown in the fourth column of Table 2.

Following Lund's example, in this study the lowest correlation

coefficient applied so far was +0.7. Hence of the 246 maps examined for the summer of 1968 all but 28 maps (approximately 11% of the total) were correlated by a value of +0.70 or higher with one or more of the type-representative maps. The question is, whether one can reduce the number of unclassifiable cases by lowering the limit of the acceptable correlation values. To test this, a second computer correlation has been carried out and correlation coefficients equal to or greater than +0.6 were listed. Through this second run, correlation has been performed only for the type-representative maps and the unclassifiable cases. If this lower correlation value is acceptable as a sufficient indication of representativeness then the number of unclassifiable cases is reduced from 11% to 6% of the total cases. The effect of the lowered correlation coefficients to +0.6 is demonstrated in the fifth column of Table 2. The greatest change occurred among the unclassifiable cases whose number was almost halved. Two maps were added to the type D and type R, while only one map increase was found in the types: E,F,I,K,L,N,O,U, and V.

A third correlation run, when correlation values $\geq$+0.5 were listed, resulted in a further reduction of the 15 unclassifiable cases to four maps, that is, 1.63% of the total cases. By lowering the "lowest acceptable correlation coefficient" to $\geq$+0.5 it would have been possible to place eleven more maps into the "Map Type Calendar" already shown in Table 3. Rearrangement of the maps due to the lowest correlation values of less than 0.6 but higher than 0.5 is indicated in Table 3 but unlisted in Table 2. After the third run of calculation it seemed necessary to check the validity of the theoretical classification by consulting actual maps.

An inspection of the eleven maps brought into the classification through the third correlation run referred to above does in fact reveal a definite resemblance to some of the weather types already established. However, the low correlations do not warrant unconditional acceptance of this third amendment to the pressure pattern classification. Both Lund's experiment and the present study revealed that the number of unclassifiable cases could be reduced but not eliminated by the lowering of the acceptable correlation values. The visual inspection of the maps showed that systems with deep or weak lows frequently correlated with their representative maps at a correlation coefficient of slightly higher than +0.6. No visual correlation was ever apparent between >+0.5 and <+0.6. Consequently, it was decided to use +0.6 as the dividing point between map patterns and to reject the value of 0.5 as the lowest acceptable correlation coefficient.

The classification method and technique described made possible the separation of the pressure types and the classification of the individual weather maps by presenting the types in static pictures. The time-dependent nature of the arctic circulation and the recurrence of the weather types which have as yet not received mention will be demonstrated through the correlation matrix.

c) Correlation Matrix

In order to assess the importance and the potential of the correlation matrix in the classification, it was necessary to observe the shape and the pattern of the matrix. Not every correlation coefficient was plotted on the matrix but only those correlation values

of $\geq$0.6. These values were not evenly distributed but clustered in recognizable patterns, especially along the diagonal of the matrix as illustrated in Tables 1 and 4. Clusters along the diagonal formed smaller and larger triangles and the off-diagonal concentration of the correlation values into certain patterns could also be observed. In several instances the shapes of the triangles were not fully covered by high correlation values. Only the outline of the triangles were recognizable. The empty spots in the triangles of the Tables 1 and 4 are believed to be caused by the variability of weather and correlation values at lower than 0.6. If six hourly observations had been used, these gaps might have been reduced since the twice daily observations at 00 and 12 GMT cannot provide more than two daily snapshots of the continuously changing weather phenomena.

It seems from scrutiny of Tables 1 and 4 that clusters can be formed by a persistent pressure pattern. This conclusion was reached after these clusters were broken down into the occurrences of the component weather types by the indication on the matrix of only the correlation values associated with a given type of weather. In Table 4, for example, the correlation values of type C weather are circled. It can be seen that if these circled maps were eliminated the clusters would disappear both in Tables 1 and 4. Off-diagonal concentrations along the columns and rows of the cluster-triangles demonstrated the cyclic recurrences of type C weather which was itself representative of a particular synoptic regime. In both the vertical and horizontal column of Table 4 type C weather can be seen to have twice reappeared 4.5 days after its previous occurrence. The persistence of this type was also expressed through the size of the area occupied by the clusters. A similar representation of the

correlation values for any other type is possible on the matrix and the cyclic nature of any type can be demonstrated. Besides the classification potential of the correlation matrix, another potential technique of using the matrix can also be offered here. This technique would make possible the study of the cyclic reappearances of the weather systems. A strong type C weather spell might have been compared with upper tropospheric pressure waves. 300 mb pressure waves might have been resolved into their harmonic wave components and their possible association with the cycles of the surface pressure types might have been sought. These are interesting aspects but the discussion of these relations is omitted in this study.

In addition to these observations it is suggested that this method of classification can be applied not only to map patterns but to the classification of, for example, radiosonde ascents, radiation curves, wind profiles, temperature curves of a site, and to many other curves provided that the relationship among the curves is linear. Unfortunately the relationship among the pressure maps as pointed out by Hare et al. (19), and Robinson et al. (46) is not linear. Strictly speaking the specification of the maps should have been done with orthogonal polynomials but the error introduced with the assumption of a linear relationship is, as pointed out by Robinson et al. (46), insignificant. Therefore, one can interpret with confidence the results obtained using Lund's method of classification.

CHAPTER 3

INTERPRETATION OF THE CLASSIFICATION RESULTS

a) Interpretation of, and experimenting with, the classification results

To be able to judge the validity of the method of classification used one must first examine the success of the separation of the type-representative maps. It was assumed that if there was a similarity between type-representative maps then the types had not been successfully separated. Therefore these maps were correlated with each other and the calculation proved that none of them correlated with one another at a correlation value of $\geq +0.5$. The absence of a high positive correlation between the type-representative maps suggests that the separation of the type-representative maps was successful. Further support of this suggestion is provided by the visual inspection of the individual maps within each type. This indicated that the classification was quite sensitive even in the detection of the localized small-scale isobaric features which showed up as small waves on the isobars.

After the positive correlation run, another experiment was conducted on the type-representative maps taking into consideration the negative correlation coefficients. An assumption was made that a correlation run of the opposite pressure patterns would result in a high negative correlation. The dissimilarity between the type-representative maps, observable also by the visual inspection of these maps, is quantitatively portrayed

through the high negative correlation coefficients presented in Table 5B. The most remarkable examples are shown by the type-representative maps of N and C at a correlation value of -0.811.

After the completion of the statistical experimentation on the type-representative maps the next task is the critical review of the type mean maps in Figures 3B - 24B. Visual inspection and comparison of the type mean maps with the individual maps clearly shows that the mean maps are simplified reproductions of the type-representative maps. The deviations of the individual pressure maps from the mean maps presented by the Figures 3C - 24C reveal only localized increases in the standard deviations. An additional generalization of the large-scale features is provided through further experiments. A positive correlation run of the type-mean maps revealed that type A mean map was highly correlated with type L, U, I, and D mean maps and similarly type E mean map highly correlated with type V and T maps, as has been shown in Table 5A. Hence one can notice that the grouping of the pressure types in terms of the large-scale formations would be statistically possible using Lund's method. A further generalization, that is, a grouping of the large-scale weather systems is feasable if the motion of the pressure patterns is examined in a moving corrdinate system.

The constant pressure patterns, which have so far been studied only at a fixed system, in fact move, rotate, and deform horizontally with a velocity C relative to the fixed system. Hence the changes of the pressure values with the lapse of time can be looked upon in a moving coordinate system moving with the pressure pattern and expressed by Petterssen's (44)

formula:

$$\frac{dp}{dt} = \frac{\partial p}{\partial t} + C \cdot \nabla p \cdot \qquad (9)$$

Applying this concept, through the visual inspection of the mean maps, one can easily recognize the following changes:

a) if type A mean pressure pattern is shifted 5 degrees of latitude distance to the northwest, it corresponds to a type L mean map;

b) if type A mean pressure pattern is rotated 70 degrees to the west around its cyclone centre in the Foxe Basin, type A pattern becomes a type U mean map;

c) if the two cyclone centres of the type A mean map are separated a distance of 15 degrees latitude along the same trough axis, it is the same as type I mean map; and

d) if the upper cyclone centre of the type A mean map is shifted a distance of 15 degrees latitude to the southwest, the pattern is like that of a type D mean map.

Similar observation of the type E mean pressure pattern reveals that:

a) the type E mean pattern becomes type V if its two cyclone centres are meriodionally separated, and

b) the type E mean map becomes type T if its two cyclones are separated along a northeast-southwest axis.

Hence through the preceeding correlation of the type mean maps and the consideration of the displacement of the pressure patterns it can be argued that weather types A, L, U, I, and D seem to comprise a general group. Similarly the weather systems E, V, and T can be interpreted as another general group of weather. Hence the principle of generalization or

grouping of weather types has been demonstrated although the interpretation and the discussion of the weather types needs to be done for the individual types separately.

In addition to generalization or grouping of the weather systems it is necessary to examine the dominance of the weather types by taking into consideration their persistence or variability. Despite the variability of arctic weather, type C was dominant during the end of May and early June, for example, with a persistence of 168 hours in one spell; type D in early May lasted 108 hours, while others existed for less than 12 hours and for as long as 72 hours. The non-persistent or rare types tended to occur either in early May or the end of August. This suggests that these patterns are really more representative of conditions in another season than of summer weather. Patterns Z and R are recognizable only by the end of August while types C, J, K, M, N, and S with their May and June appearances are rather transitional types from winter to summer circulation.

The frequency with which one type was followed either by itself or by another type is shown in Table 6. (The table must be read from the top downward). The whole numbers indicate the frequency with which one pressure type was transformed into another type and the figures in brackets express the percentage of the succession. The column totals in Table 6 are equal to the total occurrences within that type. Type C, with the highest persistence, reappeared in 80% of the cases while the less stable pattern, type V, repeated itself only in 25% of the cases. For all the 22 types the pressure patterns reappeared in an average of 57% of the cases.

The experimentation with the positive and negative correlation on the time-dependent, persistent, and transitional weather types suggests the need for a synoptic interpretation of the weather types. The preceeding statistical analysis cannot explain the relationship between the weather types and the characteristics of the physical processes likely responsible for precipitation. The synoptic interpretation of the types however can be expected to throw some light on this relationship.

b) Synoptic interpretation of the large- and small-scale pressure features of the weather types

Synoptic interpretation of the pressure types will be done through the joint consideration of the maps already used for classification purposes, and the maps of the thermo-dynamic and kinetic characteristics. The following are included in the classification maps:

i) the location of the centres of closed cyclones and anticyclones as compiled from the individual maps (Figures 3D-24D) where dots indicate cyclone centres and little squares the centres of highs;

ii) the mean surface pressure maps (Figures 3B-24B); and

iii) The standard deviation maps (Figures 3C-24C). The thermo-dynamic characteristics, the thickness and vorticity advections, can be obtained by means of Ferguson's (15) method from the 500 mb thickness and absolute vorticity maps. The kinetic parameters can be deduced from some of the related streamline patterns (Figures 25, 26, 27, 28). By the discussion of these parameters a general synoptic background is provided for the interpretation of the closed cyclones and anticyclones, which are the large-scale pressure features of the weather types. Finally the synoptic aspects

of the lower boundary layer producing small-scale weather features will be discussed taking into consideration the kinetic variables.

i) Interpretation of the large-scale pressure features. When dealing with the large-scale features of the weather types an interpretation of the pressure centres is presented firstly in relation to

a) the mean pressure, type representative maps, and secondly,

b) the standard deviation maps.

The survey of the locations of the pressure pattern centres has been carried out over the whole map area which is much larger than the section classified. Reference to Figures 3D to 24D indicates that cyclone centres occur along the trough lines or cyclonic areas, while anticyclone centres occur along the ridges and around the high centres of the mean maps of all the weather systems. If the dots and squares are mixed over a region it indicates that the weather systems are variable. A mixture is, for example, observable over the southwest corner of the type D weather maps during middle August. Since the pressure sampling network did not extend over the southwest corner of the map area, the existence of the arctic front associated with the strong trough zone of the type D representative map is not apparent when this classification technique is applied. As a result of the intensification of this low system and its intrusion in between the two high centres during late summer a correlation smaller than 0.70 occurred between the individual and the type-representative map. The localized variability of the large-scale patterns can be detected not only through the mixture of the low and high pressure centres but also through the observation of the related maps of the standard deviations.

In order to obtain information about the pressure centres in relation to the standard deviation maps, the pattern of both pressure centres and standard deviation were compared to the heat regimes of the large-scale pressure features. Visual inspection and comparison of the related pressure centres and the standard deviation maps suggested that weather types in which high pressure was dominant, were associated with low standard deviations. The highest standard deviations over anticyclonic areas occupied the western and north-western warm sections of the anticyclones. The most variable weather types were always associated with the low pressure dominated features and stable weather always occupied the cold sections of the anticyclones. When the mixture of the low and high pressure centres occurred over the warm sectors of the weather systems it was found that the magnitudes of the related standard deviations (caused by the localized succession of the lows and highs) were higher than the magnitudes found over the homogeneous sectors of the pressure centre maps. Over low pressure systems the highest standard deviations similarly coincided with the warm sectors of the cyclones, that is, with the location of cyclogenesis. The close agreement between the patterns of the standard deviation maps and the cold and warm temperature regimes of the mean pressure patterns led to the consideration of the thermo-dynamic parameters of the pressure types.

For the general description of the thermo-dynamic characteristics a comparison has been made between the charts of 500 mb thickness, vorticity, and standard deviation. After the inspection and comparison of these charts was completed, it was found that the highest standard deviation over the western and northwestern sections of the anticyclonic areas was associated with a strong and warm southerly wind component. These conditions were

found for the high pressure dominated types: C, D, F, G, M, N, and Z. The position of the maximum thickness advection was always in good agreement, when calculated according to equations (2) and (6), with the southerly flow regimes of the closed cyclone centres. This was true for the southeasterly and easterly sectors of the low pressure systems. After this qualitative investigation, a case study of the map of July 3, 12 GMT, 1968 was conducted, and it was found that the maximum thickness and vorticity advections coincided with the positions of the highest standard deviations. After this case study the investigation was extended to all the type A individual maps. The analysis of the 500 mb thickness (A_h) and vorticity advection ($A\zeta_a$) fields for all the individual type A maps however revealed that half of the maps were found without significant advection fields or, if positive vorticity advection existed, there was no thickness advection field associated with it. The centres of the maximum warm advections were indicated with dots and the centres of the maximum cold advections were represented by X marks in Figure 29. The position of the maximum positive vorticity advections ($A\zeta_a$), that is, cyclonic rotation, of the type A individual maps (Figure 30) were marked with dots and the anticyclonic rotation centres with X symbols. The superimposition of the Figure 29 on Figure 30 suggested that the sum of the large-scale vertical velocity parameters, ($A_h + A\zeta_a$) of equation (6), seldom reached a positive value that could possibly produce precipitation. The lack of coincidence of the 500 mb, + A_h, and + $A\zeta_a$ patterns suggested the possibility of random vertical velocity distribution not only within the type A weather group but within other types as well. One might assume that the kinetic components of the vertical velocities introduced in equation (8) would show the same random appearance as the time-distributions of the thermo-dynamic variables. For this reason,

then the kinetic parameters of the large-scale pressure features will be interpreted next.

The kinetic parameters were derived from the 3-dimensional, actual wind conditions demonstrated for selected cases through the surface, 850, 700, 600, and 500 mb streamlines of the type A, D, and E representative weather conditions in the Figures 25, 26, 28, and for the one type U weather shown in Figure 27. The construction of the streamlines has been carried out with the same technique used and recommended by Soucier (48), Petterssen (44), and Kagawa (29). In the figures, the presentation of the 500 mb streamlines is omitted for the sake of convenient demonstration. Visual inspection of the streamlines and their pressure patterns reveals that the surface streamlines deviate substantially from the surface pressure patterns. The upper streamlines however well resemble their related pressure maps from the 850 mb level upward. The centres of the closed low and high pressure features and their related confluence and difluence points for the selected cases are in close agreement at all levels. In support of this qualitative observation, a quantitative correlation of the streamlines with their related pressure patterns will be provided.

On the basis of the visual inspection of the streamlines it was expected that kinetic analysis in support of the observation would show either areas or structural lines along which organized streamline patterns might be shown. The kinetic analysis was accordingly aimed at the characterization of the large-scale features which had organized regional or linear structure that could not be explained in terms of local causes. The kinetic analysis was carried out for one single type U weather condition

(July 14, 1968, 12 GMT) since this particular occasion produced more precipitation at Frobisher Bay than any other day of the summer period analysed. In order to show the distribution of the horizontal velocity divergence the isotachs were superimposed on the streamline pattern of Figure 28. For this kinetic analysis the velocity divergences of the surface wind field and the associated relative vorticities were calculated along a grid of 170 points. The calculation was performed with Graham's (17) Del Computer and the results (both positive cyclonic and negative anticyclonic vorticities and the related values of positive divergences and negative convergences) were plotted on two maps. The technique of calculation will be presented in Chapter 5a. The kinetic expressions of the streamline features are shown on the distribution maps of relative vorticities and divergences in Figures 31 and 32. By superimposing the maps of Figure 28, 31 and 32 it is possible to observe the correlation of the confluence and difluence zones with their related divergence values. The vorticity values were read from the related map (Figure 31) along the 170 grid points and plotted against the divergences obtained from Figure 32. The point pattern of the divergence distribution was converted into two histograms and frequency polygons: one representing the kinetic conditions in anticyclonic rotation (Figure 33), and the other in cyclonic rotation (Figure 34). This association between the relative vorticities of the surface air currents and the related velocity divergences resulted in a wide scatter of dots with a central concentration of a circular pattern. Figure 33 has shown that the mean divergence, 0.04×10^{-5} sec^{-1}, was very close to zero, that is, the anticyclonic flow even on the surface generally behaved geostrophically. The slight skewness, 0.55, was possibly due to the influence of the relatively few and horizontally separated zones of

divergences of large magnitudes clearly recognizable on the streamline map. Tanner's (50), and Essenvanger's (12) studies on the resolution of frequency curves into their component normal curves suggests that the slight skewness and the high kurtosis, 4.23, of Figure 33 were similarly due to component curves. By means of Tanner's (50) technique it became possible to point out one main convergence component over the cyclones of Figure 34 with a mean of -3.5×10^{-5} sec^{-1} and a divergence component centered at the value of 0.4×10^{-5}. The comparison of Figure 33 and 34 implies that the high kurtosis of Figure 33 with dominant geostrophic flow provides a much more stable weather condition than the cyclonic systems of the same weather condition with a lower kurtosis of 1.59. The comparison of Figures 33 and 34 proved that large-scale cyclonic pressure features can in general be characterized as having zones of convergences and large-scale anticyclones with divergences.

According to equation (8), and likewise in agreement with the conclusions obtained by Deordorff (10), and Kondratyev (30, 31), it can be expected that the large-scale organized convergences would be in good agreement with the large-scale vertical velocities and that these zones were made visible by characteristic cloud patterns. Visual inspection and comparison of the surface streamlines with cloud patterns indicated that cloud patterns and streamlines were closely connected. This close connection seems to be in accord with the conclusions made by Boucher and Newcomb (6). The cloud patterns of the satellite cloud pictures for the type A, E, B, and L representative weather conditions resembled so much their related surface streamlines, that one could attribute great importance to the boundary layer in the generation of the large-scale and low cloud

patterns composed of Sc, Cu, or St forms. The clouds of the representative weather systems mentioned above were lined up along the linear or curved confluence lines of the related streamline patterns. Difluent streamline structures were associated with cloudless skies. On the other hand, when wave clouds were present they formed rows at right angles to the flow of the 700 mb winds. In all the cases when wave clouds occurred, the surface, the 850 mb and the 700 mb streamlines were of the same direction.

ii) Interpretation of the small-scale pressure features. In addition to the large-scale pressure features of the different weather-type systems, the esistence of the small-scale features could be detected by the form of clouds, the wind patterns, and the pressure waves, as well as by local weather phenomena. The surface pressure waves connected with troughs and ridges for example were clearly recognized on several type-representative maps. Troughs were usually associated with one or more meso-scale cyclonic vortices, cases in point being on the type A, (Figure 25) and type D (Figure 26) surface streamline maps. At the upper level these vortices on the type D map joined and formed a much larger single cyclonic flow pattern. Ridges of the type A, D, and E representative maps were accompanied by difluent streamlines or with cyclonic outflow on the surface maps and anticyclonic vortices at upper levels, above their surface ridge areas. Since the localized surface vortices in Figure 26 were represented in the small waves of the surface isobars, their morphology might be expressed both in terms of the surface pressure values, and the streamline patterns. Hence it was expected that the small-scale features would be detected on the individual maps. The observation provided the interesting point that

within a type not every individual map exhibited small-scale pressure waves.

Small-scale flow features were noticed over the southeast coast of Baffin Island and the southwest coast of Greenland only on the 12 GMT surface synoptic charts. The local morning occurrences of the weather types A, H, I, L, and U with cyclonic centres over the Foxe Basin region were frequently associated with small-scale pressure waves and westerly surface winds on the east coast of Baffin Island flowing against the pressure gradient. When these cyclonic outflows mix with the moist southwesterly winds of the coastal Davis Strait area, they can cause coastal fog, obstructing the insolation necessary to melt sea ice. Such favourable potential conditions for coastal fog formation occurred 38 times with weather types A, H, I, L, and U during the morning observations of the 1968 summer. Similar small-scale weather features could frequently be observed along the southwest coast of Greenland, south from Egedesminde. This statement is supported by a kinetic analysis of the morning weather condition on July 14, 12 GMT. On this occasion, the relative cyclonic vorticity (Figure 31) along the southwest coastal zone of Greenland ranged between $0.5 - 2.5 \times 10^{-5}$ sec^{-1} and was associated with a velocity divergence of $0.3 - 1.4 \times 10^{-5}$ sec^{-1} (Figure 32). Therefore it can be assumed that the glaciated parts of the arctic, if associated with katabatic cyclonic outflow, could bring about meso-scale shallow streamline features especially in the early morning. These features were in fact observed frequently on the 12 GMT surface maps. The existence of these small or meso-scale surface features was never detected on the 850 mb charts since the average elevation of the inversion which took place at Egedesminde was below the 900 mb level. The continuation of the small-scale or meso-scale features

further inland could only be recognized with difficulty. The presence of these features was usually unnoticed because of the lack of local observation.

The small-scale features discussed were observed in coastal situations. However, it is desirable to see small-scale circulation features superimposed on the large-scale flow patterns for an inland situation. For this purpose a synoptic study of local wind observations at Inugsuin Fiord will be made. Daily, four surface wind observations 70 miles from the coast line at the head of the Inugsuin Fiord provided wind data for analysis. Since the wind directions were estimated by the position of a flag raised at the head of the Inugsuin Fiord, a $\pm 30^{o}$ error due to the subjective nature of the observations has been assumed. The overall frequency of the diurnal wind directions, as given in Table 7, shows a slight day time dominance of the up fiord northerly and northeasterly winds along the longitudinal axis of the fiord. The high frequency of the easterly winds from the steep and shaded tributary valley at 00 GMT shown in the Table 7 may be caused by the katabatic winds from the eastern slope of the valley. The table also shows a day-time high frequency of the easterly winds. This frequency might be attributed to large-scale geostrophic flow modified by föhn effects. These effects are revealed on the thermo-hygrograph and baragraph records which frequently show temperature rises, coinciding with falls in humidity and pressure. Barry and Jackson (4) at Tanquary Fiord N.W.T. grouped wind data to emphasize the diurnal dominance of certain wind directions. Barry's (4) example together with subjective observations suggested using a similar grouping here. If the wind direction at Inugsuin Fiord were grouped into two major regimes, one into N - NE - E,

and the other SW - W (this latter one flowing along the Inugsuin River valley, the exit of the fiord head), the diurnal march of the wind directions would be more apparent (Table 7B). The grouped up fiord flow increased from 06 till 00 GMT, while the westerly down fiord wind regime decreased during the daytime and the highest frequency occurred at local midnight (06 GMT). The 12 GMT (07 a.m. L.S.T.) wind observations at Inugsuin Fiord grouped for weather types A, H, I, L, and U and tabulated in Table 7C revealed only large-scale up fiord and meso-scale down fiord winds. The relatively low frequency of the non-geostrophic westerly winds was associated with weak pressure gradients and a mean 40% strato-cumulus cloud cover. The dominant geostrophic flow in an up fiord direction appeared with a higher wind velocity than that of the westerly winds and an almost overcast low and middle level cloud cover. It is revealed from Table 7C that the precipitation potential (cloudiness) of the large-scale weather types A, H, I, L, and U over Inugsuin Fiord was higher during the dominance of the large-scale weather than under the influence of the meso-scale features of the same weather systems.

CHAPTER 4

WEATHER TYPES AND THEIR RELATED STATION PRECIPITATION

On the basis of the conclusions concerning cloudiness at Inugsuin Fiord one might assume that large-scale individual cyclonic features, if not suppressed by small-scale patterns, could produce more precipitation than single anticyclones. This suggests that weather types with dominant large-scale cyclonic features could produce more precipitation than systems dominated by conditions of high pressure. The aim of this chapter therefore is, firstly, to group precipitation data of the standard gauging stations according to the established weather types, secondly, to analyse and interpret these data, to compare the precipitation values with the large-scale pressure patterns and, thirdly, to see whether any persistent relation exists between station precipitation and weather types.

For this reason station precipitation data have been listed, and organized for each weather type. The contribution of the weather types to station precipitation for the 1968 summer has been shown for 18 Canadian and 2 Greenland stations in Table 8. The table was constructed on the basis of the 6 hourly total precipitation data for the Canadian stations and of the 12 hourly totals for the two Greenland stations, Egedesminde and Narssarssuaq. All the stations had full coverage of data for May, June, July, and August, except one, Inugsuin Fiord for which data exist only for the period May 25 to August 23, 1968. Table 8 thus provides a comprehensive summary and cross section of the summer precipitation conditions which can be used for relevant interpretation.

After an inspection of the partial percentages of Table 8 one might consider that the major portions of the station summer precipitation totals were due only to a few weather types. The table clearly indicates that if $\geq$10% contribution is arbitrarily considered significant, the partial contributions of the weather types A, B, D, E, F, I, L, and W to station totals were quite substantial. When high partial percentages occurred they usually occurred at stations which were near the large-scale cyclones observed on the type-representative and mean surface pressure maps. Individual weather maps were similarly inspected for each station precipitation and the observations revealed that the actual precipitation totals were frequently measured within the cyclonic patterns of these weather types. The inspection also revealed that high station precipitation seldom occurred and low values were frequently observed.

It would appear from Table 8 that certain weather types never yielded precipitation at some stations and other types provided only insignificant proportions of the summer totals. Weather types C, K, M, N, S, T, and U did not exceed a 10% contribution to the total precipitation at any station. Individual weather maps revealed that low partial percentages (<10% contribution) could be attributed to one or more of several factors:

a) anticyclonic conditions near the station;

b) local disturbances in the boundary layer;

c) distant or particular relative position of the stations to the large-scale cyclones of the weather types;

d) distant position of the station to the cluster formed by the closed cyclone centres of Figures 3D-24D; and finally,

e) the proximity of the station to the small-scale surface pressure troughs, indicating the possible existence of small-scale cyclonic streamline vortices.

In addition to an analysis by weather types a comprehensive summary was made for cyclonic precipitation and anticyclonic precipitation irrespective of the weather classification type with which each was associated. A statistical experiment was carried out on the 12 hourly precipitation values of 7 arctic stations to see whether cyclones produced more precipitation than did anticyclones. These sampling stations were Eureka, Coral Harbour, Frobisher Bay, Ft. Chimo, Hall Beach, Isachsen, and Mould Bay. The purpose was to break down precipitation rates into two groups; one was accompanied with cyclonic, and the other with anticyclonic surface isobars. When the station was within the confluence zone between a cyclone and an anticyclone, the sign of the geostrophic vorticity determined under which condition that particular precipitation would be listed. On the basis of the two groups of data two histograms and two cumulative frequency distributions of the May precipitation were constructed. These are shown in Figure 37. The 100 precipitation values on the left for cyclonic flow pattern and 76 anticyclonic precipitation values on the right were derived from all the rain-producing systems that occurred in May, 1968. As expected the cyclonic precipitation was slightly higher than the anticyclonic precipitation. Precipitation from both sources was mainly in the trace and very light rainfall regimes, with a greater emphasis on this concentration for measurements from anticyclonic than from cyclonic patterns. It is shown in Figure 37 that only 10% of the total anticyclonic cases could produce precipitation totals greater than .01", whereas for cyclonic cases approximately 30% of the 12 hourly precipitation

totals were higher than .01". Moreover 10% of the cyclonic precipitation totals exceeded .10". The shapes of the two cumulative frequency curves suggest that cyclone dominated types provided higher contributions to the summer total precipitation than the high pressure dominated types.

It would appear, therefore, that weather types can be ranked according to their partial contribution to the summer total precipitation of the 20 stations listed in Table 8. If $\geq$10% contribution is arbitrarily considered significant, the rank of the weather types in the production of precipitation can be written as types: E,A,W,B,F,I,L,V,D,R,J,P, and Z. The high contribution of the unclassifiable cases is partially due to the inherent shortcomings of the weather type classification applied in this study. Only patterns were classified and constant pressure gradients were assumed for the instantaneous weather systems of various intensities. Thomas and Thompson (51) reported large variations in the annual amount of station precipitation over the whole arctic and attributed these differences to the occurrence of synoptic conditions of variable intensities that were also expressed in the cloud patterns. Hence the variation in precipitation could be understood from cloud patterns as well.

It is to be noted that the spiralling cloudy and cloudless patterns of the large-scale cyclones, as observed on the satellite photos of the type-representative maps A (Figure 35), B, E (Figure 36), and L, for example, cannot provide homogeneous precipitation patterns, even over the central area of the cyclones. The expected amount of precipitation which can be measured by a sampling station should largely depend on its position relative to the cloud cover. Hence both space and time variation in precipitation can be understood from cloud patterns.

The variable aspect of precipitation can be interpreted more conveniently from statistical tables than from cloud patterns. Consequently, it was decided to use this method to describe in detail the variable nature and the internal structure of the partial precipitation values (Tables 9-31). The amount of precipitation <.01", called a trace, was listed in the tables but excluded from the type totals. The calculated mean precipitations and their related standard deviations for each type for each station resulted in higher standard deviations than mean values owing to the haphazard nature of precipitation. The presentation of the mean and standard deviation results was omitted in this study since Tables 9-31 and Figure 37 revealed that most of the weather types occurred more frequently without, rather than with, precipitation and the bulk of station precipitation was produced by only a few cases. The excessive time-variation of the station precipitation for each type is clearly indicated in Tables 9-31. The spatial variations, however, could not be deduced from these tables directly.

Sharp differences in the spatial distribution of the daily precipitation were noticed by Barry and Jackson (4). Similar discrepancies have been observed in this study in the spatial distribution of precipitation due to each weather type: weather types G and O for example contributed significantly to the station total at Inugsuin Fiord while at other stations the contribution of these types remained very low (Table 8). The outstanding control of the local topography on precipitation is clearly portrayed through the comparison of the type O station precipitation measured at Clyde and Inugsuin Fiord which are 75 miles apart (Table 23). Type O weather systems precipitated only .19" water or equivalent moisture at Clyde while 1.70" was measured at the head of Inugsuin Fiord. The reduction of the precipitation

at Clyde was possibly due to the lee effect of the orography while the mountain ranges were responsible for the orographically-induced uplift, and additional precipitation at Inugsuin Fiord. The 43% contribution of type O precipitation to the summer total at Inugsuin Fiord should not be over-emphasized, however, since the summer total of Inugsuin precipitation was calculated for a shorter period than the whole summer. Conclusions on the relative anomaly of the type G precipitation at Inugsuin Fiord (Table 15) should not be carried too far on the basis of the three occurrences.

The high variation of station precipitation shown in Table 8, and Tables 9-31 suggest that statistically not much relationship can be pointed out between moving weather systems and their related station precipitation totals measured in a fixed, coordinate system. Both the occurences and the amounts of individual precipitation totals within the types in no way showed any systematic pattern of distribution. In Table 32 there are two examples showing the time variations of the precipitation which occurred at two stations. This table presents the precipitation associated with type A weather at Coral Harbour, and that for type E weather at Frobisher Bay. Both stations were close to their respective low centres and these two types were highly ranked according to their partial contributions to the summer precipitation totals. Table 32 does not indicate an adequate connection between station precipitation and the related weather systems deduced for the whole Canadian Archipelago. When no precipitation was recorded, a good relationship could be observed between pressure features and the cloudless sections of the weather types where high pressure patterns were predominant and the standard deviation maps (Figures 3C-24C) indicated low values. High persistence was shown by certain pressure types that never produced precipitation at some stations.

For example, not even a trace was reported in Inugsuin Fiord when the weather types C, D, E, I, J, K, and S prevailed. By contrast, relationship between station precipitation and weather types was loose and requires some comment.

It seems reasonable to assume that a classification of cyclones considered in a coordinate system moving with the cyclone centres would result in a better relationship between pressure patterns and station precipitation than that achieved by the procedures used so far. The large-scale of the present classification has provided a good general description of weather types but when the objective is to classify weather conditions in terms of precipitation then Yorgensen et al.'s (28), and Korte et al.'s (32) "moving cyclone classification" is likely to be more effective. To apply the methods used in these two studies to the arctic, however, is unpractical. The authors depended on several hundreds of rain gauges for their classification areas and the fact that there are only a few arctic gauging stations would make it impossible to provide more than a maximum of 3 or 4 precipitation measurements for each of the areas covered by any one closed cyclone. Figure 37 provides another reason for the rejection of "moving cyclone classification" for the arctic. This figure clearly reveals that precipitation was frequently associated with anticyclonic pressure patterns. Consequently, a better relationship can be expected between the pressure patterns and station precipitation only at those portions of the weather systems that are associated with large-scale vertical velocities. Hence it is now necessary to determine the role of vertical velocities in producing precipitation. This will be examined with reference only to the two weather types, A, and E, since these two weather types caused the highest partial contribution to the summer total precipitation of many stations.

CHAPTER 5

INITIAL PRECIPITATION RATES OF SELECTED WEATHER CONDITIONS

a) Calculation techniques of the total vertical velocities and precipitation rates

The synoptic interpretation of the pressure patterns in an earlier chapter (Chapter 3(b)), provided a two-dimensional evaluation of the large and small-scale pressure features associated with the different weather types. However, it has been demonstrated in this last chapter that there is an inadequate statistical relationship between the two-dimensional surface weather-systems and the precipitation recorded at a given station. Hence, attention should now be drawn to examining the three-dimensional physical processes of the precipitation field.

Among the underlying physical processes the pseudo-adiabatic cooling expressed in the actual vertical velocity is considered in all precipitation models to be the most important generator of large-scale precipitation. Following this work of Harley (21), (22), Penner (42), (43), Petterssen (44), and many others it is considered here that the total vertical velocity of a precipitation field is the resultant of component processes, such as the large-scale vertical velocity ($-\omega_{\epsilon}$), effective vertical velocity ($\omega_{E\epsilon}$), orographic vertical velocity (ω_{m}), and latent heat vertical velocity (ω_{L}). The theoretical presentation of these components has been omitted here, as it is adequately discussed in the references. Consequently, information will be given only on the techniques of calculation

used in the present study. Both single and multi-layered models will be used for the calculation of the vertical velocities and with these results a tool will be provided in section b of this chapter to explain the relationship between vertical velocity and precipitation.

i) Large-scale vertical velocity ($-\omega_6$). Vertical velocity of a single-layer model. The first component of total vertical velocity, large-scale vertical velocity ($-\omega_6$), for a single-layer model has been calculated with Penner's equation (7) by using Ferguson's (13), (15) "Advection Scale" and McPherson et al.'s (38) "Component Vertical Velocity Chart". The large-scale vertical velocities were expressed in pressure coordinates, in $\omega_6 \times 10^{-3}$ mb sec^{-1} units (or mb per 1000 sec, numerically almost equal to 1 cm sec^{-1}). For ascent, the vertical motion was considered negative and for descent it was considered to be positive.

Vertical velocity of a multi-layered model. Vertical velocities in a multi-layered atmosphere have been calculated according to equation (8) by considering the divergence fields and by making the assumption of continuity. The success of calculation in equation (8) depended on the representativeness of the calculated divergences.

To approximate the representativeness of the divergence values, winds have been sampled from the isogon and isotach charts of the surface and the standard pressure surfaces at the three apices of sixty equilateral triangles with a height of 3^{o} latitude distance (3.34×10^{5} metres). Each triangle was numbered and the locations of the triangles were fixed on a transparent overlay constructed for the polar-stereographic charts in a

scale of 1:20,000,000, as shown in Figure 38. The upside-down, unnumbered triangles were omitted from the divergence calculation. It was intended that the divergence field would be smoothed by the omission of these areas. According to Landers (34), this smoothing is desirable when the main objective is to calculate large-scale vertical velocities.

For the computerized calculation of divergences, Graham's (17), and Ferguson's (14) combined methods have been used by summing up the partial velocity divergences at the three apices of the equilateral triangles and dividing by the height of the triangle. Finally, the calculated divergence values were corrected according to Panofsky's (40), (41) correction term. This correction was due to the convergence of meridians. The significant effect of latitude and the magnitude of the meridional wind components on the values of divergences have been demonstrated in the correction chart (Figure 39) constructed with Panofsky's (40), (41) formula. It should be mentioned that the chart has also been used to correct relative vorticities (ζ). Figures 31 and 32 already, introduced in chapters 1(a) and 3(b), were also corrected according to Figure 39. When the corrections were executed the calculation of divergences was considered complete.

Before calculating the vertical velocities another correction is necessary since the vertical velocity is reduced by the height above mean sea level. The elevation of the surface has been offset by correcting the expression p_1 in equation (8). To achieve this correction a table of deductable pressure values was constructed (by assuming the validity of the U.S. Standard Atmosphere) for 15 triangles (Table 33). Then with the corrected surface pressure values the vertical velocities were calculated

according to equation (8) for the top of each successive layer, using Bellamy's (5) step-wise method. Penner's (43) and Harley's (21) arguments that the vertical velocity at 600 mb level was the representative value for large-scale precipitation processes were similarly applied for both equations (7) and (8). Therefore large-scale vertical velocities ($-\omega_6$) were calculated for the 600 mb surface.

ii) Effective vertical velocity (ω_{E6}). The second component, the effective vertical velocity expressing the sum of the large-scale vertical velocity ($-\omega_6$) and an increment (ω_s) proportional to the initial unsaturation of the atmosphere, has been calculated using Harley's (22) empirical approximations for the Δt = 6 hourly period and 600 mb surface. The effective vertical velocity component based on empirical approximations has been termed here "prognostic effective vertical velocity".

iii) Orographic vertical velocity (ω_m). The estimation of the orographic vertical velocity has been made using Harley's (21) tables and charts based on Vederman's (53) model. However, due attention was paid to the important role played by temperature inversion and atmospheric stability in orographic uplift as has been envisaged by Elliott et al. (11), and Bugaev et al. (8). The consideration of stability must not be neglected because the high frequency of the arctic summer inversions has been found by Vowinckel et al. (54) over the polar ocean. Similarly frequent inversions are expected during the summer on the Canadian Archipelago. Therefore, despite Harley's (21) technique of using geostrophic winds for the calculation of the orographic vertical velocities, in this study the surface streamlines were used in the calculation when the surface elevation was less than 2500 feet. Above this level the wind field of the 850 mb streamlines was used

for the assessment of the orographic vertical velocities. It was also assumed that the bending effect of the orography on the airstream pattern would be taken into consideration by using streamline data. In other words, streamlines were interpreted in this study following Namias' (39) method as being the orthographic projections of the horizontal wind components on the undulating terrain in that they reflect the combined effects of bending, friction, and stability.

For the practical calculation of the orographic uplift selected streamlines were used with a simplified or smoothed contour map of the arctic (Figure 40). As a demonstration of the application of the simplified orography, vertical velocities were calculated with Harley's (21) tables for the whole arctic, assuming northerly and southerly winds in Figure 41, and easterly and westerly winds in Figure 42 at a wind speed of 10 m sec^{-1}.

iv) Latent heat vertical velocity (ω_L). For the calculation of this parameter Harley's (21) method has been accepted. The method uses a graphical process for finding the latent heat vertical velocity using the 700 mb temperature. By adding the latent heat vertical velocity to the sum of the components so far discussed, the total vertical velocity becomes known.

v) Rate of precipitation (P_R). A knowledge of the total vertical velocity and precipitable moisture made possible the calculation of the expected amount of precipitation or the rate of precipitation at the time of observation. The amount of the precipitable water was readily estimated using Fergusons's (16) method based on the dew point values from three levels. Harley's (22) chart for adjusting precipitable water to orographic elevation was also consulted for the construction of the maps showing the

amount of precipitable water. The rate of precipitation was obtained using Harley's (21) method. Maps of the precipitable water adjusted to orography were superimposed over the total vertical velocity charts and the precipitation rates were read directly from Harley's (21) chart.

b) Synoptic interpretation of the large-scale vertical velocities and precipitation rates caused by two weather conditions

With the computing techniques presented in the previous section a sequence of calculations was performed on the type A and E representative weather conditions and the distribution of the component processes was calculated one-by-one for both cases. In this section the calculated distribution of the component processes will be compared with the related satellite cloud pictures. Localized deviations of the actual processes from the calculated values will also be detected and an explanation will be sought for meso-scale cloud features by the analysis of the three-dimensional motion field. With the knowledge of the variation of the three-dimensional component vertical velocities, the relation between station precipitation and the total vertical velocities will be described for the two weather conditions.

i) Large-scale vertical velocities. The distribution of the large-scale vertical velocity ($-\omega_6$), the first component process, has been calculated for the type A weather condition using Penner's equation (7) for a single-layer atmosphere. Generally one might say that no thickness and vorticity advection field was detected on the 500 mb level with the exception of the southern region. Most of the map area, therefore, was characterized with

parallel contours, thickness, and vorticity lines. A vertical velocity component due to the thickness advection, could be detected only over the Labrador-Ungava region and the southern portion of the Davis Strait area. The advection of the absolute vorticity brings about a wider field of large-scale vertical velocity than the thickness advection. The component vertical velocities are not presented for this weather condition. However, the type A isanabats due to their thickness and vorticity advections are shown in Figure 43. The positions of the surface fronts (Figure 3A) and the southerly flow regimes of the surface and upper level streamlines (Figure 25) are in good agreement with the negative field of vertical velocities (Figure 43). The comparison of the 500 mb pressure map with the isanabats of the 600 mb level revealed that ascending motion took place in advance of the 500 mb trough and a descending regime has been observed in front of the ridges just as it was predicted at the end of chapter 1(b). Again applying the single layer model for the calculation of the large-scale vertical velocity of the type E weather condition, one might clearly observe that the pattern of the vertical velocity component due to thickness advection (Figure 44) was associated with the confluencing southerly flow regime of the surface, 850 mb, and 700 mb level streamlines (Figure 27). The pattern of the vertical velocity component due to vorticity advection is shown in Figure 45. One can clearly observe in this figure that the cyclonic vortices were shifted with the curved general flow counterclockwise around the central part of the map area. The sum of the two components, the large-scale vertical velocity, calculated with Penner's equation (7) is presented in Figure 46. The 500 mb pressure patterns and the 600 mb isanabats indicate the same relation with each other as has been shown above for the type A weather condition. The two-dimensional demonstration of the 600 mb vertical velocities by Figure 43 and 46 could

not suggest the three-dimensional structure of the isanabat field. The consideration of a multi-layered atmosphere could be expected to reveal more detail. Therefore to increase the sensitivity of the calculation the vertical velocity pattern was also calculated for both weather conditions using equation (8).

The result of the vertical velocity calculation according to equation (8) is presented in the 600 mb isanabat maps of type A and E representative weather conditions given in Figures 47 and 48. The calculations were based on three atmospheric layers: surface - 850 mb; 850 - 700 mb; and 700 - 600 mb.

Vertical velocities, divergences, and relative vorticities were calculated for the surface, 850, 700, 600 and 500 mb levels. The results were listed in computer output sheets. However, by accepting Harley's (21) technique only the 600 mb isanabat maps were drawn and the rest of the data were consulted only in the three-dimensional analysis. No tables exhibiting these data are presented in this study, although the relevant values will be quoted in the text. Type A large-scale vertical velocity in Figure 47 and isanabats of the type E representative weather condition in Figure 48 produced a much larger field of negative vertical velocity than that obtained from a single-layer model. The cloud patterns showed more agreement with the isanabats estimated using the divergence method than with the vertical velocities obtained using Penner's equation (7).

In order to demonstrate the high sensitivity of the calculation obtained by means of equation (8), a vertical streamline cross-section was

constructed between Fort Chimo and Alert in Figure 49 for the type A representative weather condition. The centres of the sampling triangles, orography, and the horizontal surface winds were drawn along the horizontal axis, and pressure heights along the vertical axis of the figure. The upper numerical values indicated vertical velocities in cm sec^{-1} and the lower ones horizontal-meridional wind components in m sec^{-1}. Northerly winds were shown in the diagram with negative signs and southerlies with positive signs. Vertical velocities had zero values along the plotted dashed line. It should be noted that the scale of vertical velocity has been exaggerated one hundredfold with respect to the scale of the horizontal component. The vertical vortex between points E7 and C5 was a shallow circulation feature. The weak northerly component of the surface wind between Thule and Clyde was clearly observable from the surface streamline map. The negative sign of the surface wind was reversed at the 850 mb surface because the 0.10×10^{-5} sec^{-1} surface divergence and the 0.52×10^{-5} sec^{-1} divergence at 850 mb level over the triangle area C5 brought about descending motion. The small lateral extent and the shallow nature of this descending motion was observed with the 3-layered model but left unnoticed with the use of the single layer model since disturbances in the boundary layer were not detected in the thermodynamic conditions of the 500 mb level. Therefore it was decided to base further calculations on equation (8) and to disregard the isanabats assessed with Penner's equation (7). Hence the selection of the 3-dimensional model and the rejection of the single-layer model was justifiable and the former model seemed especially useful in the explanation of agreements and discrepancies between the cloud patterns and isanabats and the detection of small-scale atmospheric features.

By using the 3-dimensional model for the calculation of vertical velocities, especially good agreement has been found between the negative vertical velocity field and the cloud pattern of the type A weather condition over Baffin Bay and Davis Strait region shown in Figure 35. Similarly good agreement has been found for the same weather condition over the sampling triangle I3 covering northern James Bay and Belcher Islands. For this area the cloudless spot of Figure 35 was indicated with descending motion in Figure 47, and the sampling triangle I2 directly behind it provided high cyclonic vorticity, general ascent, and overcast alto-stratus cloud cover. The difference in cyclonic rotation between points I2 and I3 amounted to as much as $+2.2 \times 10^{-5}$ sec^{-1} in relative vorticity. This type of intensified cyclonic vorticity behind the cold front at point B of Figure 35 is similar to that which has been previously described by Adamy (1) as a secondary front. In Figure 35 this secondary front is shown by the 700 mb trough and the upper level bent occlusion just behind the disturbance on the primary cold front. The diverting effect of the 700 mb trough on the circulation pattern is clearly shown just west of point B in Figure 35.

Since the large-scale vertical velocities obtained with equation (8) were integrated up to the 600 mb level, the existence of vertical velocities below the 850 mb level was frequently suppressed by upper level subsidence and not indicated by the 600 mb isanabat maps. Furthermore the 850 mb vertical velocities were averaged for a thick 150 mb layer and low-level vertical velocities were possibly smoothed out. Hence discrepancies were expected between the 600 mb isanabats and the related cloud pictures. Indeed such discrepancies occurred over F3, F5, and G3 sampling triangles of the type A representative map in which the 600 mb descending motion was

associated with stratus and strato-cumulus cloud cover. The related surface kinetic field at points F3, F5, and G3 produced -0.53, -0.54 and -0.68 x 10^{-5} sec^{-1} convergences respectively, while for the 850 mb level at the same points 0.61, 1.92 and 1.33 x 10^{-5} sec^{-1} divergences were calculated. The type A satellite picture in Figure 35 revealed 9 cyclonic cloud belts. However, only three cloud belts were detected by the calculation of both the surface, 850 mb streamlines and the 3-dimensional vertical velocities. This discrepancy is possibly due to the scant observation network, the size of the grid distance, and the smoothing technique used. Similar discrepancies were observed during the prevalence of the type E weather condition over the Labrador and Ungava Bay region shown in Figure 36 where the stratus cloud cover could be explained by the strong surface convergence of -2.29 x 10^{-5} sec^{-1} over the sampling triangle I6. Low level strato-cumulus appeared over the sampling triangle E2. It was probably generated by a surface velocity convergence of -0.84 x 10^{-5} sec^{-1}, despite the 600 mb descending motion. The low level ascending motion was terminated below the 850 mb surface and the thin strato-cumulus cloud cover spread beneath the 850 mb level. The complicated striations in the strato-cumulus cloud pattern over the Hudson Bay area express the presence of meso-scale vortices (Figure 36), the existence of which was concealed in the streamline trough of Figure 27. Only a dense surface wind observation network would be able to expose such vortices. Hence the dominance of the boundary layer in the formation of organized strato-cumulus cloud cover is self-evident, although, its existence is hardly recognizable on the 600 mb isanabats. Thick alto-stratus cloud covers were however always identifiable within the vertical velocity field of the 600 mb surface.

The amount of strato-cumulus cloud cover was always in excess of the alto-stratus clouds for both type A and E weather conditions. Hence one might suggest that vertical velocities due to organized boundary layer processes in lateral extent surpassed the area of the large-scale vertical velocities extending up-to or higher than the 600 mb level. According to the writers personal observations at Inugsuin Fiord, arctic snow-showers were frequently associated with low level strato-cumulus cloud cover. Judging by the great lateral extent and frequent occurrence of strato-cumulus cloudiness, there is likely to be greater possibility for shower-type of precipitation than for heavy snow-fall. This suggestion has been confined in the two weather conditions examined in depth. Nevertheless, on the basis of Figure 37 it would be possible to use this as a general principle for the rest of the weather types. Generalization based only on large-scale vertical velocity would provide better results if the other component vertical velocities were also taken into consideration.

ii) Effective Vertical Velocities. The distribution of the effective vertical velocity for the type A representative weather condition is shown in Figure 50. According to Harley's (21) recommendation the increment (ω_s) was related to Δt = 6 hourly interval. The type A weather system existed 24 hours before and persisted 36 hours after the observation. It has been assumed therefore that the calculated precipitation, with the consideration of the 6 hourly interval, might be comparable to the actual 6 hourly total precipitation. The high degree of unsaturation greatly reduced the size of the negative vertical velocity field and the actual cloud cover was more extensive than suggested by the effective vertical velocity. Due to persistent weather the actual Δt might have a value of 36 hours, and therefore

the positive increment (ω_s), working against the negative vertical velocity, would become zero. Consequently somewhat weak ascent could bring about cloud cover. A persistent weak ascent with its adiabatic cooling could also cause more cloudiness than a short-lived strong uplift.

Another map of the effective vertical velocity representing the type E weather condition has been shown in Figure 51. The weak ascending motion at the edge of the sampling triangle network, at points I2 and I3, over the southern part of the Hudson Bay has been eliminated on Figure 51 because of the high unsaturation found at 700 mb level. The weak ascent over southern Hudson Bay associated with 90% relative humidity near the surface, however, has produced cloud cover at an elevation lower than the 700 mb surface. The great extent of the cloud cover of Figure 36 suggests the dominant role of the low level saturation in cloud formation. This suggests that the calculation of effective vertical velocities based on the unsaturation observed at the 850 mb level, rather than on the dew point depressions of 700 mb as recommended by Harley (21), would provide an effective vertical velocity pattern revealing a much better agreement with the actual cloud cover than the pattern that was based on the 700 mb dew-point spread.

iii) Orographic Vertical Velocity. Orographic vertical velocities are shown in Figures 52 and 53. Figure 52 was calculated using Harley's (24) method and Figure 53 using streamline winds. The magnitude of the ω_m patterns due to strong geostrophic winds (Figure 52) surpassed the value of the orographic vertical velocity estimated with the weak streamline winds. Differences in the magnitudes of the ω_m patterns obtained with

gradient wind and those calculated with streamline winds were quite significant all over the arctic, especially over south Greenland and Ellesmere Island. The sums of the effective and orographic vertical velocities ($\omega_{E6}+\omega_m$) are presented in Figure 54 for type A weather and in Figures 55 and 56 for the type E representative weather condition.

iv) Latent Heat Vertical Velocity. The latent heat vertical velocity component has been added graphically to the isanabat fields of ($\omega_{E6}+\omega_m$) and the result, the total vertical velocity, for the type A representative weather condition is presented in Figure 57, and for type E in Figure 58. The isanabat field was slightly increased for both cases with the component ω_L added. As a generalization one might observe that this addition did not change the position of the zero total vertical velocity isanabats substantially from the zero lines of large-scale vertical velocities but rather that it modified the intensities of the patterns.

v) Rate of Precipitation. The calculation of precipitation rates using Harley's (21) chart required the knowledge of total vertical velocities and the distribution of precipitable water. The latter, unadjusted to surface elevation, was calculated using Ferguson's (16) overlay for the type A and E representative weather conditions. The results of their analysis are presented in Figures 59 and 60. One can easily observe that the areas of high precipitable water values shown in these two figures were associated with the confluence of moist southerly streamlines shown in Figures 25 and 27. By contrast the regions of confluence of the northerly dry air correspond well with the troughs of lower precipitable water values shown in Figures 59 and 60. The overwhelming influence of the surface streamline

patterns on the distribution of precipitable moisture indicated by these correspondences suggests that the atmospheric water vapour was concentrated beneath the 850 mb surface. Similar observations over the arctic have already been reported by Barry and his associates (3), (4). The agreement between the surface streamline patterns and the "precipitable water adjusted to orography" is demonstrated clearly in Figures 61 and 62.

A comparison of the precipitation recorded at selected stations with the calculated precipitation by the method described above is presented in Table 34 for the type A weather condition. Only slight discrepancies have been found between the measured and calculated amounts. Good agreement has been found for the following stations: Isachsen, Frobisher Bay, Port Harrison, Inugsuin Fiord, and Clyde. Slight discrepancies occurred at Alert and Baker Lake where traces were reported when the calculated effective vertical velocity suggested that condensation was impossible due to high unsaturation at the 700 mb surface. However the weak vertical velocity of -0.75×10^{-3} mb sec^{-1} at Alert on the 850 mb level might have brought about a precipitation rate of -.02" since the air at the 850 mb elevation was saturated. A similar condition was found at Baker Lake. Calculation for vertical velocity revealed subsidence for this station at the 600 mb level. There was a weak ascent of -0.42×10^{-3} mb sec^{-1} in the saturated layer below the 850 mb surface which was able to form a shower-type of precipitation of 0.01". Clearly, therefore, Harley's (21) contention that vertical velocity at the 600 mb level is a dominant cause of precipitation did not apply in this case. The discrepancy between calculated and measured precipitation at Goose Bay was possibly due to edge effect since this station was outside the sampling network. Great discrepancy has been found

for Coral Harbour where the heavy precipitation of 1.15" for a 12 hourly period was possibly brought about by the intrusion of the precipitation along the saturated 850 mb surface where the clouds and the associated precipitations were intruding with the 850 mb streamlines. Similar intrusions of heavy cloud layers into the subsiding zones of cyclones have previously been reported by Deardorff (10), and Kondratyev (30).

A comparison between the calculated and measured precipitation for type E weather is presented in Table 35. The values for initial precipitation rates shown approximate well the actual values for Resolute and Frobisher Bay. The eastward moving streamline pattern in Figure 58 probably caused the high precipitation prior to the observation over Fort Chimo. The underestimation shown in the table for Baker Lake and Mould Bay was possibly due to the edge effect around the sampling network. A slight convergence of -0.03×10^{-5} sec^{-1} over Isachsen might have produced shower-type trace in the saturated layer beneath the 850 mb level. The lack of measurable precipitation, despite the 0.03" precipitation rate calculated for Clyde, might be due to lee effects and evaporation in the dry lower atmosphere which had a mean relative humidity of 85% and a temperature of $+5^{o}C$.

Careful consideration of the agreements and discrepancies between the calculated and observed precipitation discussed above suggests a sequence of thoughts and conclusions. A first source of error between calculated and observed values was possibly due to the calculation of mean divergences within the layer, between the surface and 850 mb. This first layer sometimes proved to be too thick a layer for effective calculation since vertical velocities and saturation producing clouds occurred well below the 850 mb level. Hence it is believed that the introduction of an intermediate

height between the surface and the 850 mb level for the calculation of the large-scale vertical velocities would increase the accuracy of calculation.

A second source of discrepancy can be attributed to low level saturation. The existence of a saturated layer associated with weak ascent below the 600 mb level would favour cloud formation despite the results of the calculations done for the 600 mb level. This low saturated layer, as indicated for example by the type A and E representative weather conditions, has been termed here, "active layer" and it usually took place at a height lower than the 850 mb surface. Because of this active layer the calculation of the total precipitable moisture from the surface to 500 mb level seemed to be largely meaningless if the actual condensation took place at an elevation lower than the 700 mb surface. Hence it is necessary to emphasize the inactive role of the atmospheric moisture lying above the active layer in the condensation leading to precipitation. In the majority of cases, however, the vertical velocity was not terminated below the 850 mb level rather increased upward. Under these conditions the consideration of the total precipitable moisture did not overestimate the precipitation rate.

Despite the various discrepancies mentioned it would appear that with the available observation network it is possible to obtain reasonably accurate information about precipitation characteristics under given weather conditions when streamline technique is applied in the interpolation of the surface wind field. The main objective, the characterization and synoptic interpretation of the vertical velocity parameters, and of the processes producing precipitation has been completed for two types of weather conditions. The generalizations and conclusions drawn from these two cases

might be a useful tool in the formation of a model for the study of the atmospheric water balance.

CONCLUSION

This first attempt at a quantitative weather classification for the whole Canadian Archipelago in terms of surface pressure types provided a useful characterization of the different large-scale pressure patterns and also of some of the small-scale features superimposed. However, subjecting such a large area to classification introduced the problem of including conditions over small areas, such as Inugsuin Fiord and Southern Hudson Bay. These smaller areas could be characterized with less types than could the whole area. Indeed, it may well be that to have confined the study to small areas would have produced a better relationship between the station precipitation and the pressure patterns than the study, as a whole, has shown. However the reduction of the area to be classified might result in the filering out of the large-scale lower tropospheric waves, the only links, that might provide an explanation of the relation between local and macro-scale weather conditions. According to Figure 37 only a low percentage of the total snow occurrences could significantly contribute to the station totals, and therefore one might attribute greater glacio-hydrological significance to these few cases than to the rest of the occurrences. However no special attention was paid to these extraordinary cases since the purpose of this study was to characterize the weather systems and the precipitation in general over the whole Archipelago and not over a small portion of the arctic. Hence there was no reason to reduce the classification area and to study only weather conditions with high precipitation. For a mass synoptic analysis of the arctic precipitation patterns it is suggested that the manual streamline analyses and the

graphical addition of the parameters so far practised for the assessment of the precipitation characteristics should be substituted by a completely computerized technique, and that the introduction of an intermediate level between the surface and the 850 mb height would increase the accuracy of calculations.

An important reason for making this study was to try to formulate a model for the study of the atmospheric water balance that might be used, despite the scattered precipitation data over the arctic, to provide information on the precipitation patterns associated with different weather types. The experience gained suggests that any estimation of the atmospheric water balance would involve sampling streamline wind data along the same triangular network as shown in Figure 38, and evaluating precipitable water by calculations, which should be adjusted to orography. In addition the importance of the active layer should be considered if attention is to be drawn to the determination of precipitation patterns, and attention must be drawn to the correction of the moisture-flux divergences due to convergence of meridians as shown in Figure 39. However, water balance calculations, considering all these factors, would be just as complicated as the assessment of the initial precipitation. Furthermore the results of the moisture-flux divergences would indicate, not the precipitation but rather the differences between precipitation and evaporation if the terms for storage and runoff were disregarded. Hence precipitation investigation by calculating the initial precipitation patterns by the techniques described in this thesis seems a more feasible procedure than to attempt to estimate precipitation through moisture-flux divergences.

References

1) Adamy, L., 1967: "Interpretation and Use of Meteorological Satellite Data," Időjárás, Vol. 71, No. 2, pp. 110-112.

2) Barry, R.G., 1966: "Meteorological Aspects of the Glacial History of Labrador-Ungave with Special Reference to Atmospheric Vapour Transport", Geographical Bulletin, Vol. 8, No. 4, pp. 319-340.

3) Barry, R.G. and Fogarasi, S., 1968: "Climatology Studies of Baffin Island, Northwest Territories", Department of Energy, Mines and Resources, Inland Waters Branch, Ottawa, Technical Bulletin, No. 13.

4) Barry, R.G. and Jackson, C.I., 1969: "Summer Weather Conditions at Tanguary Fiord, N.W.T., 1963-67", Arctic and Alpine Research, Vol. 1, No. 3, pp. 169-180.

5) Bellamy, I.C., 1949: "Objective Calculations of Divergence, Vertical Velocity, and Vorticity", Bulletin of the American Meteorological Society, Vol. 30, No. 2, pp. 45-49.

6) Boucher, R.J. and Newcomb, R.J., 1962: "Synoptic Interpretation of Some Tirox Vortex Patterns: a preliminary cyclone model", Journal of Applied Meteorology, Vol. 1, No. 2, pp. 127-136.

7) Bryson, R.A. and Kuhn, P.M., 1961: "Stress-Differential Induced Divergence with Application to Littoral Precipitation", Erdkunde, Band 15, pp. 287-294.

8) Bugaev, V.A. and Musaeljan, S.A., 1967: "On Orographic Disturbances of the Eastward Air Transport Generated by the Relief of Antarctica", Polar Meteorology, WMO, Technical Note, 87, Proceedings of the WMO-SCAR-ICPM Symposium on Polar Meteorology, pp. 250-262.

9) Court, A., 1957: "Climatology: Complex Dynamic, and Synoptic", Annals of the Association of the American Geographers, Vol. 47, p. 25.

10) Deardorff, J.W., 1963: "Satellite Cloud Photos and Large-Scale Vertical Motion", Journal of Applied Meteorology, Vol. 2, pp. 173-175.

11) Elliott, R.D., and Shaffer, R.W., 1962: "The Development of Quantitative Relationships between Orographic Precipitation and Air-Mass Parameters for Use in Forecasting and Cloud Seeding Evaluation", Journal of Applied Meteorology, Vol. 1, No. 2, pp. 218-228.

12) Essenwanger, O., 1954: "Neue Methode der Zerlegung von Häufigkeitsverteilungen in Gauss'sche Normalkurven und Ihre Anvendung in der Meteorologie", Berichte der Deutschen Wetterdienstes, Report, No. 10, Bad Kissingen, 34 p.

13) Ferguson, H.L., 1961: "A Geostrophic Advection Scale for Constant Pressure Surfaces", Canadian Department of Transport, Meteorological Branch, circ. No. 3516.

14) Ferguson, H.L. 1964: "Divergence and Vorticity Computations", Canadian Department of Transport, Meteorological Branch, Training Section, Internal Publication, No. 86.

15) Ferguson, H.L., 1963: "A Geostrophic Advection Scale for Polar Stereographic Charts", Canadian Department of Transport, Meteorological Branch, Circ. 3857.

16) Ferguson, H.L., 1962: "A Tephigram Overlay for Computing Precipitable Water", Canadian Department of Transport, Meteorological Branch, Circ. 3653.

17) Graham, R.D., 1953: "A New Method of Computing Vorticity and Divergence", Bulletin of the American Meteorological Society, Vol. 34, No. 2, pp. 68-74.

18) Hare, F.K., 1968: "The Arctic", Quarterly Journal of the Royal Meteorological Society, Vol. 94, No. 42, pp. 439-459.

19) Hare, F.K., Godson, W.L., Macfarlane, M.A., Wilson, C.W., 1957: "Specification of Pressure Fields and Flow Patterns in Polar Regions, Theories and Techniques", Arctic Meteorology Research Group, McGill University, Publication in Meteorology, No. 5, January, 1957.

20) Harley, W.S., 1964: "Use of the Advection Scale in the Determination of Vertical Velocity", Canadian Department of Transport, Meteorological Branch, Circ. 4052.

21) Harley, W.S., 1963: "An Operational Method for Quantitative Precipitation Forecasting", Canadian Department of Transport, Meteorological Branch, Circ. 3852.

22) Harley, W.S., Dragert, H. and Rutherford, I.D., 1964: "The Determination of Spot Values of Vertical Velocity and Precipitation Rate", Canadian Department of Transport, Meteorological Branch, Circ. 4139.

23) Hastenrath, S.L., 1967: "Rainfall Distribution and Regime in Central America", Archive für Meteorologie, Geofysik und Bioklimatology, Band 15, Heft 3, pp. 201-241.

24) Hromov, S.P., 1952: "Szinoptikus Meteorologia Alapjai", 1st edition, Akadémia Kiadó, Budapest, Hungarian Translation of: ОСНОВЫ СИНОПТИЧЕСКОЙ МЕТЕОРОЛОГИИ, 835 p.

25) Jarvis, E.C., 1963: "The Relationship of Surface Pressure Tendency to Fields of 500 mb Vorticity Advection and Tropospheric Thermal Advection", Canadian Department of Transport, Meteorological Branch, circ. 3901.

26) Jarvis, E.C., 1966: "The Analysis and Interpretation of Precipitation Patterns", Canadian Department of Transport, Meteorological Branch, Circ. 4510.

27) Jarvis, E.C., 1967: "The Use of Surface Streamline Analysis in Short Range Forecasting, Short-Range Forecast Techniques", Canadian Department of Transport, Meteorological Branch, Circ. 4534.

28) Jorgensen, D.L., Klein, W.H., and Korte, A.F., 1967: "A Synoptic Climatology of Winter Precipitation from 700 mb Lows for Intermountain Areas of the West", Journal of Applied Meteorology, Vol. 6, No. 5, pp. 782-790.

29) Kagawa, N.H., 1966: "A Technique for Streamline Analysis", Canadian Department of Transport, Meteorological Branch, Circ. 4374.

30) Kondratyev, K.Ya., 1966: "Synoptic Analysis of Meteorological Satellite Cloud Pictures", Part 1, Időjárás, Vol. 70, No. 4, pp. 198-210.

31) Kondratyev, K. Ya., 1966: "Synoptic Analysis of Meteorological Satellite Cloud Pictures", Part 2, Időjárás, Vol. 70, No. 5, pp. 266-275.

32) Korte, A.F., Jorgensen, D.L. and Klein, W.H., 1968: "Probabilities of Station Precipitation in the Western Plateau States from 850 mb Lows during Winter", Unpublished manuscript, 49th Annual Meeting of the American Geophysical Union, April 8-11, 1968, Washington, D.C.

33) Kuhn, P.M., 1953: "A Generalized Study of Precipitation Forecasting, Part 2. A Graphical Computation of Precipitation", Monthly Weather Review, Vol. 81, No. 8, pp. 222-232.

34) Landers, H., 1955: "A Three-Dimensional Study of the Horizontal Velocity Divergence", Journal of Meteorology, Vol. 12, No. 5, pp. 415-427.

35) Lee, R., 1961: "On Forecasting the Development of Surface Pressure Systems", Canadian Department of Transport, Meteorological Branch, Circ. 3503.

36) Lund, I.A., 1963: "Map Pattern Classification by Statistical Methods", Journal of Applied Meteorology, Vol. 2, pp. 56-65.

37) Lydolph, P.E., 1957: "A Comparative Analysis of the Dry Western Littoras", Annals of the Association of the American Geographers, Vol. 47, pp. 213-230.

38) McPherson, G.A., Thompson, F.D., Tibbles, L.G., and Treidl, R.G., 1969: "The Meaning and Application of Advection Fields in Analysis and Forecasting", Canadian Department of Transport, Meteorological Branch, Circ. 715.

39) Namias, J., 1951: "General Aspects of Extended-Range Forecasting", American Meteorological Society, Compendium of Meteorology, pp. 802-813.

40) Panofsky, H.A., 1951: "Large-Scale Vertical Velocity and Divergence", American Meteorological Society, Compendium of Meteorology, pp. 639-646.

41) Panofsky, H.A., 1946: "Methods of Computing Vertical Motion in the Atmosphere", Journal of Meteorology, Vol. 3, No. 2, pp. 45-49.

42) Penner, C.M., 1960: "The Vorticity Concept and Its Application to Forecasting", Canadian Department of Transport, Meteorological Branch, Refresher Course Notes, Unpublished.

43) Penner, C.M., 1963: "An Operational Method for the Determination of Vertical Velocities", Journal of Applied Meteorology, Vol. 2, pp. 235-241.

44) Petterssen, S., 1956: "Weather Analysis and Forecasting", 2nd Edition, Vol. 1, 2, McGraw Hill Book Co. Inc., New York.

45) Petterssen, S., 1950: "Some Aspects of the General Circulation of the Atmosphere", Centenary Proceedings of the Royal Meteorological Society, Centenary Symposium on the General Circulation, Oxford, 30th of March, pp. 120-155.

46) Robinson, A.H. and Bryson, R.A., 1957: "A Method for Describing Quantitatively the Correspondence of Geographical Distributions", Annals of the Association of the American Geographers, Vol. 47, pp. 379-391.

47) Saltzman, B., 1968: "Surface Boundary Effects on the General Circulation and Macroclimate, A Review of the Theory of the Quasi-Stationary Perturbations in the Atmosphere", Meteorological Monographs, Vol. 18, No. 30.

48) Saucier, W., 1965: "Principles of Meteorological Analysis", The University of Chicago Press, Chicago and London, 4th Edition.

49) Sutcliffe, R.C. and Forsdyke, A.G., 1950: "Theory of the Use of Upper Air Thickness Patterns in Forecasting", Quarterly Journal of the Royal Meteorological Society, Vol. 76, No. 328, pp. 187-217.

50) Tanner, W.F., 1963: "Detachment of Gaussian Components from Zig-Zag Curves", Journal of Applied Meteorology, Vol. 2, pp. 119-121.

51) Thomas, M.K., Thompson, H.A., 1960: "Heavy Rainfall in the Canadian Arctic During August, 1960", Weatherwise, Vol. 15, No. 4, pp. 153-167.

52) Thompson, Y.C. and Collins, G.O., 1953: "A Generalized Study of Precipitation Forecasting, Part 1; Computation of Precipitation from the Fields of Moisture and Wind", Monthly Weather Review, Vol. 81, No. 4, pp. 91-100.

53) Vederman, J., 1961: "Forecasting Precipitation with the Aid of High Speed Computer", Monthly Weather Review, Vol. 89, No. 7, pp. 243-250.

54) Vowinckel, E. and Orvig, S., 1967: "The Inversion over the Polar Ocean", Polar Meteorology, WMO, Technical Note 87, Proceedings of the WMO-SCAR-ICPM, Symposium on Polar Meteorology, Geneva 5-9 Sept. 1966, pp. 39-59.

T A B L E S

Numbered from 1 to 35

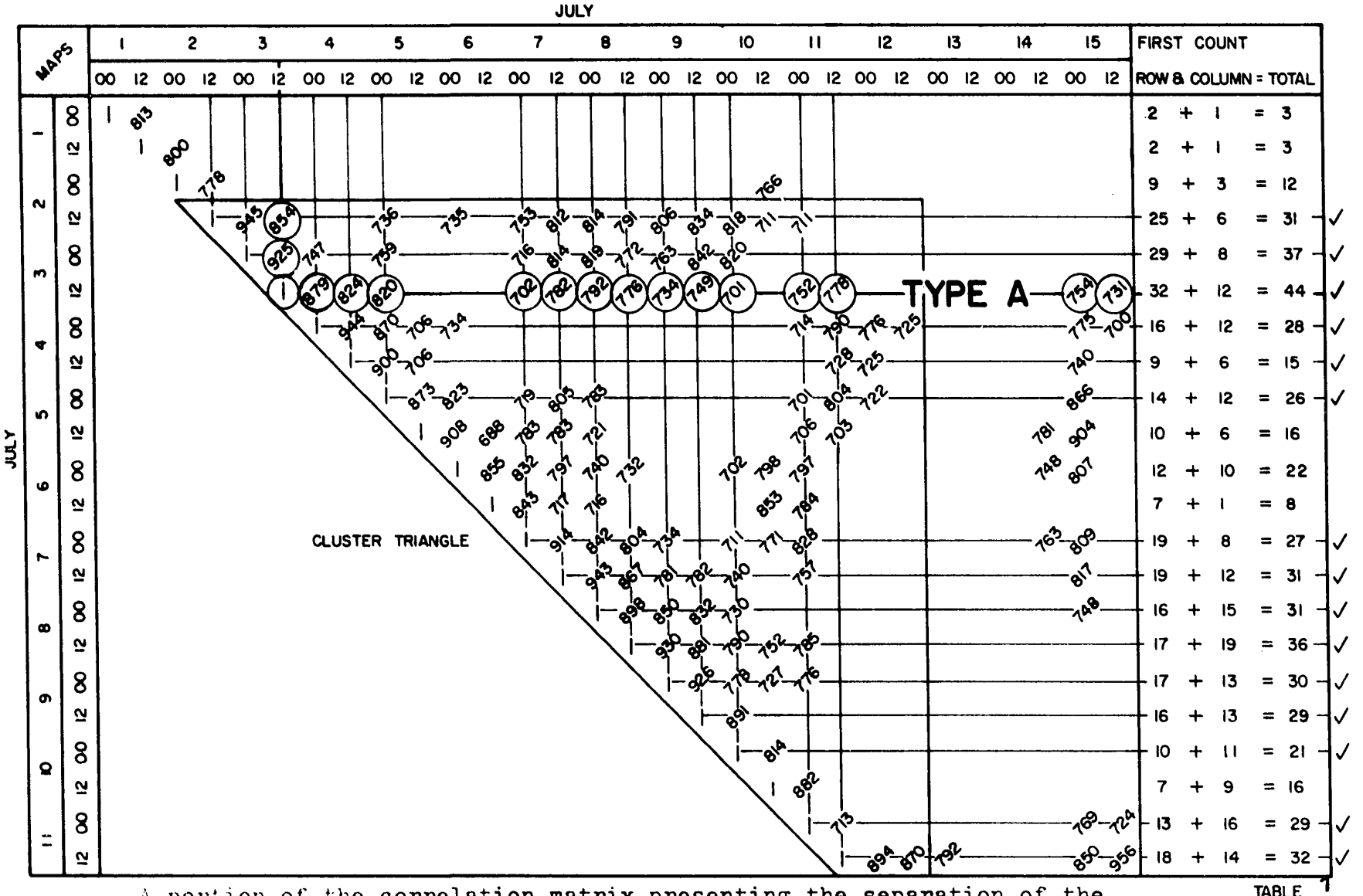

A portion of the correlation matrix presenting the separation of the pressure type " A " as a result of the first count

Type	Representative Map of the Type	No. of Cases With r ≥ + .7	No. of Cases After Re-arrangement	No. of Cases With r ≥ + .6	Mean Correlation Coefficient Within the Whole Group
A	July 3 12 GMT	44	27	27	.810
B	July 28 00 "	24	19	19	.808
C	June 1 12 "	20	20	20	.853
D	May 2 12 "	16	20	22	.805
E	Aug. 2 00 "	15	14	15	.811
F	May 13 12 "	12	12	13	.792
G	June 25 12 "	11	10	10	.808
H	June 17 00 "	10	7	7	.840
I	July 2 00 "	9	9	10	.770
J	June 7 12 "	8	9	9	.866
K	May 25 12 "	7	7	8	.823
L	July 12 00 "	6	12	13	.827
M	May 17 00 "	5	6	6	.818
N	May 15 12 "	4	4	5	.808
O	July 17 12 "	4	4	5	.821
P	Aug. 15 12 "	4	5	7	.810
R	Aug. 29 12 "	4	4	4	.885
S	May 8 00 "	3	5	5	.826
T	June 29 00 "	3	4	4	.892
U	July 5 12 "	3	10	11	.818
V	Aug. 1 00 "	3	7	8	.830
Z	Aug. 22 00 "	3	3	3	.882
W	Unclassifiable	r <.7, 28	r <.7, 28	r <.6, 15	<.6

Summarized information about the types

Table 2

MAP TYPE CALENDAR

Date	Hour	May	June	July	August
1	00	M .744	C .951	W	V
	12	D .931	C	I .800	E .801
2	00	D .977	C .896	I	E
	12	D	C .877	A .854	E .830
3	00	D .990	C .832	A .925	E .766
	12	D .972	C .781	A	V .820
4	00	D .882	P .590	A .879	E .871
	12	D .838	P .682	A .824	E .851
5	00	D .807	D .727	U .873	E .897
	12	D .710	D .739	U	E .836
6	00	A .710	D .766	U .908	E .728
	12	E .672	J .857	U .688	A .847
7	00	T .776	J .968	U .783	A .853
	12	S .782	J	U .783	A .794
8	00	S	J .867	A .792	E .765
	12	S .833	C .756	A .776	E .823
9	00	V .815	C .800	A .734	V .884
	12	A .792	C .776	A .749	V .679
10	00	A .890	C .807	P .849	I .814
	12	A .738	K .782	I .766	I .715
11	00	L .834	S .750	A .752	D .763
	12	L .759	E .718	L .894	D .829
12	00	N .686	B .782	L	B .777
	12	F .874	B .803	L .928	D .806
13	00	F .930	B .770	L .864	D .758
	12	F	I .711	H .878	D .653
14	00	F .858	A .780	H .875	D .684
	12	F .751	U .712	U .781	D .713
15	00	N .837	U .830	U .904	P .909
	12	N	L .823	L .858	P
16	00	N .783	L .881	L .775	P .827
	12	M .713	L .805	L .717	P .691
17	00	M	H	O .829	U .736
	12	M .880	H .916	O	A .718
18	00	D .718	H .715	O .885	A .826
	12	J .738	H .580	O .726	A .807
19	00	J .780	N .737	B .514	A .751
	12	J .806	F .715	B .709	B .754
20	00	J .917	F .755	B .754	B .742
	12	J .864	F .749	I .716	B .726
21	00	G .739	F .731	I .795	D .580
	12	K .693	F .693	E .786	Z .753
22	00	K .837	M .755	E .828	Z
	12	K .778	M .821	V .816	Z .895
23	00	S .546	D .735	A .582	G .771
	12	C .756	B .870	A .560	G .793
24	00	G .816	B .807	D .720	G .771
	12	K .760	C .806	A .728	G .776
25	00	K .917	G .832	I .725	G .744
	12	K	G	I .667	G .549
26	00	K .819	G .840	P .715	W
	12	S .769	O .505	B .781	W
27	00	B .759	O .667	B .885	F .740
	12	B .761	H .730	B .957	F .778
28	00	C .750	H .771	B	F .734
	12	C .870	T .929	B .918	F .564
29	00	C .924	T	B .798	R .890
	12	C .921	T .865	A .856	R
30	00	C .924	V .787	A .873	R .924
	12	C .880	W	A .825	R .728
31	00	C .871		A .769	L .618
	12	C .894		V .842	L .586

Table 3

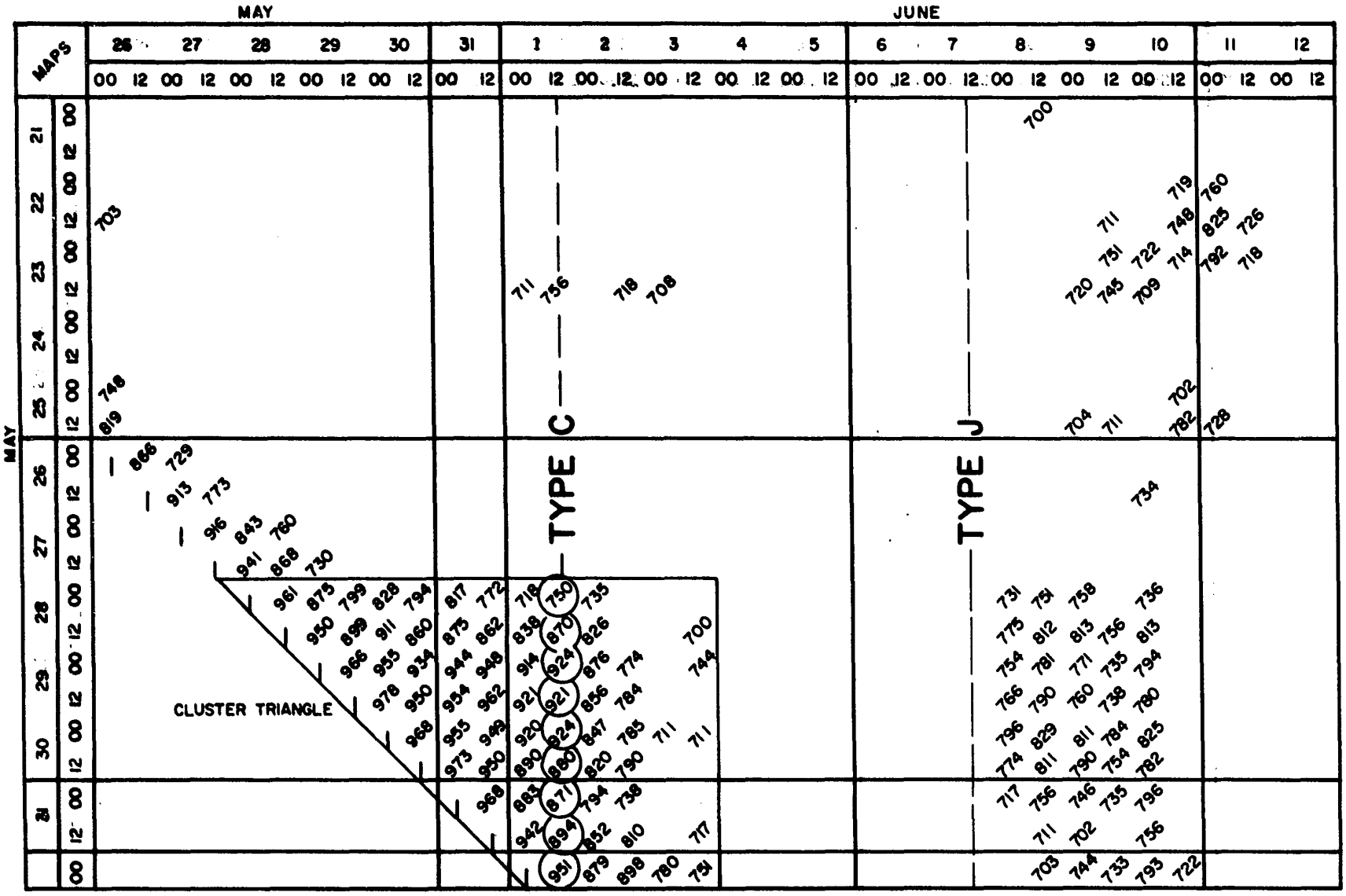

A portion of the correlation matrix with the upper part of the type " C " cluster triangle

Table 4

Type	A	mean map	correlated	with	type	L	mean map	at	r	=	0.770
"	A	"	"	"	"	"	U	"	"	"	r	=	0.769
"	A	"	"	"	"	"	I	"	"	"	r	=	0.738
"	A	"	"	"	"	"	D	"	"	"	r	=	0.719
"	E	"	"	"	"	"	V	"	"	"	r	=	0.869
"	E	"	"	"	"	"	T	"	"	"	r	=	0.724

Positive correlation of the type mean maps with each other when $r \geq + 0.7$ A

Type	N	representative map	correlated	with	type	C	representative map	at	r	=	-0.811
"	D	"	"	"	"	"	R	"	"	"	r	=	-0.790
"	H	"	"	"	"	"	G	"	"	"	r	=	-0.772
"	G	"	"	"	"	"	U	"	"	"	r	=	-0.754
"	F	"	"	"	"	"	V	"	"	"	r	=	-0.750
"	F	"	"	"	"	"	B	"	"	"	r	=	-0.746
"	C	"	"	"	"	"	U	"	"	"	r	=	-0.733

Negative correlation of the type representative maps with each other when $r \leq -0.7$

Table 5 B

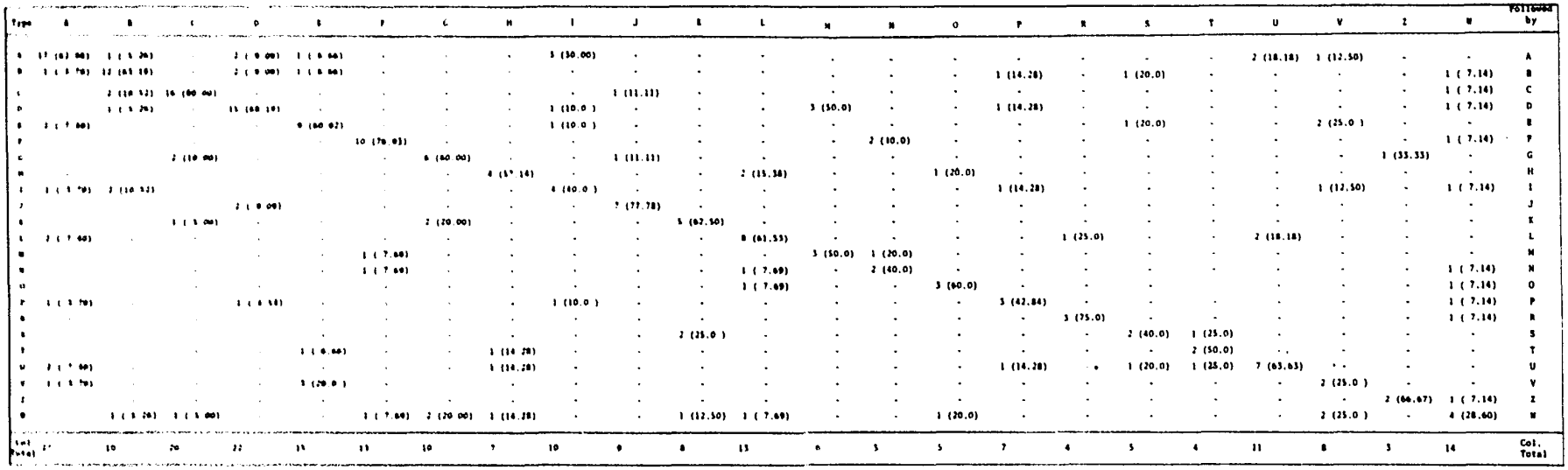

Type	A	B	C	D	E	F	G	H	I	J	K	L	M	N	O	P	R	S	T	U	V	Z	W	Followed by
A	17 (62.96)	1 (5.26)		2 (9.09)	1 (6.66)				3 (30.00)											2 (18.18)	1 (12.50)			A
B	1 (3.70)	12 (63.16)		2 (9.09)	1 (6.66)											1 (14.28)		1 (20.0)					1 (7.14)	B
C		2 (10.52)	16 (80.00)							1 (11.11)													1 (7.14)	C
D		1 (5.26)		15 (68.18)					1 (10.0)				5 (50.0)			1 (14.28)							1 (7.14)	D
E	2 (7.40)				9 (60.02)				1 (10.0)									1 (20.0)			2 (25.0)			E
F						10 (76.9)								2 (10.0)									1 (7.14)	F
G			2 (10.00)				6 (60.00)			1 (11.11)												1 (33.33)		G
H								4 (57.14)				2 (15.38)			1 (20.0)									H
I	1 (3.70)	2 (10.52)							4 (40.0)							1 (14.28)					1 (12.50)		1 (7.14)	I
J				2 (9.09)						7 (77.78)														J
K			1 (5.00)				2 (20.00)				5 (62.50)													K
L	2 (7.40)											8 (61.53)					1 (25.0)			2 (18.18)				L
M						1 (7.69)							5 (50.0)	1 (20.0)										M
N						1 (7.69)						1 (7.69)		2 (40.0)									1 (7.14)	N
O												1 (7.69)			3 (60.0)								1 (7.14)	O
P	1 (3.70)			1 (4.54)					1 (10.0)							5 (42.84)							1 (7.14)	P
R																	3 (75.0)						1 (7.14)	R
S											2 (25.0)							2 (40.0)	1 (25.0)					S
T					1 (6.66)			1 (14.28)											2 (50.0)					T
U	2 (7.40)							1 (14.28)								1 (14.28)		1 (20.0)	1 (25.0)	7 (63.63)				U
V	1 (3.70)				5 (70.0)																2 (25.0)			V
Z																						2 (66.67)	1 (7.14)	Z
W		1 (5.26)	1 (5.00)			1 (7.69)	2 (20.00)	1 (14.28)			1 (12.50)	1 (7.69)			1 (20.0)						2 (25.0)		4 (26.60)	W
Col. Total	27	19	20	22	15	13	10	7	10	9	8	13	6	5	5	7	4	5	4	11	8	3	14	Col. Total

Frequency of type transitions from one observation to the next

Table 6

HOUR GMT	Wind Directions								
	N	NE	E	SE	S	SW	W	NW	Calm
06	13	14	14	8	1	9	9	5	7
12	10	20	15	11	2	6	9	2	5
18	12	23	13	15	3	9	3	2	1
00	11	18	22	9	2	6	6	4	3

A

Frequency of wind directions of the 6 hourly observations, Inugsuin Fiord, May 25 - August 13, 1968.

HOUR GMT	Gradient or upfiord winds	Nongradient or downfiord winds
06	41	18
12	45	15
18	48	12
00	51	12

B

Frequency of the grouped wind directions, Inugsuin Fiord, May 25 - August 13, 1968.

Wind Directions	N	NE	E	SE	S	SW	W	NW	Calm
Frequency	8	9	11	-	-	1	3	-	-
Average wind speed in kts	10	15	5	-	-	3	5	-	-
Average cloudiness in %	95	95	70	-	-	25	40	-	-

C

Frequency of wind directions with average wind speed and cloudiness for the weather types A, H, I, L, and U, 12 GMT observations, Inugsuin Fiord, May 25 - August 13, 1968.

Table 7

Station	Percentage of the Summer Total Precipitation Due to Weather Type																						
	A	B	C	D	E	F	G	H	I	J	K	L	M	N	O	P	R	S	T	U	V	Z	W
Alert	6.96	17.91	3.81	2.15	8.12	-	.49	4.31	11.94	1.65	.99	.99	.66	-	-	15.09	5.30	2.32	6.94	.99	6.96	-	2.32
Baker Lake	9.69	4.34	2.34	.66	22.07	2.34	-	1.00	18.72	-	3.67	.66	.33	-	2.34	.66	-	.33	2.67	-	13.71	.33	14.04
Churchill	4.91	10.00	6.72	6.39	14.42	2.78	-	11.63	20.32	.16	-	5.90	2.13	.16	.32	2.29	8.19	.16	-	.98	.81	1.14	.49
Clyde	11.89	-	2.70	5.58	12.52	-	-	.33	1.86	1.18	.16	28.59	-	-	3.21	-	-	-	-	8.62	.16	-	20.13
Coppermine	21.32	.47	-	8.09	17.61	2.38	9.52	-	16.66	9.04	.47	.95	-	1.90	-	.95	-	-	.47	-	3.80	-	6.19
Coral Harbour	39.67	1.76	.47	-	7.62	1.40	-	.11	1.64	-	3.16	.70	1.05	3.99	8.80	2.58	12.91	-	2.34	8.33	.35	-	3.05
Egedesminde	6.85		.88	3.98	7.74	5.31	1.54	4.64	1.77	-	-	17.25	-	.44	2.87	2.21	-	1.32	2.65	2.21	13.71	.44	24.11
Eureka	7.93	15.87		12.69	22.22	25.39	1.58	1.58	-	1.58	-	-	-	-	-	3.17	-	-	-	-	1.58	-	6.34
Fort Chimo	30.18	8.70	.15	16.21	15.46	-	.15	5.55	1.80	.45	-	.75	1.35	-	-	1.95	-	.90	.30	5.55	2.25	1.35	6.90
Frobisher Bay	17.05	.73		1.62	8.52	.48	.97	25.70	4.99	.12	-	3.04	.24	-	2.92	4.99	.24	2.31	.12	7.18	5.11	-	10.59
Goose Bay	17.47	10.62	.06	7.33	3.77	4.89	4.68	.62	-	3.70	.27	15.16	2.23	.06	-	5.31	-	-	.97	5.80	.07	5.38	11.53
Hall Beach	11.20	.57	.57	5.41	2.87	3.73	9.48	2.01	3.44	.86	1.14	22.98	4.59	8.62	-	2.01	5.74	1.43	-	8.62	3.73	-	2.87
Imgsuin Fiord	3.46	1.27		-	-	.25	16.79	12.21	-	-	-	6.36	.50	M	43.25	-	M	-	9.66	2.79	2.79	M	.50
Isachsen	9.21		5.78	15.02	20.23	10.40	1.15	-	-	1.15	4.62	-	4.62	4.62	-	.57	12.13	1.15	-	.57	2.89	-	5.78
Mould Bay	3.57		1.78	1.78	12.50	3.57	5.35	-	1.78	28.57	8.92	1.78	1.78	3.57	-	-	-	-	-	-	7.14	-	17.85
Narssarssuaq	11.93	5.42	3.46	1.05	41.62	-	-	.75	-	-	-	1.50	.60	-	-	.45	5.27	-	1.05	3.01	13.12	-	7.69
Natchequon	11.79	2.71		8.68	5.32	1.37	5.80	3.17	4.67	.05	.71	2.87	.47	-	1.31	3.53	-	1.55	1.01	4.55	4.85	.53	8.94
Port Harrison	6.02	25.04	-	3.10	17.86	4.66	-	1.35	7.96	-	-	.19	-	-	-	4.85	-	-	-	6.79	8.54	1.16	12.42
Resolute	1.65	4.65	.99	1.99	5.52	17.27	5.98	1.99	.66	3.98	4.31	.99	3.65	1.99	1.32	-	.66	.33	-	-	20.26	.66	20.26
Sachs Harbour	1.13	7.13		-	3.30	32.23	4.95	-	.82	2.47	-	-	-	1.65	-	-	-	-	-	-	-	38.84	4.13

Type contribution to station precipitation

Table 8

Total Occurrence of Weather Type A: 27

Station	Number of Cases with Measurable Precipitation	Occurrence of Trace	Cases with no Precipitation (Trace Excluded)	Precipitation in Inches		
				Summer Total	Type Total	Percentage of the Summer Total
Alert	4	4	19	6.03	.42	6.96 %
Baker Lake	5	4	18	2.99	.29	9.69
Churchill	5	3	19	6.10	.30	4.91
Clyde	7	4	16	5.91	.88	14.89
Coppermine	6	1	20	2.10	.45	21.42
Coral Harbour	10	3	14	8.52	3.38	39.67
Egedesminde	4	-	23	4.52	.31	6.85
Eureka	1	1	25	.63	.05	7.93
Fort Chimo	16	2	9	6.60	2.01	30.18
Frobisher Bay	14	3	10	8.21	1.40	17.05
Goose Bay	8	3	16	14.31	2.50	17.47
Hall Beach	8	3	16	3.48	.39	11.20
Inugsuin Fiord (n = 19)	5	-	14	3.93	.14	3.56
Isachsen	3	8	16	1.73	.16	9.24
Mould Bay	1	2	24	.56	.02	3.57
Narssarssuaq	10	-	17	6.63	.99	14.93
Nitchequon	19	1	7	16.70	2.47	14.79
Port Harrison	6	5	16	5.15	.31	6.02
Resolute	3	2	22	3.01	.14	4.65
Sachs Harbour	2	1	24	1.21	.05	4.13

Precipitation Related to Weather Type: A

Table 9

Total Occurrence of Weather Type B: 19

Station	Number of Cases with Measurable Precipitation	Occurrence of Trace	Cases with no Precipitation (Trace Excluded)	Precipitation in Inches		
				Summer Total	Type Total	Percentage of the Summer Total
Alert	10	4	5	6.03	1.08	17.91 %
Baker Lake	2	1	16	2.99	.13	4.34
Churchill	5	1	13	6.10	.61	10.00
Clyde	-	3	16	5.91	-	-
Coppermine	1	-	18	2.10	.01	.47
Coral Harbour	3	2	14	8.52	.15	1.76
Egedesminde	-	-	19	4.52	-	-
Eureka	1	-	18	.63	.10	15.87
Fort Chimo	5	1	13	6.60	.58	8.70
Frobisher Bay	2	1	16	8.21	.06	.73
Goose Bay	9	2	8	14.31	1.52	10.62
Hall Beach	2	4	13	3.48	.02	.57
Inugsuin Fiord (n = 16)	2	-	14	3.93	.05	1.27
Isachsen	-	8	11	1.73	-	-
Mould Bay	-	1	18	.56	-	-
Narssarssuaq	4	-	15	6.63	.36	5.42
Nitchequon	13	-	6	16.70	4.30	25.74
Port Harrison	7	-	12	5.15	1.29	25.04
Resolute	2	2	15	3.01	.14	4.65
Sachs Harbour	2	-	17	1.21	.09	7.43

Precipitation Related to Weather Type: B

Table 10

Total Occurrence of Weather Type C : 20

Station	Number of Cases with Measurable Precipitation	Occurrence of Trace	Cases with no Precipitation (Trace Excluded)	Precipitation in Inches		
				Summer Total	Type Total	Percentage of the Summer Total
Alert	5	1	14	6.03	.23	3.81 %
Baker Lake	2	-	18	2.99	.07	2.34
Churchill	5	2	13	6.10	.41	6.72
Clyde	3	2	15	5.91	.16	2.70
Coppermine	-	-	20	2.10	-	-
Coral Harbour	2	-	18	8.52	.04	.47
Egedesminde	2	-	18	4.52	.04	.88
Eureka	-	1	19	.63	-	-
Fort Chimo	1	-	19	6.60	.01	.15
Frobisher Bay	-	4	16	8.21	-	-
Goose Bay	1	2	17	14.31	.01	.06
Hall Beach	2	-	18	3.48	.02	.57
Inugsuin Fiord	-	-	19	3.93	-	-
Isachsen (n = 19)	4	11	5	1.73	.10	5.78
Mould Bay	1	5	14	.56	.01	1.78
Narssarssuaq	3	-	17	6.63	.23	3.46
Nitchequon	-	-	20	16.70	-	-
Port Harrison	-	-	20	5.15	-	-
Resolute	2	5	13	3.01	.03	.99
Sachs Harbour	-	1	19	1.21	-	-

Precipitation Related to Weather Type: C

Table 11

Total Occurrence of Weather Type D : 22

Station	Number of Cases with Measurable Precipitation	Occurrence of Trace	Cases with no Precipitation (Trace Excluded)	Precipitation in Inches		
				Summer Total	Type Total	Percentage of the Summer Total
Alert	3	2	17	6.03	.13	2.15 %
Baker Lake	1	4	17	2.99	.02	.66
Churchill	5	4	13	6.10	.39	6.39
Clyde	8	2	12	5.91	.33	5.58
Coppermine	4	1	17	2.10	.17	8.09
Coral Harbour	-	3	19	8.52	-	-
Egedesminde	2	-	20	4.52	.18	3.98
Eureka	3	-	19	.63	.08	12.69
Fort Chimo	7	5	10	6.60	1.08	16.21
Frobisher Bay	5	7	10	8.21	.38	4.62
Goose Bay	10	1	11	14.31	1.05	7.33
Hall Beach	4	2	16	3.48	.12	3.44
Inugsuin Fiord (n = 10)	-	-	10	3.93	-	-
Isachsen	2	7	13	1.73	.26	15.02
Mould Bay	1	3	18	.56	.01	1.78
Narssarssuaq	2	-	20	6.63	.07	1.05
Nitchequon	12	2	8	16.70	1.45	8.68
Port Harrison	6	1	15	5.15	.16	3.10
Resolute	3	-	19	3.01	.06	1.99
Sachs Harbour	-	2	20	1.21	-	-

Precipitation Related to Weather Type: D

Table 12

Total Occurrence of Weather Type E : 15

Station	Number of Cases with Measurable Precipitation	Occurrence of Trace	Cases with no Precipitation (Trace Excluded)	Precipitation in Inches		
				Summer Total	Type Total	Percentage of the Summer Total
Alert	6	1	8	6.03	.49	8.12 %
Baker Lake	5	-	10	2.99	.66	22.07
Churchill	8	1	6	6.10	.88	14.42
Clyde	4	1	10	5.91	.74	12.52
Coppermine	7	-	8	2.10	.37	17.61
Coral Harbour	5	1	9	8.52	.65	7.62
Egedesminde	6	-	9	4.52	.35	7.74
Eureka	2	-	13	.63	.14	22.22
Fort Chimo	7	3	5	6.60	1.03	15.46
Frobisher Bay	4	3	8	8.21	.70	8.52
Goose Bay	4	-	11	14.31	.54	3.77
Hall Beach	2	-	13	3.48	.10	2.87
Inugsuin Fiord	-	-	14	3.93	-	-
Isachsen (n = 14)	3	5	7	1.73	.35	20.23
Mould Bay	3	6	6	.56	.07	12.50
Narssarssuaq	11	-	4	6.63	2.76	41.62
Nitchequon	5	1	9	16.70	.89	5.32
Port Harrison	5	3	7	5.15	.92	17.86
Resolute	3	2	10	3.01	.10	3.32
Sachs Harbour	1	2	12	1.21	.04	3.30

Precipitation Related to Weather Type: E

Table 13

Total Occurrence of Weather Type F : 13

Station	Number of Cases with Measurable Precipitation	Occurrence of Trace	Cases with no Precipitation (Trace Excluded)	Precipitation in Inches		
				Summer Total	Type Total	Percentage of the Summer Total
Alert	-	-	13	6.03	-	- %
Baker Lake	2	-	11	2.99	.07	2.34
Churchill	3	2	8	6.10	.17	2.78
Clyde	-	-	13	5.91	-	-
Coppermine	2	-	11	2.10	.05	2.38
Coral Harbour	4	1	8	8.52	.12	1.40
Egedesminde	2	-	11	4.52	.24	5.30
Eureka	4	-	9	.63	.16	25.39
Fort Chimo	-	1	12	6.60	-	-
Frobisher Bay	2	2	9	8.21	.04	.48
Goose Bay	7	2	4	14.31	.70	4.89
Hall Beach	5	3	5	3.48	.13	3.73
Inugsuin Fiord (n = 5)	1	-	4	3.93	.01	.25
Isachsen	5	4	4	1.73	.18	10.40
Mould Bay	1	6	6	.56	.02	3.57
Narssarssuaq	-	-	13	6.63	-	-
Nitchequon	2	-	11	16.70	.23	1.37
Port Harrison	3	-	10	5.15	.24	4.66
Resolute	6	3	4	3.01	.52	17.27
Sachs Harbour	4	3	6	1.21	.39	32.23

Precipitation Related to Weather Type: F

Table 14

Total Occurrence of Weather Type G: 10

Station	Number of Cases with Measurable Precipitation	Occurrence of Trace	Cases with no Precipitation (Trace Excluded)	Precipitation in Inches		
				Summer Total	Type Total	Percentage of the Summer Total
Alert	3	3	4	6.03	.03	.49 %
Baker Lake	-	-	10	2.99	-	-
Churchill	-	1	9	6.10	-	-
Clyde	-	2	8	5.91	-	-
Coppermine	4	2	4	2.10	.20	9.52
Coral Harbour	-	1	9	8.52	-	-
Egedesminde	1	-	9	4.52	.07	1.54
Eureka	1	-	9	.63	.01	1.58
Fort Chimo	1	1	8	6.60	.01	.15
Frobisher Bay	2	2	6	8.21	.08	.97
Goose Bay	3	-	7	14.31	.67	4.68
Hall Beach	3	3	4	3.48	.33	9.48
Inugsuin Fiord (n = 3)	1	-	2	3.93	.66	16.79
Isachsen	2	1	7	1.73	.02	1.15
Mould Bay	1	1	8	.56	.03	5.35
Narssarssuaq	-	-	10	6.63	-	-
Nitchequon	4	1	5	16.70	.97	5.80
Port Harrison	-	-	10	5.15	-	-
Resolute	5	1	4	3.01	.18	5.98
Sachs Harbour	2	2	6	1.21	.06	4.95

Precipitation Related to Weather Type: G

Table 15

Total Occurrence of Weather Type H : 7

Station	Number of Cases with Measurable Precipitation	Occurrence of Trace	Cases with no Precipitation (Trace Excluded)	Precipitation in Inches		
				Summer Total	Type Total	Percentage of the Summer Total
Alert	2	-	5	6.03	.26	4.31 %
Baker Lake	2	1	4	2.99	.03	1.00
Churchill	5	-	2	6.10	.71	11.63
Clyde	2	-	5	5.91	.02	.33
Coppermine	-	-	7	2.10	-	-
Coral Harbour	1	1	5	8.52	.01	.11
Egedesminde	2	-	5	4.52	.21	4.64
Eureka	1	-	6	.63	.01	1.58
Fort Chimo	1	-	6	6.60	.37	5.55
Frobisher Bay	3	-	4	8.21	2.11	25.70
Goose Bay	3	-	4	14.31	.09	.62
Hall Beach	2	-	5	3.48	.07	2.01
Inugsuin Fiord (n = 7)	2	-	5	3.93	.48	12.21
Isachsen	-	1	6	1.73	-	-
Mould Bay	-	-	7	.56	-	-
Narssarssuaq	2	-	5	6.63	.05	.75
Nitchequon	1	1	5	16.70	.53	3.17
Port Harrison	1	-	6	5.15	.07	1.35
Resolute	1	2	4	3.01	.06	1.99
Sachs Harbour	-	-	7	1.21	-	-

Precipitation Related to Weather Type: H

Table 16

Total Occurrence of Weather Type I : 10

Station	Number of Cases with Measurable Precipitation	Occurrence of Trace	Cases with no Precipitation (Trace Excluded)	Precipitation in Inches		
				Summer Total	Type Total	Percentage of the Summer Total
Alert	3	1	6	6.03	.72	11.94 %
Baker Lake	6	1	3	2.99	.56	18.72
Churchill	5	-	5	6.10	1.24	20.32
Clyde	1	-	9	5.91	.11	1.86
Coppermine	3	-	7	2.10	.35	16.66
Coral Harbour	3	2	5	8.52	.14	1.64
Egedesminde	3	-	7	4.52	.08	1.76
Eureka	-	-	10	.63	-	-
Fort Chimo	2	-	8	6.60	.12	1.80
Frobisher Bay	2	-	8	8.21	.41	4.99
Goose Bay	-	3	7	14.31	-	-
Hall Beach	4	1	5	3.48	.12	3.44
Inugsuin Fiord (n = 10)	-	-	10	3.93	-	-
Isachsen	-	4	6	1.73	-	-
Mould Bay	1	3	6	.56	.01	1.78
Narssarssuaq	-	-	10	6.63	-	-
Nitchequon	3	1	6	16.70	.78	4.67
Fort Harrison	3	-	7	5.15	.41	7.96
Resolute	1	2	7	3.01	.02	.66
Sachs Harbour	1	-	9	1.21	.01	.82

Precipitation Related to Weather Type: I

Table 17

Total Occurrence of Weather Type J : 9

Station	Number of Cases with Measurable Precipitation	Occurrence of Trace	Cases with no Precipitation (Trace Excluded)	Precipitation in Inches		
				Summer Total	Type Total	Percentage of the Summer Total
Alert	3	-	6	6.03	.10	1.65 %
Baker Lake	-	2	7	2.99	-	-
Churchill	1	1	7	6.10	.01	.16
Clyde	1	-	8	5.91	.07	1.18
Coppermine	1	1	7	2.10	.19	9.04
Coral Harbour	-	1	8	8.52	-	-
Egedesminde	-	-	9	4.52	-	-
Eureka	1	2	6	.63	.01	1.58
Fort Chimo	2	-	7	6.60	.03	.45
Frobisher Bay	1	1	7	8.21	.01	.12
Goose Bay	6	2	1	14.31	.53	3.70
Hall Beach	2	1	6	3.48	.03	.86
Inugsuin Fiord (n = 4)	-	-	4	3.93	-	-
Isachsen	1	3	5	1.73	.02	1.15
Mould Bay	2	2	5	.56	.16	28.57
Narssarssuaq	-	-	9	6.63	-	-
Nitchequon	1	-	8	16.70	.01	.05
Port Harrison	-	-	9	5.15	-	-
Resolute	3	2	4	3.01	.12	3.98
Sachs Harbour	2	-	7	1.21	.03	2.47

Precipitation Related to Weather Type: J

Table 18

Total Occurrence of Weather Type K : 8

Station	Number of Cases with Measurable Precipitation	Occurrence of Trace	Cases with no Precipitation (Trace Excluded)	Precipitation in Inches		
				Summer Total	Type Total	Percentage of the Summer Total
Alert	2	2	4	6.03	.06	.99 %
Baker Lake	2	2	4	2.99	.11	3.67
Churchill	-	1	7	6.10	-	-
Clyde	1	1	6	5.91	.01	.16
Coppermine	1	-	7	2.10	.01	.47
Coral Harbour	2	2	4	8.52	.27	3.16
Egedesminde	-	-	8	4.52	-	-
Eureka	-	4	4	.63	-	-
Fort Chimo	-	3	5	6.60	-	-
Frobisher Bay	-	3	5	8.21	-	-
Goose Bay	1	-	7	14.31	.04	.27
Hall Beach	2	4	2	3.48	.04	1.14
Inugsuin Fiord (n = 4)	-	-	4	3.93	-	-
Isachsen	4	4	-	1.73	.08	4.62
Mould Bay	3	3	2	.56	.05	8.92
Narssarssuaq	-	-	8	6.63	-	-
Nitchequon	2	-	6	16.70	.12	.71
Port Harrison	-	-	8	5.15	-	-
Resolute	3	2	3	3.01	.13	4.31
Sachs Harbour	-	5	3	1.21	-	-

Precipitation Related to Weather Type: K

Table 19

Total Occurrence of Weather Type L: 13

Station	Number of Cases with Measurable Precipitation	Occurrence of Trace	Cases with no Precipitation (Trace Excluded)	Precipitation in Inches		
				Sumner Total	Type Total	Percentage of the Summer Total
Alert	3	-	10	6.03	.06	.99 %
Baker Lake	1	1	11	2.99	.02	.66
Churchill	2	3	8	6.10	.36	5.90
Clyde	6	-	7	5.91	1.69	28.59
Coppermine	2	-	11	2.10	.02	.95
Coral Harbour	1	3	9	8.52	.06	.70
Egedesminde	6	-	7	4.52	.78	17.25
Eureka	-	-	13	.63	-	-
Fort Chimo	2	1	10	6.60	.05	.75
Frobisher Bay	4	2	7	8.21	.25	3.04
Goose Bay	7	1	5	14.31	2.17	15.16
Hall Beach	9	1	3	3.48	.80	22.98
Inugsuin Fiord (n = 10)	2	2	6	3.93	.25	6.36
Isachsen	-	1	12	1.73	-	-
Mould Bay	1	-	12	.56	.01	1.78
Narssarssuaq	2	-	11	6.63	.10	1.50
Nitchequon	4	-	9	16.70	.48	2.87
Port Harrison	1	-	12	5.15	.01	.19
Resolute	2	1	10	3.01	.03	.99
Sachs Harbour	-	-	13	1.21	-	-

Precipitation Related to Weather Type: L

Table 20

Total Occurrence of Weather Type M : 6

Station	Number of Cases with Measurable Precipitation	Occurrence of Trace	Cases with no Precipitation (Trace Excluded)	Precipitation in Inches		
				Summer Total	Type Total	Percentage of the Summer Total
Alert	2	-	4	6.03	.04	.66 %
Baker Lake	1	1	4	2.99	.01	.33
Churchill	2	-	4	6.10	.13	2.13
Clydo	-	-	6	5.91	-	-
Coppermine	-	-	6	2.10	-	-
Coral Harbour	1	-	5	8.52	.09	1.05
Egedesminde	-	-	6	4.52	-	-
Eureka	-	1	5	.63	-	-
Fort Chimo	1	-	5	6.60	.09	1.35
Frobisher Bay	1	1	4	8.21	.02	.24
Goose Bay	5	1	-	14.31	.32	2.23
Hall Beach	3	-	3	3.48	.16	4.59
Inugsuin Fiord (n = 2)	2	-	-	3.93	.02	.50
Isachsen	2	3	1	1.73	.08	4.62
Mould Bay	1	2	3	.56	.01	1.78
Narssarssuaq	1	-	5	6.63	.04	.60
Nitchequon	1	-	5	16.70	.08	.47
Port Harrison	-	-	6	5.15	-	-
Resolute	1	4	1	3.01	.11	3.65
Sachs Harbour	-	1	5	1.21	-	-

Precipitation Related to Weather Type: M

Table 21

Total Occurrence of Weather Type N : 5

Station	Number of Cases with Measurable Precipitation	Occurrence of Trace	Cases with no Precipitation (Trace Excluded)	Precipitation in Inches		
				Summer Total	Type Total	Percentage of the Summer Total
Alert	-	-	5	6.03	-	- %
Baker Lake	-	-	5	2.99	-	-
Churchill	1	-	4	6.10	.01	.16
Clyde	-	-	5	5.91	-	-
Coppermine	1	-	4	2.10	.04	1.90
Coral Harbour	2	-	3	8.52	.34	3.99
Egedesminde	1	-	4	4.52	.02	.44
Eureka	-	-	5	.63	-	-
Fort Chimo	-	-	5	6.60	-	-
Frobisher Bay	-	-	5	8.21	-	-
Goose Bay	1	1	3	14.31	.01	.06
Hall Beach	4	-	1	3.48	.30	8.62
Inugsuin Fiord (n = 0)	M	M	M	3.93	M	M
Isachsen	3	1	1	1.73	.08	4.62
Mould Bay	1	2	2	.56	.02	3.57
Narssarssuaq	-	-	5	6.63	-	-
Nitchequon	-	-	5	16.70	-	-
Port Harrison	-	-	5	5.15	-	-
Resolute	2	1	2	3.01	.06	1.99
Suchs Harbour	1	1	3	1.21	.02	1.65

Precipitation Related to Weather Type: N

Table 22

Total Occurrence of Weather Type 0 : 5

Station	Number of Cases with Measurable Precipitation	Occurrence of Trace	Cases with no Precipitation (Trace Excluded)	Precipitation in Inches		
				Summer Total	Type Total	Percentage of the Summer Total
Alert	-	-	5	6.03	-	- %
Baker Lake	1	-	4	2.99	.07	2.34
Churchill	1	-	4	6.10	.02	.32
Clyde	1	-	4	5.91	.19	3.21
Coppermine	-	-	5	2.10	-	-
Coral Harbour	1	-	4	8.52	.75	8.80
Egedesminde	2	-	3	4.52	.13	2.87
Eureka	-	1	4	.63	-	-
Fort Chimo	-	-	5	6.60	-	-
Frobisher Bay	1	-	4	8.21	.24	2.92
Goose Bay	-	-	5	14.31	-	-
Hall Beach	-	2	3	3.48	-	-
Inugsuin Fiord (n = 5)	5	-	-	3.93	1.70	43.25
Isachsen	-	-	5	1.73	-	-
Mould Bay	-	-	5	.56	-	-
Narssarssuaq	-	-	5	6.63	-	-
Nitchequon	1	-	4	16.70	.22	1.31
Port Harrison	-	-	5	5.15	-	-
Resolute	1	-	4	3.01	.04	1.32
Sachs Harbour	-	-	5	1.21	-	-

Precipitation Related to Weather Type: 0

Table 23

Total Occurrence of Weather Type P : 7

Station	Number of Cases with Measurable Precipitation	Occurrence of Trace	Cases with no Precipitation (Trace Excluded)	Precipitation in Inches		
				Summer Total	Type Total	Percentage of the Summer Total
Alert	3	1	3	6.03	.91	15.09 %
Baker Lake	2	1	4	2.99	.02	.66
Churchill	4	1	2	6.10	.14	2.29
Clyde	-	1	6	5.91	-	-
Coppermine	2	1	4	2.10	.02	.95
Coral Harbour	3	2	2	8.52	.22	2.58
Egedesminde	1	-	6	4.52	.10	2.21
Eureka	1	-	6	.63	.02	3.17
Fort Chimo	1	-	6	6.60	.13	1.95
Frobisher Bay	1	1	5	8.21	.41	4.99
Goose Bay	3	2	2	14.31	.76	5.31
Hall Beach	3	-	4	3.48	.07	2.01
Inugsuin Fiord (n = 3)	-	1	2	3.93	-	-
Isachsen	1	4	2	1.73	.01	.57
Mould Bay	-	-	7	.56	-	-
Narssarssuaq	1	-	6	6.63	.03	.45
Nitchequon	4	1	2	16.70	.59	3.53
Port Harrison	3	-	4	5.15	.25	4.85
Resolute	-	1	6	3.01	-	-
Sachs Harbour	-	-	7	1.21	-	-

Precipitation Related to Weather Type: P

Table 24

Total Occurrence of Weather Type R: 4

Station	Number of Cases with Measurable Precipitation	Occurrence of Trace	Cases with no Precipitation (Trace Excluded)	Precipitation in Inches		
				Summer Total	Type Total	Percentage of the Summer Total
Alert	3	-	1	6.03	.32	5.30 %
Baker Lake	-	-	4	2.99	-	-
Churchill	3	-	1	6.10	.50	8.19
Clyde	-	-	4	5.91	-	-
Coppermine	-	-	4	2.10	-	-
Coral Harbour	3	-	1	8.52	1.10	12.91
Egedesminde	-	-	4	4.52	-	-
Eureka	-	2	2	.63	-	-
Fort Chimo	-	-	4	6.60	-	-
Frobisher Bay	1	1	2	8.21	.02	.24
Goose Bay	-	-	4	14.31	-	-
Hall Beach	1	1	2	3.48	.20	5.74
Inugsuin Fiord (n = 0)	M	M	M	3.93	M	M
Isachsen	3	1	-	1.73	.21	12.13
Mould Bay	-	1	3	.56	-	-
Narssarssuaq	2	-	2	6.63	.35	5.27
Nitchequon	-	-	4	16.70	-	-
Port Harrison	-	-	4	5.15	-	-
Resolute	1	1	2	3.01	.02	.66
Sachs Harbour	-	1	3	1.21	-	-

Precipitation Related to Weather Type: R

Table 25

Total Occurrence of Weather Type S : 5

Station	Number of Cases with Measurable Precipitation	Occurrence of Trace	Cases with no Precipitation (Trace Excluded)	Precipitation in Inches		
				Summer Total	Type Total	Percentage of the Summer Total
Alert	1	-	4	6.03	.14	2.32 %
Baker Lake	1	-	4	2.99	.01	.33
Churchill	1	1	3	6.10	.01	.16
Clyde	-	2	3	5.91	-	-
Coppermine	-	-	5	2.10	-	-
Coral Harbour	-	-	5	8.52	-	-
Egedesminde	2	-	3	4.52	.06	1.32
Eureka	-	-	5	.63	-	-
Fort Chimo	1	1	3	6.60	.06	.90
Frobisher Bay	2	1	2	8.21	.19	2.31
Goose Bay	-	1	4	14.31	-	-
Hall Beach	1	-	4	3.48	.05	1.43
Inugsuin Fiord (n = 2)	-	-	2	3.93	-	-
Isachsen	2	2	1	1.73	.02	1.15
Mould Bay	-	2	3	.56	-	-
Narssarssuaq	-	-	5	6.63	-	-
Nitchequon	2	-	3	16.70	.26	1.55
Port Harrison	-	1	4	5.15	-	-
Resolute	1	2	2	3.01	.01	.33
Sachs Harbour	-	-	5	1.21	-	-

Precipitation Related to Weather Type: S

Table 26

Total Occurrence of Weather Type T : 4

Station	Number of Cases with Measurable Precipitation	Occurrence of Trace	Cases with no Precipitation (Trace Excluded)	Precipitation in Inches		
				Summer Total	Type Total	Percentage of the Summer Total
Alert	2	-	2	6.03	.42	6.96 %
Baker Lake	1	-	3	2.99	.08	2.67
Churchill	-	-	4	6.10	-	-
Clyde	-	3	1	5.91	-	-
Coppermine	1	-	3	2.10	.01	.47
Coral Harbour	1	-	3	8.52	.20	2.34
Egedesminde	2	-	2	4.52	.12	2.65
Eureka	-	2	2	.63	-	-
Fort Chimo	1	1	2	6.60	.02	.30
Frobisher Bay	1	1	2	8.21	.01	.12
Goose Bay	1	-	3	14.31	.14	.97
Hall Beach	-	-	4	3.48	-	-
Inugsuin Fiord (n = 3)	3	-	-	3.93	.38	9.66
Isachsen	-	1	3	1.73	-	-
Mould Bay	-	1	3	.56	-	-
Narssarssuaq	2	-	2	6.63	.07	1.05
Nitchequon	1	-	3	16.70	.17	1.01
Port Harrison	-	-	4	5.15	-	-
Resolute	-	1	3	3.01	-	-
Sachs Harbour	-	-	4	1.21	-	-

Precipitation Related to Weather Type: T

Table 27

Total Occurrence of Weather Type U: 11

Station	Number of Cases with Measurable Precipitation	Occurrence of Trace	Cases with no Precipitation (Trace Excluded)	Precipitation in Inches		
				Summer Total	Type Total	Percentage of the Summer Total
Alert	3	1	7	6.03	.06	.99 %
Baker Lake	-	-	11	2.99	-	-
Churchill	2	-	9	6.10	.06	.98
Clyde	3	1	7	5.91	.51	8.62
Coppermine	-	-	11	2.10	-	-
Coral Harbour	6	1	4	8.52	.71	8.33
Egedesminde	2	-	9	4.52	.10	2.21
Eureka	-	-	11	.63	-	-
Fort Chimo	2	-	9	6.60	.37	5.55
Frobisher Bay	2	1	8	8.21	.59	7.18
Goose Bay	6	-	5	14.31	.83	5.80
Hall Beach	4	1	6	3.48	.30	8.62
Inugsuin Fiord	3	1	6	3.93	.11	2.79
(n = 10) Isachsen	1	2	8	1.73	.01	.57
Mould Bay	-	-	11	.56	-	-
Narssarssuaq	2	-	9	6.63	.20	3.01
Nitchequon	6	-	5	16.70	.76	4.55
Port Harrison	3	1	7	5.15	.35	6.79
Resolute	-	-	11	3.01	-	-
Sachs Harbour	-	-	11	1.21	-	-

Precipitation Related to Weather Type: U

Table 28

Total Occurrence of Weather Type V : 8

Station	Number of Cases with Measurable Precipitation	Occurrence of Trace	Cases with no Precipitation (Trace Excluded)	Precipitation in Inches		
				Summer Total	Type Total	Percentage of the Summer Total
Alert	2	2	4	6.03	.42	6.96 %
Baker Lake	3	1	4	2.99	.41	13.71
Churchill	2	-	6	6.10	.05	.81
Clyde	1	2	5	5.91	.01	.16
Coppermine	2	-	6	2.10	.08	3.80
Coral Harbour	1	-	7	8.52	.03	.35
Egedesminde	5	-	3	4.52	.62	13.71
Eureka	1	2	5	.63	.01	1.58
Fort Chimo	4	1	3	6.60	.15	2.25
Frobisher Bay	4	1	3	8.21	.42	5.11
Goose Bay	1	-	7	14.31	.01	.07
Hall Beach	2	2	4	3.48	.13	3.73
Inugsuin Fiord (n = 7)	2	-	5	3.93	.11	2.79
Isachsen	1	2	5	1.73	.05	2.89
Mould Bay	2	3	3	.56	.04	7.14
Narssarssuaq	6	-	2	6.63	.87	13.12
Nitchequon	5	-	3	16.70	.81	4.85
Port Harrison	4	-	4	5.15	.44	8.54
Resolute	4	1	3	3.01	.61	20.26
Sachs Harbour	-	1	7	1.21	-	-

Precipitation Related to Weather Type: V

Table 29

Total Occurrence of Weather Type Z : 3

Station	Number of Cases with Measurable Precipitation	Occurrence of Trace	Cases with no Precipitation (Trace Excluded)	Precipitation in Inches		
				Summer Total	Type Total	Percentage of the Summer Total
Alert	-	-	3	6.03	-	- %
Baker Lake	1	-	2	2.99	.01	.33
Churchill	1	-	2	6.10	.07	1.14
Clyde	-	-	3	5.91	-	-
Coppermine	-	-	3	2.10	-	-
Coral Harbour	-	1	2	8.52	-	-
Egedesminde	2	-	1	4.52	.02	.44
Eureka	-	-	3	.63	-	-
Fort Chimo	1	1	1	6.60	.09	1.35
Frobisher Bay	-	-	3	8.21	-	-
Goose Bay	2	-	1	14.31	.77	5.38
Hall Beach	-	-	3	3.48	-	-
Inugsuin Fiord (n = 0)	M	M	M	3.93	M	M
Isachsen	-	1	2	1.73	-	-
Mould Bay	-	-	3	.56	-	-
Narssarssuaq	-	-	3	6.63	-	-
Nitchequon	1	1	1	16.70	.09	.53
Port Harrison	1	-	2	5.15	.06	1.16
Resolute	1	1	1	3.01	.02	.66
Sachs Harbour	2	-	1	1.21	.47	38.84

Precipitation Related to Weather Type: Z

Table 30

Total Occurrence of Weather Type W : 15

Station	Number of Cases with Measurable Precipitation	Occurrence of Trace	Cases with no Precipitation (Trace Excluded)	Precipitation in Inches		
				Summer Total	Type Total	Percentage of the Summer Total
Alert	3	2	10	6.03	.14	2.32 %
Baker Lake	2	3	10	2.99	.42	14.04
Churchill	2	1	12	6.10	.03	.49
Clyde	5	1	9	5.91	1.19	20.13
Coppermine	3	2	10	2.10	.13	6.19
Coral Harbour	1	-	14	8.52	.26	3.05
Egedesminde	6	-	9	4.52	1.09	24.11
Eureka	1	1	13	.63	.04	6.34
Fort Chimo	5	1	9	6.60	.46	6.90
Frobisher Bay	4	2	9	8.21	.87	10.59
Goose Bay	10	-	5	14.31	1.65	11.53
Hall Beach	3	3	9	3.48	.10	2.87
Inugsuin Fiord (n = 8)	1	-	7	3.93	.02	.50
Isachsen	3	4	8	1.73	.10	5.78
Mould Bay	4	-	11	.56	.10	17.85
Narssarssuaq	2	-	13	6.63	.51	7.69
Nitchequon	6	2	7	16.70	1.49	8.94
Port Harrison	3	-	12	5.15	.64	12.42
Resolute	5	2	8	3.01	.61	20.26
Sachs Harbour	2	2	11	1.21	.05	4.13

Precipitation Related to Weather Type: W

Table 31

FROBISHER BAY STATION 2402300 TYPE E

DATE	HOUR	PRECIPITATION
68 5 6	12	T
68 6 11	12	0
68 7 21	12	0
68 7 22	0	0
68 8 1	12	0
68 8 2	0	T
68 8 2	12	0
68 8 3	0	0
68 8 4	0	.09
68 8 4	12	T
68 8 5	0	0
68 8 5	12	0
68 8 6	0	.46
68 8 8	0	.07
68 8 8	12	.08
		.70

MEAN ---------- .0467

STANDARD DEVIATION ---------- .1190

CORAL HARBOUR STATION 2301000 TYPE A

DATE	HOUR	PRECIPITATION
68 5 6	0	0
68 5 9	12	0
68 5 10	0	T
68 5 10	12	0
68 6 14	0	.18
68 7 2	12	0
68 7 3	0	.55
68 7 3	12	1.15
68 7 4	0	.25
68 7 4	12	.04
68 7 8	0	0
68 7 8	12	.27
68 7 9	0	0
68 7 9	12	0
68 7 11	0	0
68 7 24	12	.77
68 7 29	12	.03
68 7 30	0	0
68 7 30	12	0
68 7 31	0	0
68 8 6	12	.11
68 8 7	0	0
68 8 7	12	0
68 8 17	12	0
68 8 18	0	T
68 8 18	12	T
68 8 19	0	.03
		3.38

MEAN ---------- .1252

STANDARD DEVIATION ---------- .2758

Type E station precipitation for Frobisher Bay and type A precipitation for Coral Harbour during the summer of 1968

Table 32

Triangle		Value Deductible from the Surface Pressure
Location	Mean Elevation	
A1	331 ft.	- 4 mb
A2	525 ft.	-12 mb
B2	863 ft.	-27 mb
B3	1,056 ft.	-35 mb
C5	469 ft.	-10 mb
D7	1,543 ft.	-57 mb
E8	950 ft.	-31 mb
F1	375 ft.	- 6 mb
F7	400 ft.	- 7 mb
F9	2,256 ft.	-78 mb
G5	363 ft.	- 5 mb
G7	769 ft.	-22 mb
H8	719 ft.	-20 mb
J1	713 ft.	-20 mb
J2	450 ft.	- 9 mb

Surface pressure corrections due to the mean elevation of the equilateral triangles

Table 33

TYPE "A" July 3, 1968, 12 GMT

STATION	Calculated P_R for 600mb $6hr^{-1}$	Observed P_R GMT 06–12	Observed P_R GMT 12–18	If discrepancies occurred: Height of the active layer	$-\omega$ at that height	Dewpoint Spread	ω_E at active height	calculated p_r for the active height
Isachsen	.03"	—	.03"	—	—	—	—	—
Frobisher Bay	.05"	.03"	T	—	—	—	—	—
Goose Bay	.13"	.72"	T	← Extrapolated value →		← Station is outside the		sampling grid →
Port Harrison	.06"	.07"	—	—	—	—	—	—
Alert	0	—	T	850mb	−0.75	Saturated	−0.75	.02"
Baker Lake	0	T	—	850mb	−0.42	Saturated	−0.42	.01"
Inugsuin Fiord	.04"	.02	—	—			—	—
Coral Harbour	0	.60	.55	≪ 850mb	Subsidence only	Saturated at 850mb	—	—
Clyde	.03"	T					—	—

Comparison of station precipitations with calculated precipitation rates.

Table 34

TYPE "E" Aug. 2, 1968, 00 GMT

STATION	Calculated P_R for 600 mb $6hr^{-1}$	Observed P_R		If discrepancies occurred				
		GMT 06–12	GMT 12–18	Height of the actice layer	$-\omega$ at that height	Dewpoint Spread	ω_E	p_r
Resolute	.03"	T	T	—	—	—	—	—
Frobisher	.02"	T	T	—	—	—	—	—
Fort Chimo	.15"	.35	T	—	—	—	—	—
Baker Lake	—	T	—	← Edge effect →				
Isachsen	—	T	T	← ≪850mb	Saturated →		Surface Convergence $-.03 \times 10^{-5} sec^{-1}$	
Mould Bay	—	.01	.03	← Edge effect →				
Clyde	.04"	—	—	← Possible Evaporation →				

Comparison of station precipitations with calculated precipitation rates.

Table 35

F I G U R E S

Numbered from 1 to 64

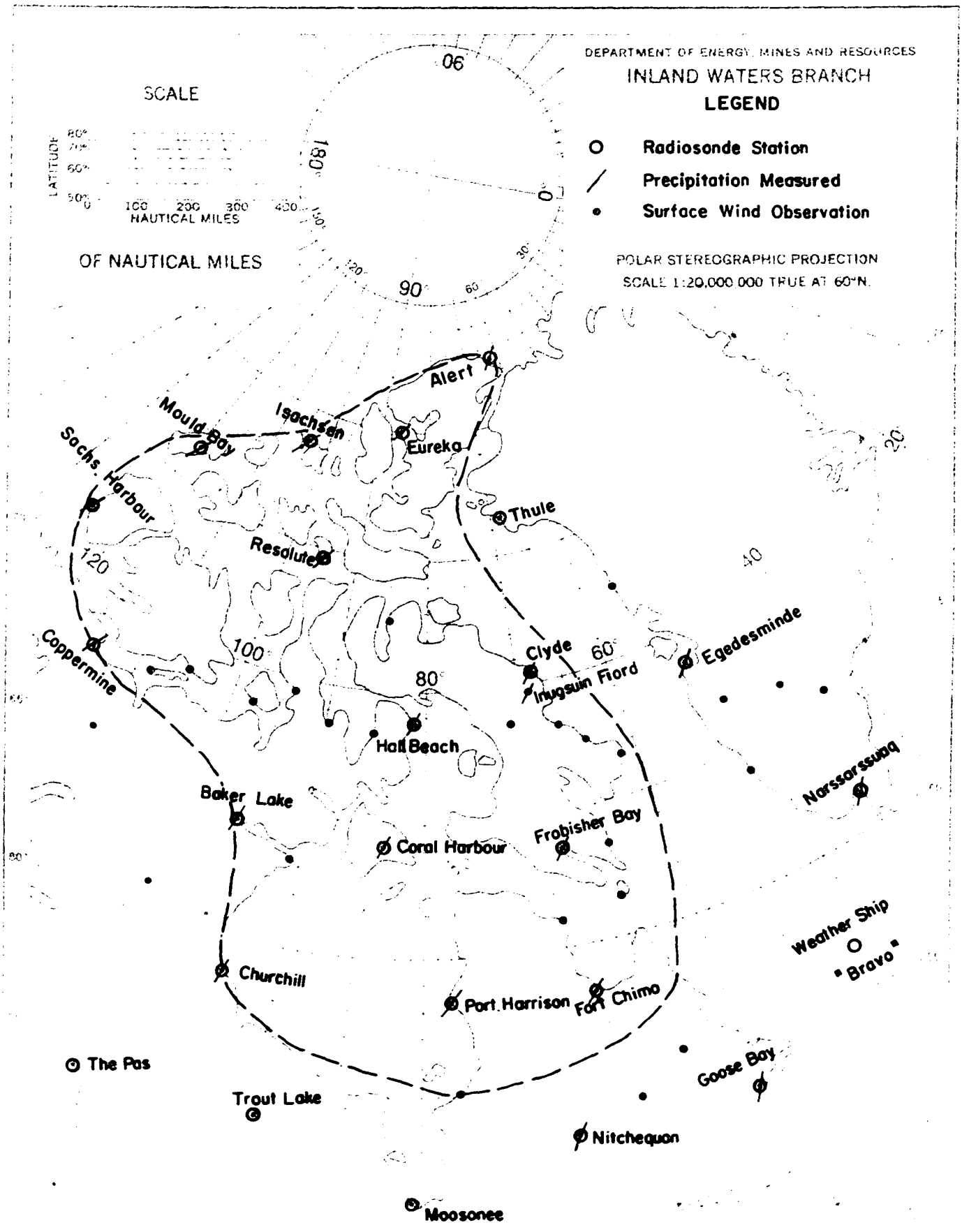

Figure 1

Surface and Upper Air Observation Network

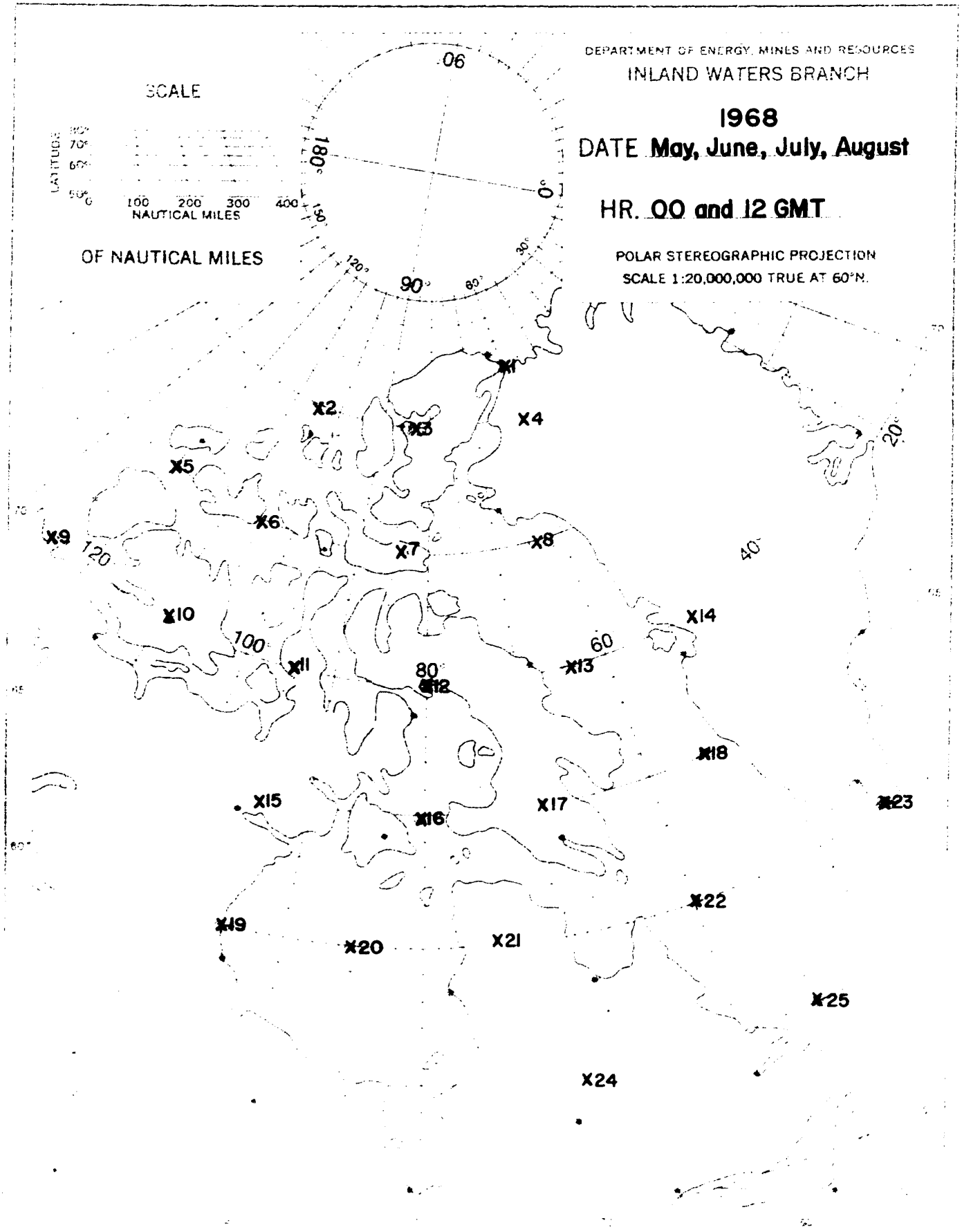

Location of the 25 Sampling Points used for Classification Figure 2

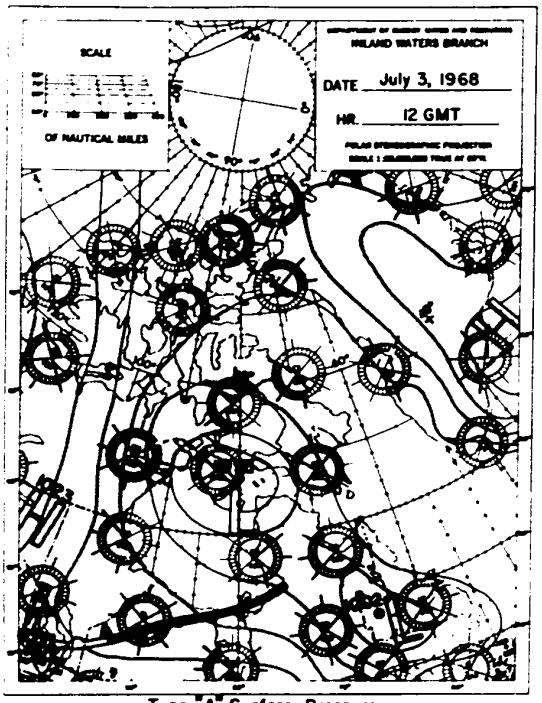

Type "A" Surface Pressure

A

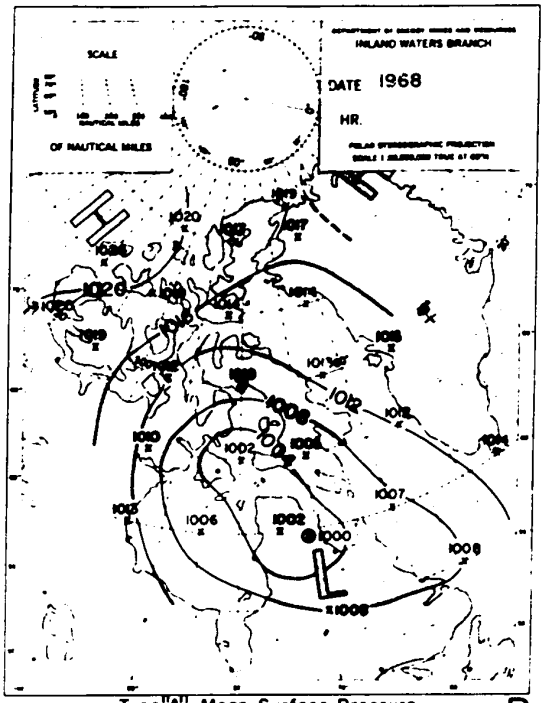

Type "A" Mean Surface Pressure

B

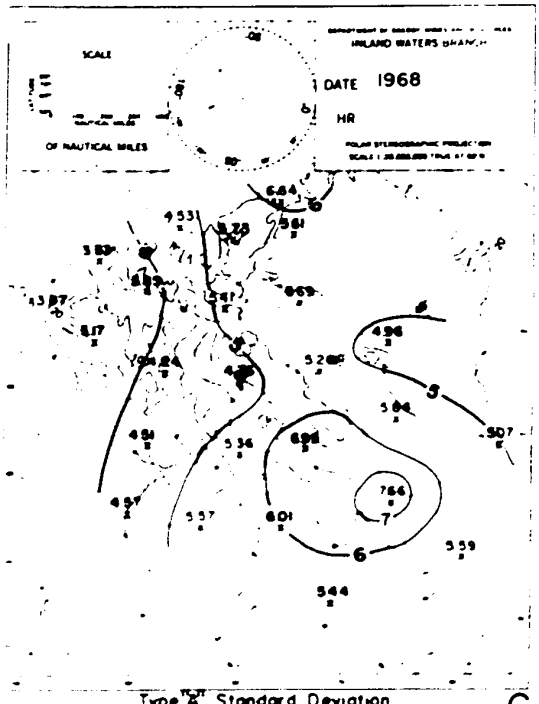

Type "A" Standard Deviation

C

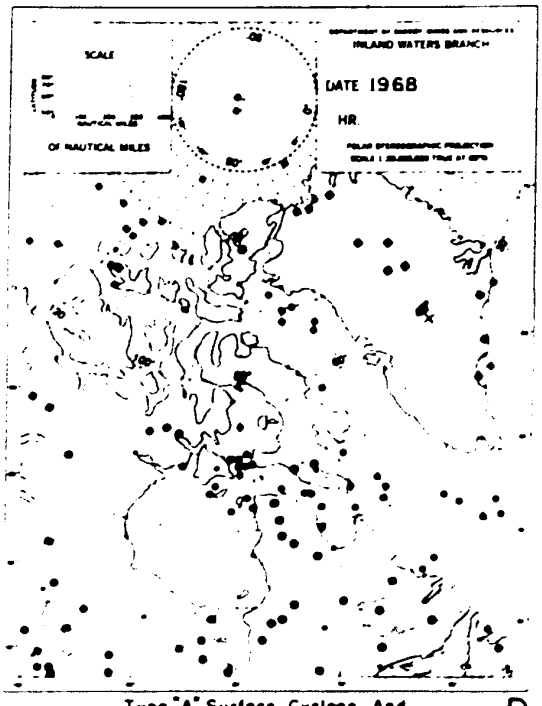

Type "A" Surface Cyclone And Anticyclone Centres

D

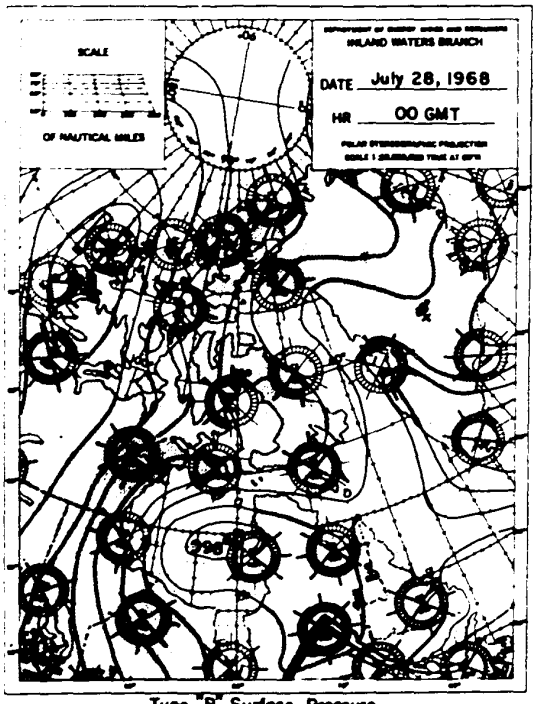

Type "B" Surface Pressure

A

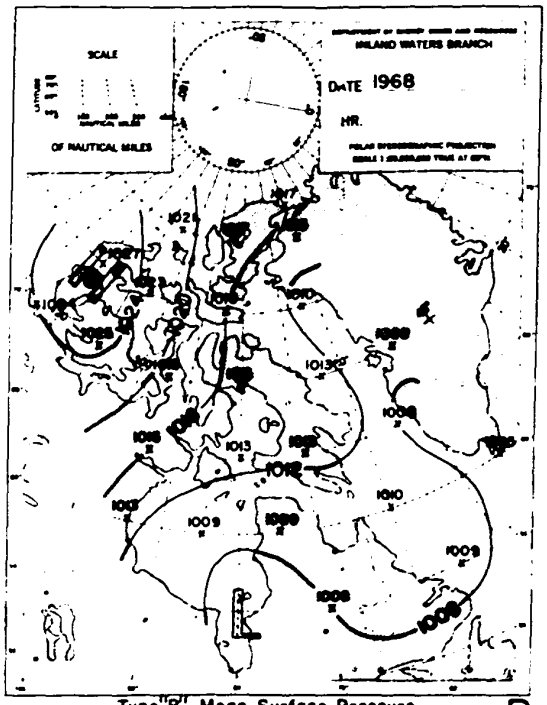

Type "B" Mean Surface Pressure

B

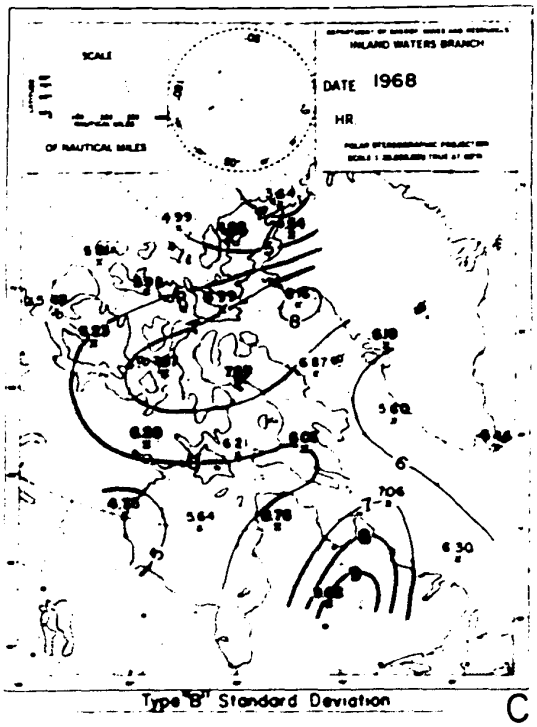

Type "B" Standard Deviation

C

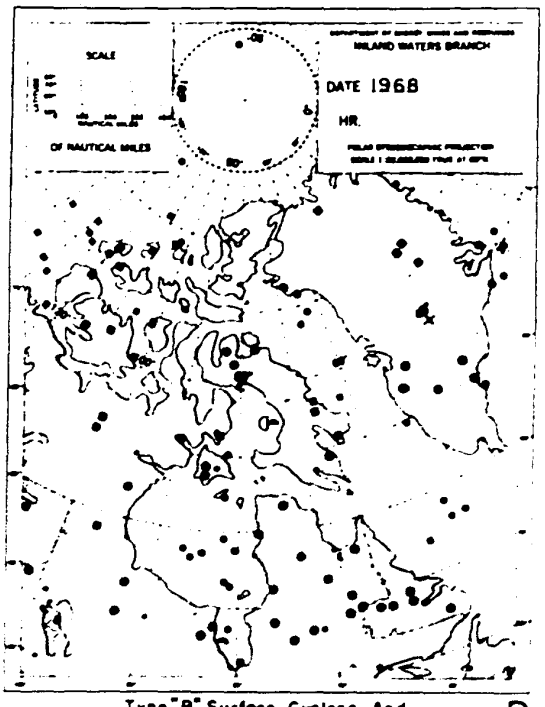

Type "B" Surface Cyclone And Anticyclone Centres

D

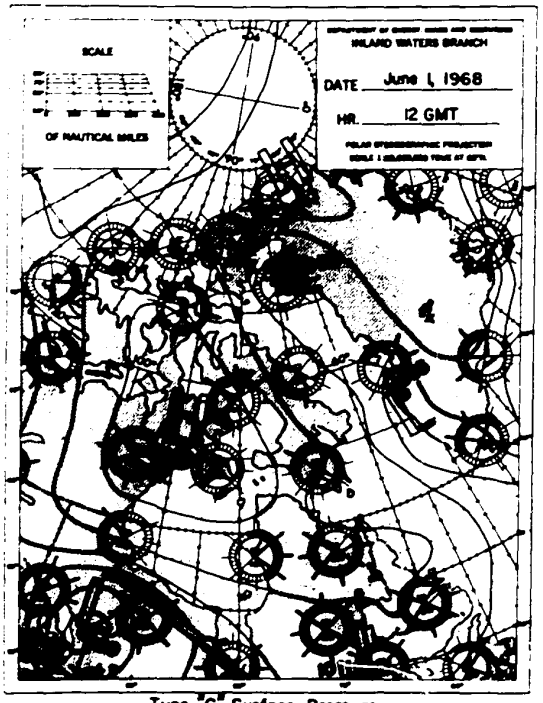

Type "C" Surface Pressure

A

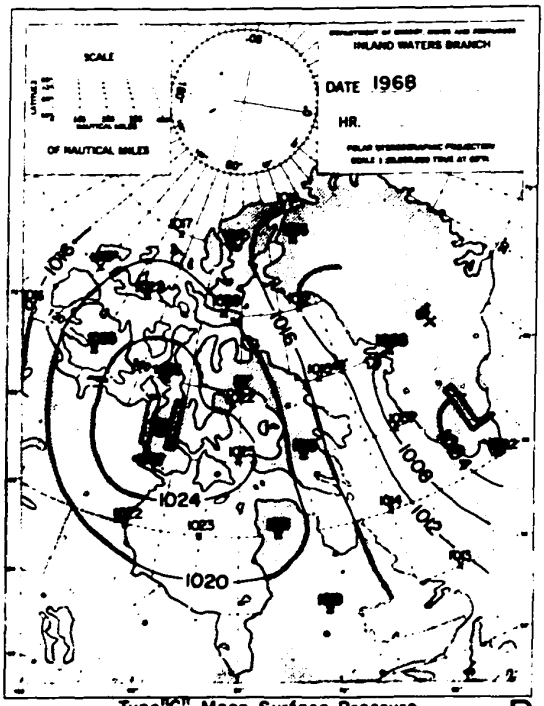

Type "C" Mean Surface Pressure

B

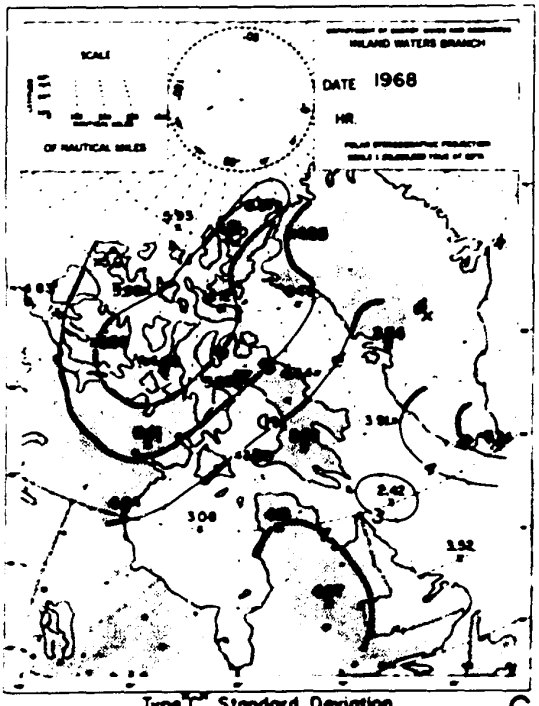

Type "C" Standard Deviation

C

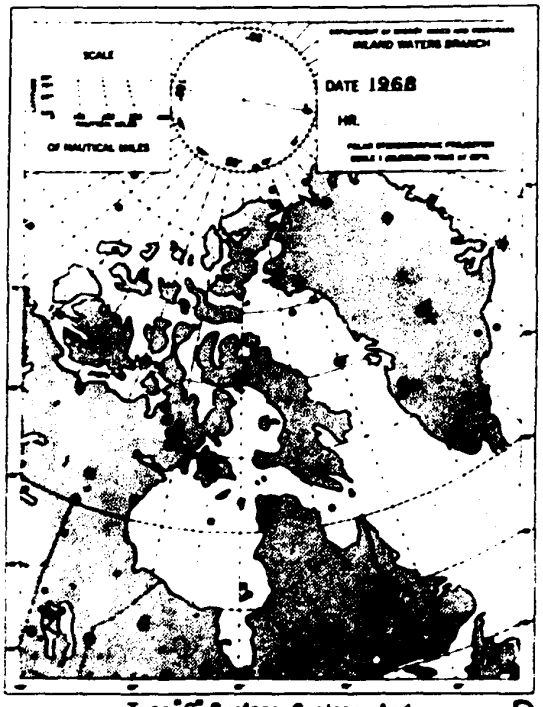

Type "C" Surface Cyclone And Anticyclone Centres

D

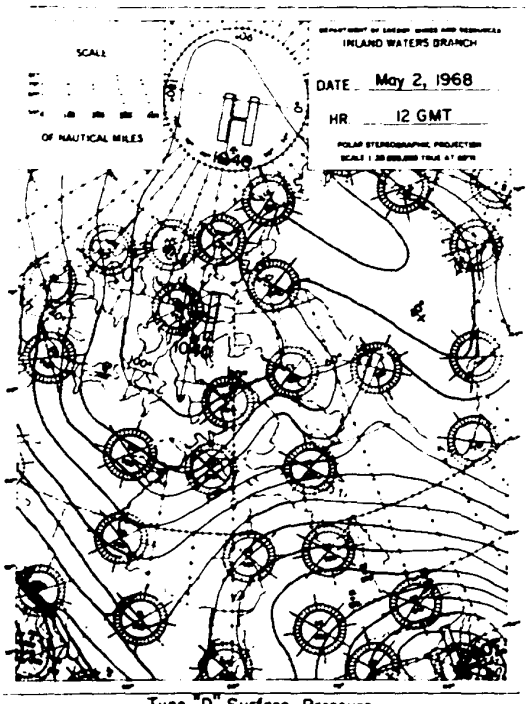

Type "D" Surface Pressure

A

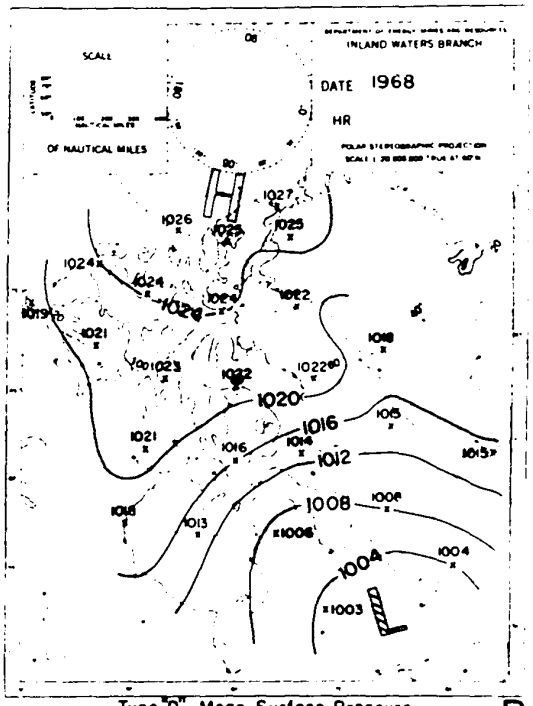

Type "D" Mean Surface Pressure

B

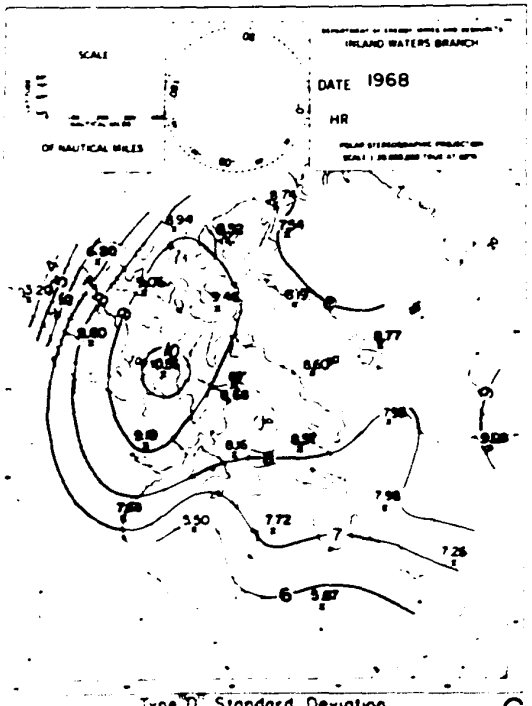

Type "D" Standard Deviation

C

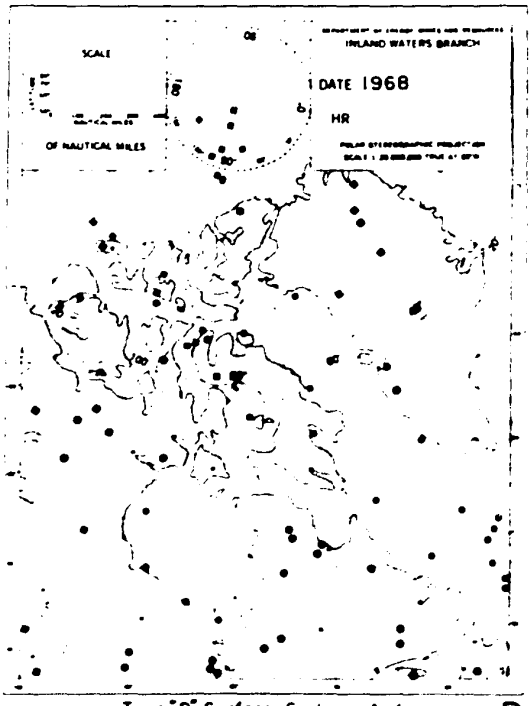

Type "D" Surface Cyclone And Anticyclone Centres

D

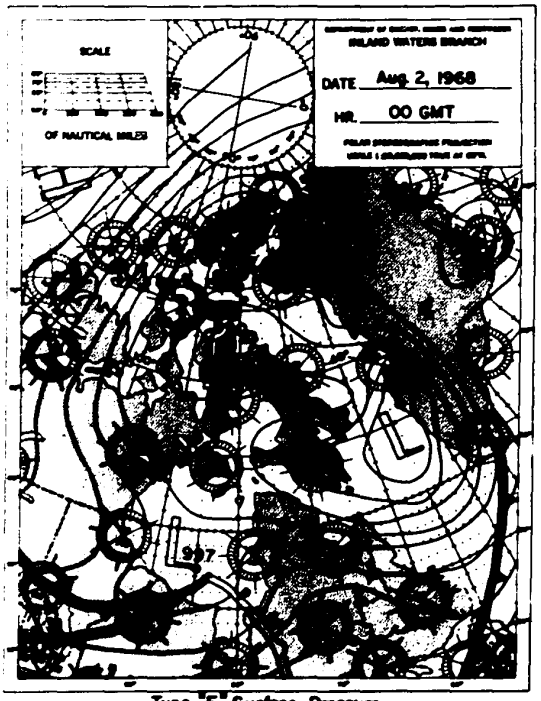

Type "E" Surface Pressure

A

Type "E" Mean Surface Pressure

B

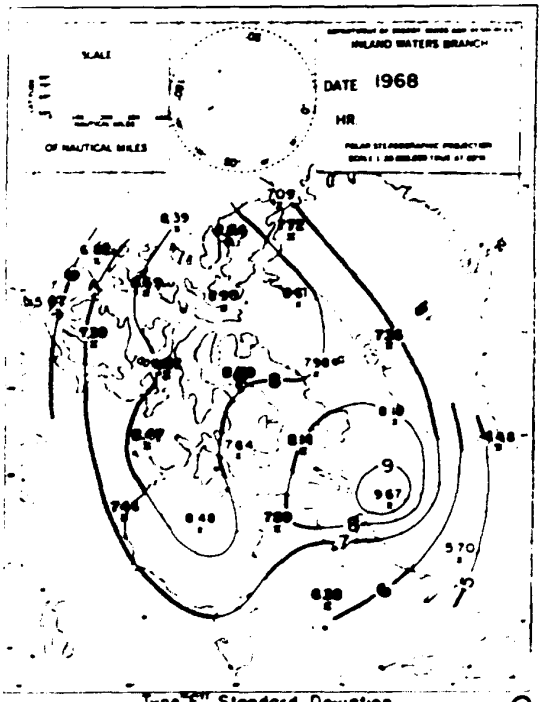

Type "E" Standard Deviation

C

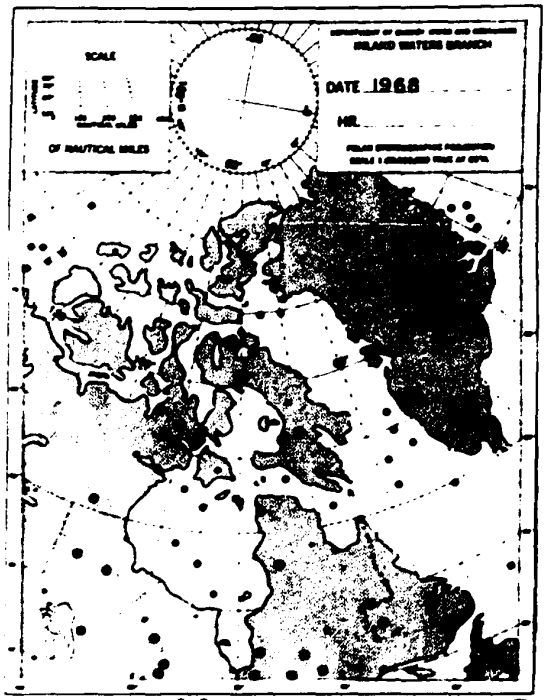

Type "E" Surface Cyclone And Anticyclone Centres

D

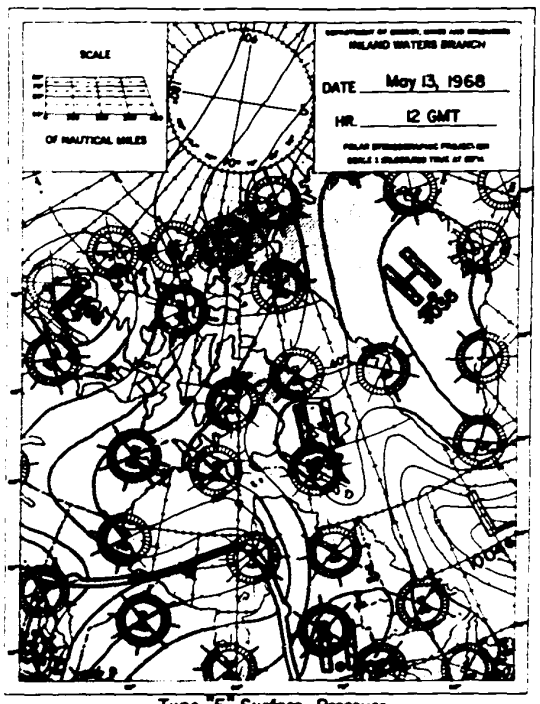

Type "F" Surface Pressure

A

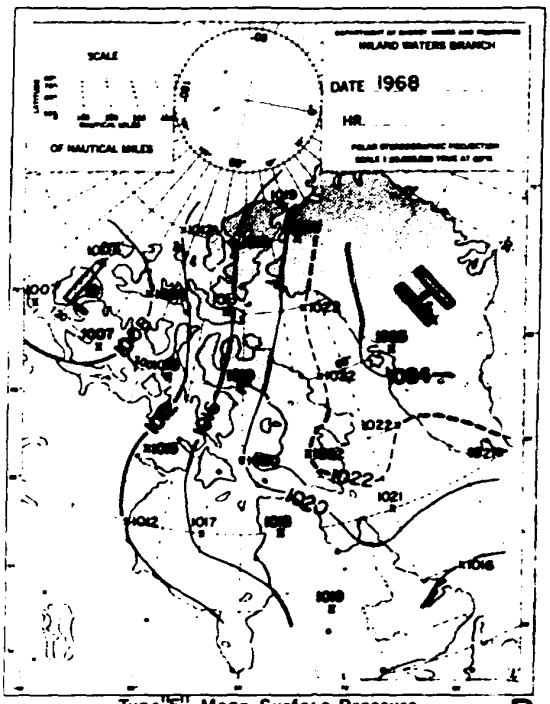

Type "F" Mean Surface Pressure

B

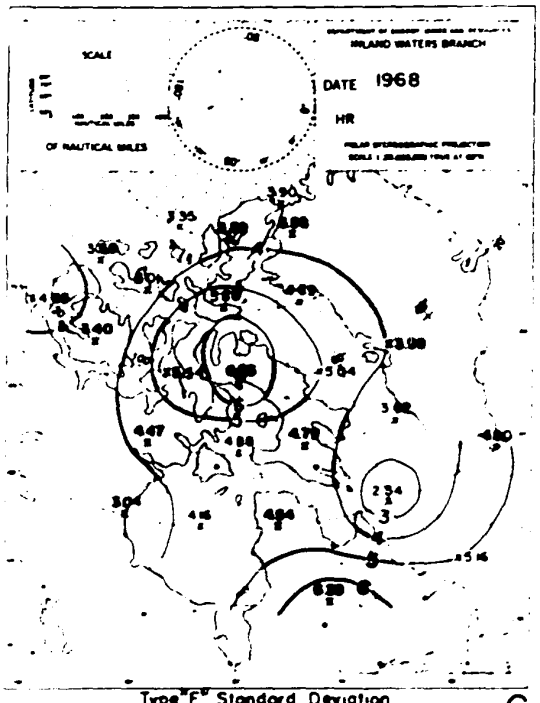

Type "F" Standard Deviation

C

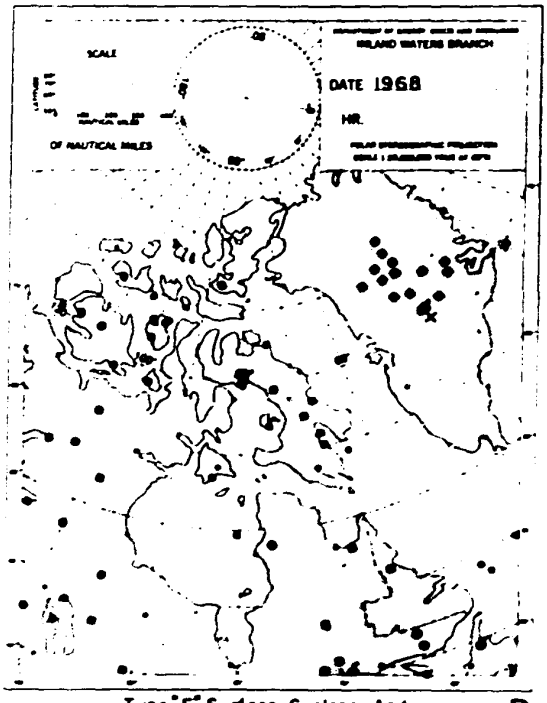

Type "F" Surface Cyclone And Anticyclone Centres

D

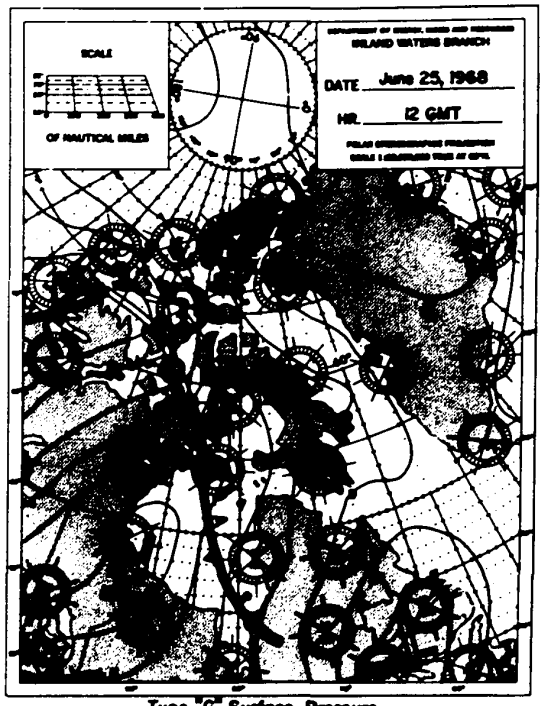

Type "G" Surface Pressure

A

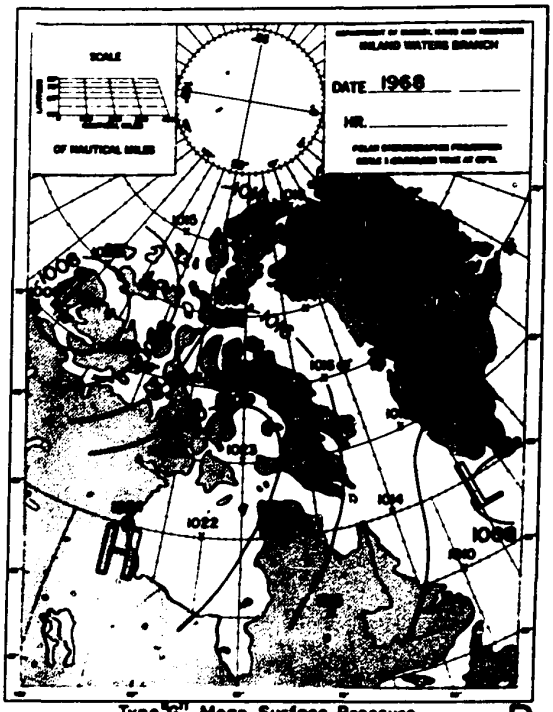

Type "G" Mean Surface Pressure

B

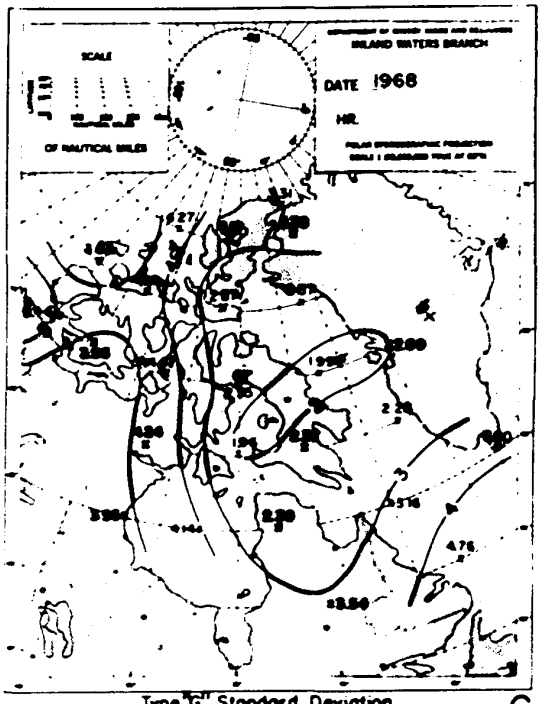

Type "G" Standard Deviation

C

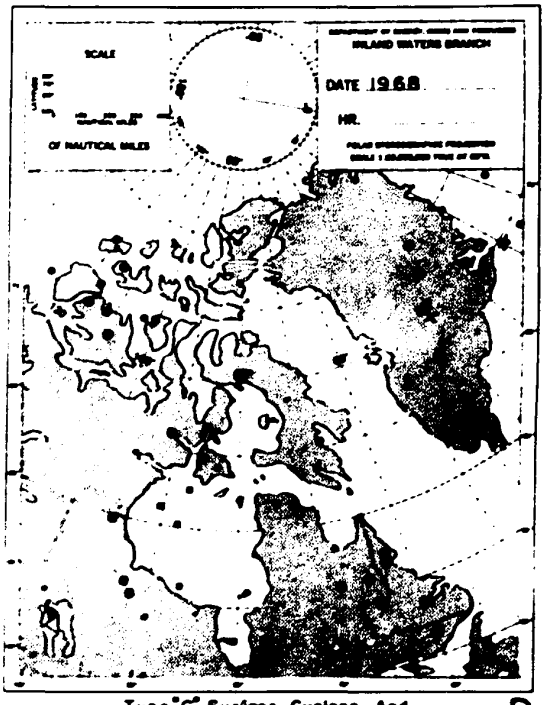

Type "G" Surface Cyclone And Anticyclone Centres

D

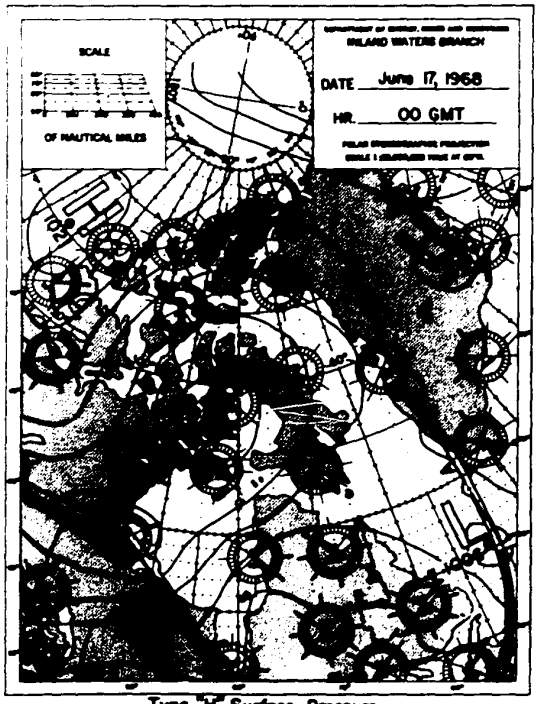

Type "H" Surface Pressure

A

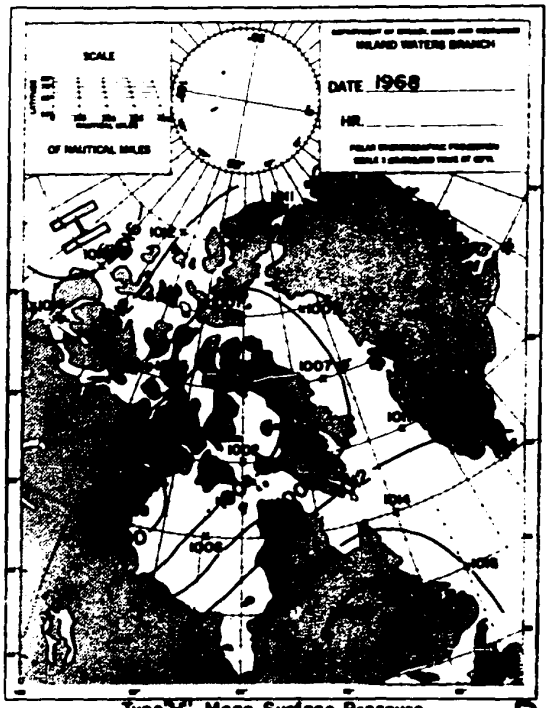

Type "H" Mean Surface Pressure

B

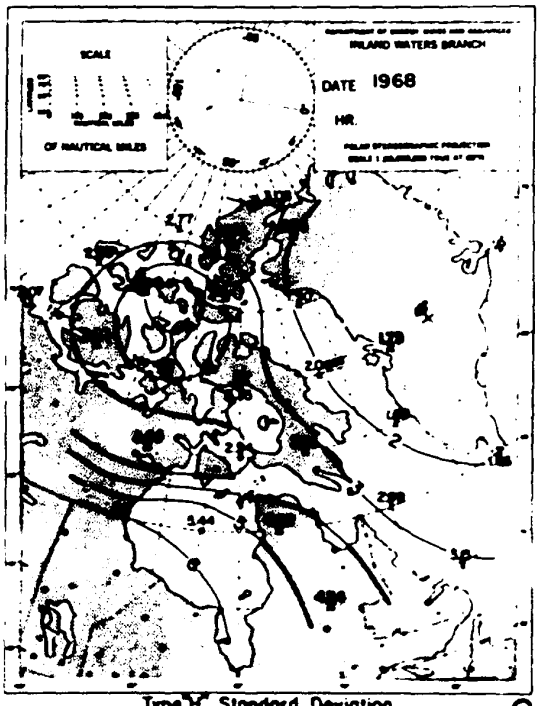

Type "H" Standard Deviation

C

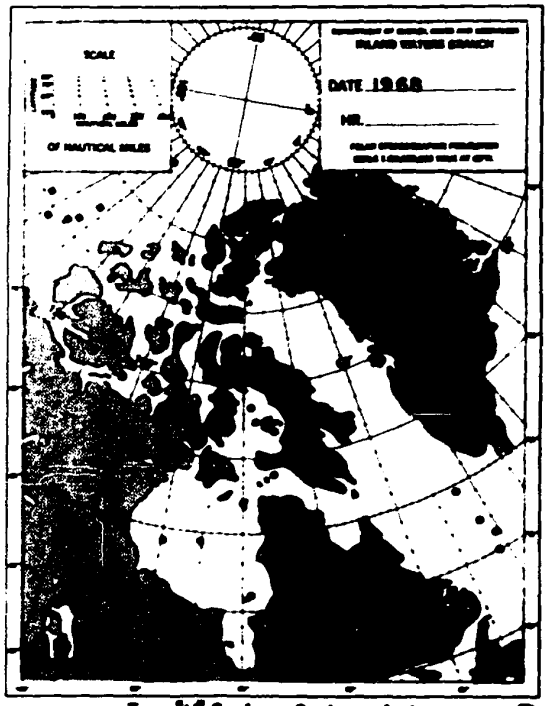

Type "H" Surface Cyclone And Anticyclone Centres

D

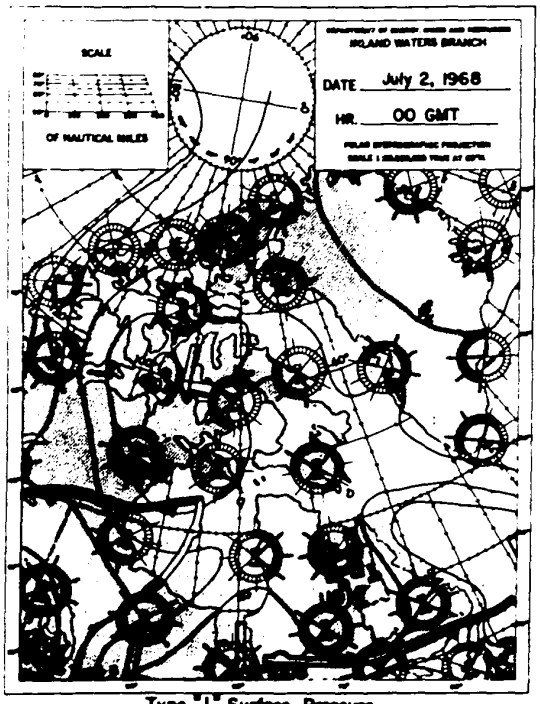

Type "I" Surface Pressure

A

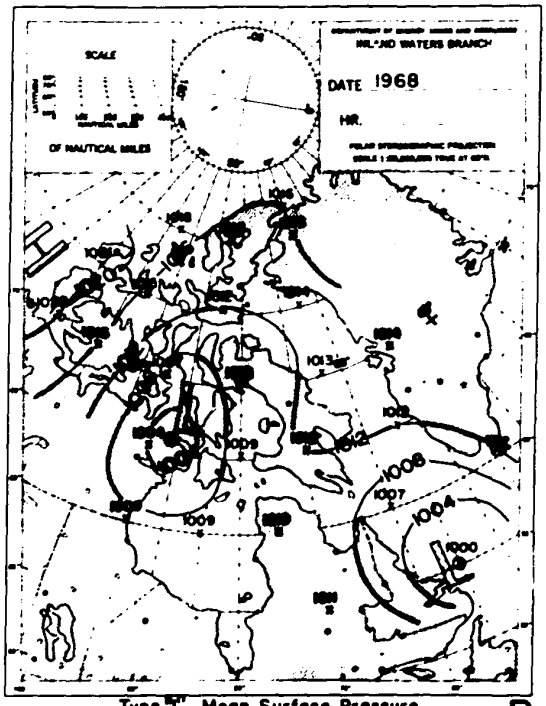

Type "I" Mean Surface Pressure

B

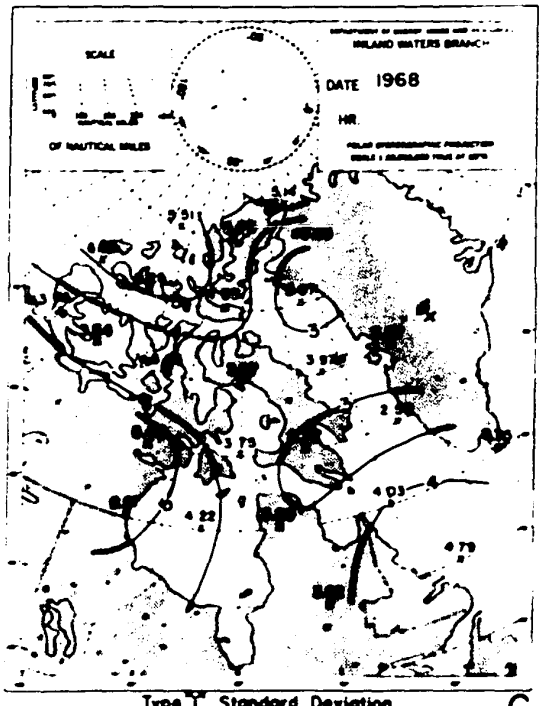

Type "I" Standard Deviation

C

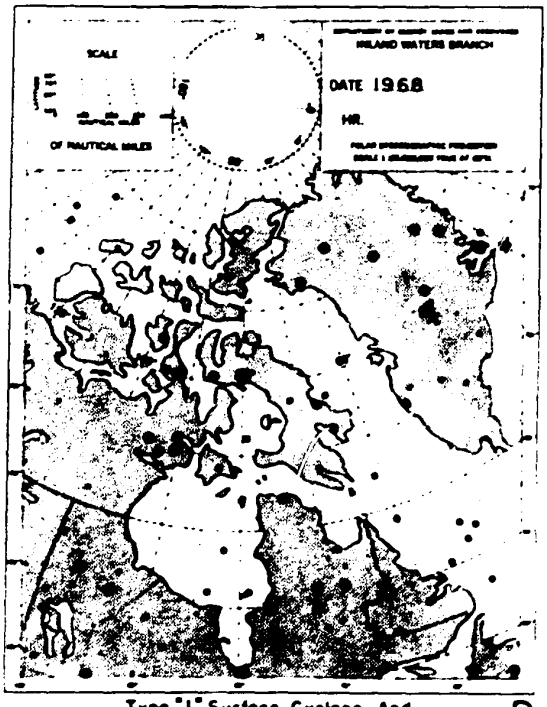

Type "I" Surface Cyclone And Anticyclone Centres

D

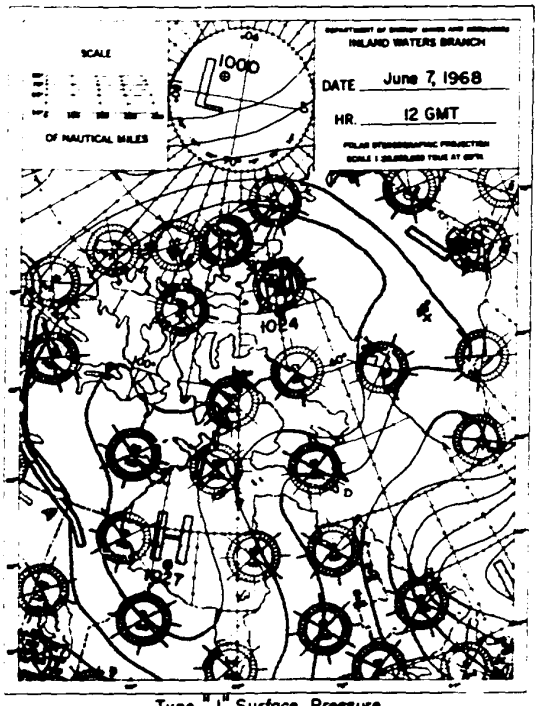

Type "J" Surface Pressure

A

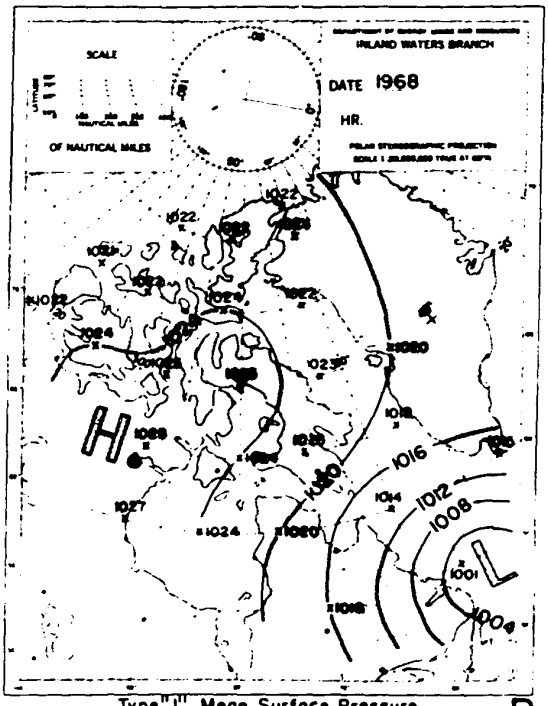

Type "J" Mean Surface Pressure

B

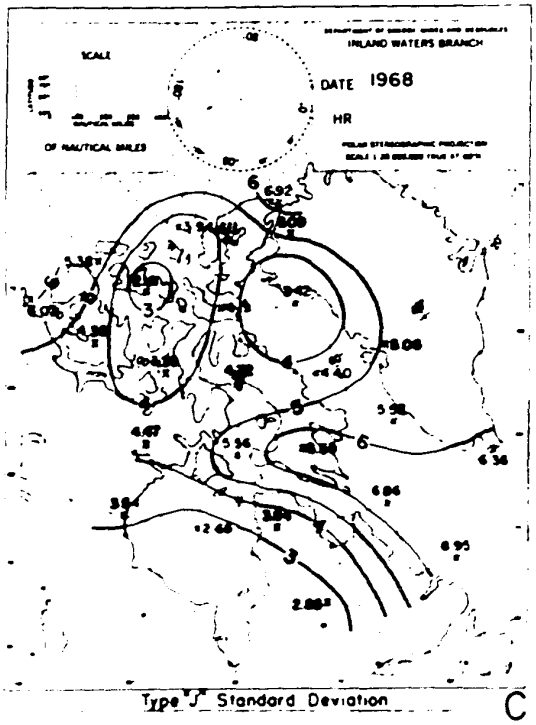

Type "J" Standard Deviation

C

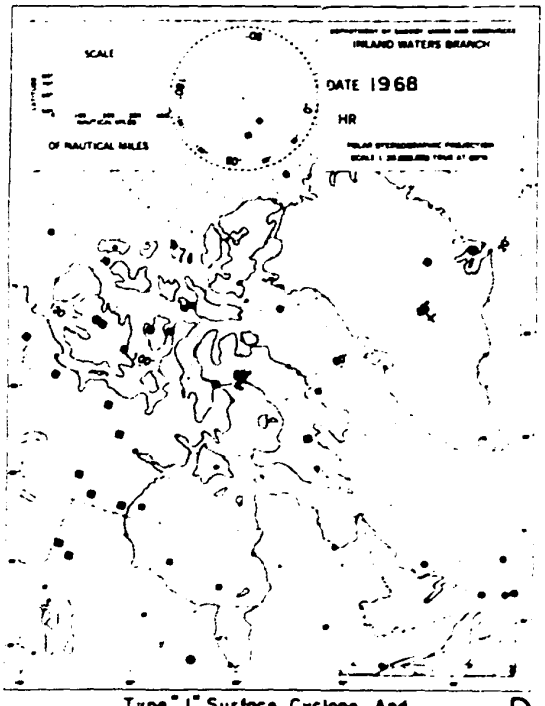

Type "J" Surface Cyclone And Anticyclone Centres

D

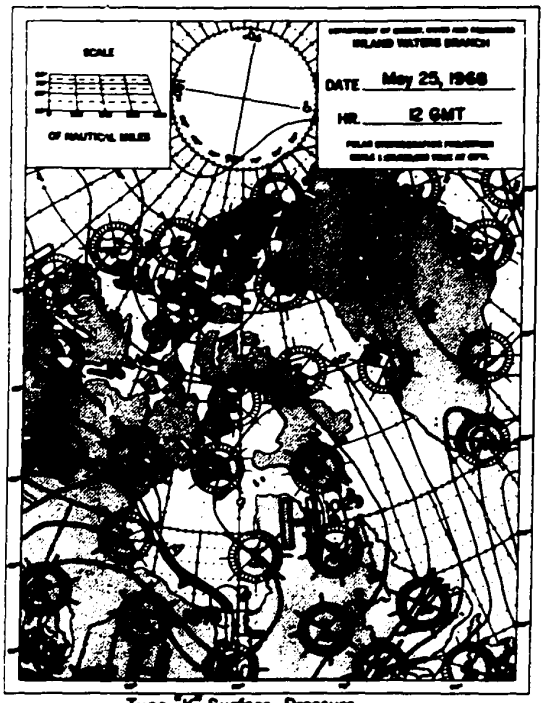

Type "K" Surface Pressure

A

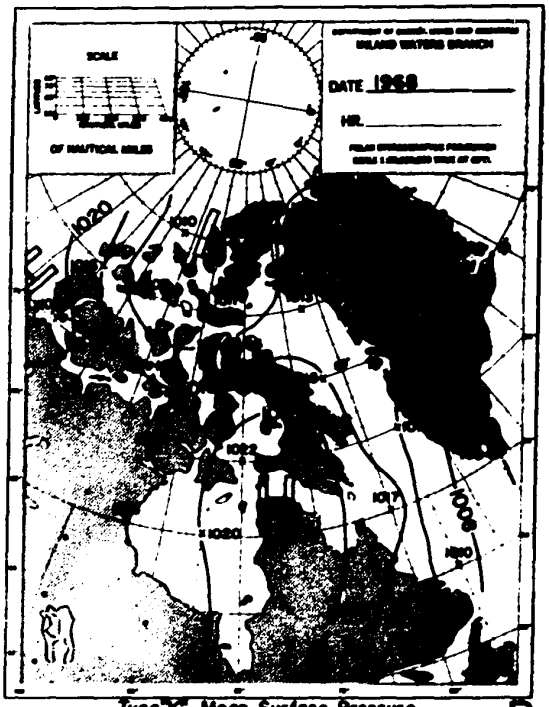

Type "K" Mean Surface Pressure

B

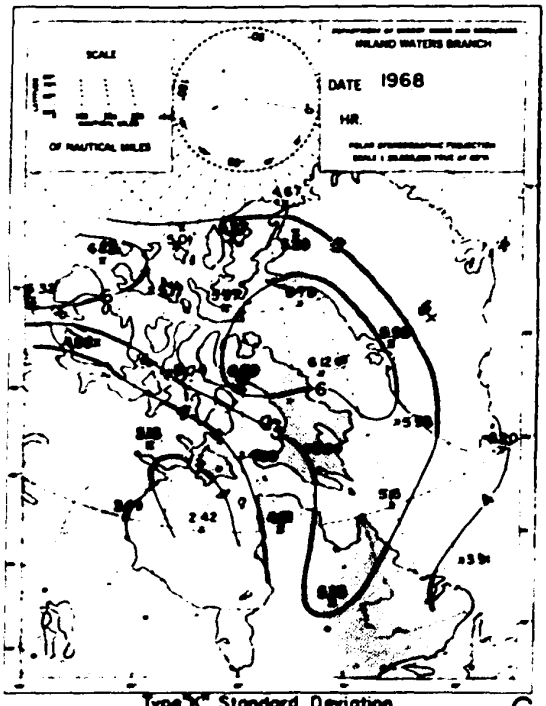

Type "K" Standard Deviation

C

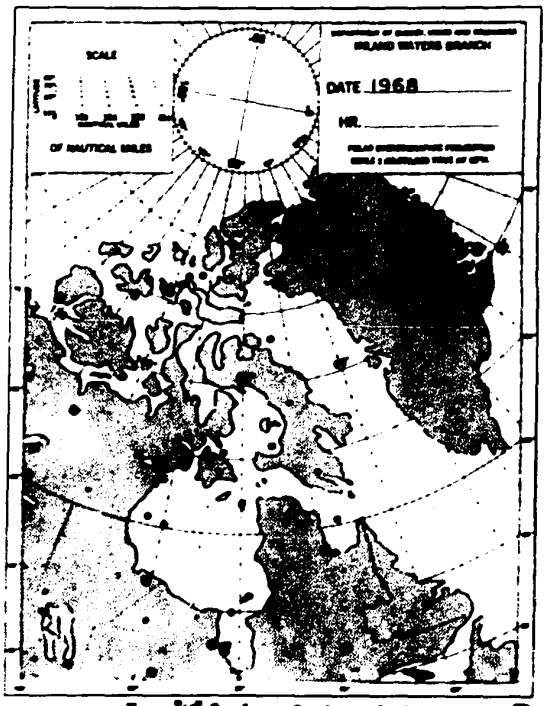

Type "K" Surface Cyclone And Anticyclone Centres

D

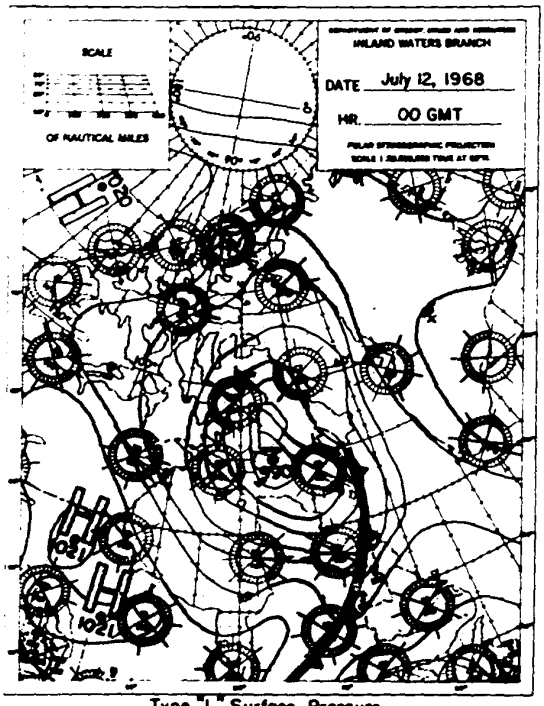

Type "L" Surface Pressure

A

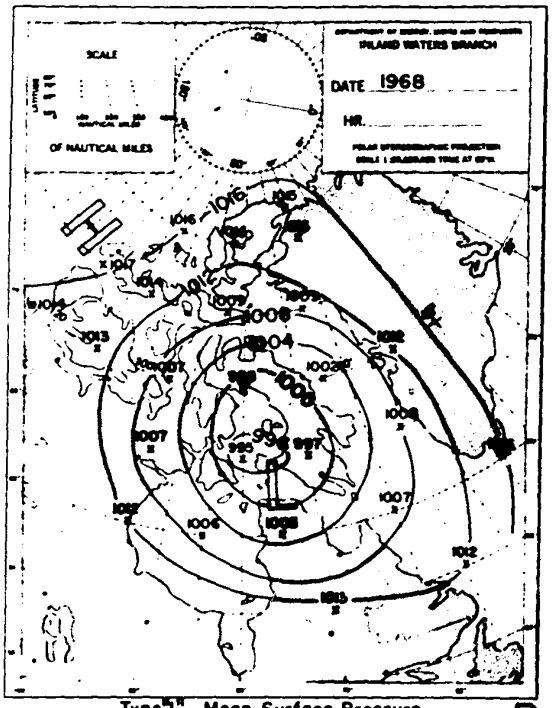

Type "L" Mean Surface Pressure

B

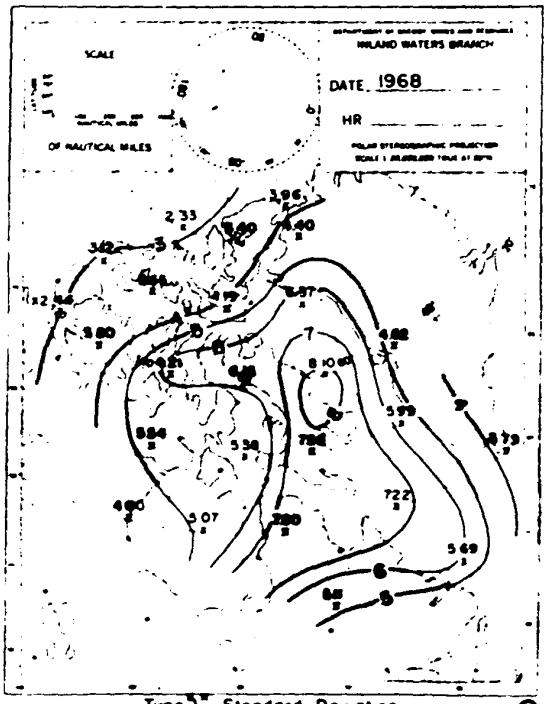

Type "L" Standard Deviation

C

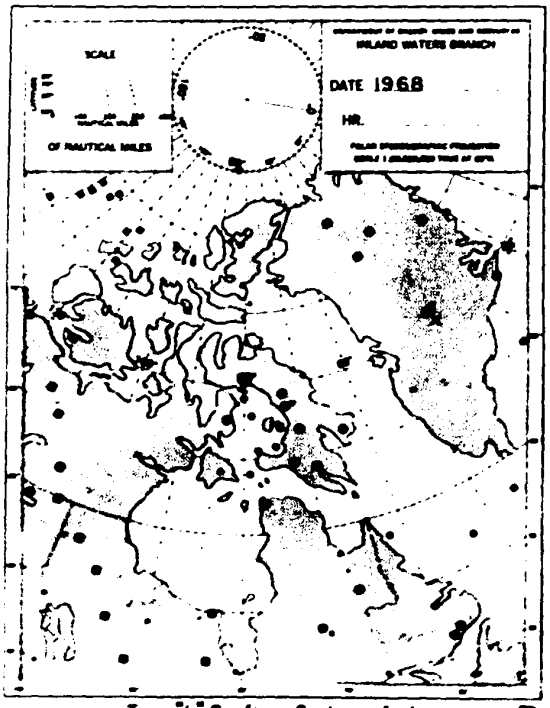

Type "L" Surface Cyclone And Anticyclone Centres

D

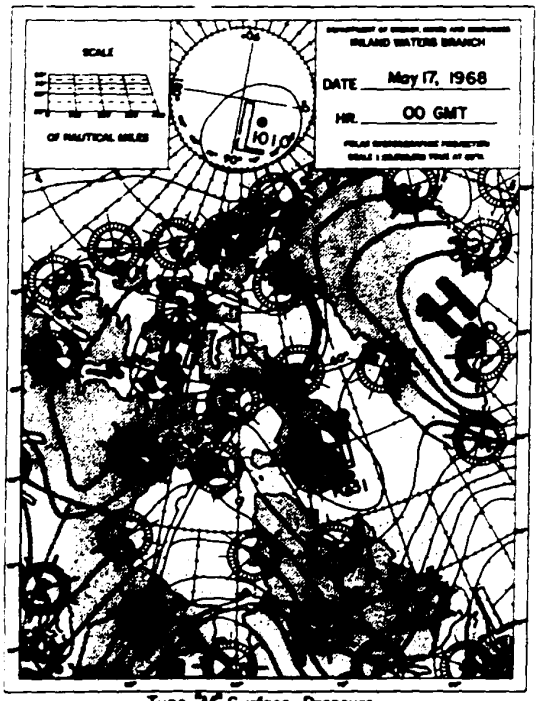

Type "M" Surface Pressure

A

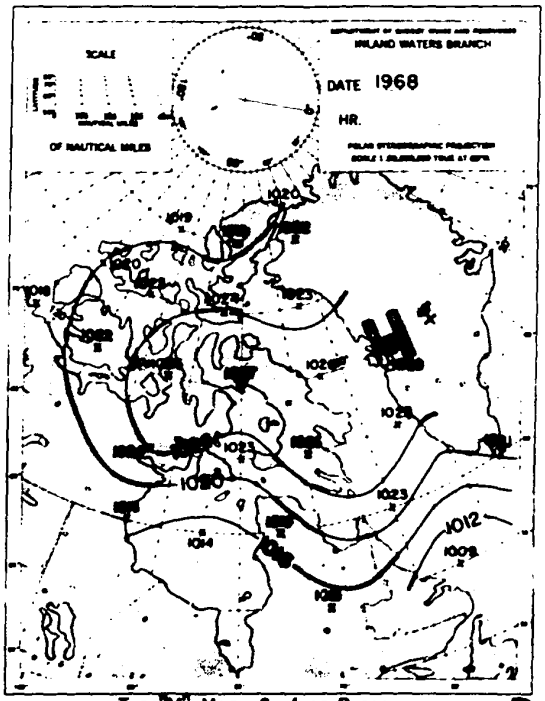

Type "M" Mean Surface Pressure

B

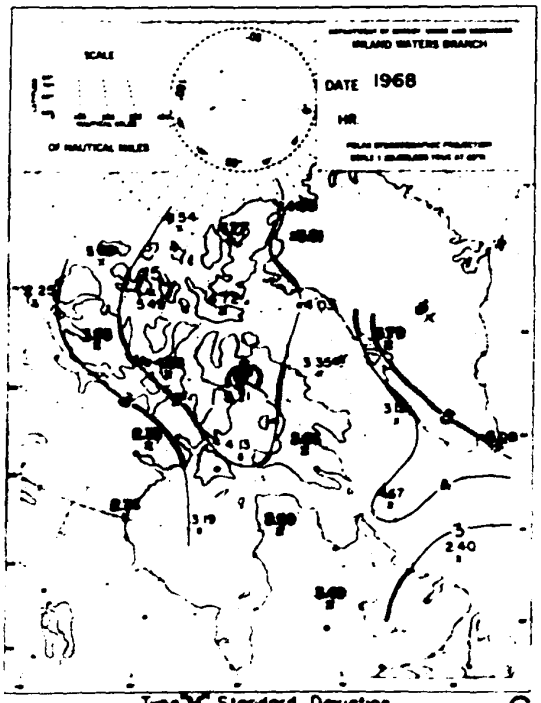

Type "M" Standard Deviation

C

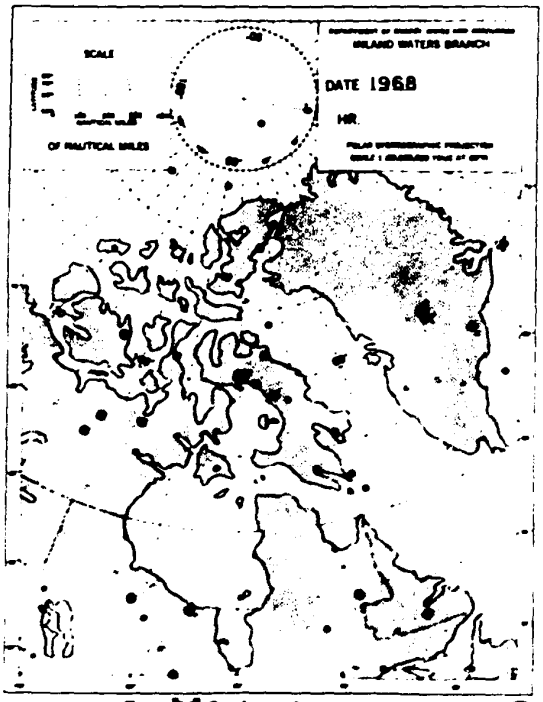

Type "M" Surface Cyclone And Anticyclone Centres

D

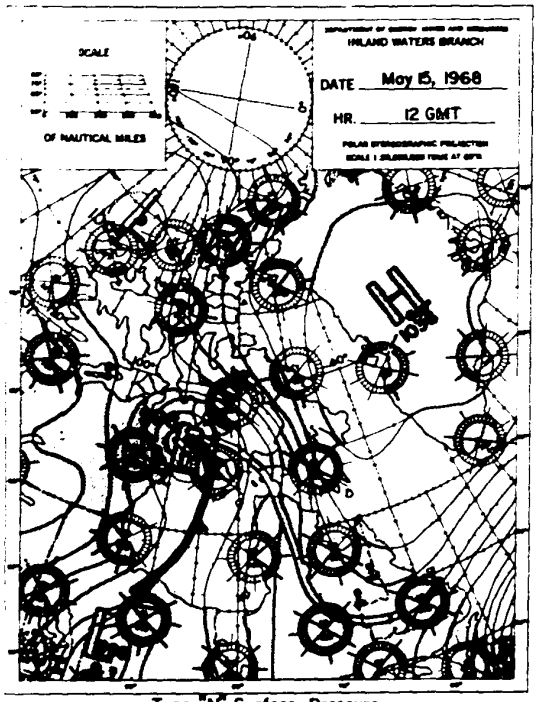

Type "N" Surface Pressure

A

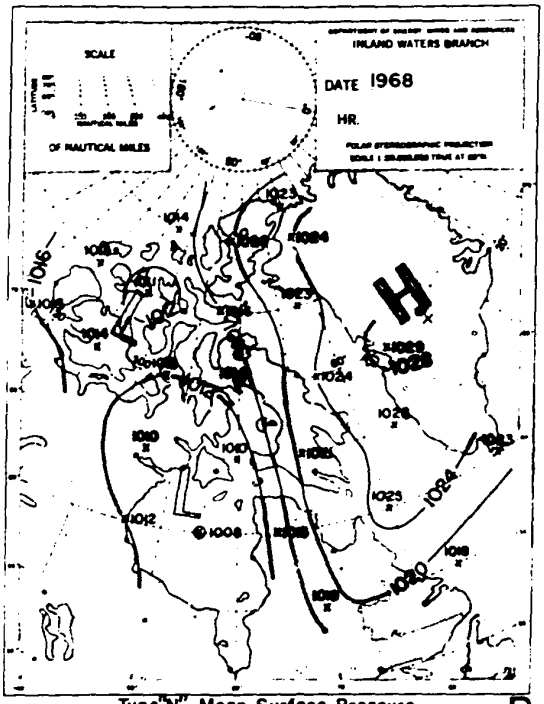

Type "N" Mean Surface Pressure

B

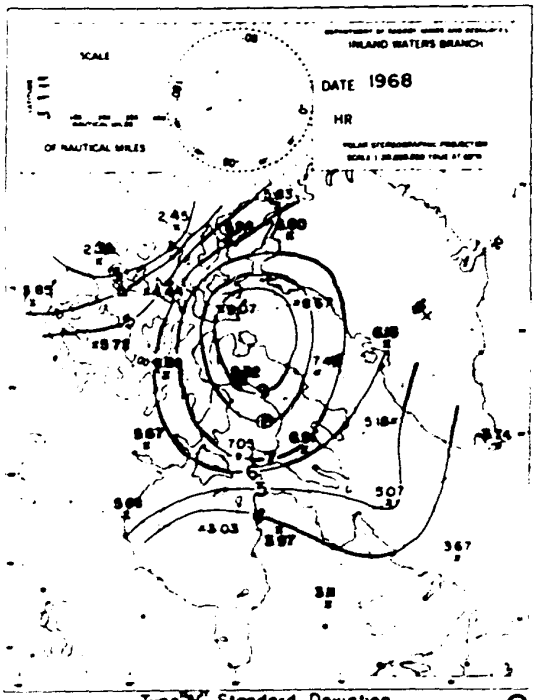

Type "N" Standard Deviation

C

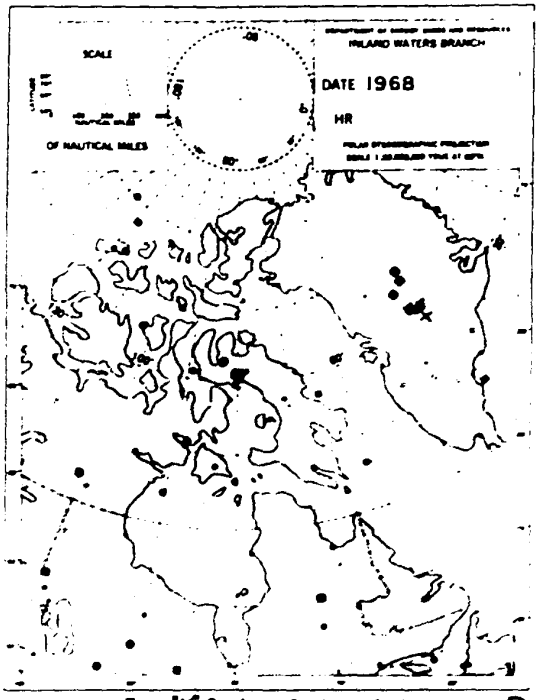

Type "N" Surface Cyclone And Anticyclone Centres

D

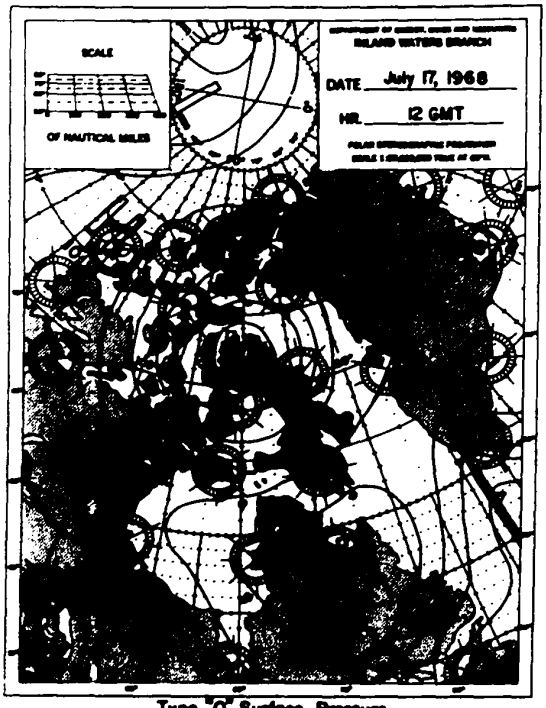

Type "O" Surface Pressure

A

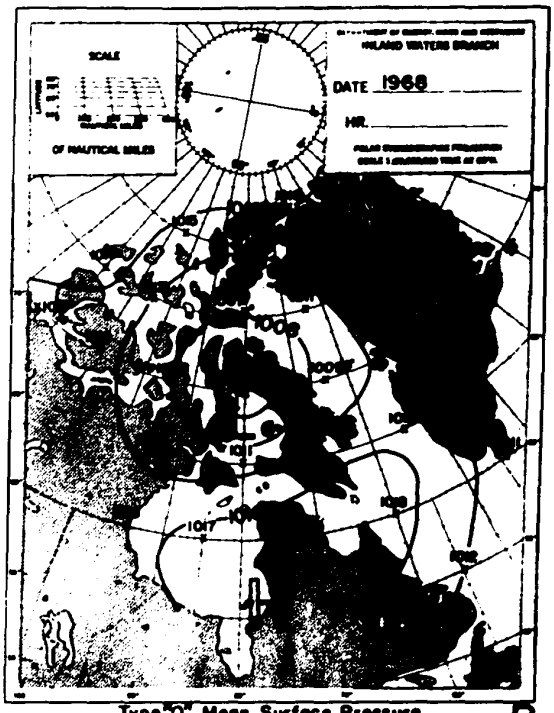

Type "O" Mean Surface Pressure

B

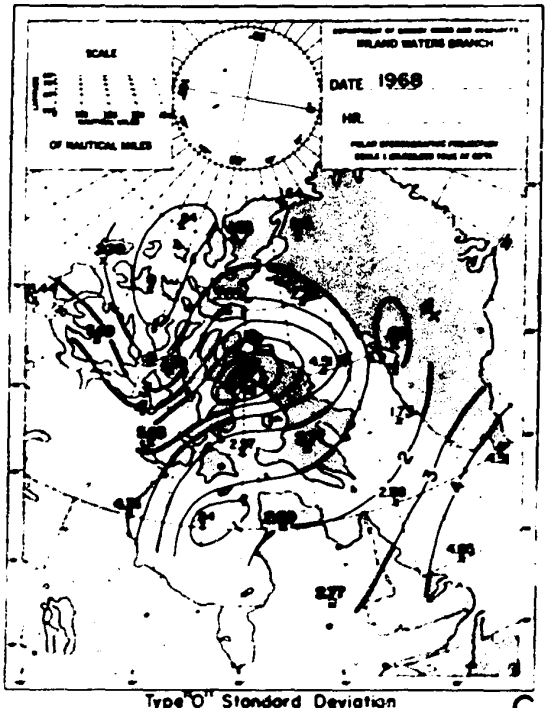

Type "O" Standard Deviation

C

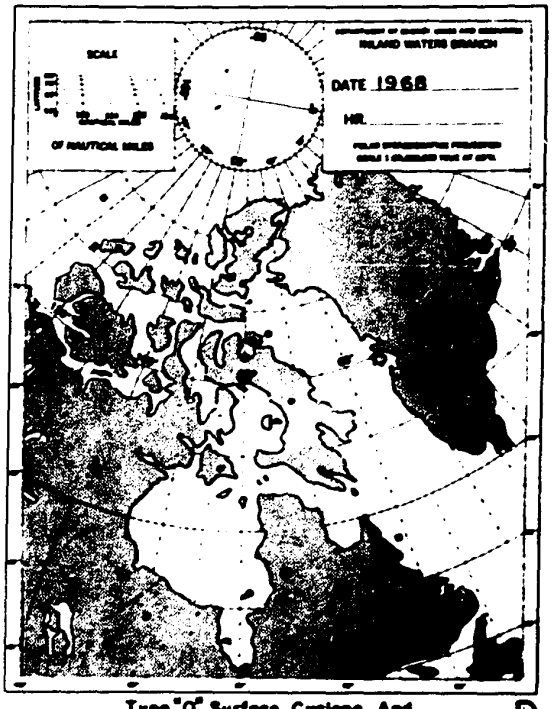

Type "O" Surface Cyclone And Anticyclone Centres

D

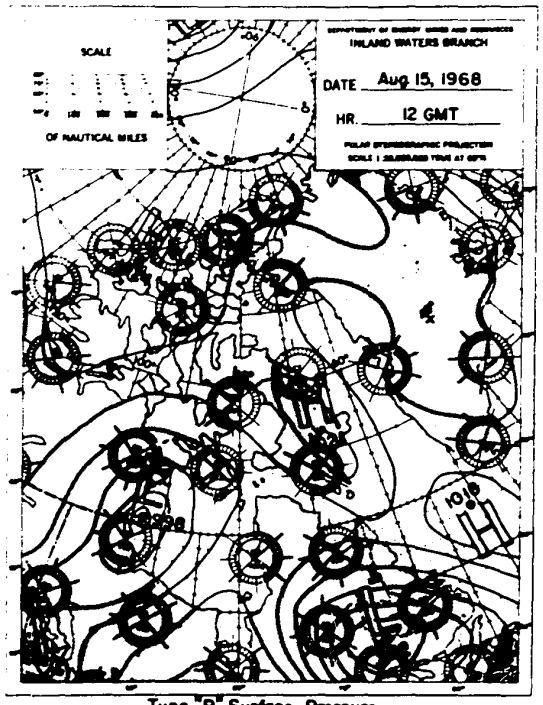

Type "P" Surface Pressure

A

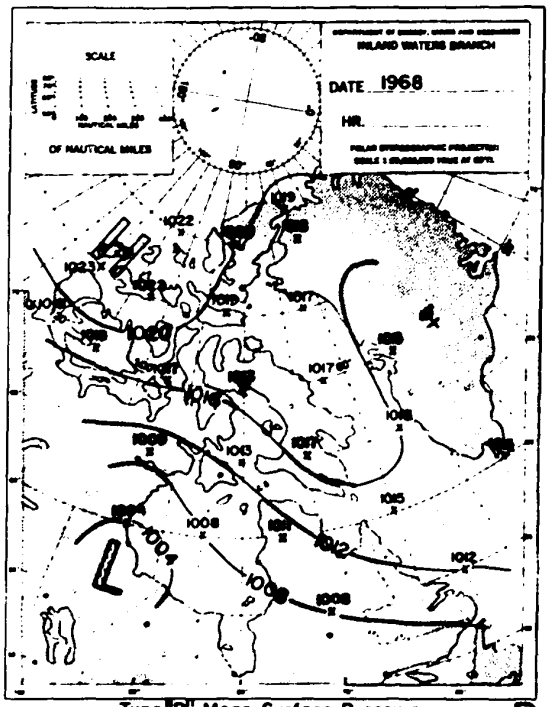

Type "P" Mean Surface Pressure

B

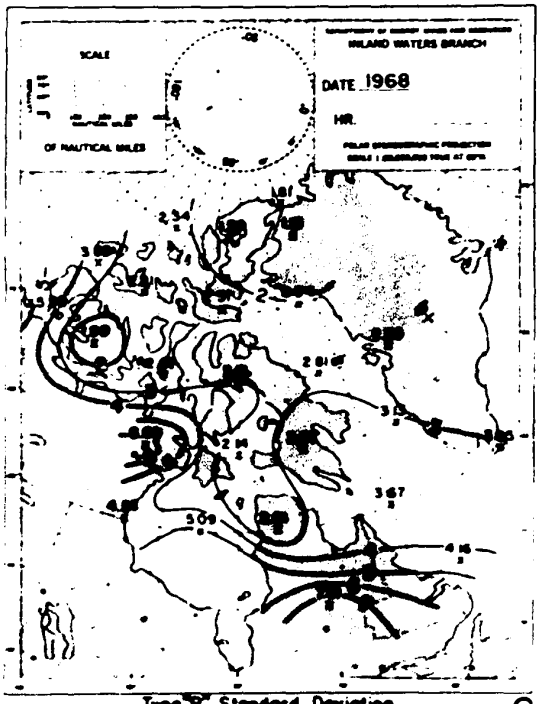

Type "P" Standard Deviation

C

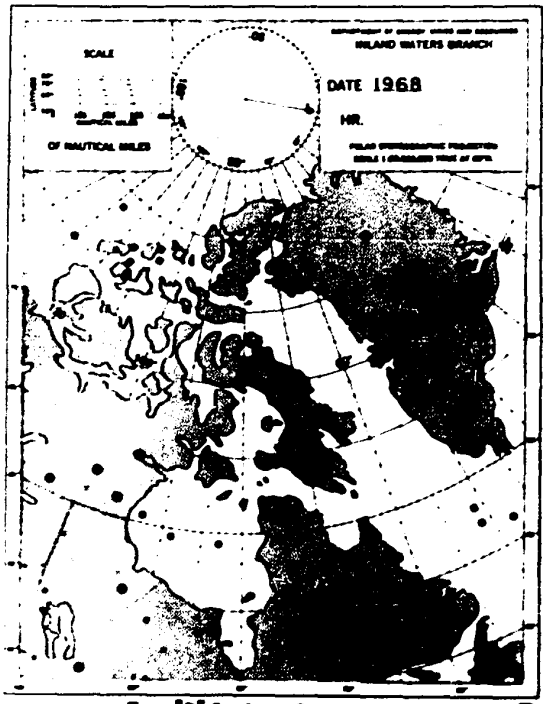

Type "P" Surface Cyclone And Anticyclone Centres

D

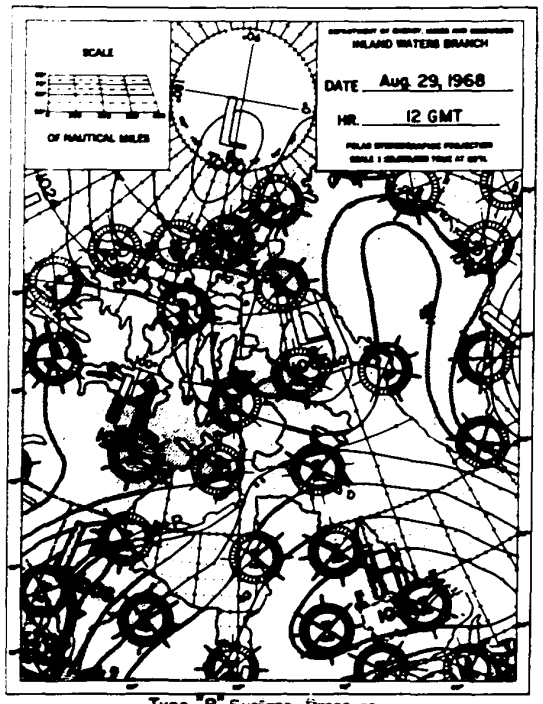

Type "R" Surface Pressure

A

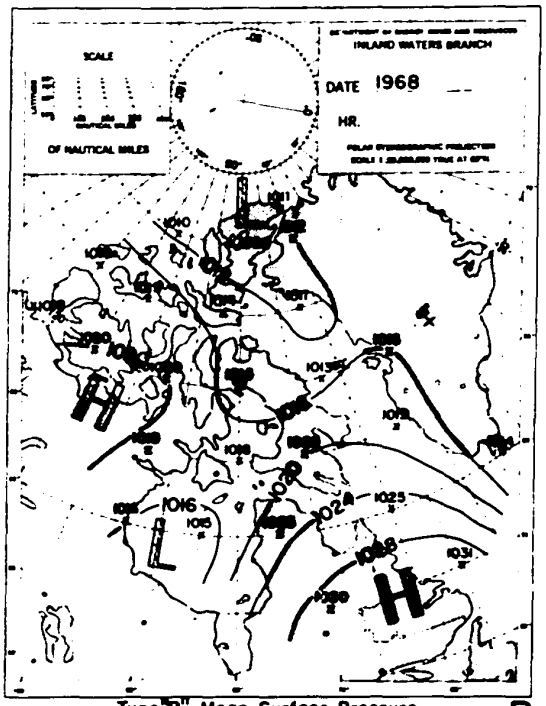

Type "R" Mean Surface Pressure

B

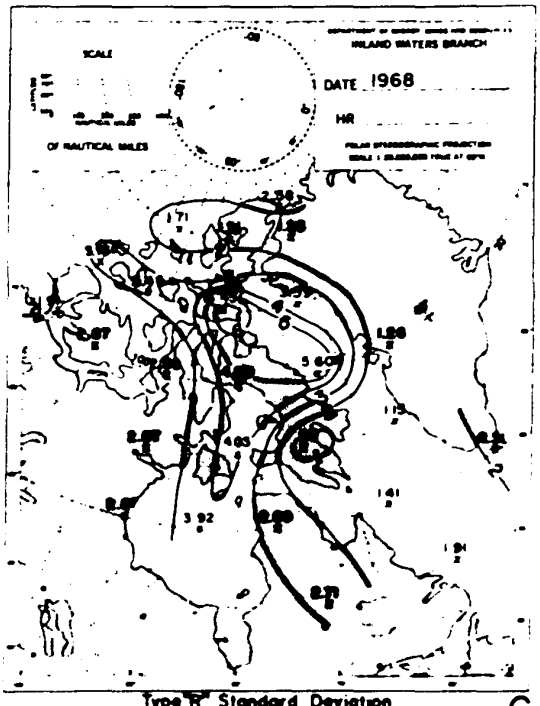

Type "R" Standard Deviation

C

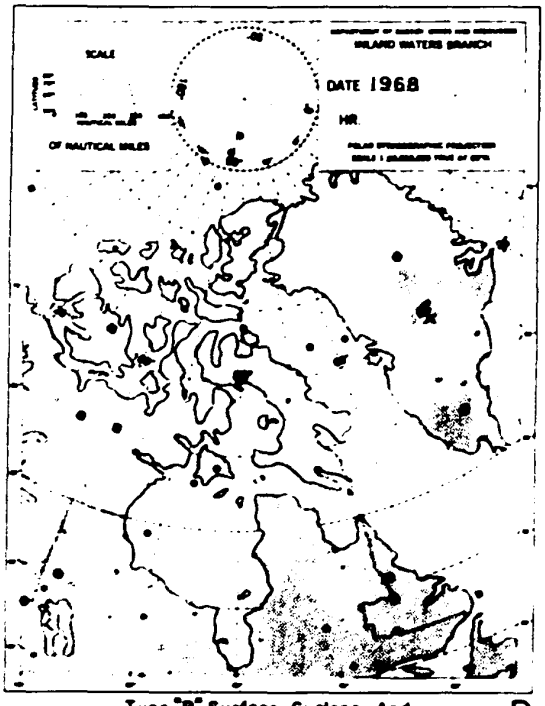

Type "R" Surface Cyclone And Anticyclone Centres

D

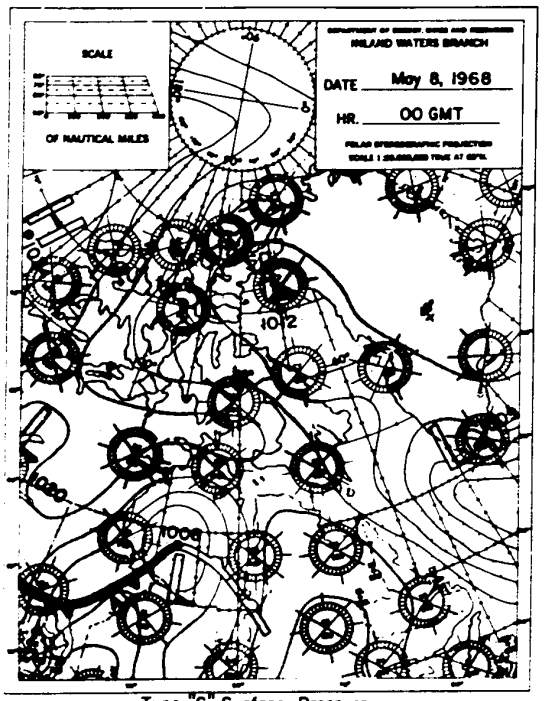

Type "S" Surface Pressure

A

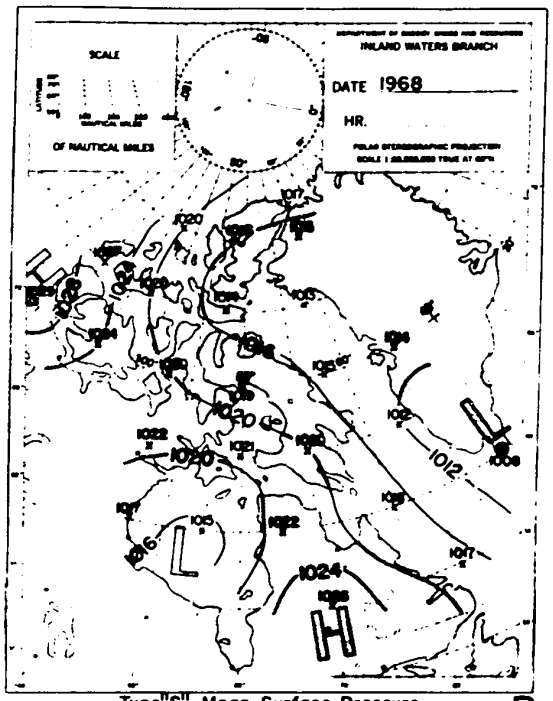

Type "S" Mean Surface Pressure

B

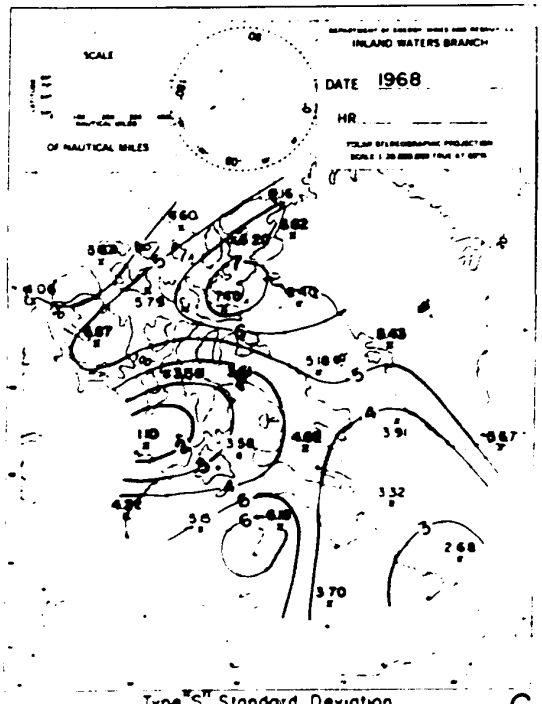

Type "S" Standard Deviation

C

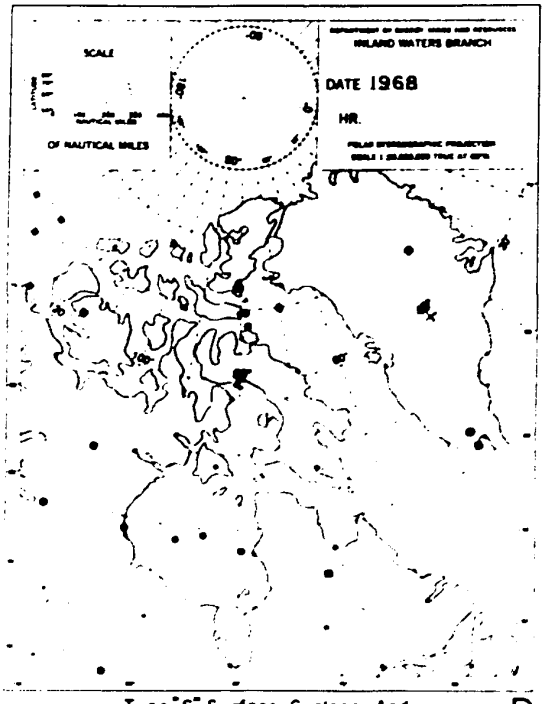

Type "S" Surface Cyclone And Anticyclone Centres

D

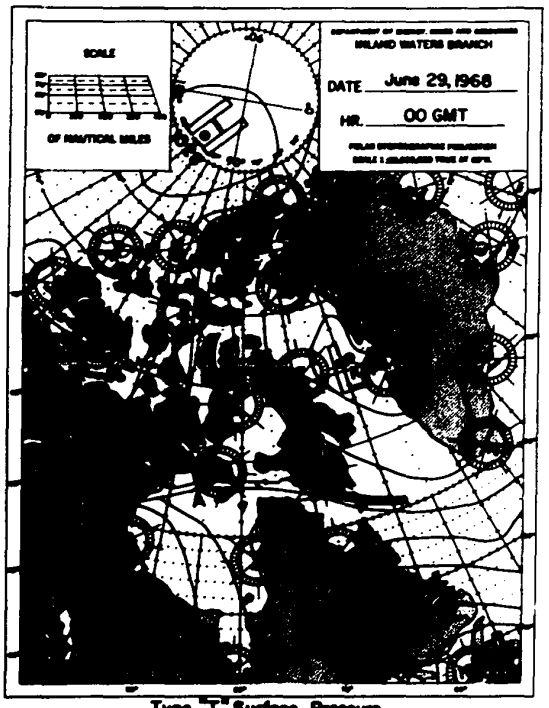

Type "T" Surface Pressure

A

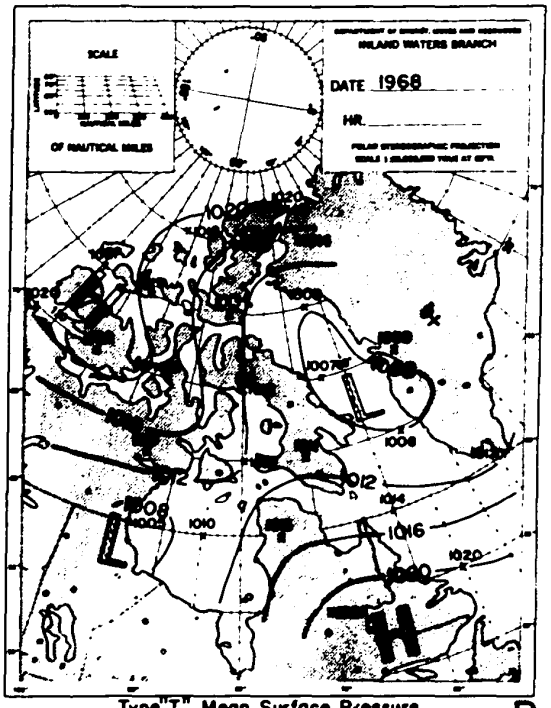

Type "T" Mean Surface Pressure

B

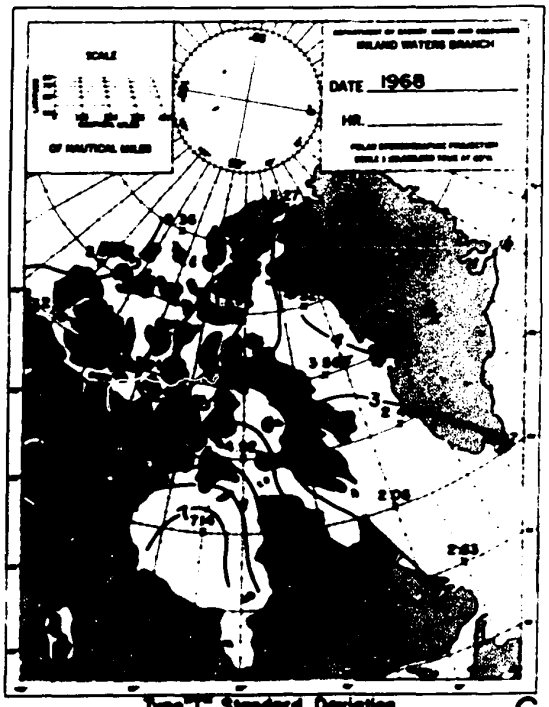

Type "T" Standard Deviation

C

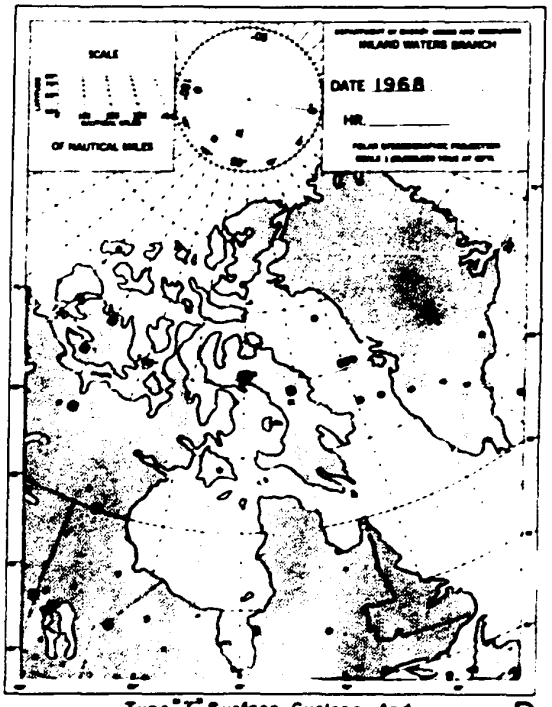

Type "T" Surface Cyclone And Anticyclone Centres

D

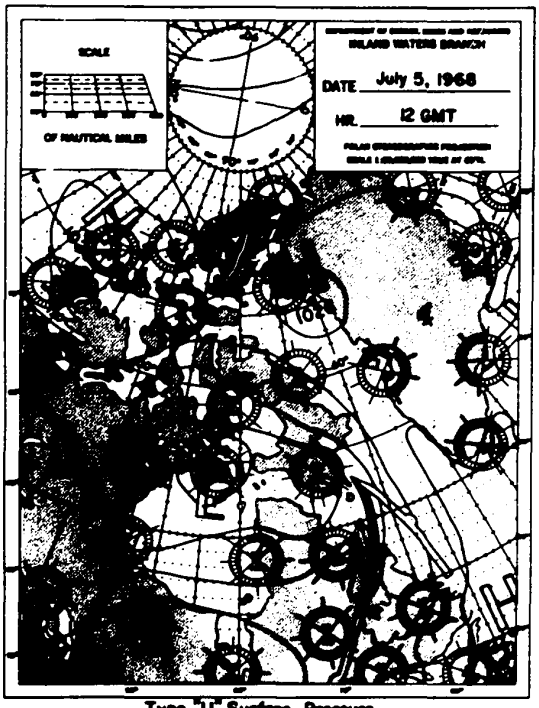

Type "U" Surface Pressure

A

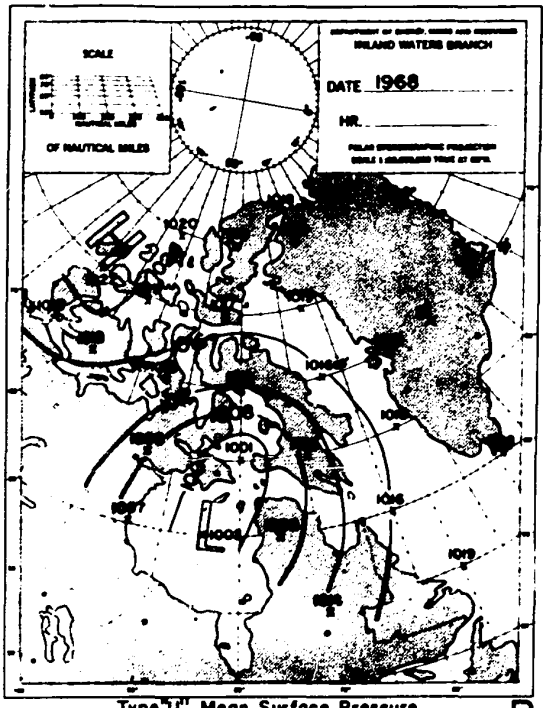

Type "U" Mean Surface Pressure

B

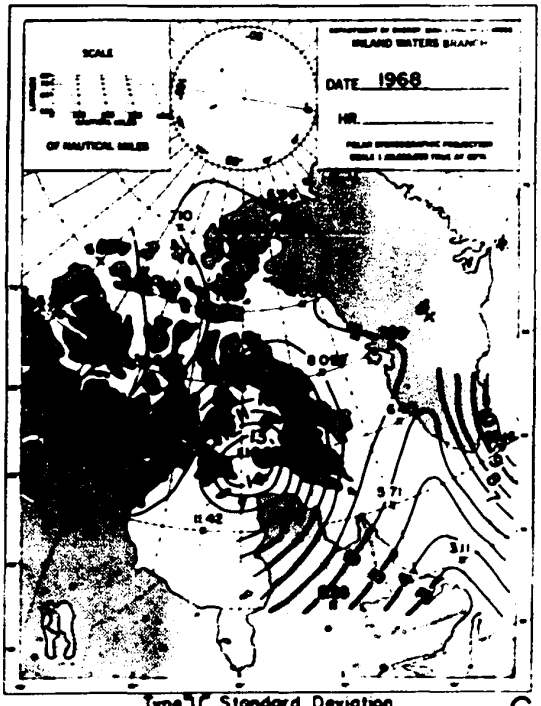

Type "U" Standard Deviation

C

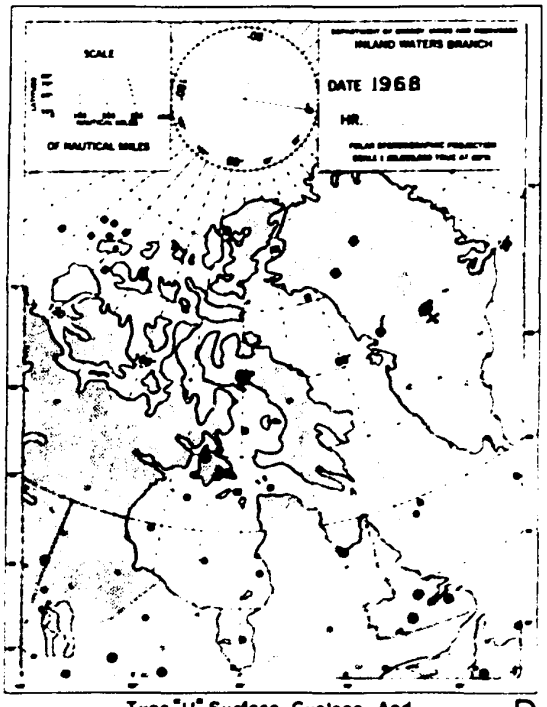

Type "U" Surface Cyclone And Anticyclone Centres

D

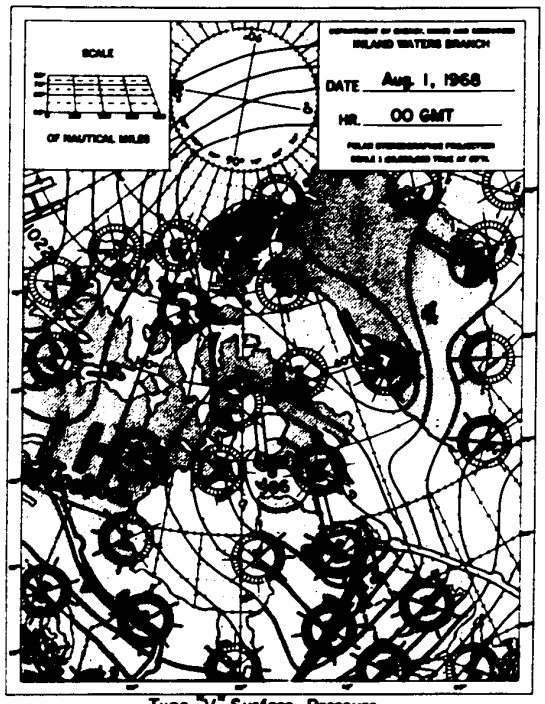

Type "V" Surface Pressure

A

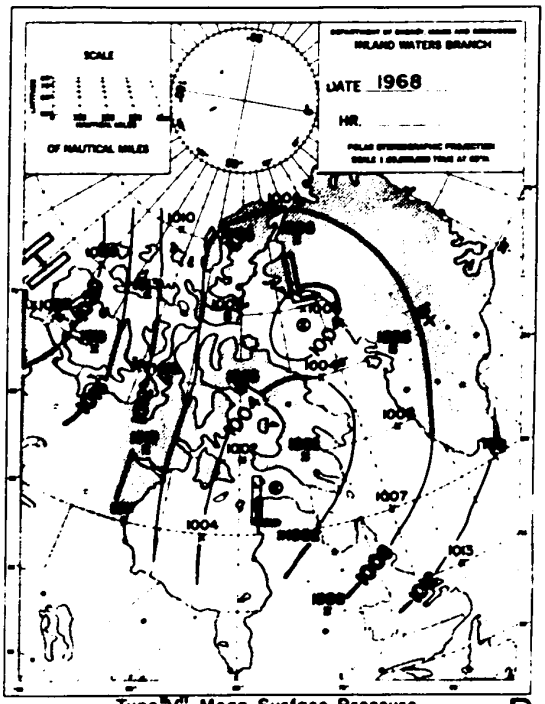

Type "V" Mean Surface Pressure

B

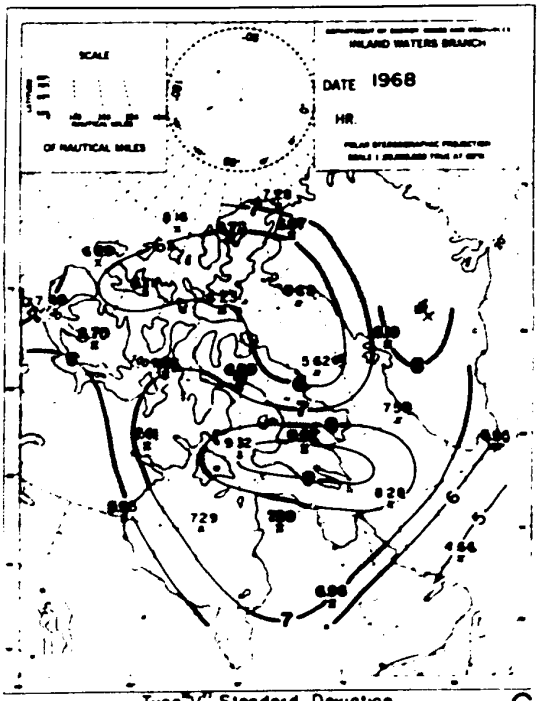

Type "V" Standard Deviation

C

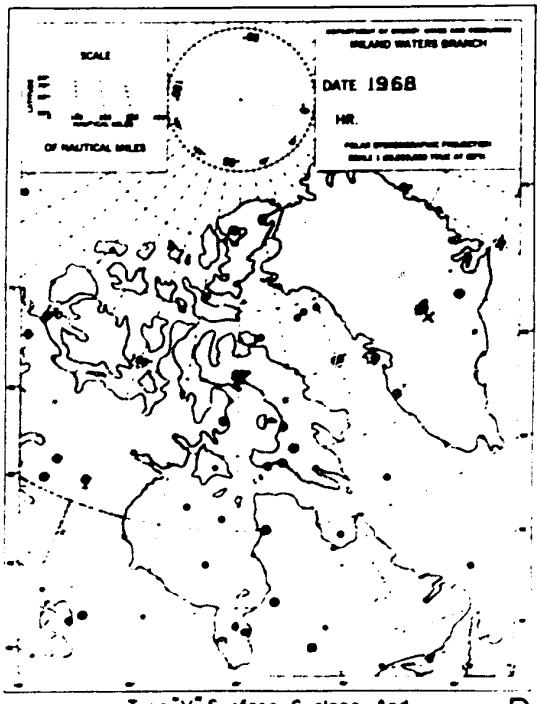

Type "V" Surface Cyclone And Anticyclone Centres

D

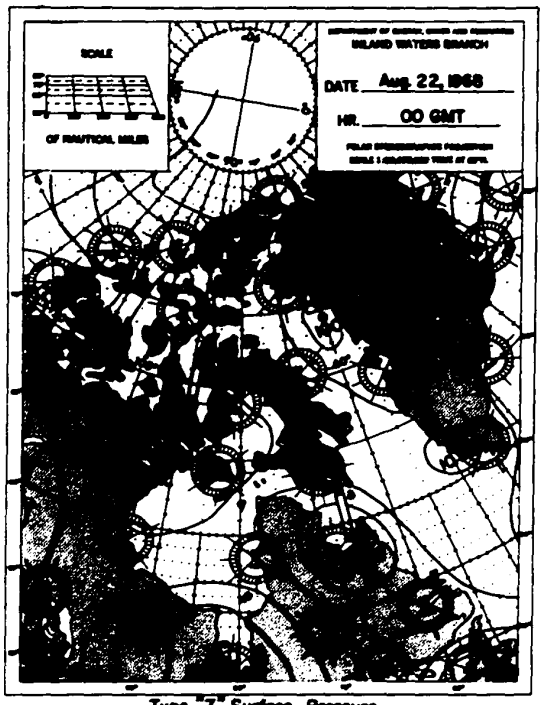

Type "Z" Surface Pressure

A

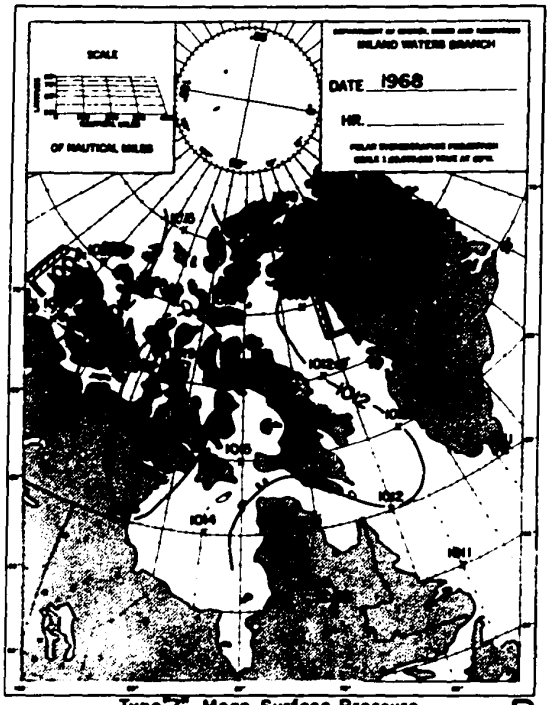

Type "Z" Mean Surface Pressure

B

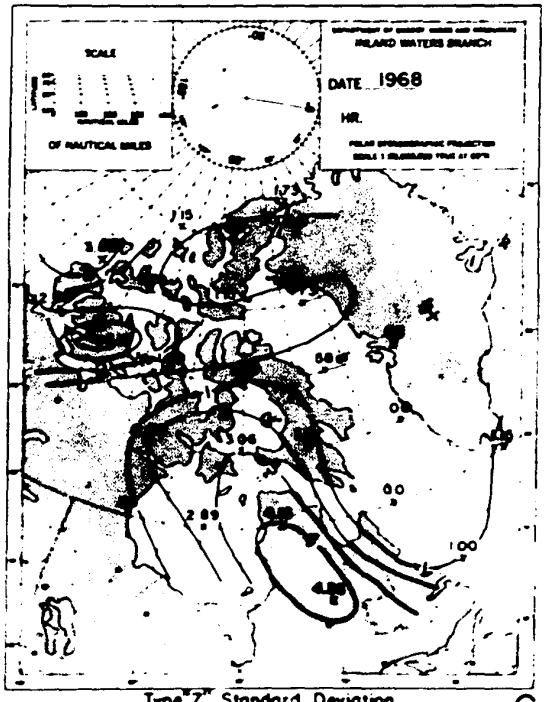

Type "Z" Standard Deviation

C

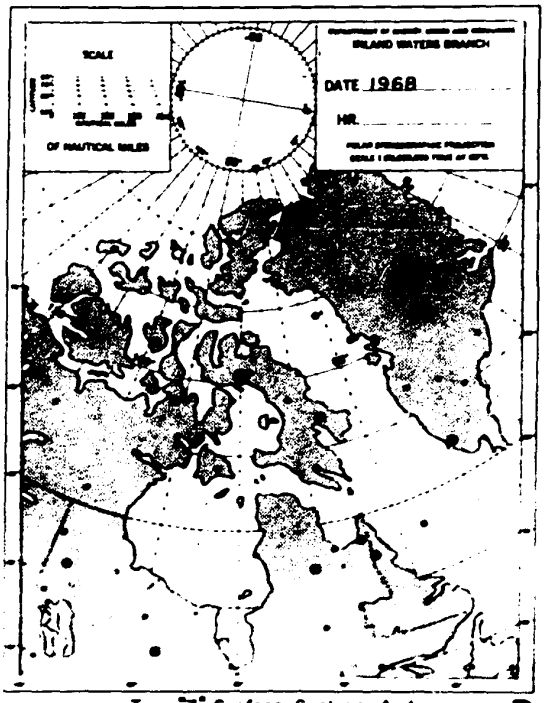

Type "Z" Surface Cyclone And Anticyclone Centres

D

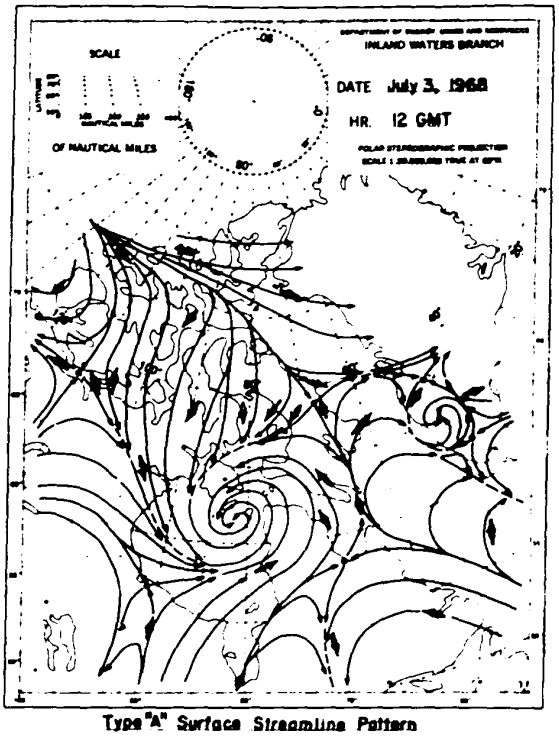

Type "A" Surface Streamline Pattern

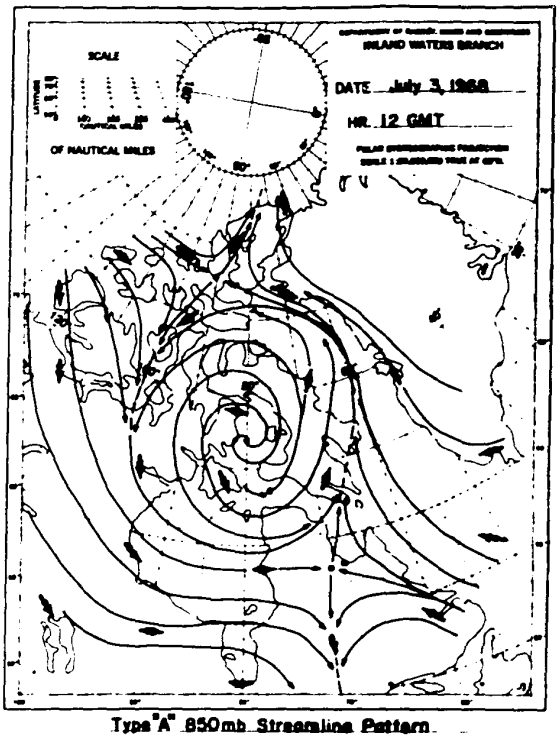

Type "A" 850mb Streamline Pattern

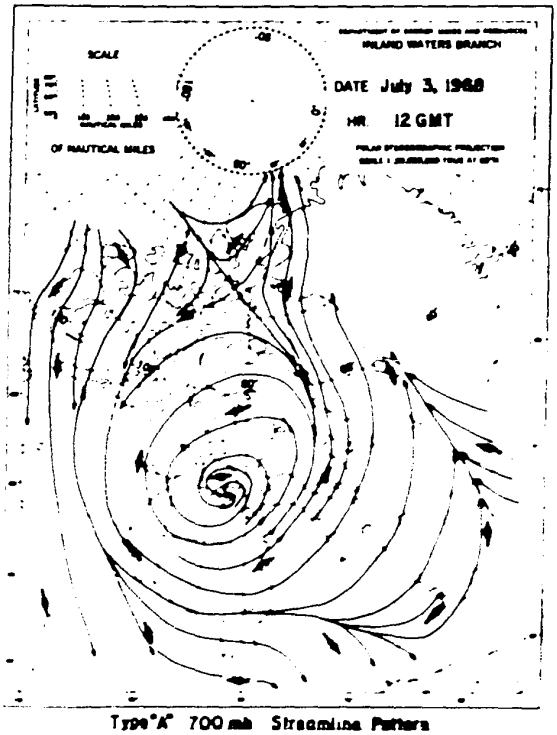

Type "A" 700 mb Streamline Pattern

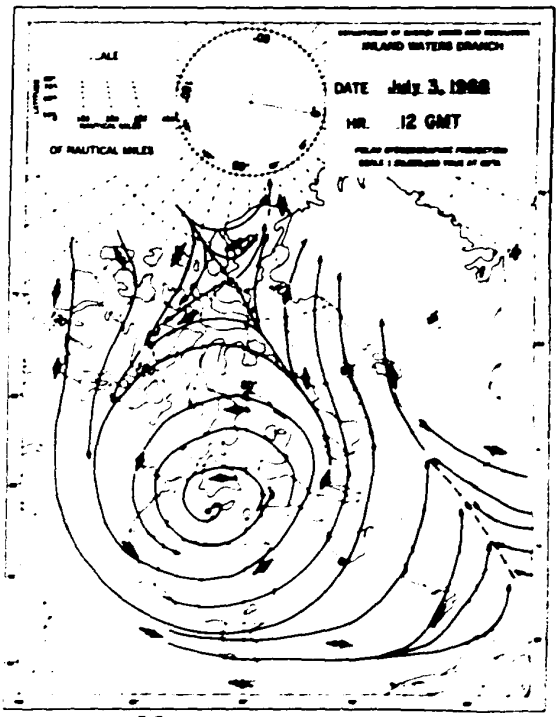

Type "A" 600mb Streamline Pattern

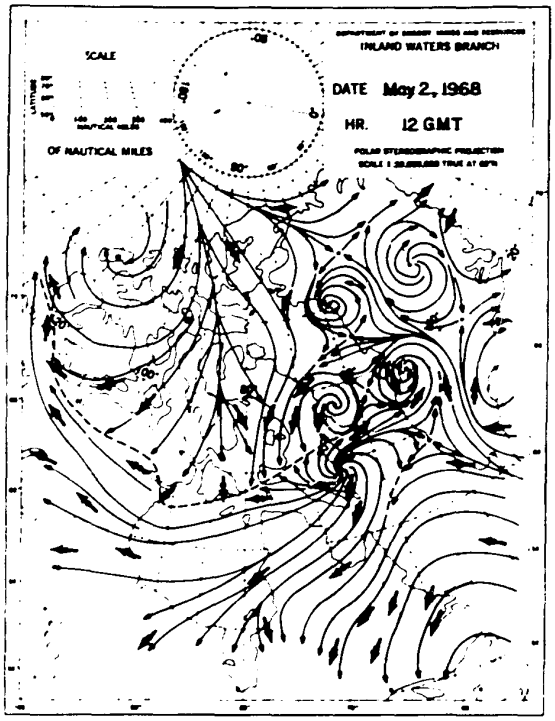

Type "D" Surface Streamline Pattern

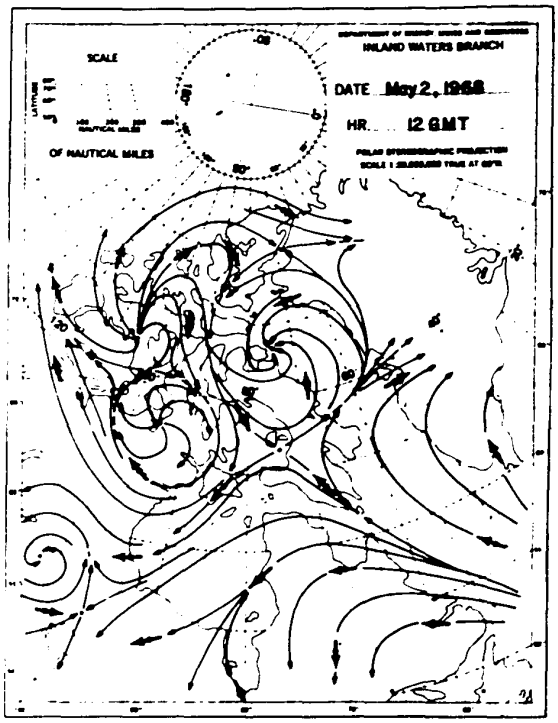

Type "D" 850 mb Streamline Pattern

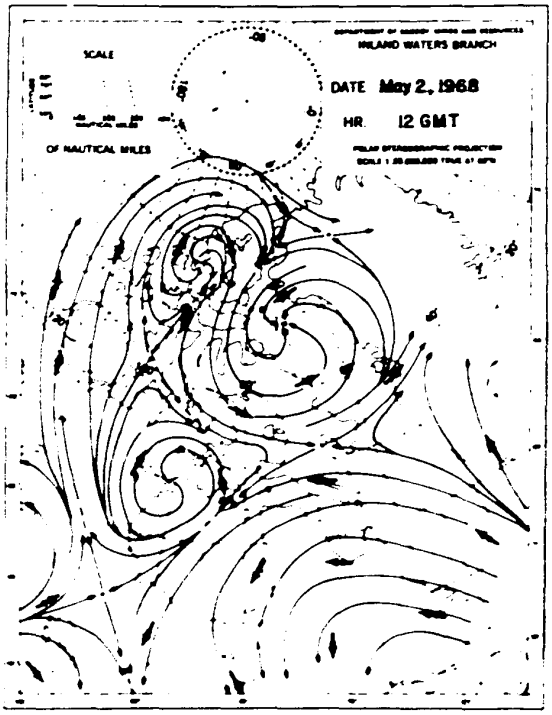

Type "D" 700 mb Streamline Pattern

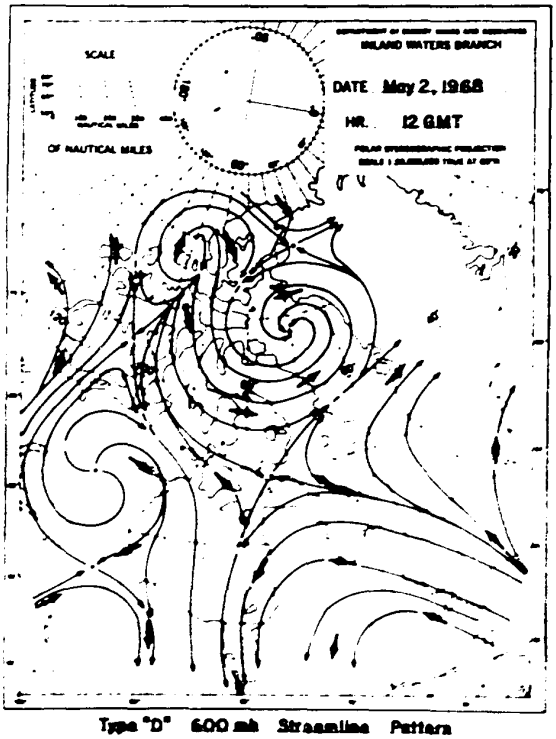

Type "D" 600 mb Streamline Pattern

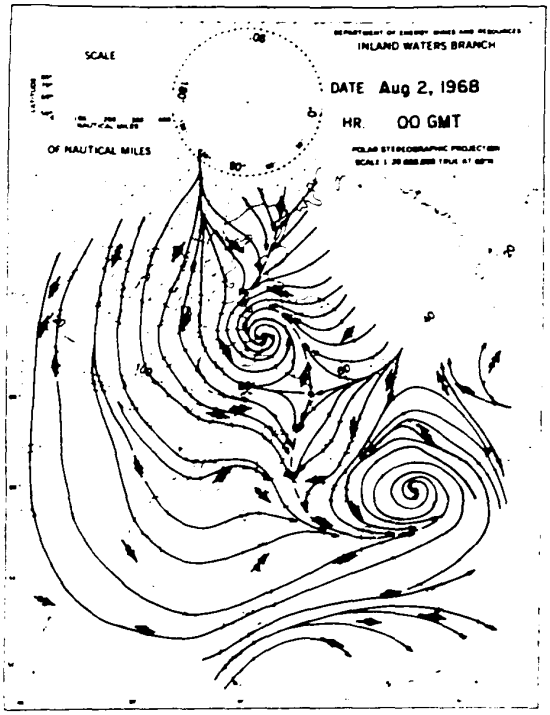

Type"E" Surface Streamline Pattern

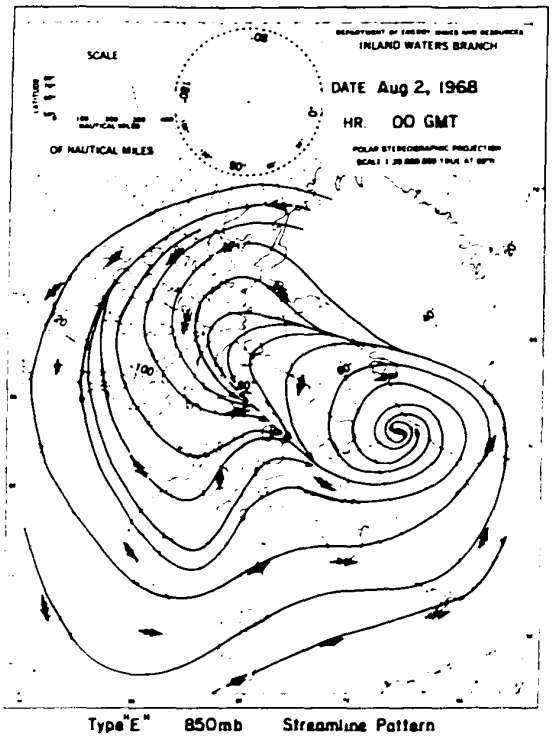

Type"E" 850mb Streamline Pattern

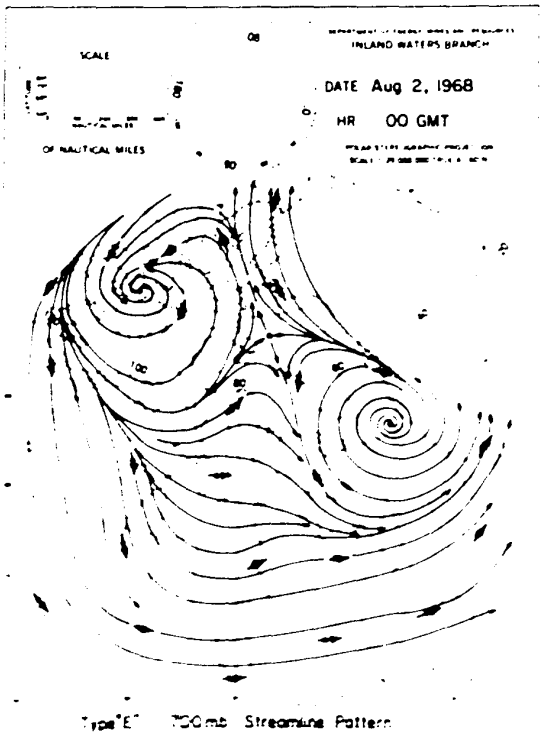

Type"E" 700mb Streamline Pattern

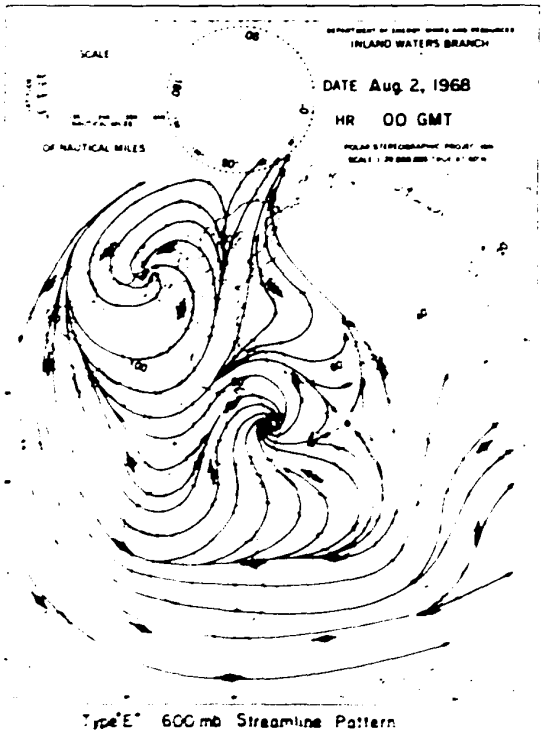

Type"E" 600mb Streamline Pattern

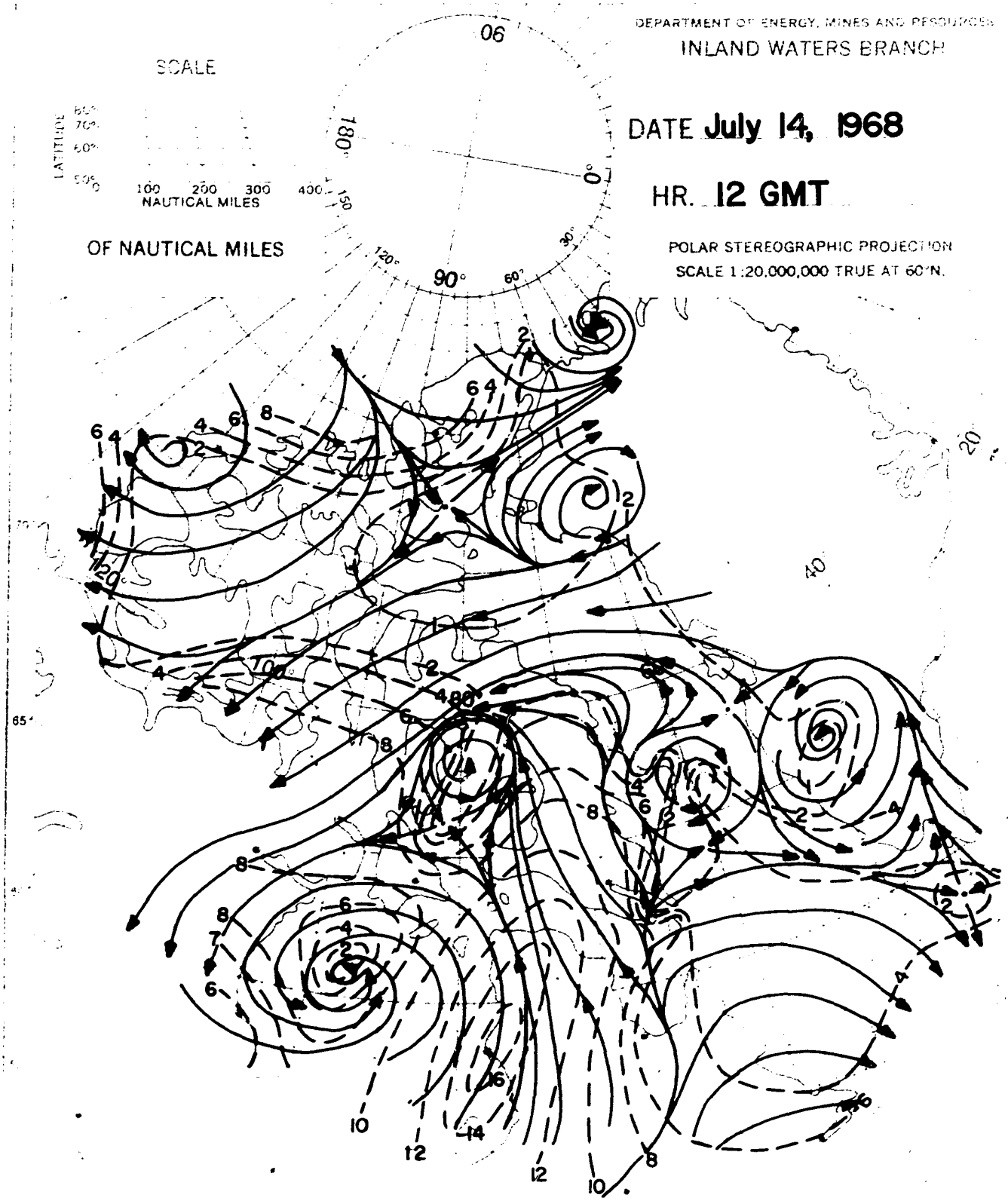

Surface Streamlines with isotachs superimposed Figure 20

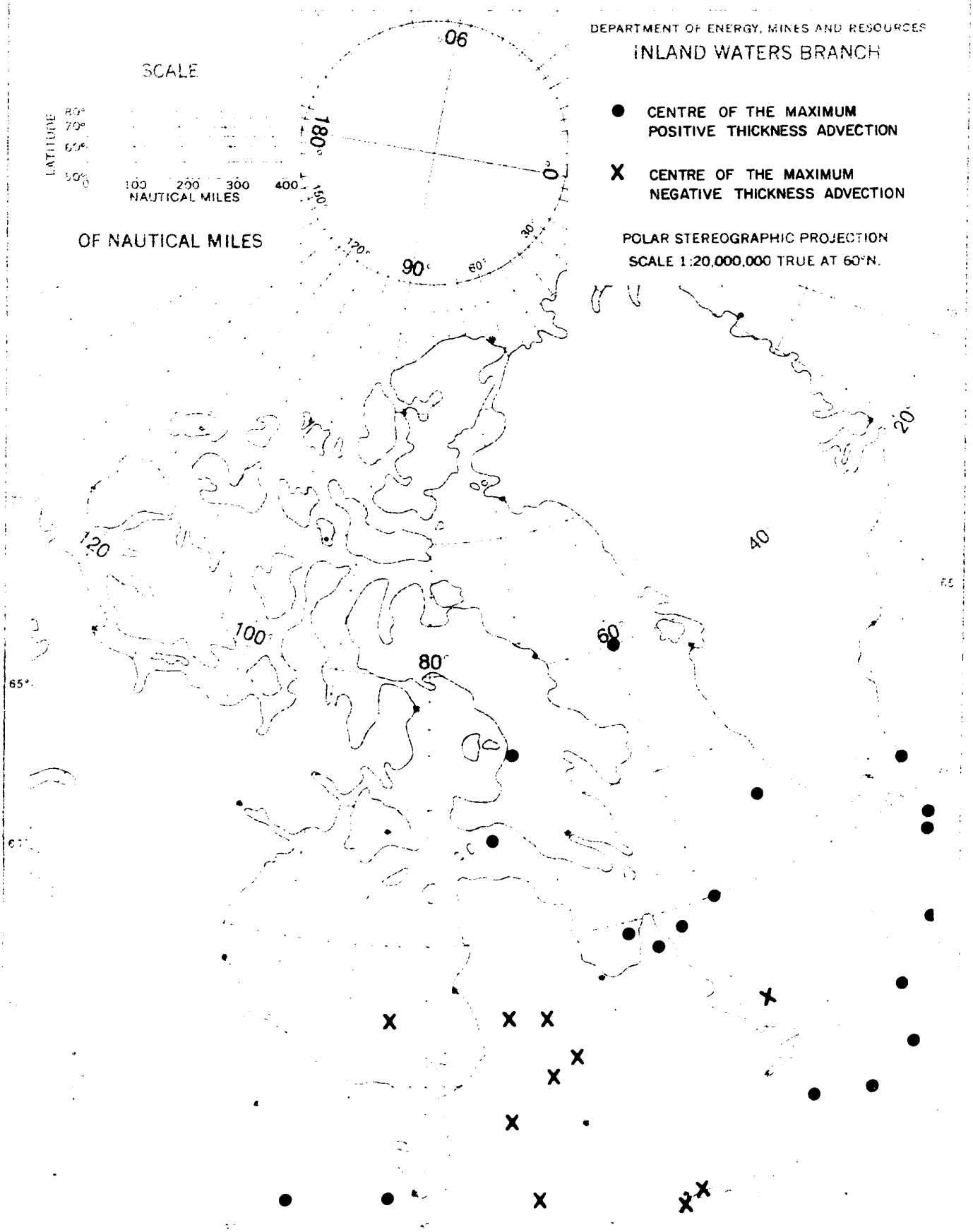

Distribution of the Centres of the Type "A" Thickness Advection Fields

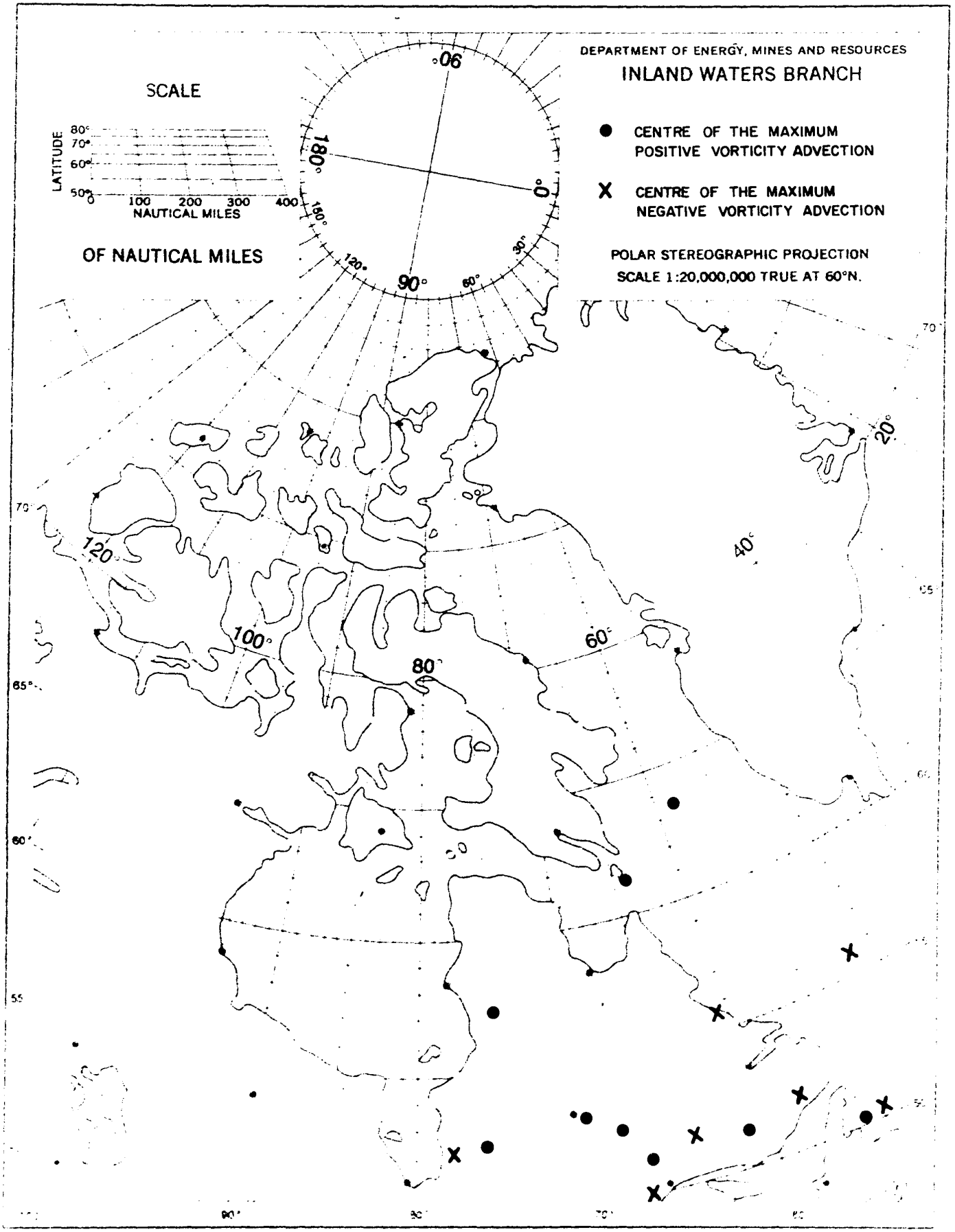

Distribution of the Centres of the Type "A" Vorticity Advection Fields

Figure 30

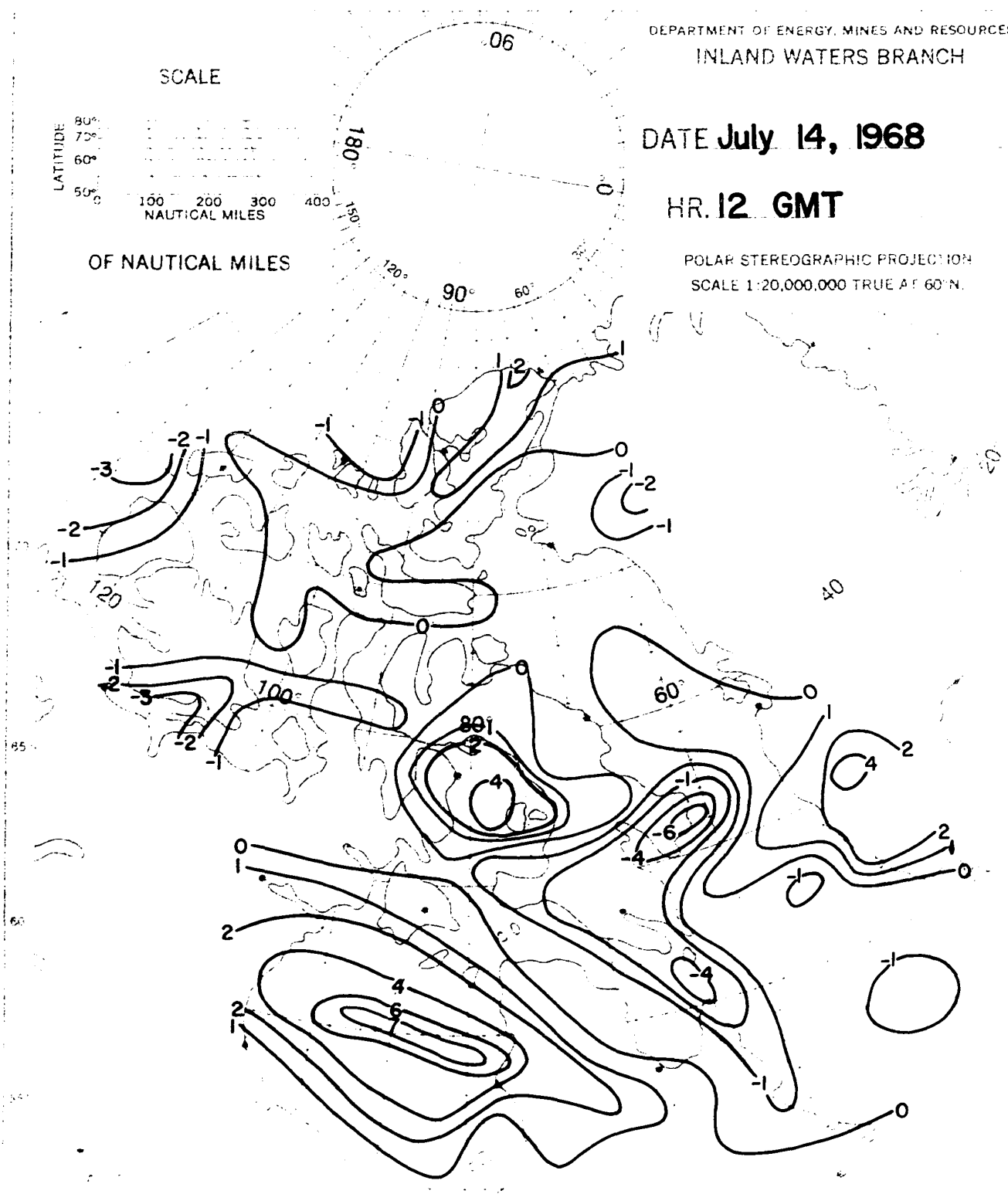

Surface relative vorticity in 10^{-5} sec^{-1} units Figure 31

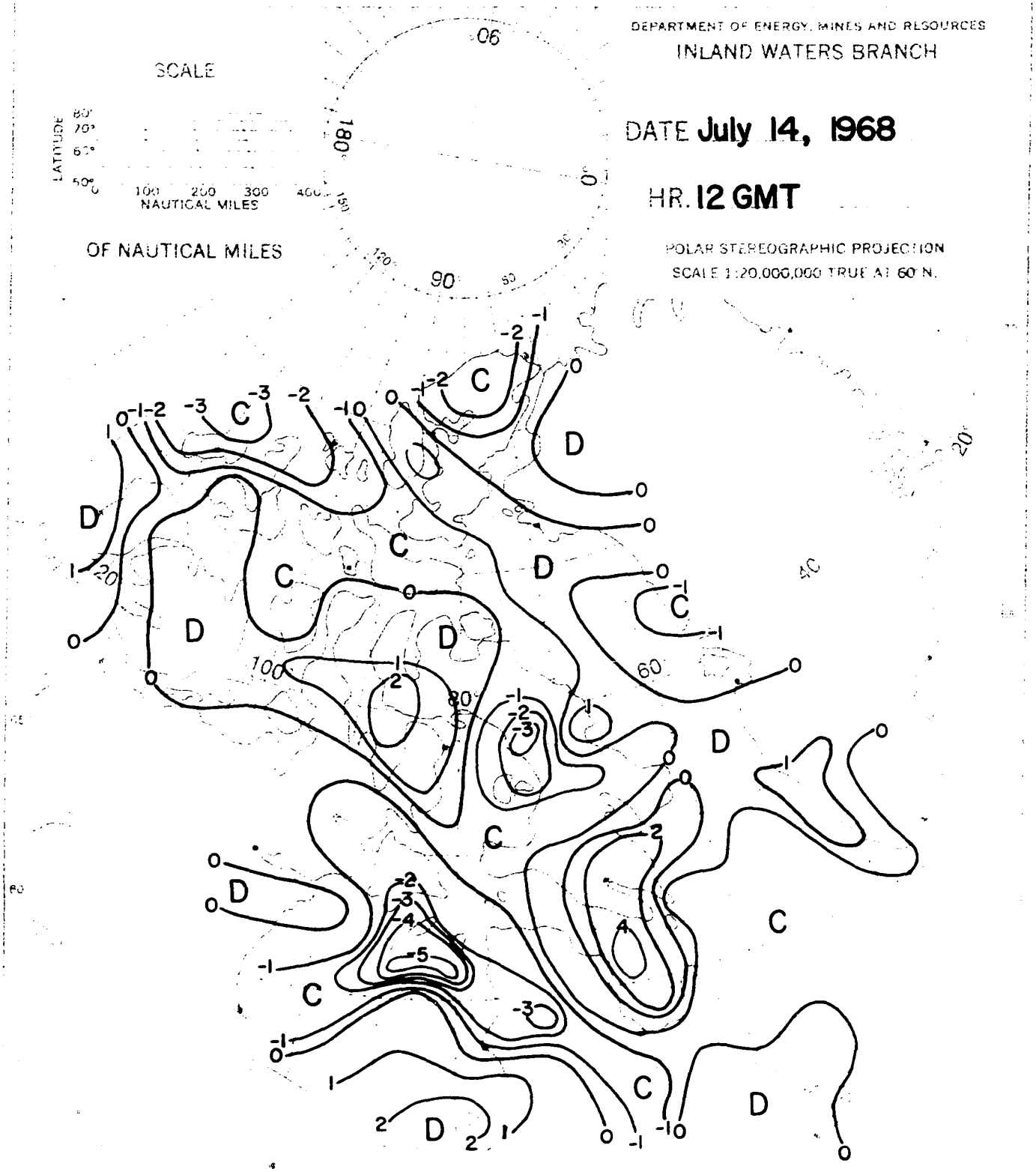

Figure 38

Surface velocity divergence in 10^{-5} sec^{-1} units

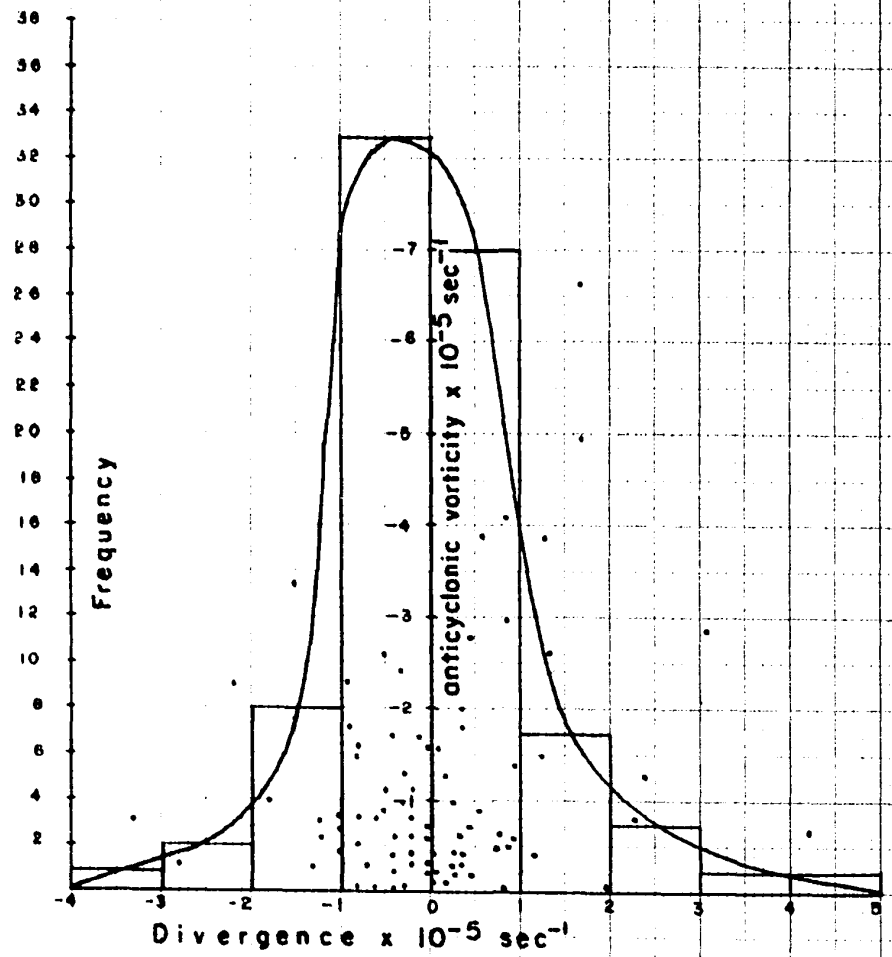

JULY 14 1968, 12 GMT
TYPE "U" SURFACE WEATHER

MEAN = 0.04 X 10^{-5} SEC^{-1}
STANDARD DEVIATION = 1.22
SKEWNESS = 0.55
KURTOSIS = 423

DIVERGENCE FREQUENCIES FOR ANTICYCLONIC FLOW

Figure 33

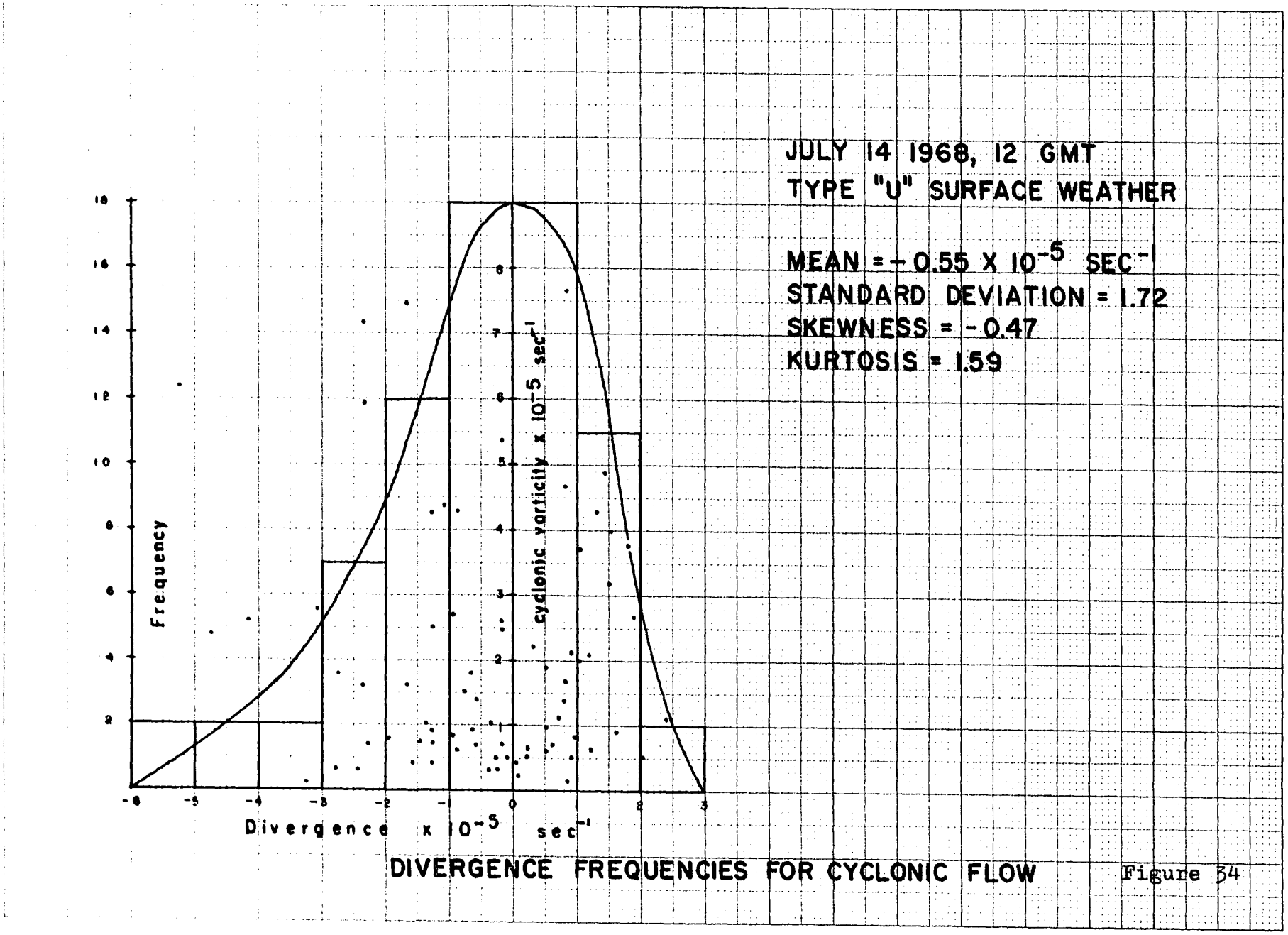

DIVERGENCE FREQUENCIES FOR CYCLONIC FLOW Figure 34

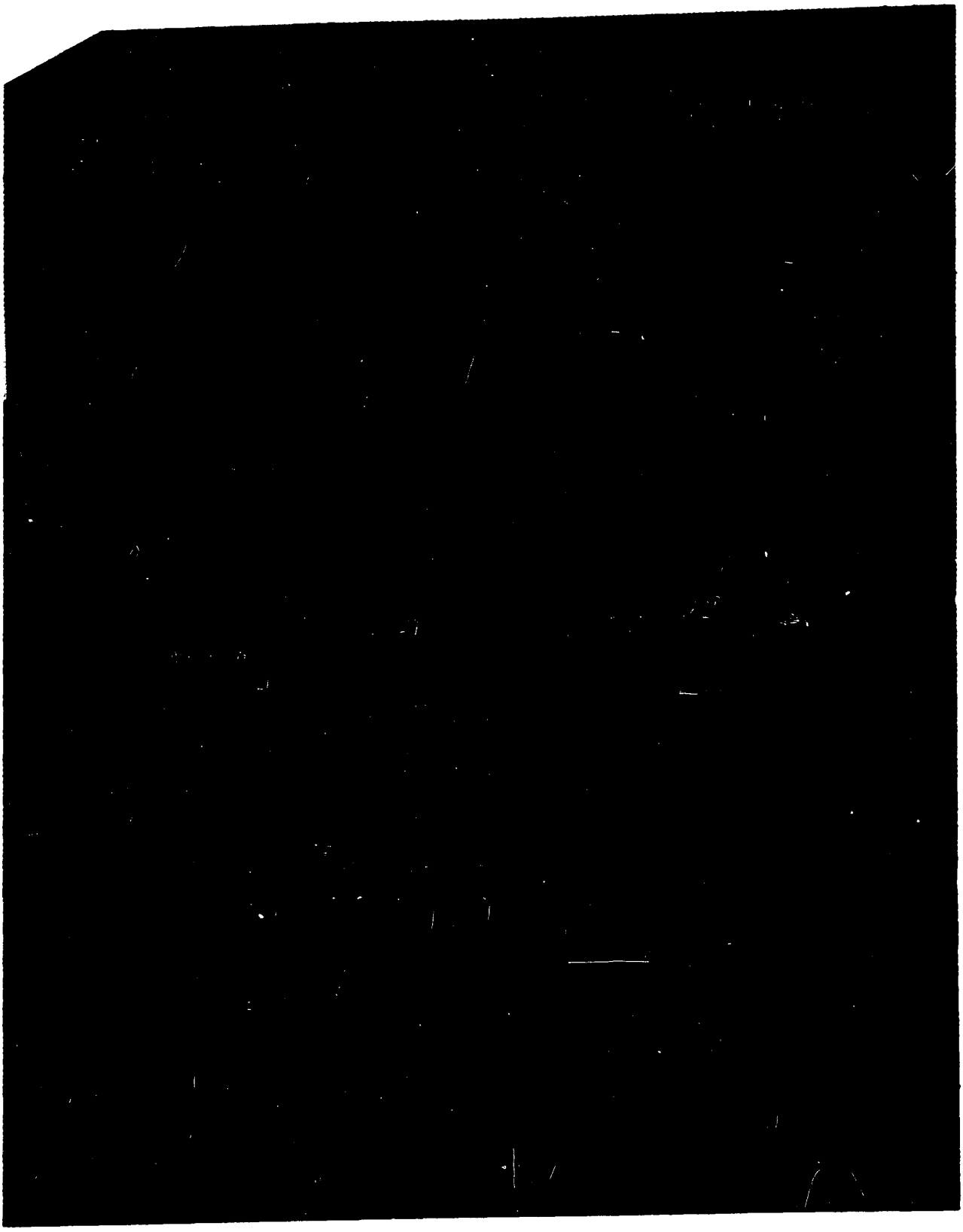

ESSA 6 Satellite Photo, July 3, 1968, 17:40 GMT Figure 35

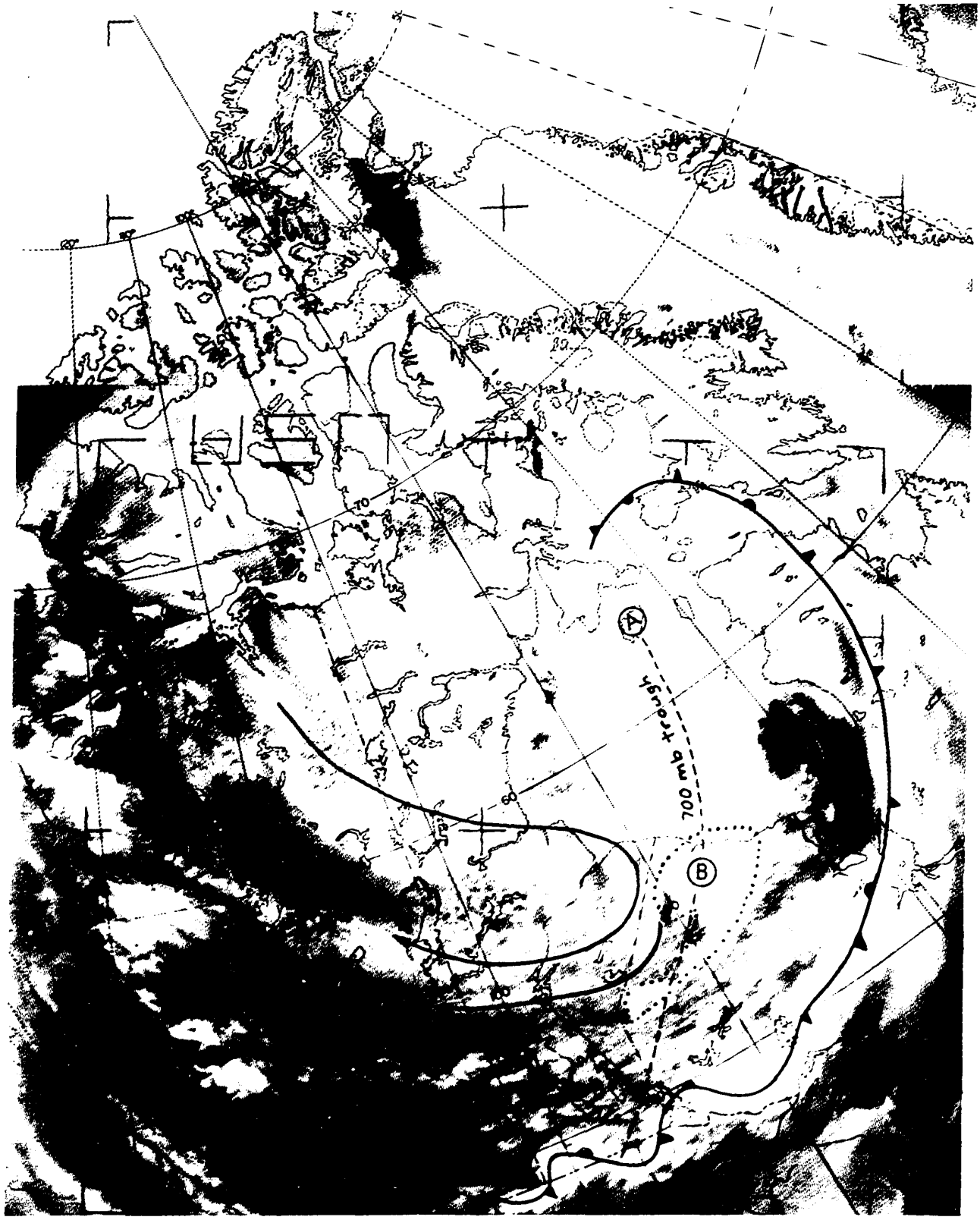
700 mb trough
A
B

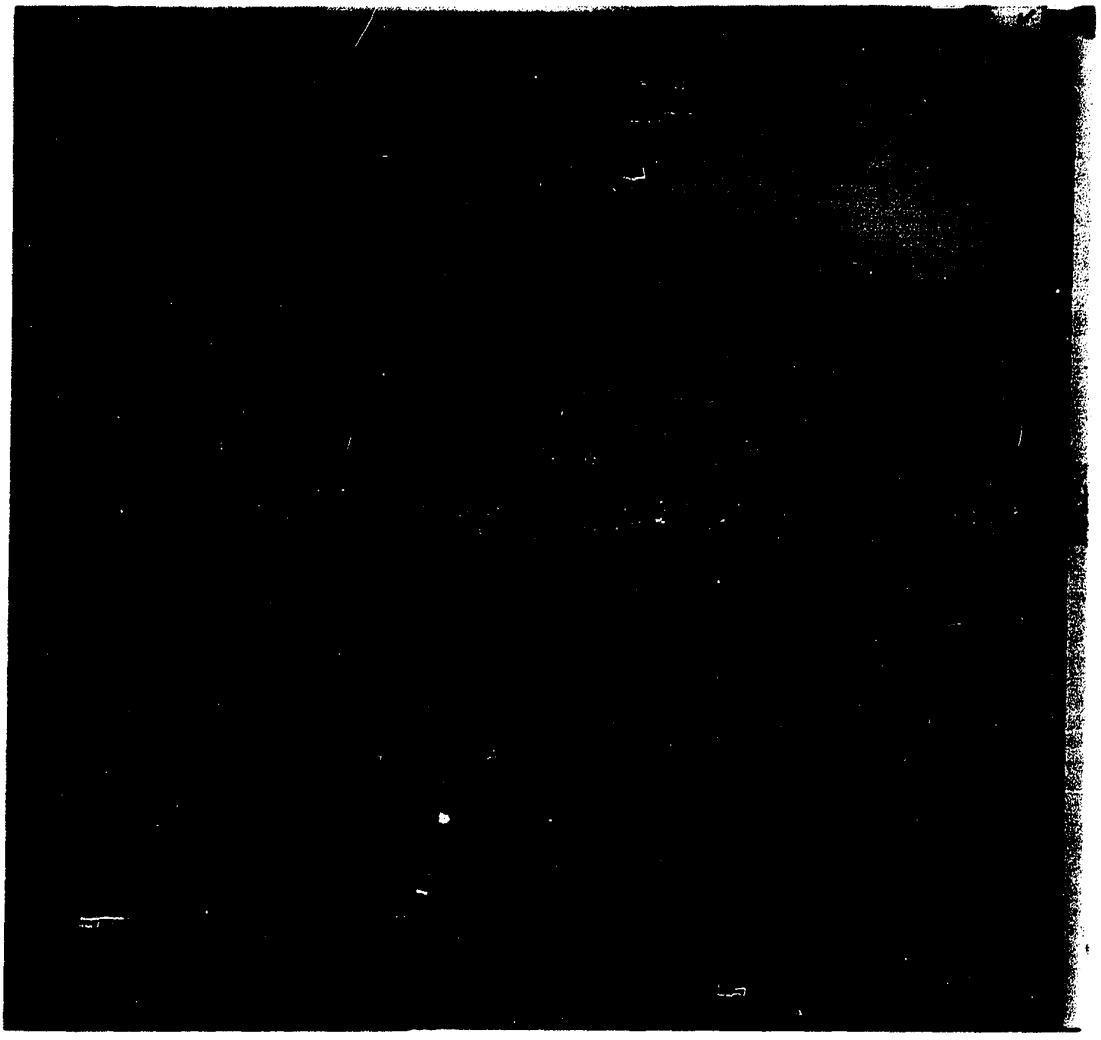

Essa 6 Satellite Photo, August 2, 1968, 17:38 GMT

Figure 36

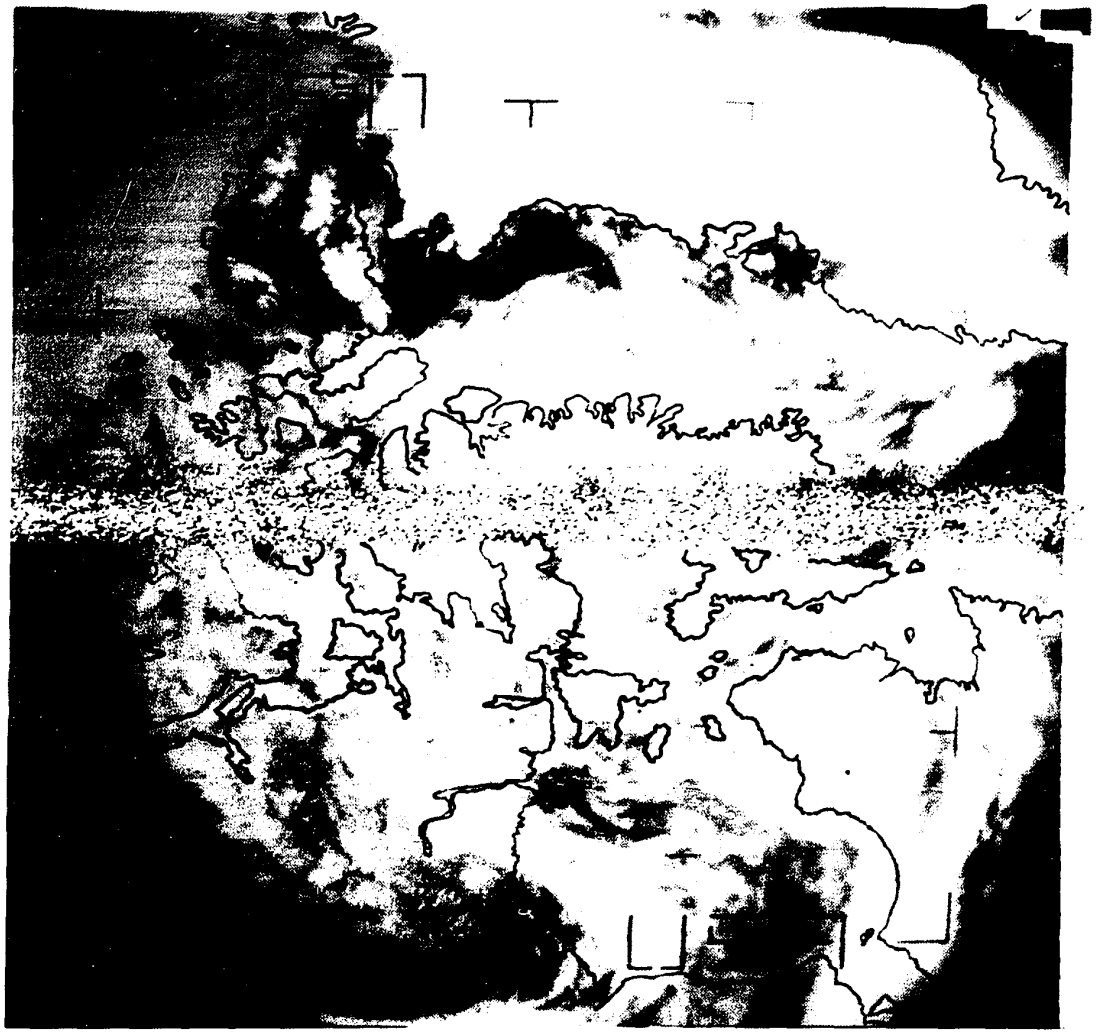

Histograms and cumulative frequency distributions of the 12 hourly rate of precipitations for 7 arctic stations during May 1968 for cyclonic and anticyclonic pressure patterns.

The 100 precipitations were associated with cyclonic surface isobars.

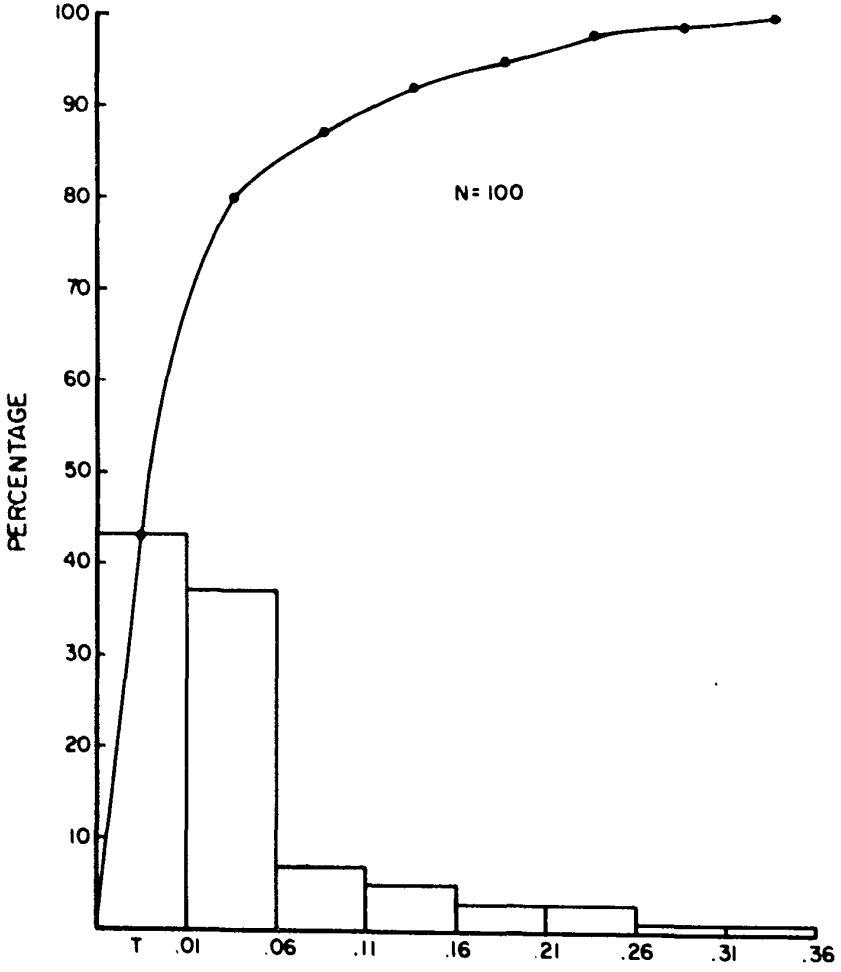

The 76 precipitations were associated with anticyclonic surface isobars.

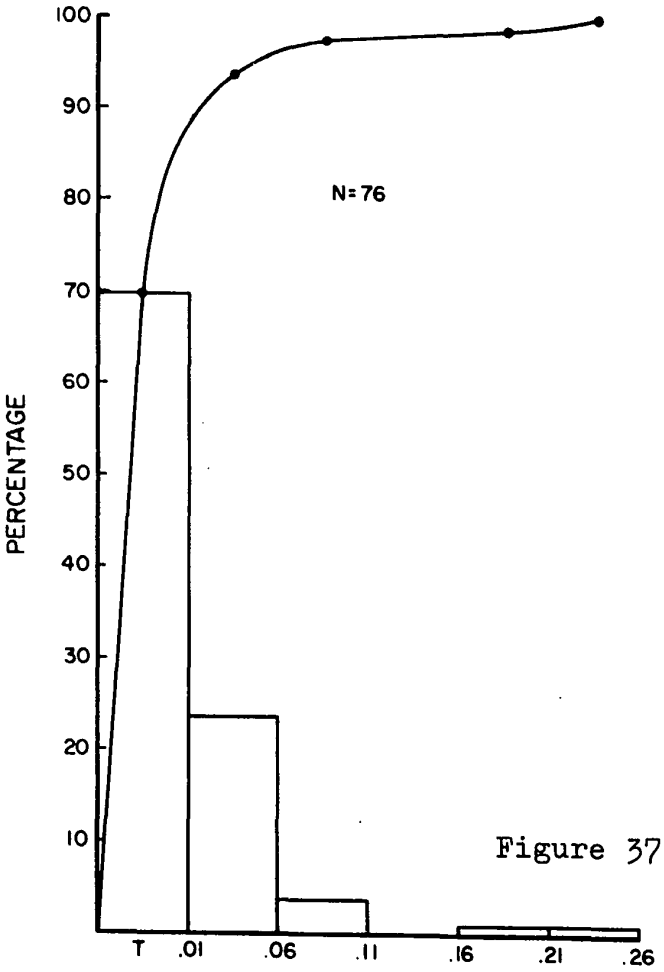

Figure 37

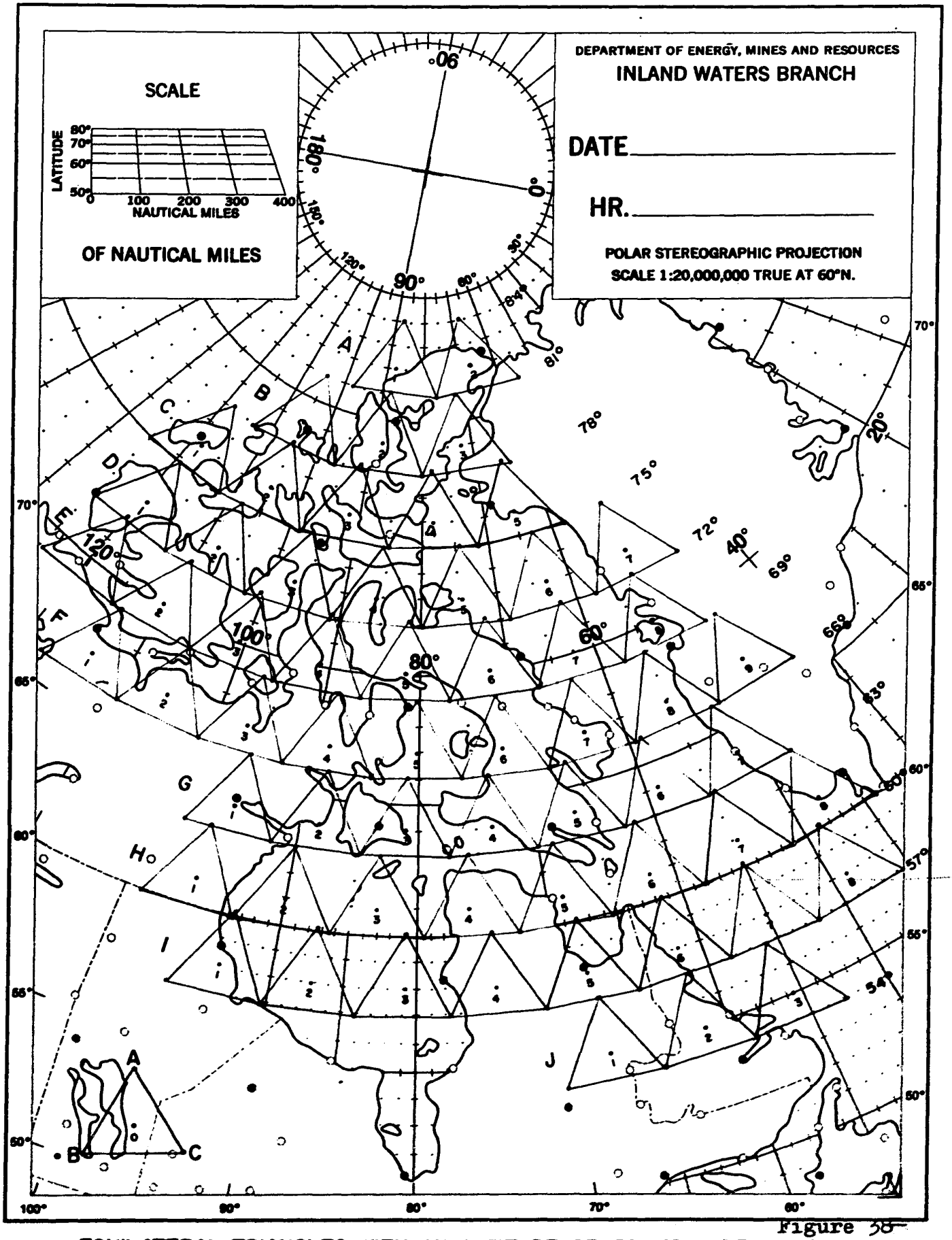

Figure 38

EQUILATERAL TRIANGLES WITH AN ALTITUDE OF 3° LATITUDE DISTANCE (3.34×10^5 M) FOR DIV $\vec{V}$ AND RELATIVE VORTICITY CALCULATION

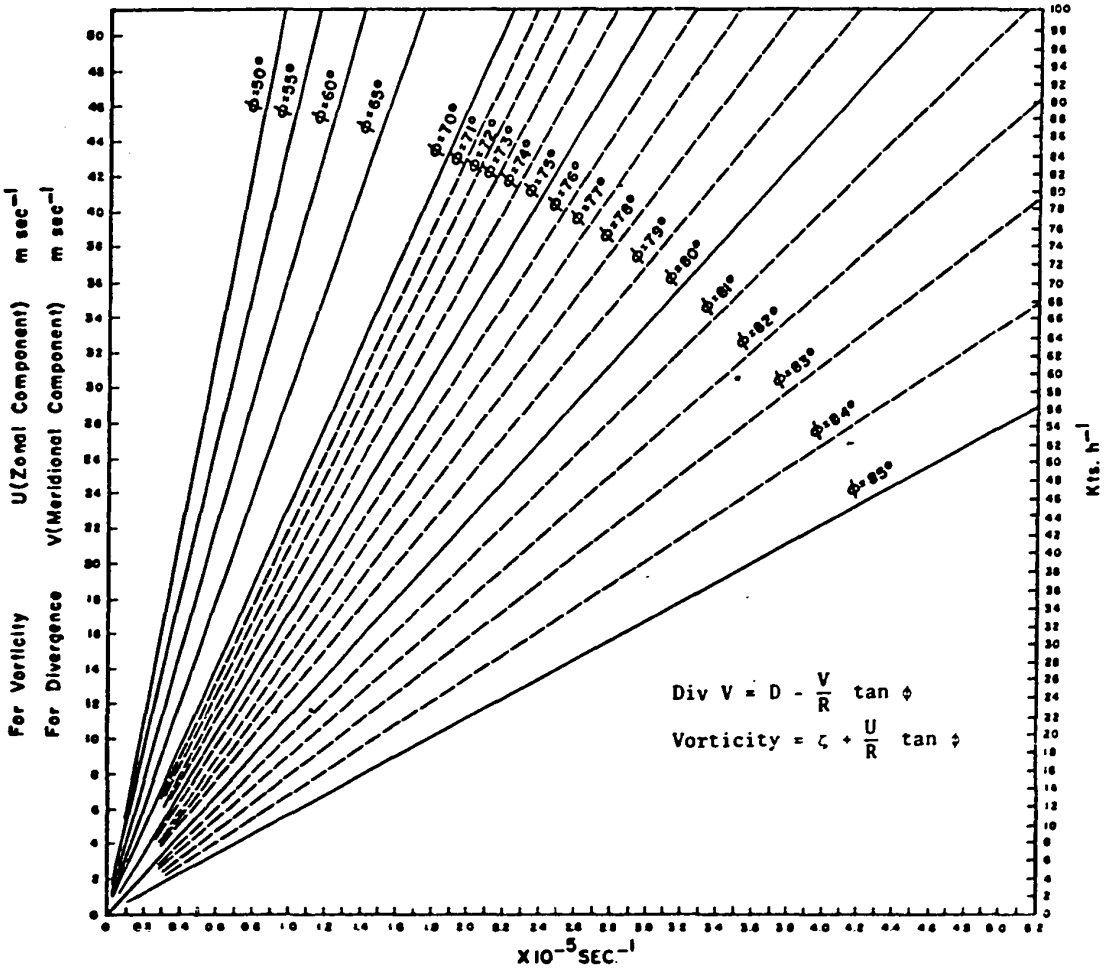

DIVERGENCE(−) AND VORTICITY(+) CORRECTION DUE TO THE CONVERGENCE OF MERIDIANS

Figure 39

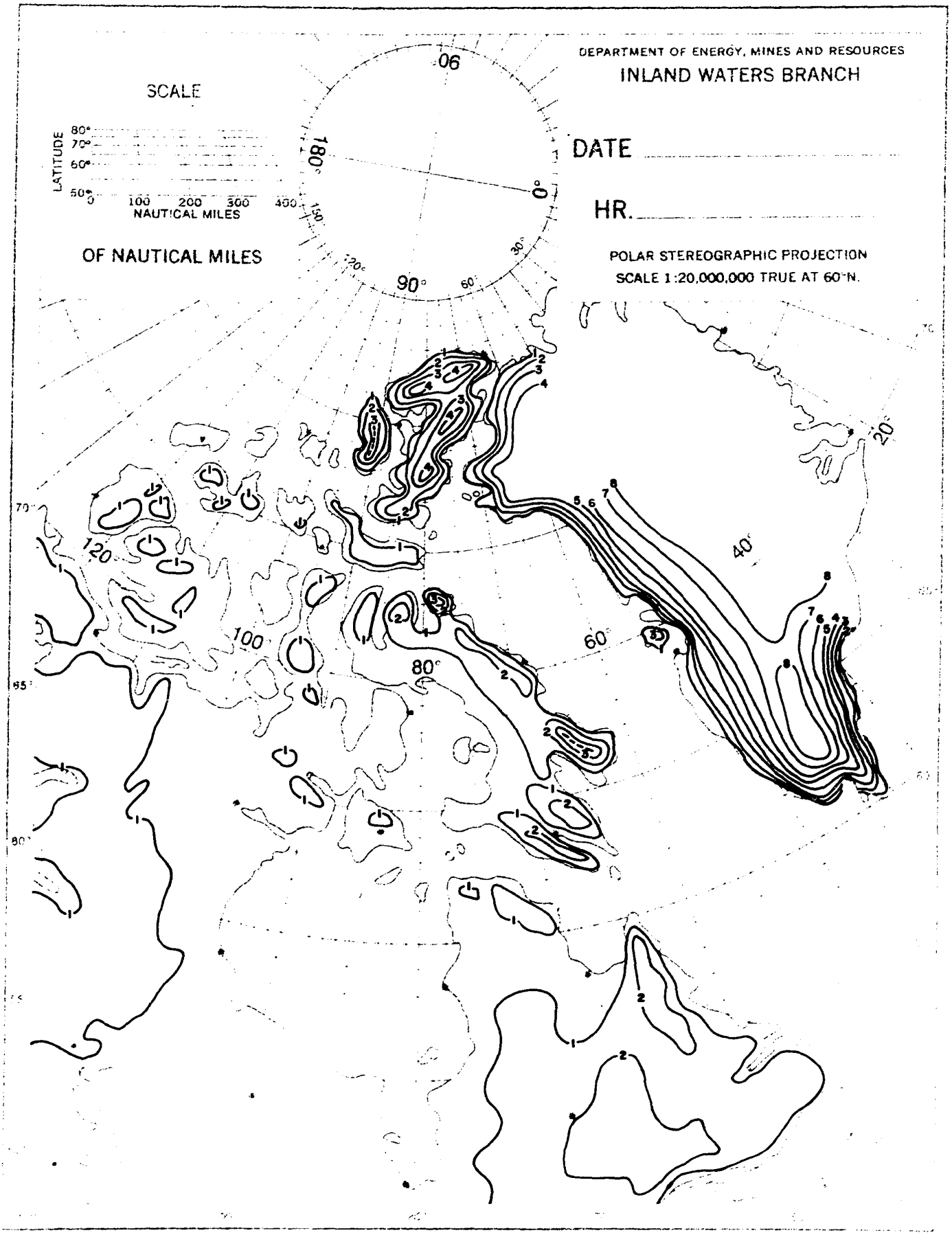

Figure 40

Smoothed orography of the Arctic Archipelago with a contour interval of 1000 ft.

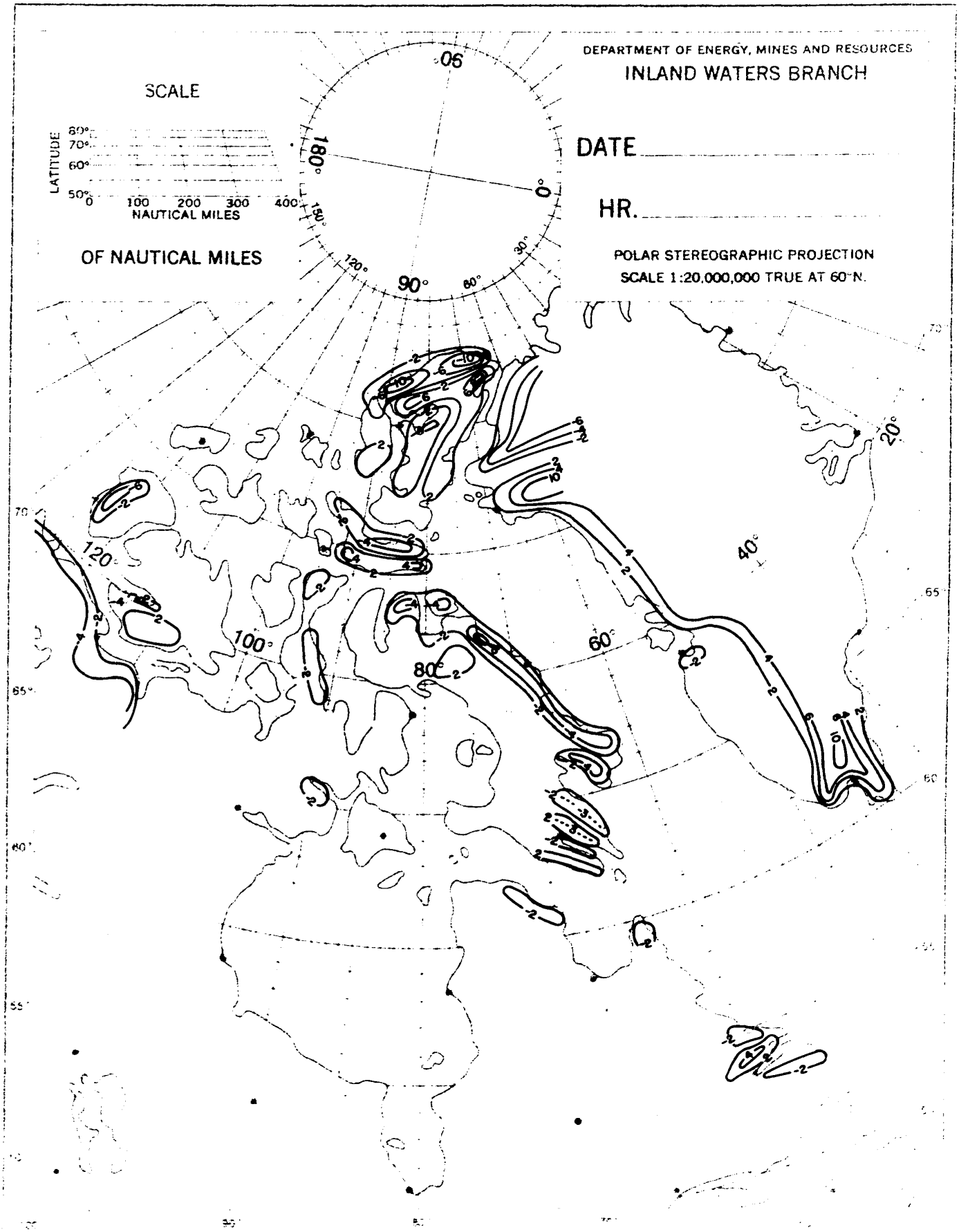

Orographic Vertical Velocity in 10^{-3} mb sec^{-1} for winds from 360° at 10 m sec^{-1} ; sign to be changed for winds from 180°

Figure 41

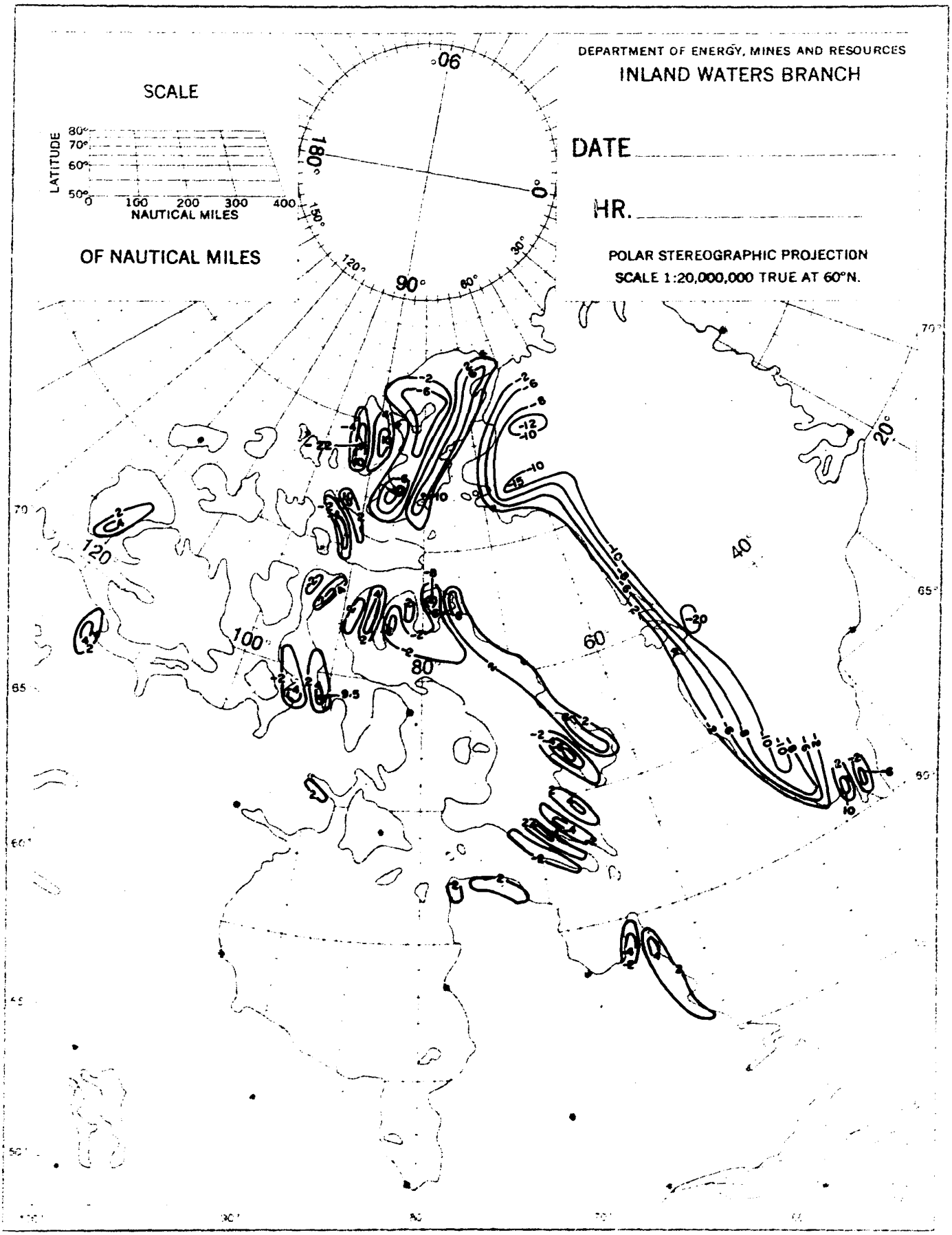

Orographic Vertical Velocity in 10^{-3} mb sec^{-1} for winds from 270° at 10 m sec^{-1} ; sign to be changed for winds from 90°

Figure 42

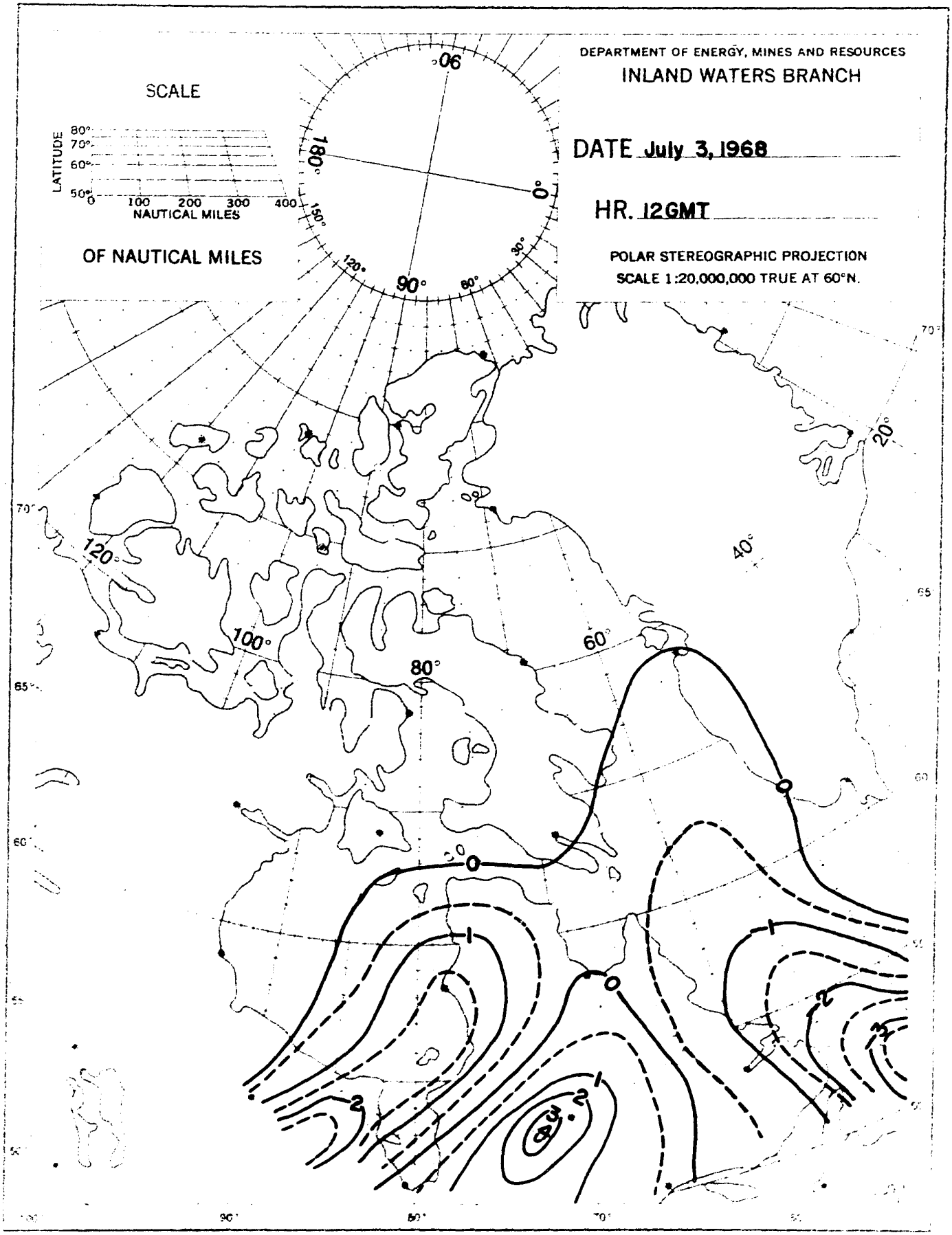

Type "A" Large-Scale Vertical Velocity ($-\omega_6$) in 10^{-3}, mb sec^{-1}; Calculated with Penner's equation. Figure 43

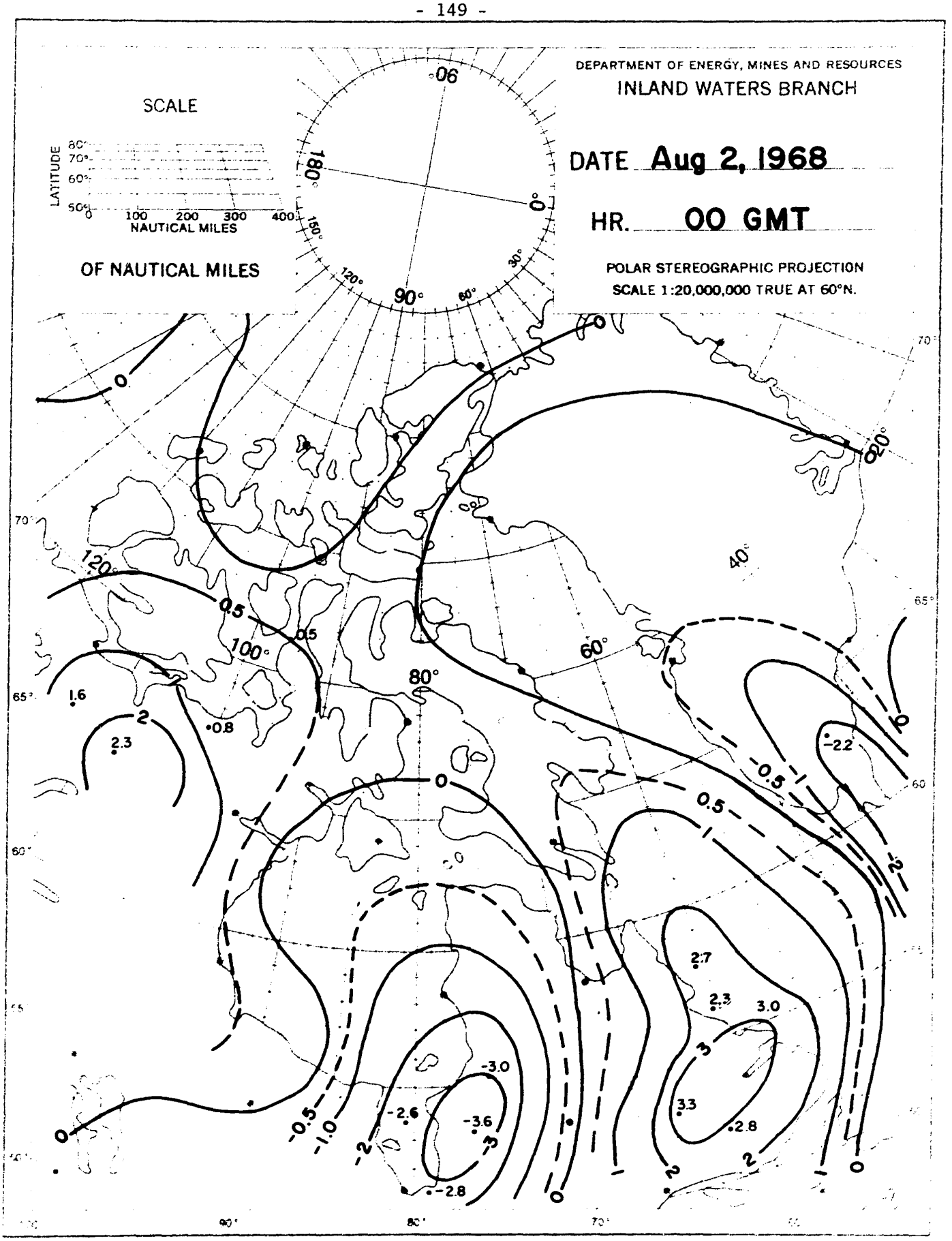

Component of Vertical Velocity Due to Thickness Advection Figure 44
in 10^{-3} mb sec^{-1} ; Type "E" Map Representative

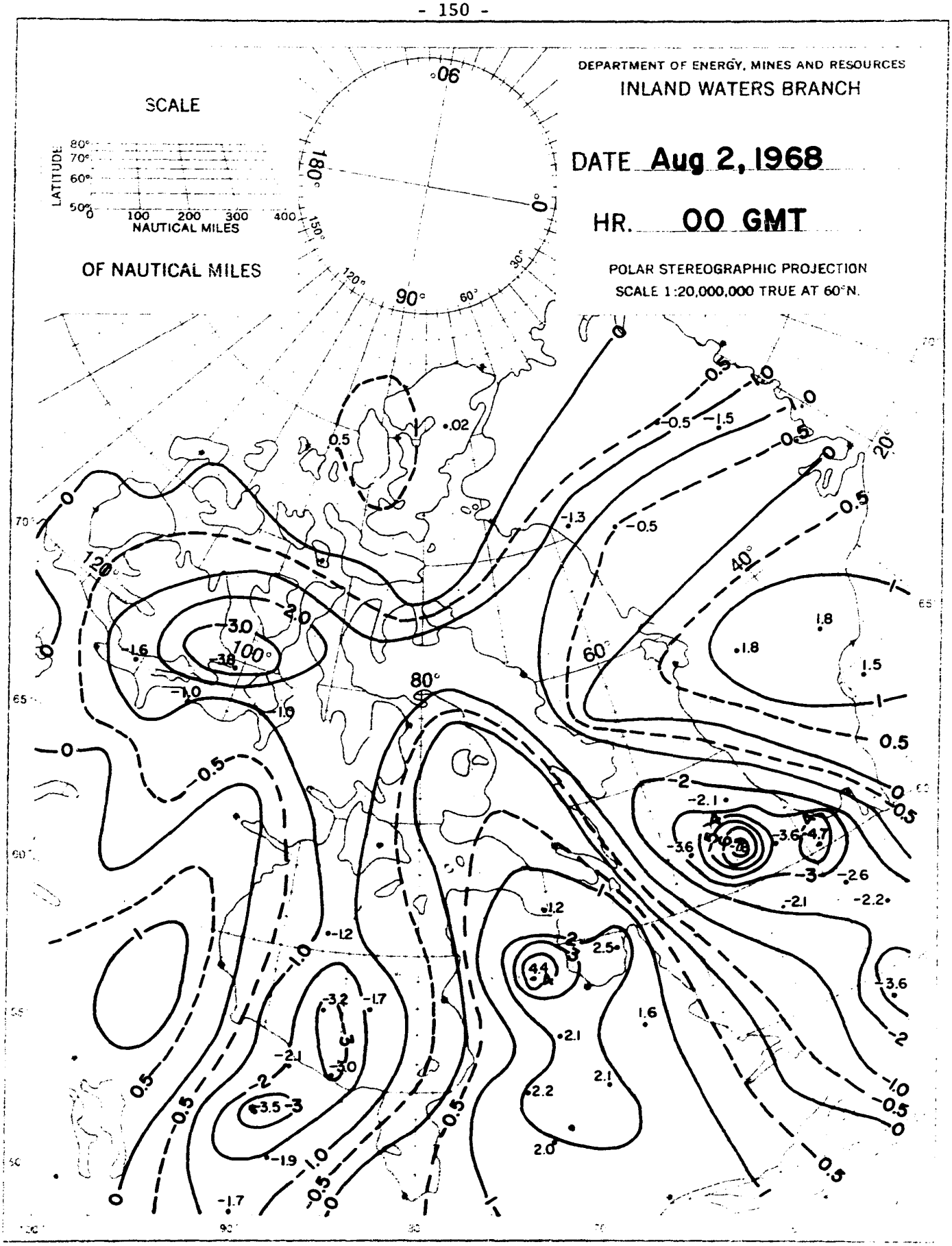

Component of Vertical Velocity Due to Vorticity Advection in 10^{-3} mb sec^{-1}; Type "E" Representative Map Figure 45

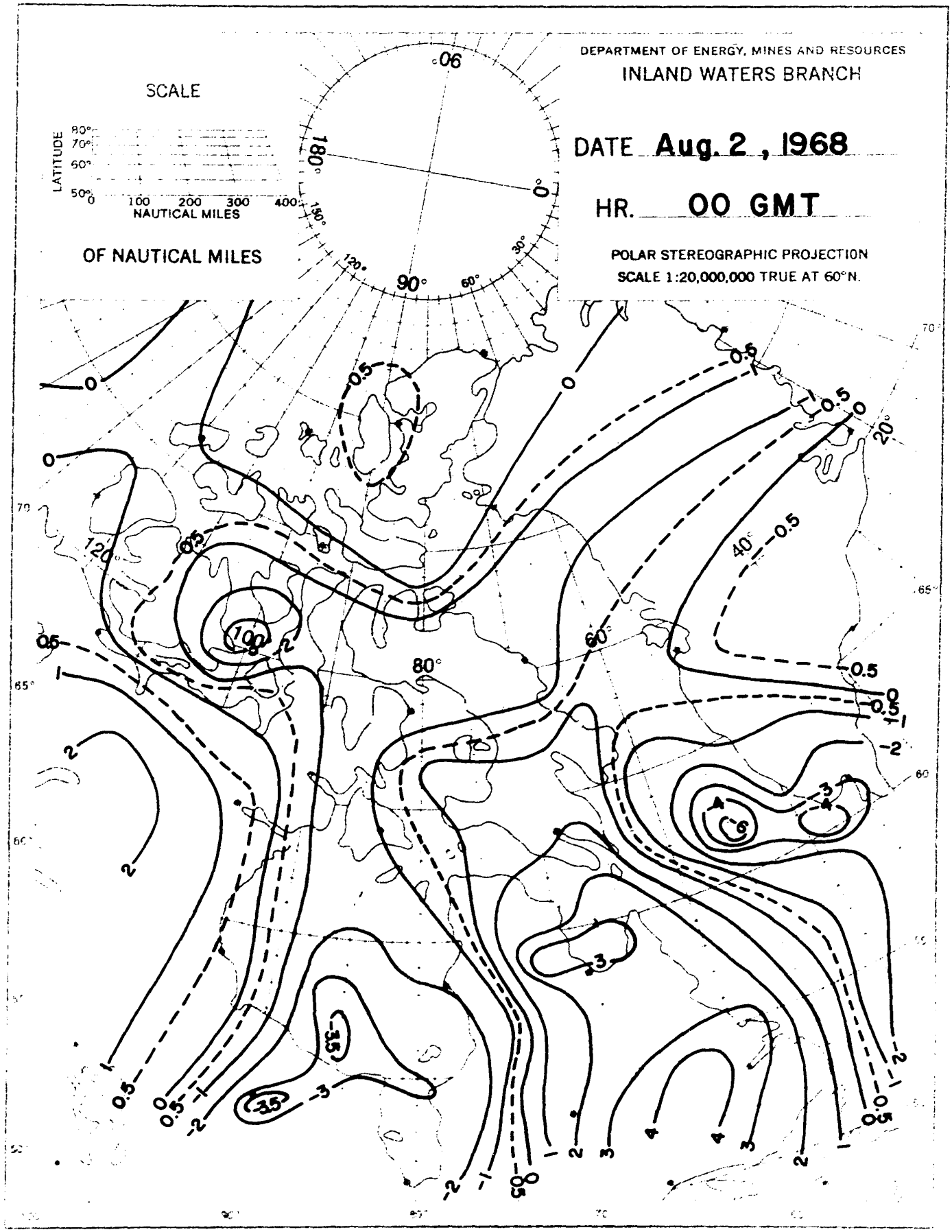

Type "E" Large-scale Vertical Velocity ($-\omega_6$) in 10^{-3} mb sec^{-1}

Figure 46

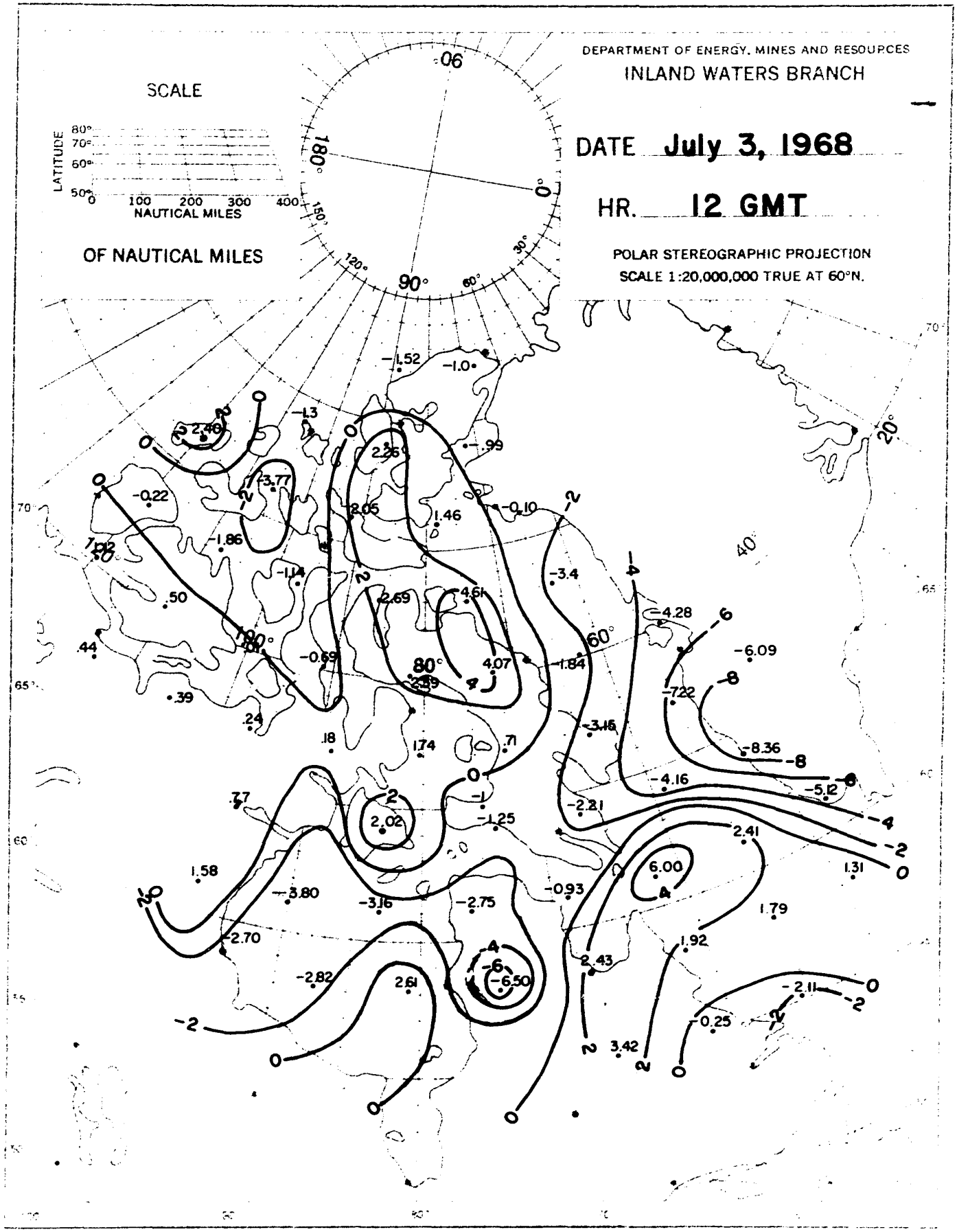

Type "A" Large Scale Vertical Velocity (ω_6) in 10^{-3}mb sec^{-1}; Calculated with Divergence Method. Figure 47

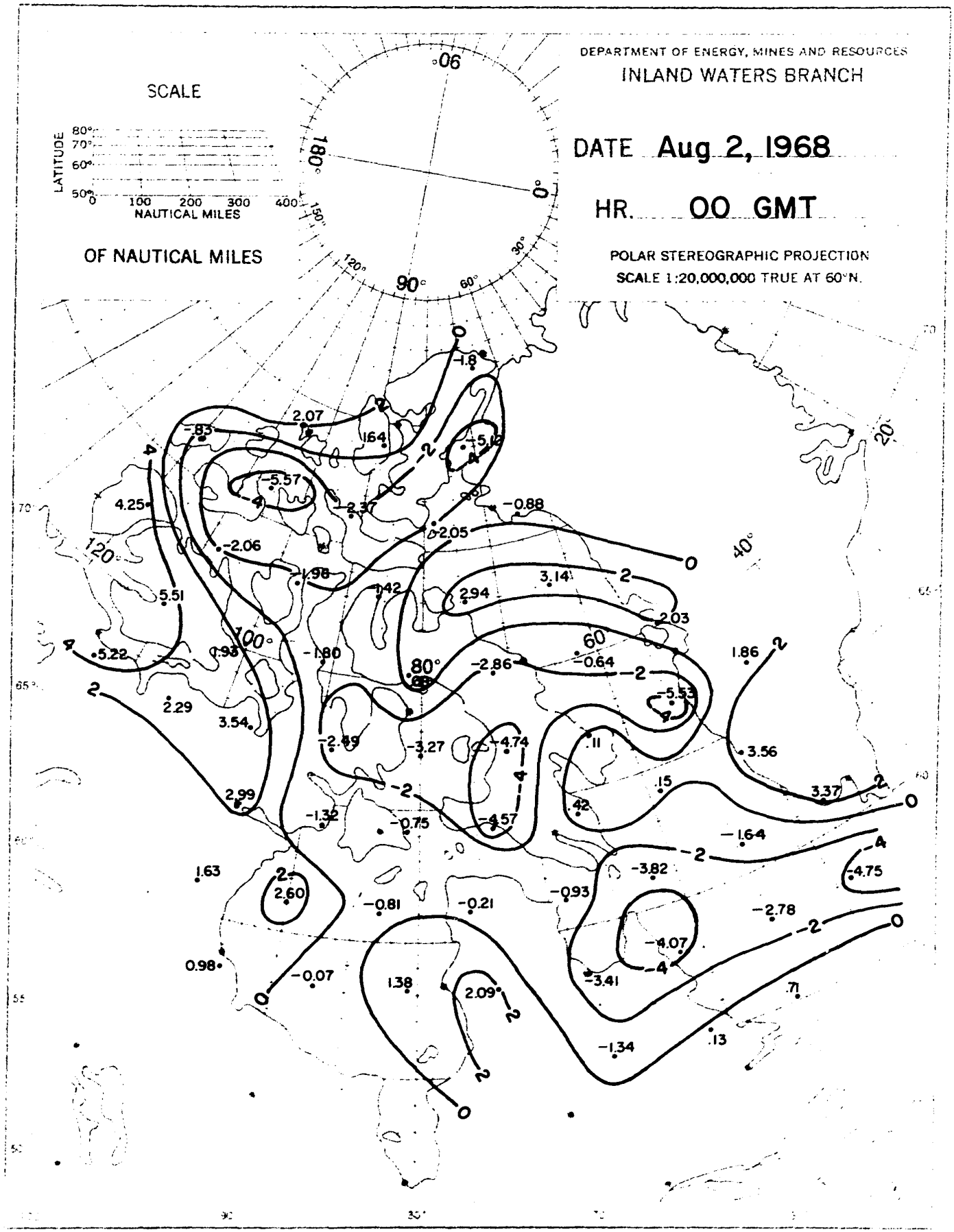

Type "E" Large Scale Vertical Velocity ($-\omega_6$) in 10^{-3} mb sec^{-1} Figure 46
Calculated with Divergence Method

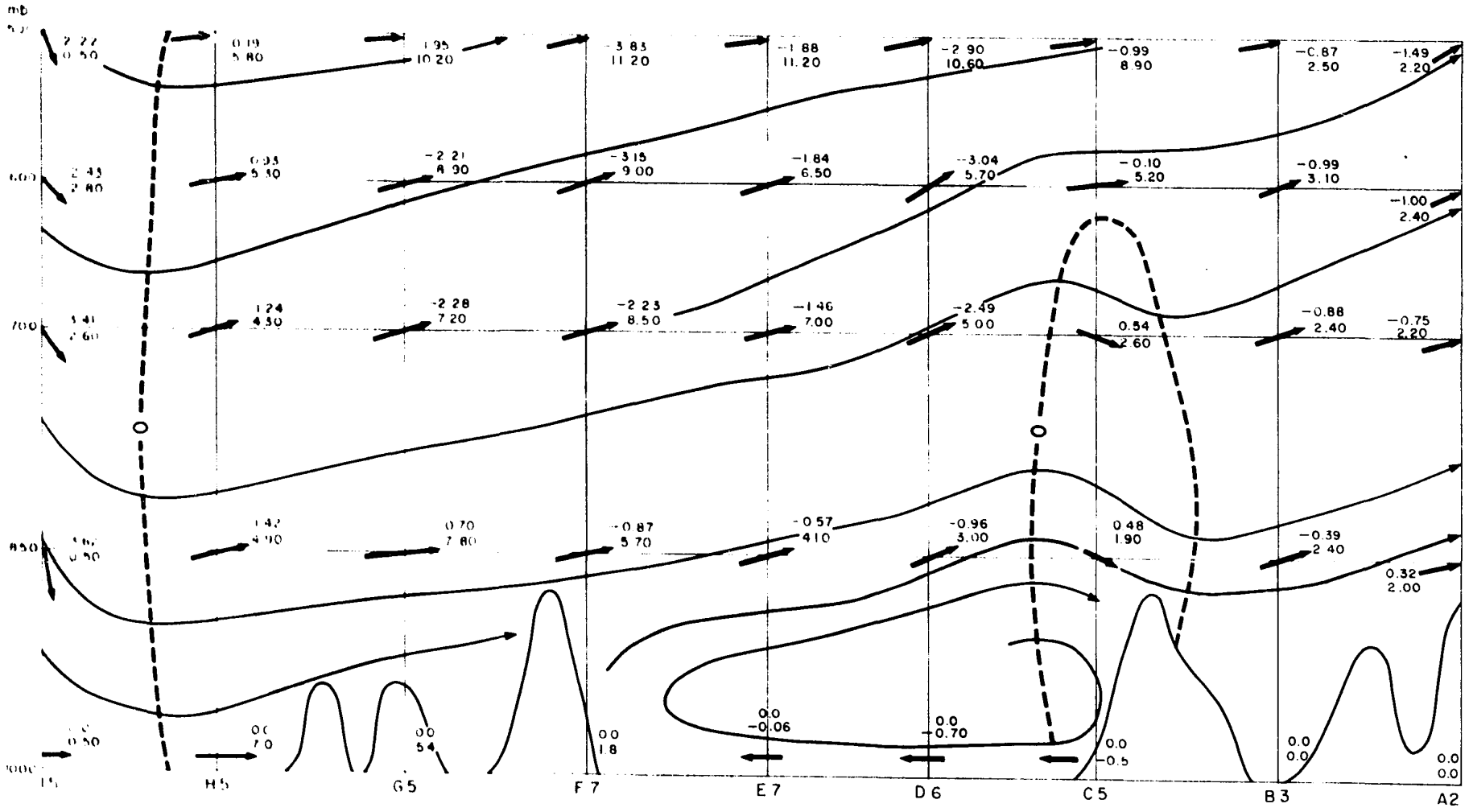

MERIDIONAL STREAMLINE CROSS SECTION, JULY 3, 1968, 12GMT

Figure 49

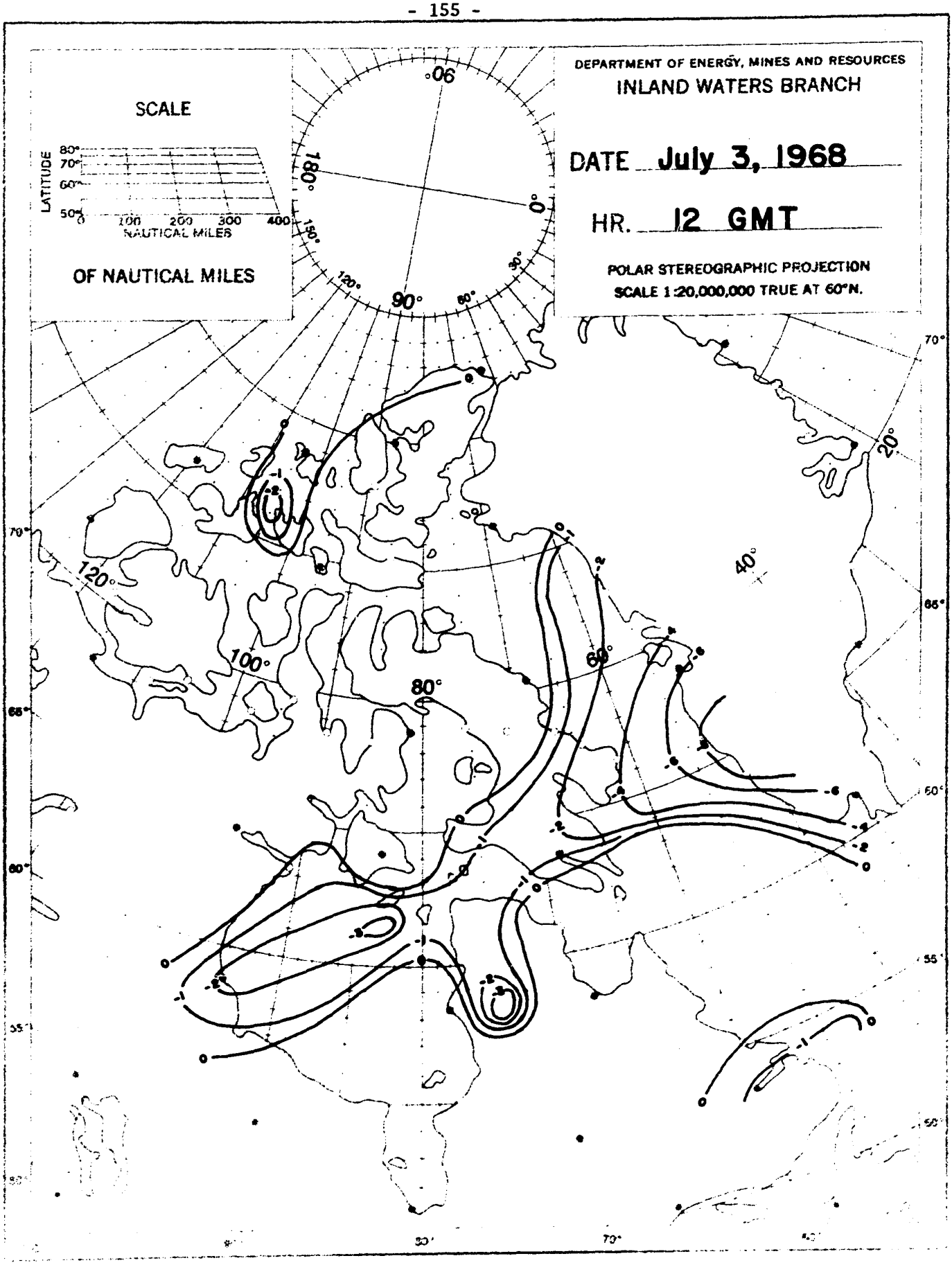

Type "A" Effective Vertical Velocity (Prognostic ω_{86}) in 10^{-3} mb sec^{-1}

Figure 50

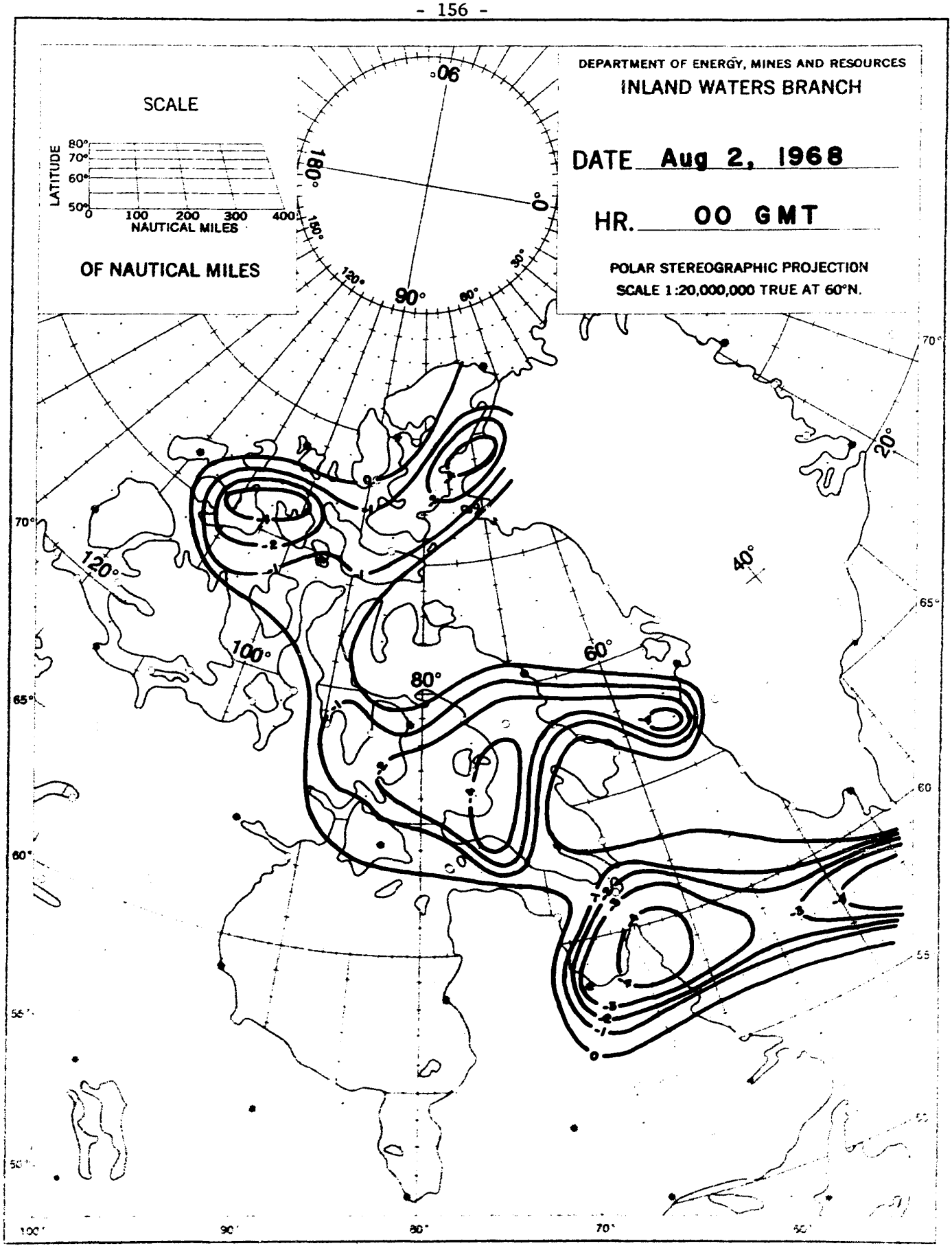

Type "E" Effective Vertical Velocity (Prognostic ω_{E6}), in 10^{-3} mb sec^{-1}; Based on Divergence Method Figure 51

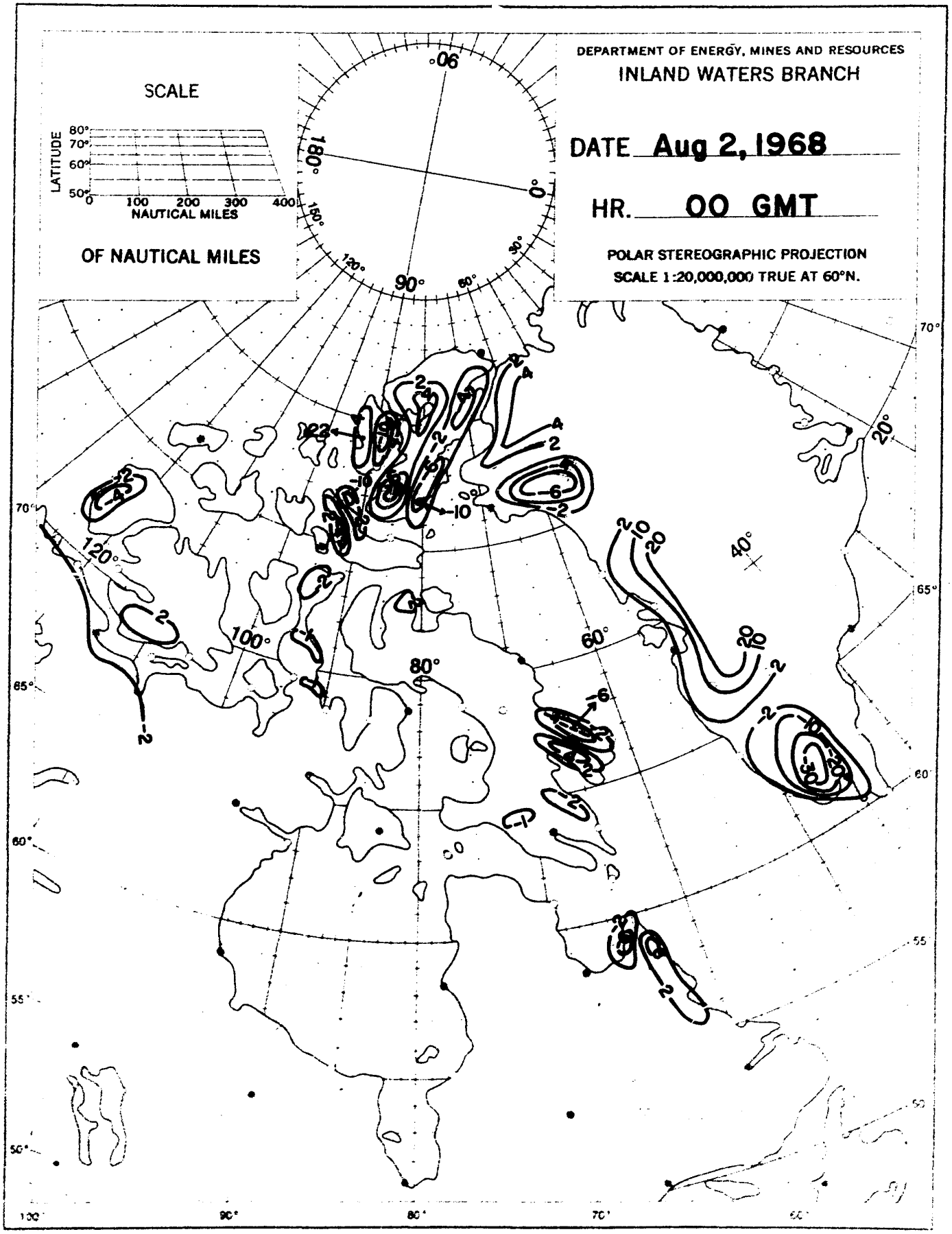

Type "E" Orographic Vertical Velocity (ω_m) Estimated with Geostrophic Wind Figure 52

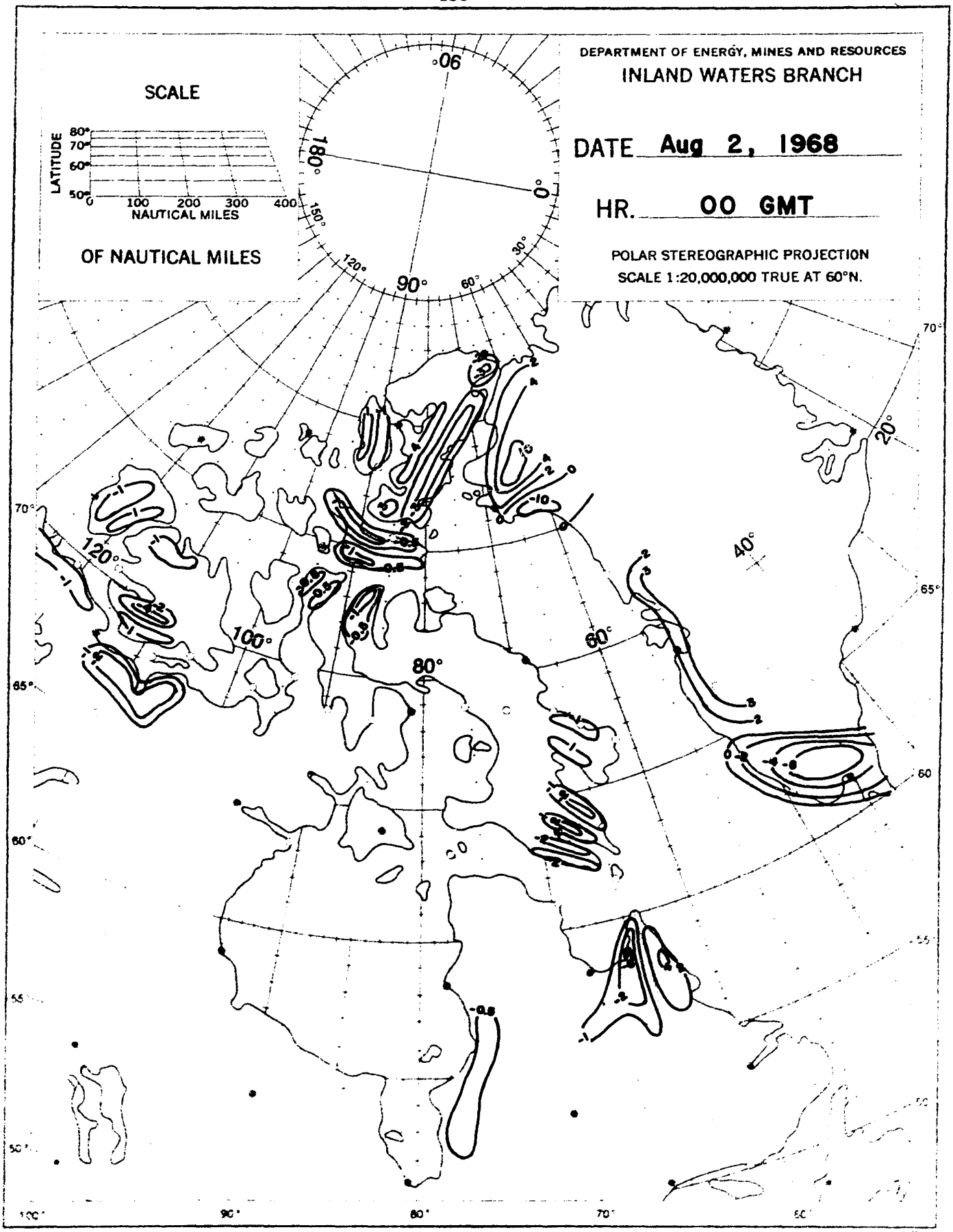

Figure 53

Type "E" Orographic Vertical Velocity (ω_m); Estimated With Streamline Wind Data

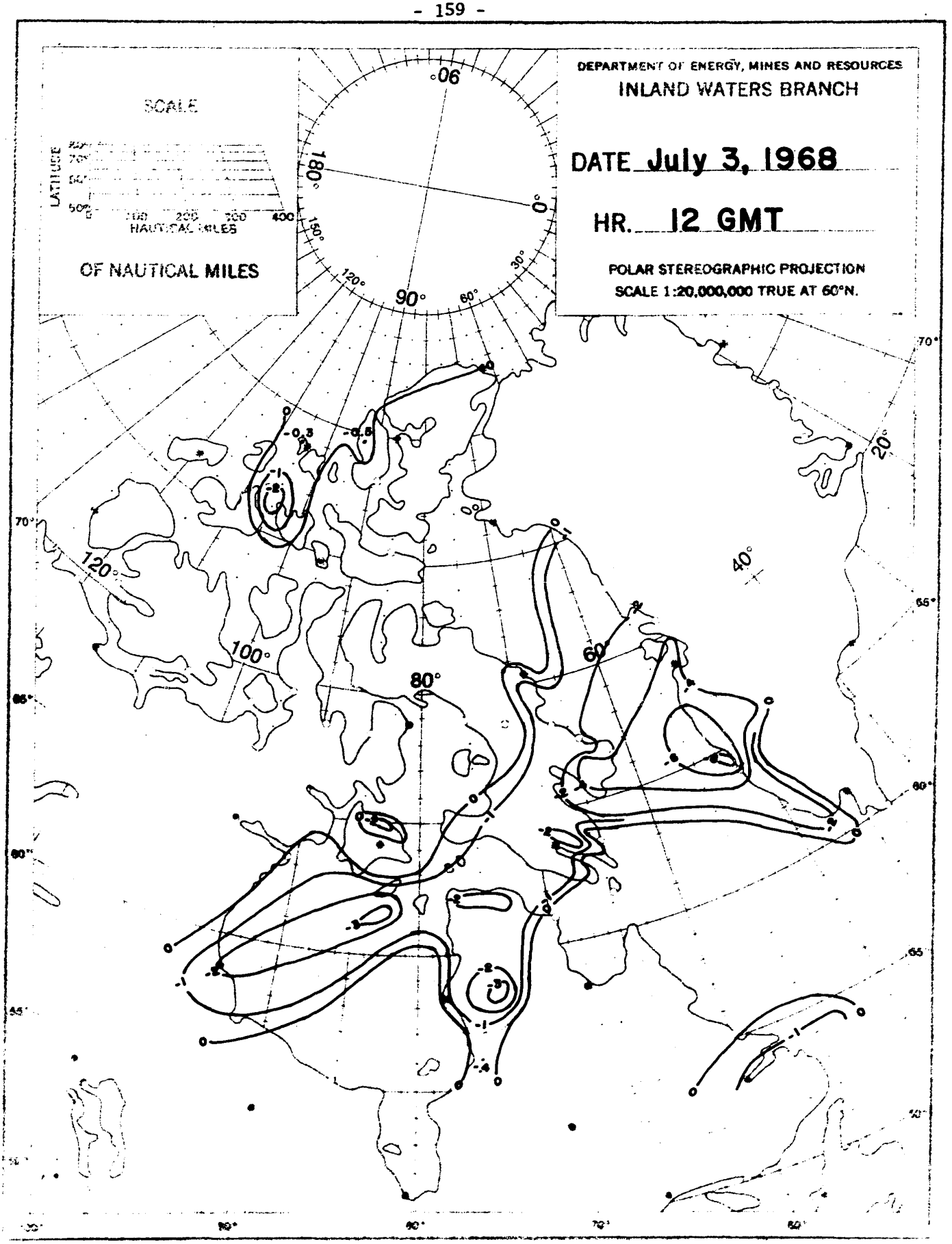

Type "A" ($\omega_{E_6} + \omega_m$) Estimated with Streamline Wind Data Figure 54

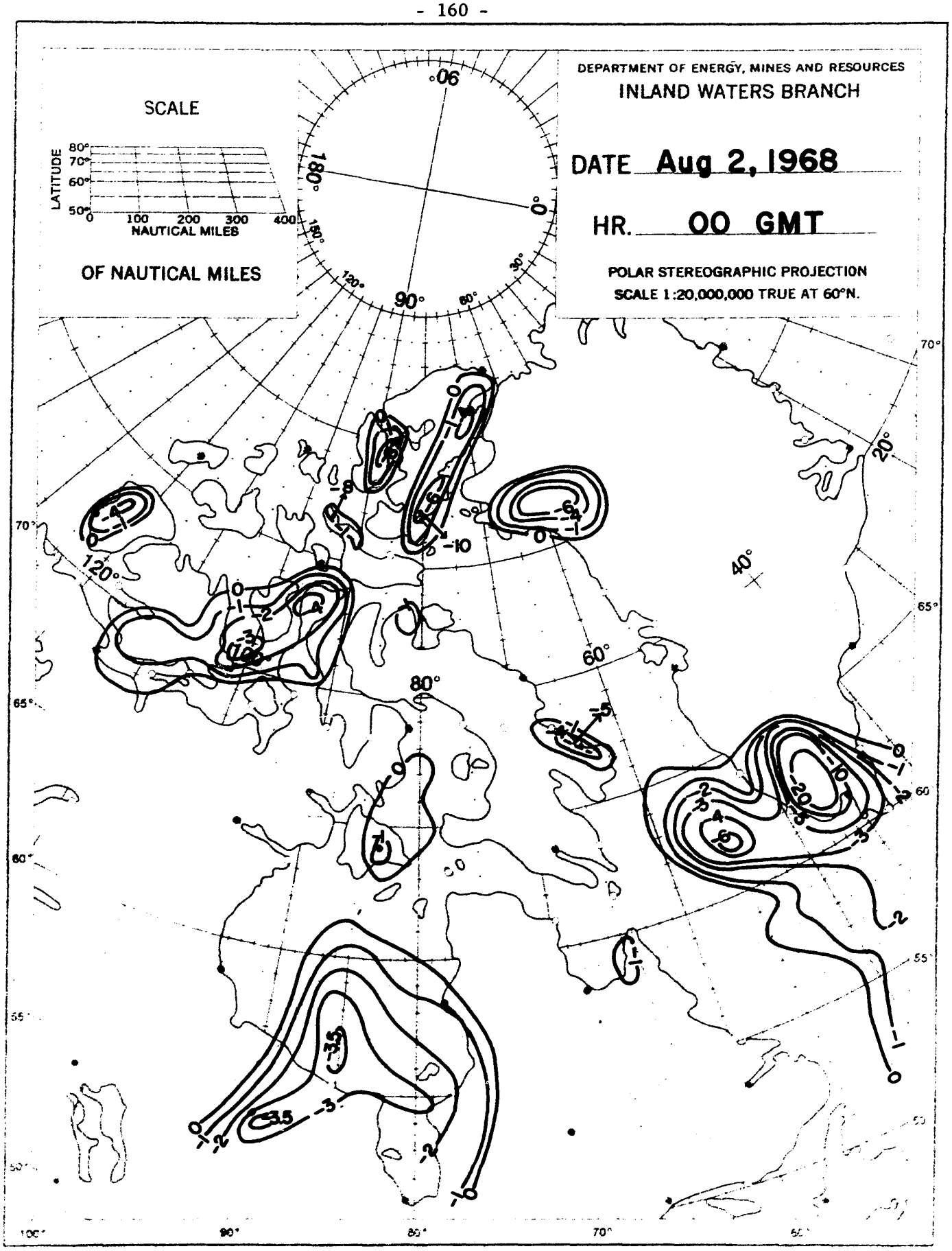

Figure 55

Type "E" ((ω)as+(ω)m) Estimated with Harley's Method Using Geostrophic Winds

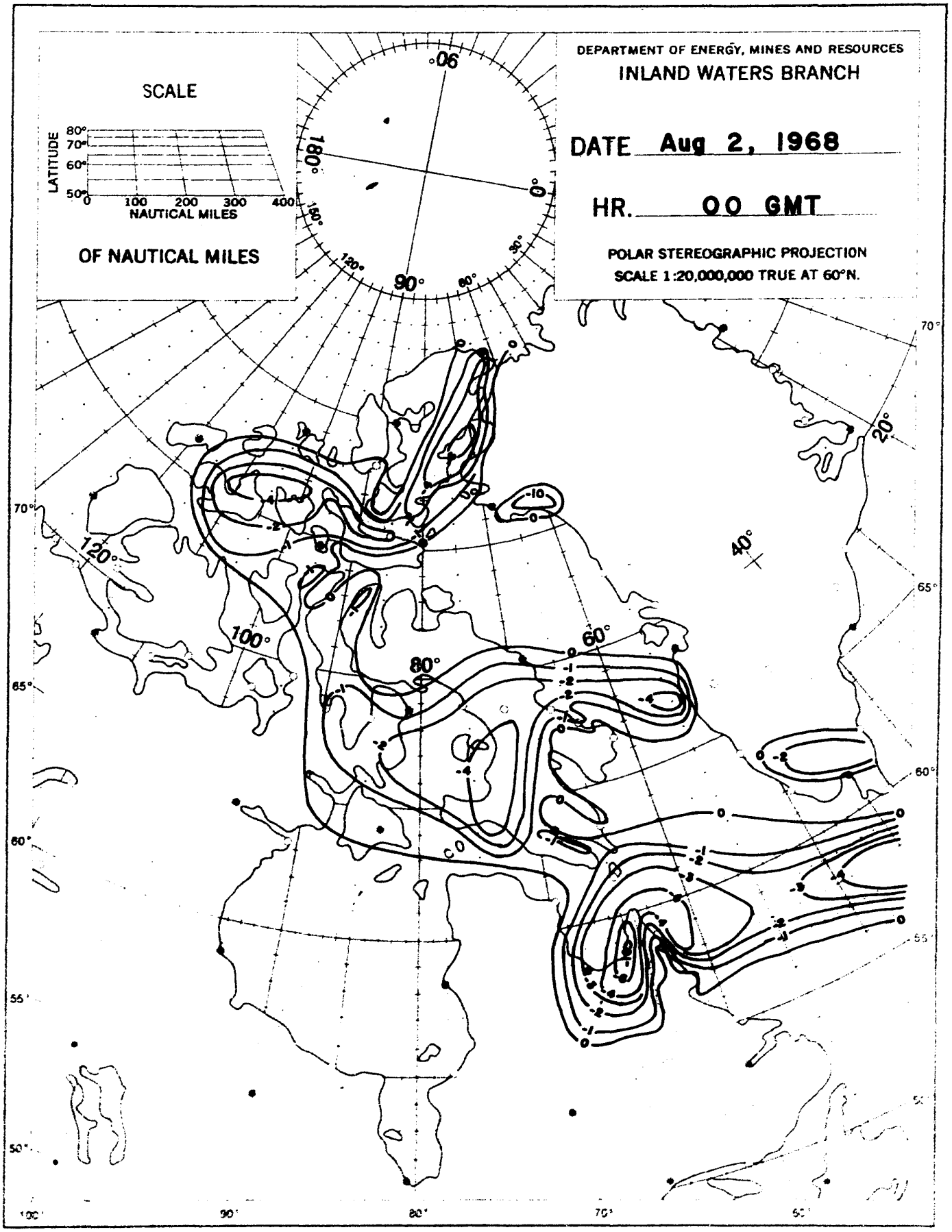

Type "E" $(\omega)_{EG} + (\omega)_{m}$; Estimated With Streamline Wind Data Figure 56

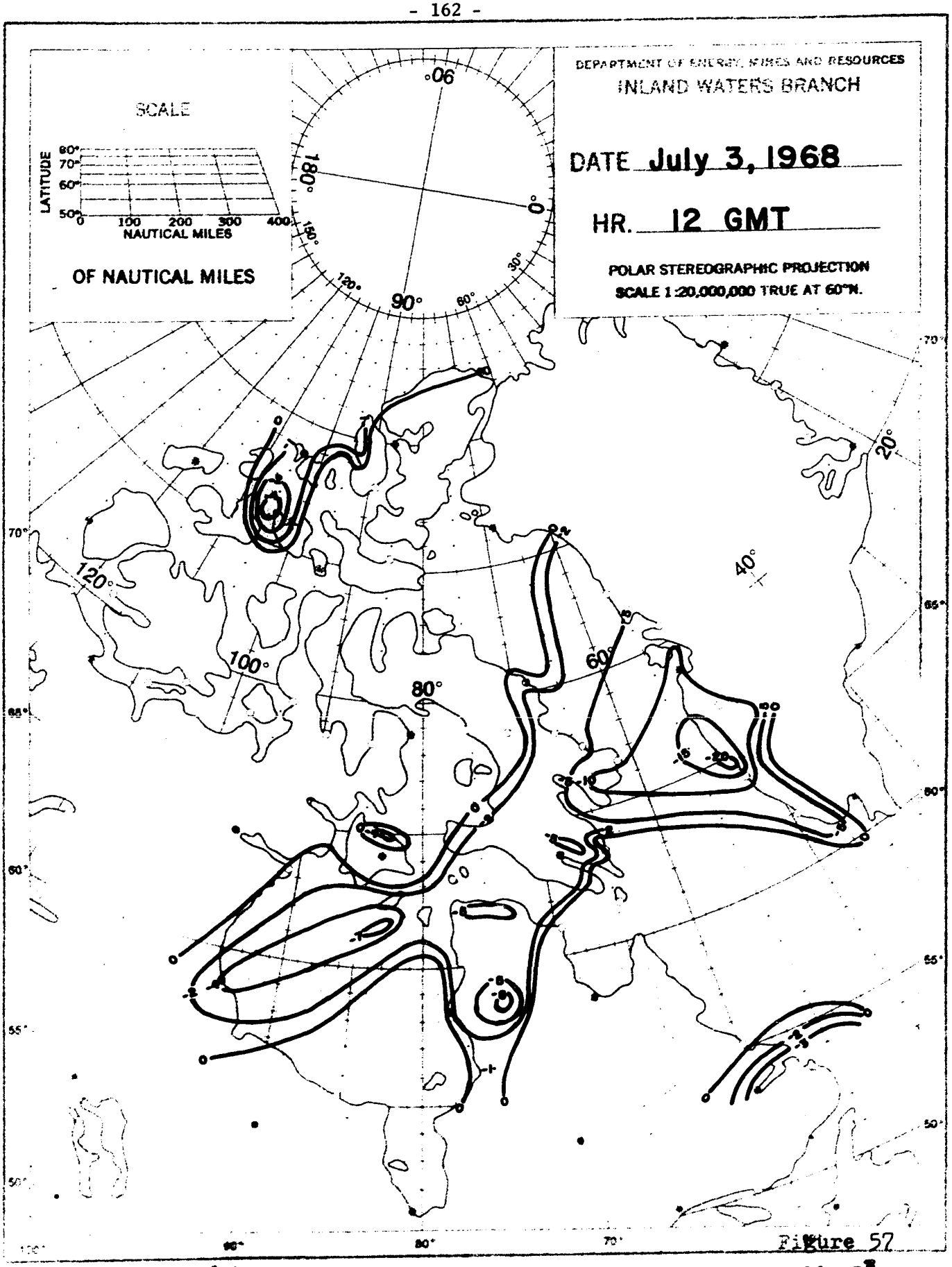

Figure 57

Type "A" Total Vertical Velocity $(\omega_{ES}+\omega_m+\omega_L)\times10^{-3}$ mb sec^{-1}
Negative Values Only

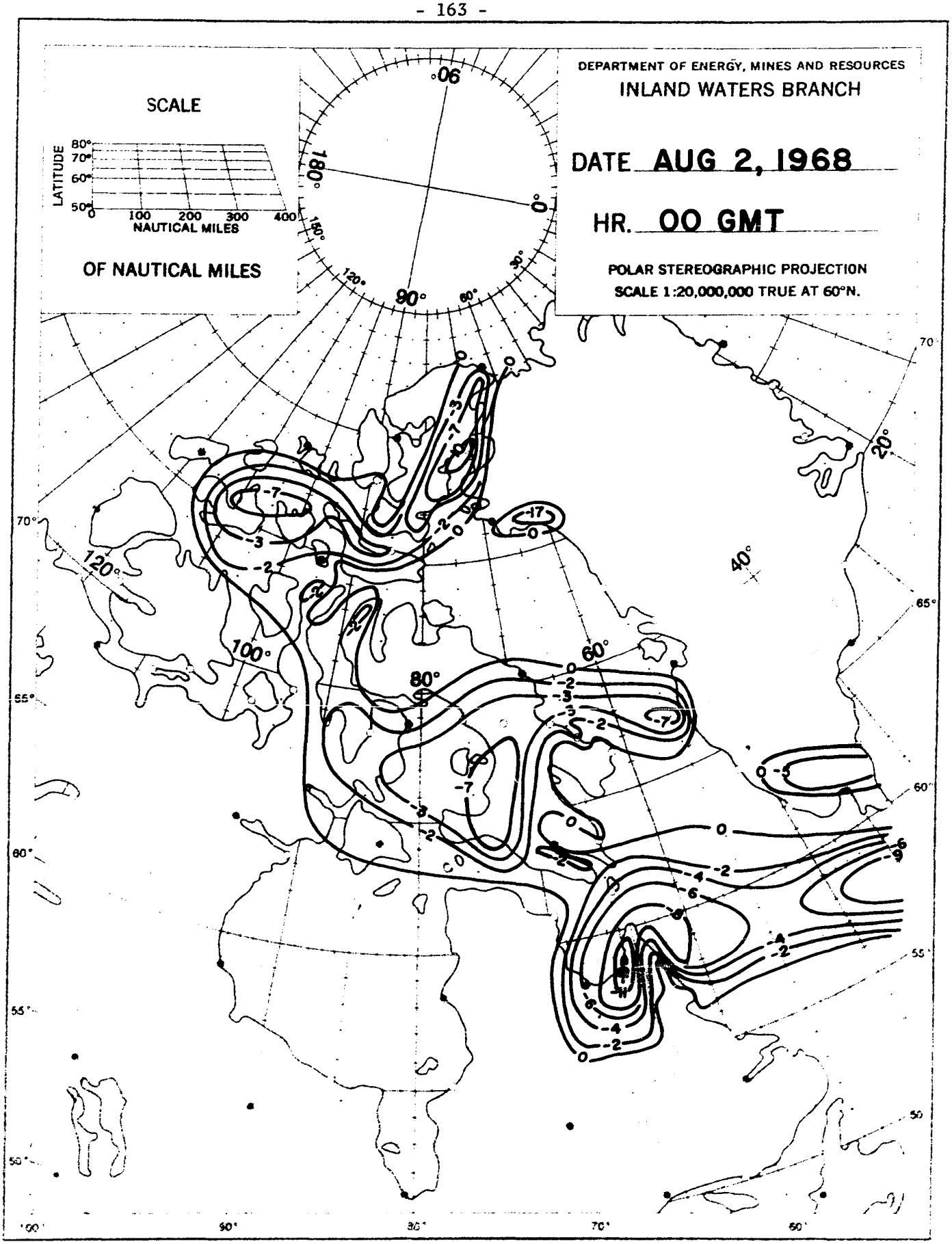

Type "E" Total Vertical Velocity ($\omega_{sc} + \omega_m + \omega_L$); Estimated With Streamline Wind Data

Figure 58

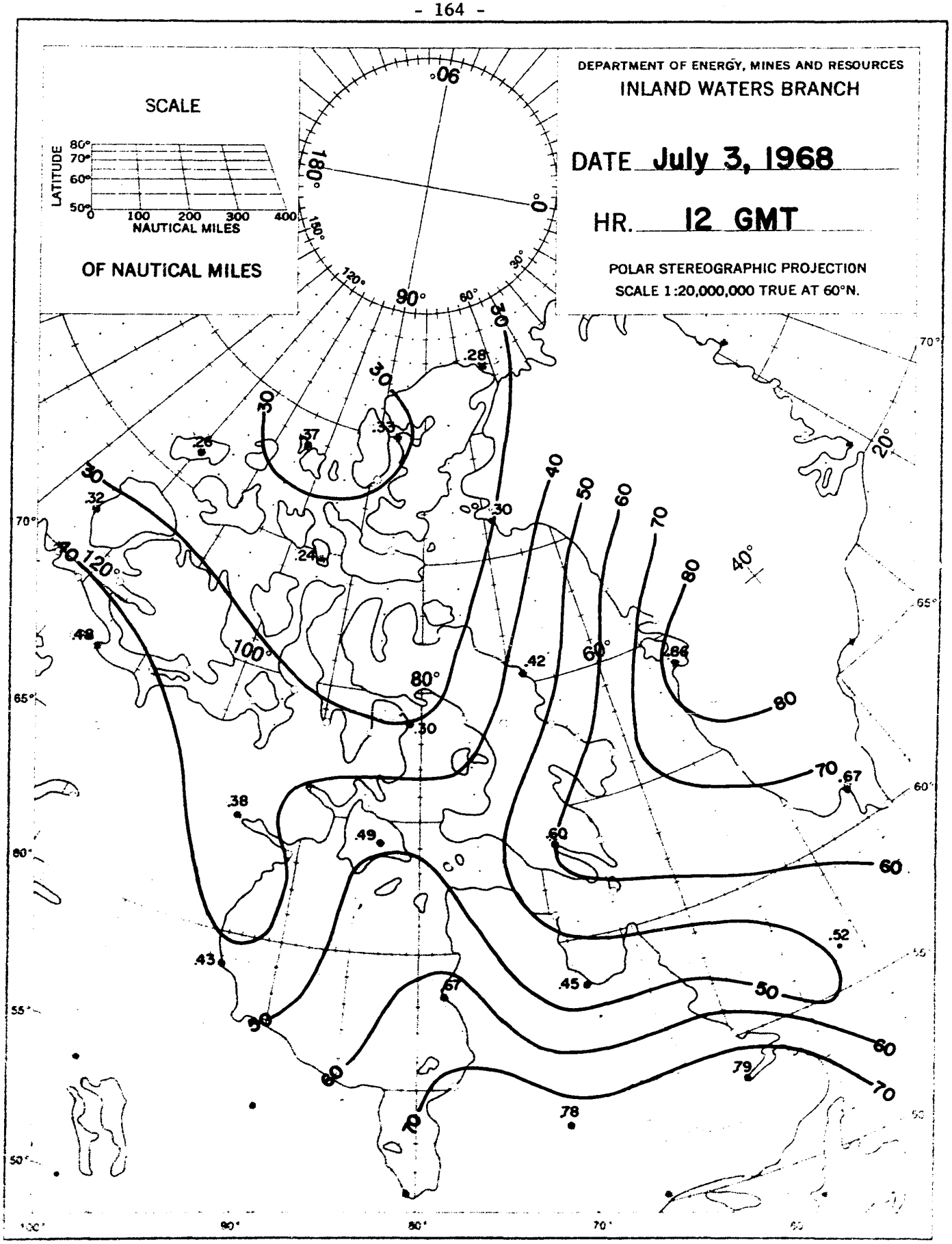

Figure 59

Precipitable Water Unadjusted to Surface Elevation in Hundredths of Inches; Type "A" Map Representative

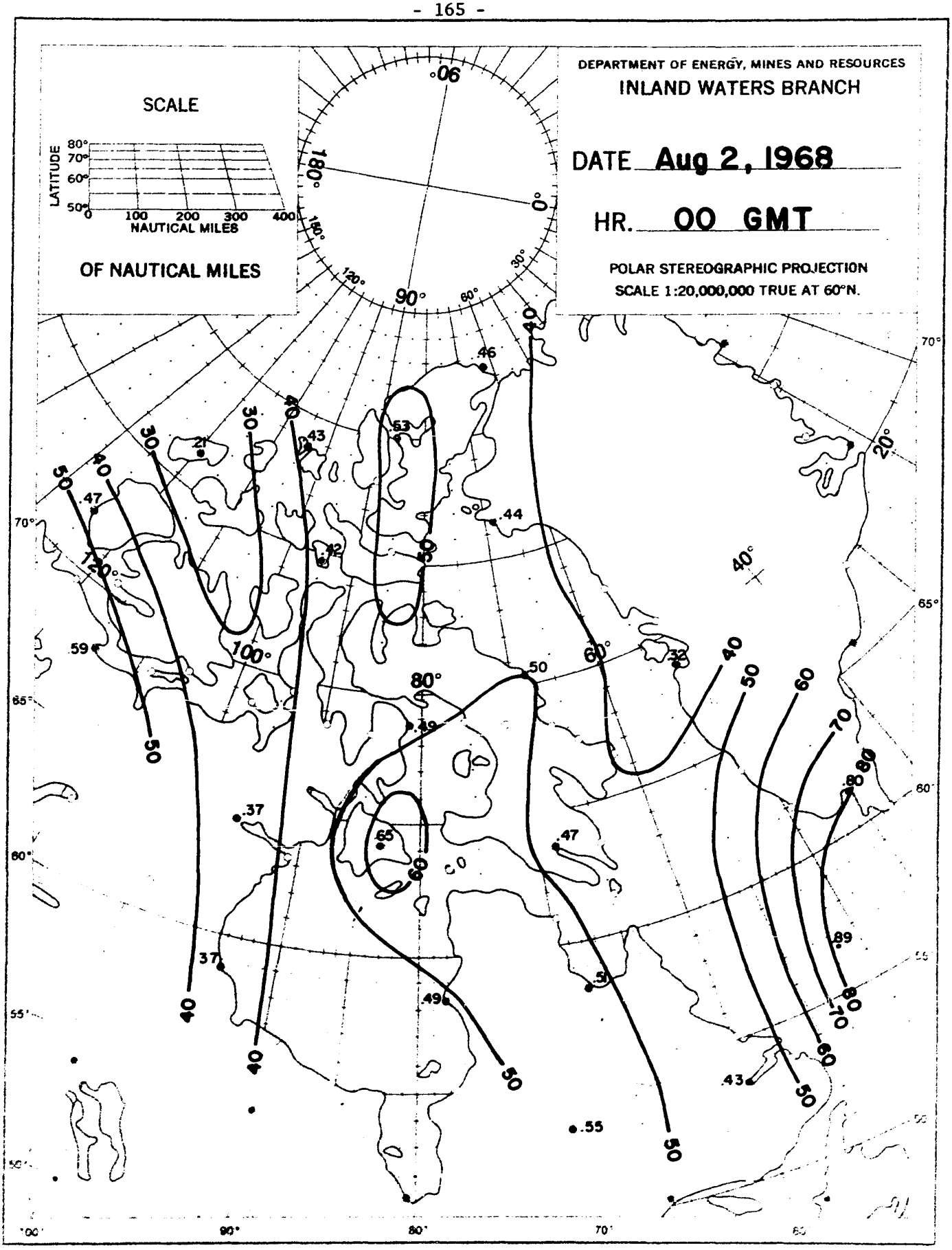

Figure 60

Precipitable Water Unadjusted to Surface Elevation in Hundredths of Inches; Type "E" Map Representative

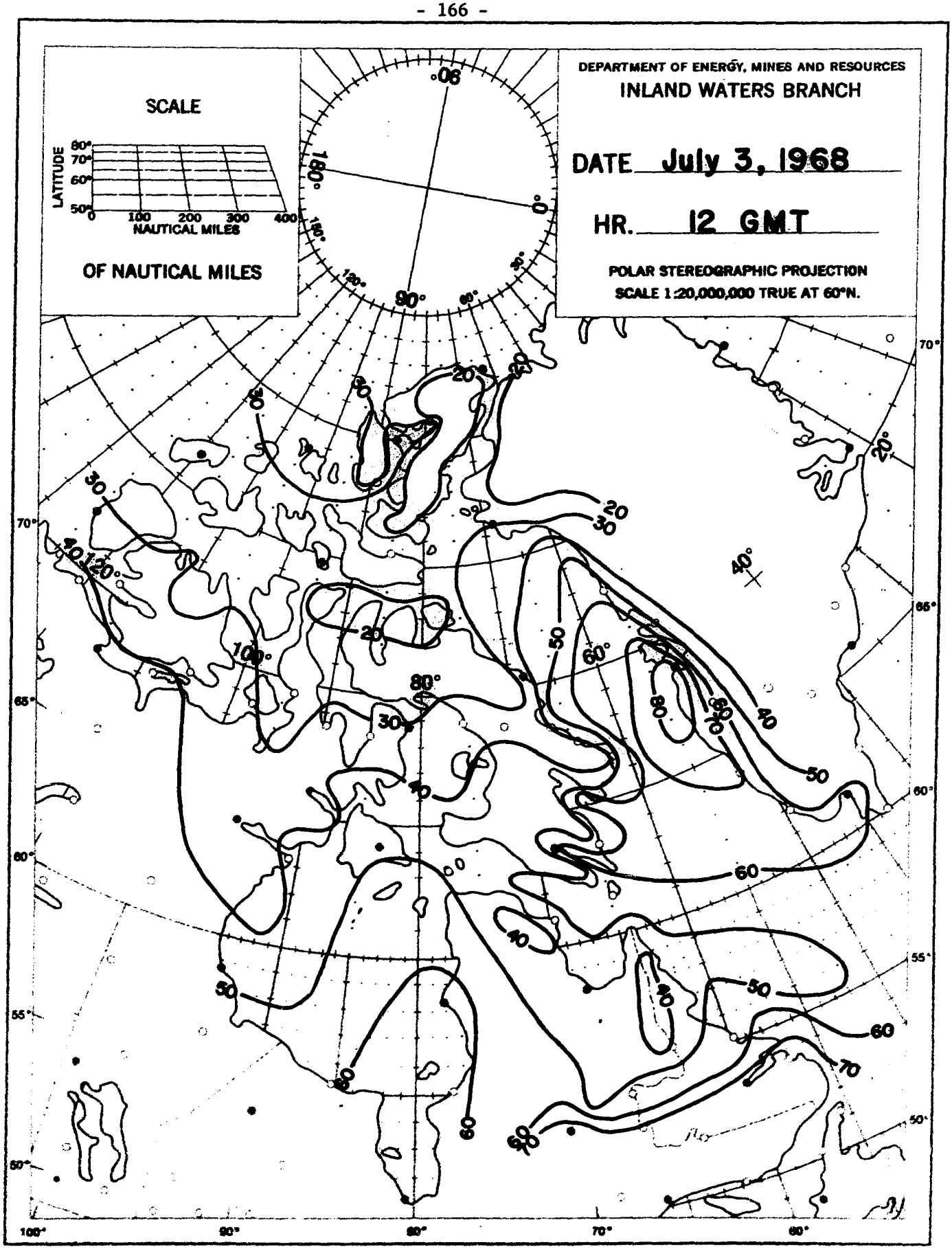

Precipitable Water Adjusted to Smoothed Orography in Hundredths of Inches, Type "A" Map Representative Figure 61

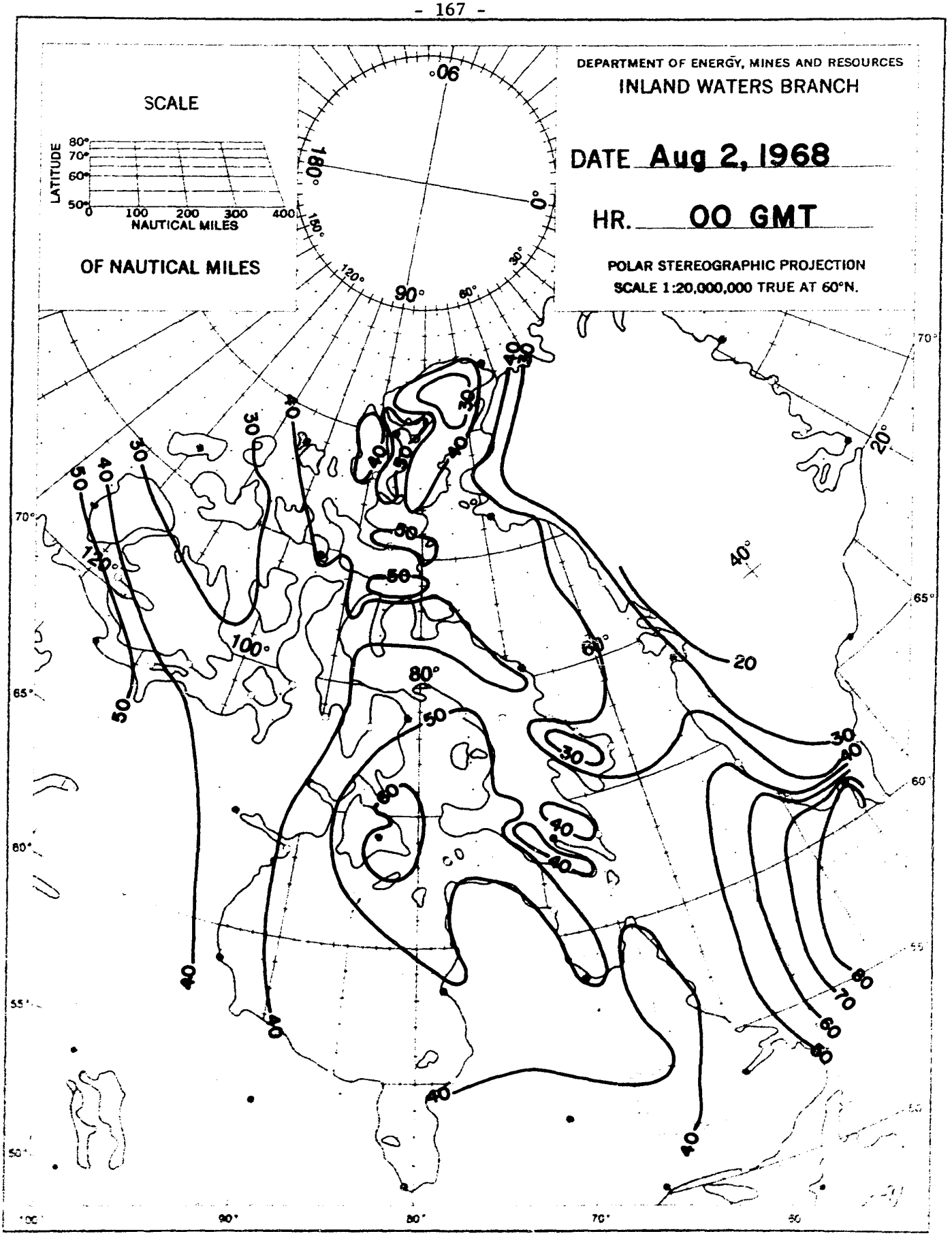

Figure 62

Precipitable Water Adjusted to Smoothed Orography in Hundredths of Inches, Type "E" Map Representative

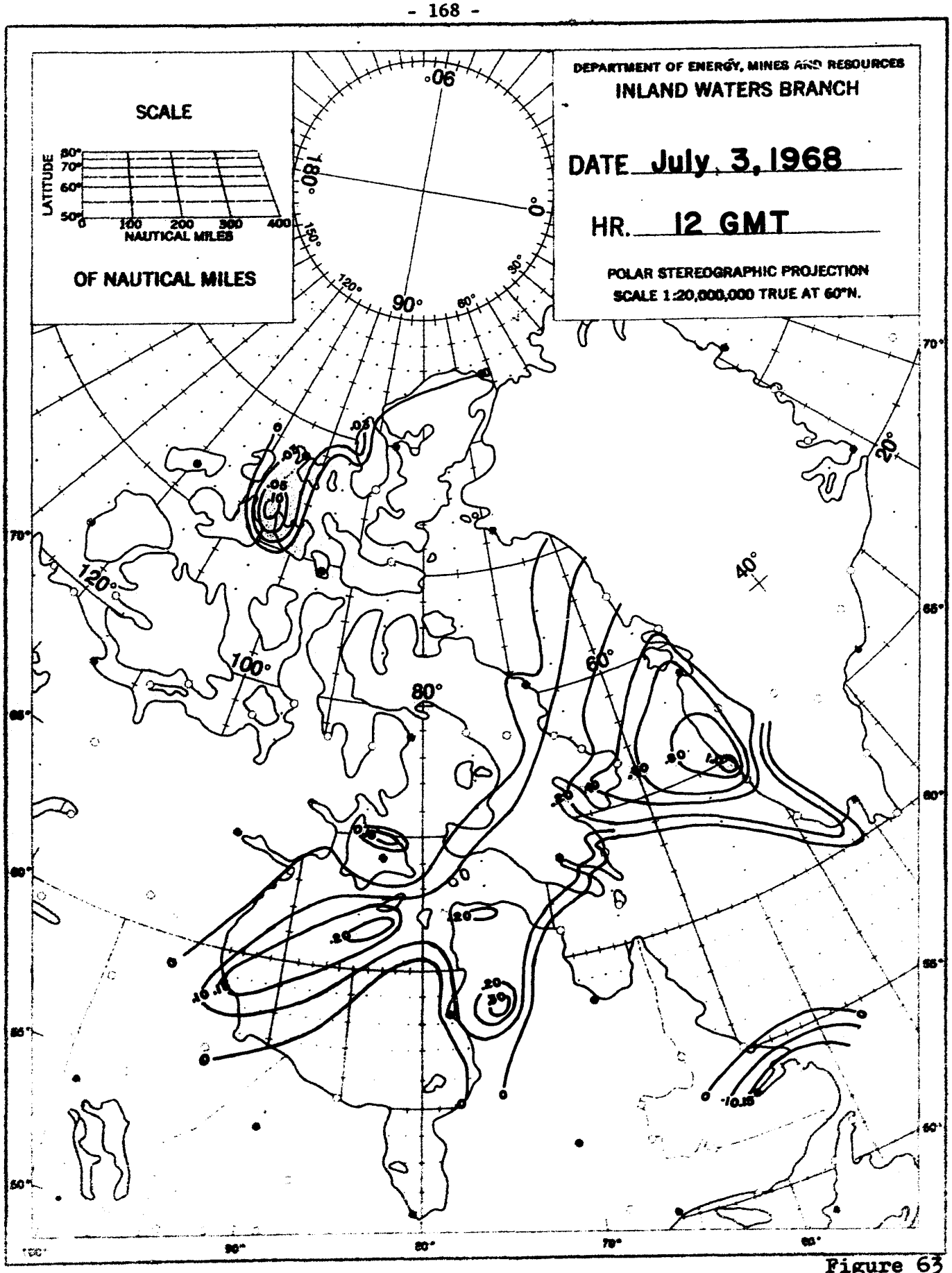

Figure 63

Rate of Precipitation for 6 Hours in Hundredths of Inches; Type "A" Representative Map

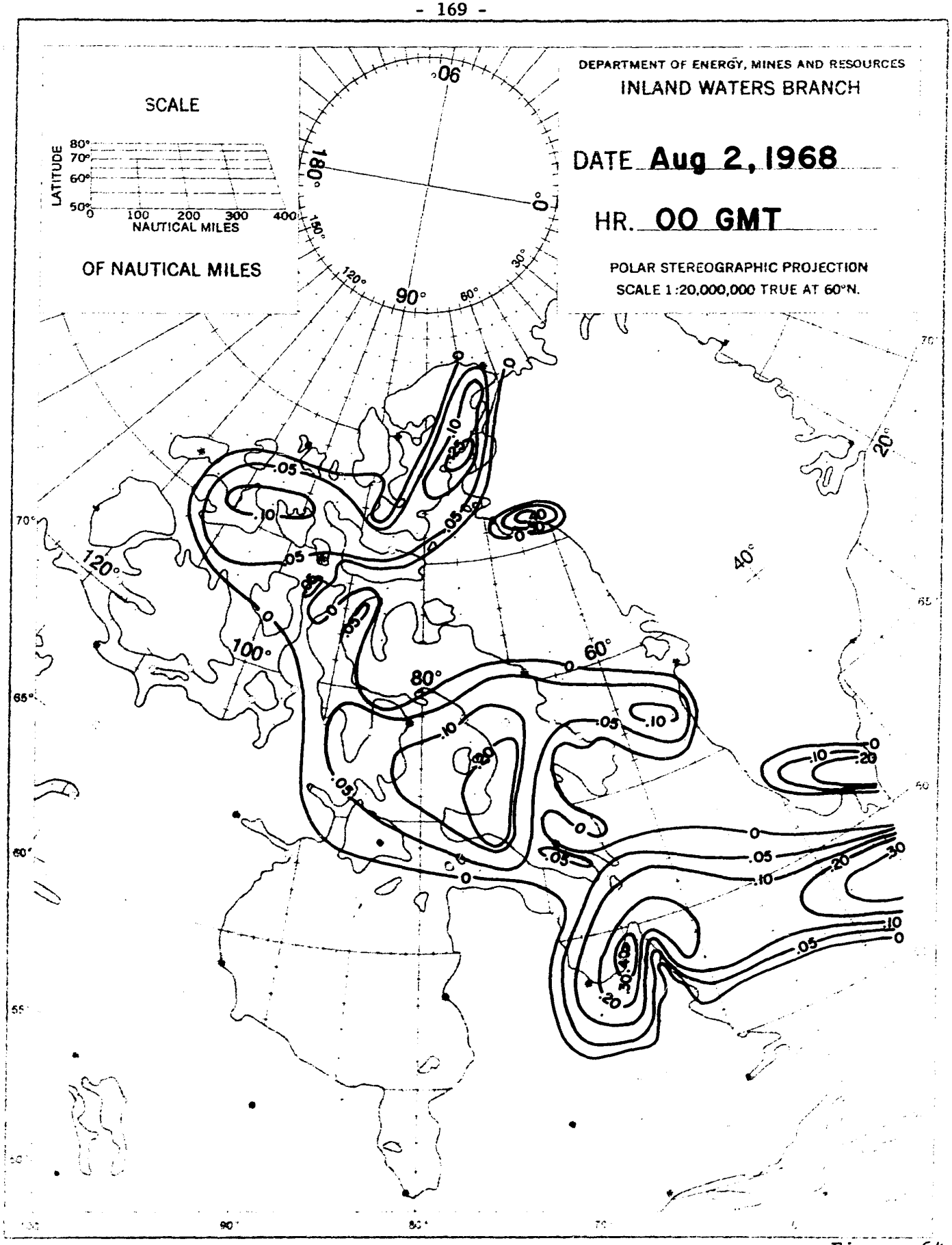

Figure 64

Rate of Precipitation for 6 Hours in Hundredths of inches; Type "E" Representative Map